UNIVERSITA' DEGLI STUDI DI MILANO

Scuola di Dottorato in Scienze Chimiche

Dipartimento di Chimica

PhD in Industrial Chemistry

XXVCycle

Electron-donor and -acceptor ligands in stabilizing and assembling Pt or Ir carbonyl clusters

(Chim 03)

Simona El Afefey

Supervisor: Prof. ALESSANDRO CERIOTTI

Coordinator: Prof. DOMINIQUE ROBERTO

A.A. 2011/2012

Abstract

1-Reactions of platinum clusters with gold-phosphane complexes

During my thesis and previous works it has been shown that $Au(PPh_3)$ fragment stabilizes unprecedented molecular structures of platinum carbonyl clusters in unusual oxidation states. Particularly, we focused on $[Pt_{19}(CO)_{22}]^{4-}$ whose trianion was obtained either chemically and electrochemically but never isolated because unstable. Moreover starting from its parent $[Pt_{19}(CO)_{24}]^{4-}$ anion we optimized the syntheses of a series of $[Pt_{19}]$ clusters bearing from one to four gold-phosphane fragments in order to obtain pure derivatives suitable for further characterization.[1] Furthermore we have tested a multidentate gold-phosphane to assemble several $[Pt_{19}]$ clusters.

- ✓ **$[Pt_{19}(CO)_{22}\{Au(PPh_3)\}]^{3-}$**

$[Pt_{19}(CO)_{22}]^{4-}$ is sufficiently nucleophilic to react with the electrophilic part of $ClAu(PPh_3)$ without requiring a dehalogenation step. The reaction is performed in acetone under nitrogen atmosphere with a molar ratio $[Pt_{19}]$: $ClAu(PPh_3)$ = 1 : 1. The reaction is monitored by IR spectroscopy: the carbonyl stretching bands of the product either in the terminal or bridging region have an upshift of about 20 cm^{-1} compared to the reagent, as we can expect for a more oxidized trianionic species. The compound was isolated as $[NBu_4]^+$ salt, but all the attempts to obtain crystals suitable for the X ray diffraction were unsuccessful. Anyway the elemental analysis of the product seems to confirm the proposed $[Pt_{19}(CO)_{22}\{Au(PPh_3)\}]^{3-}$ formula for this anion.

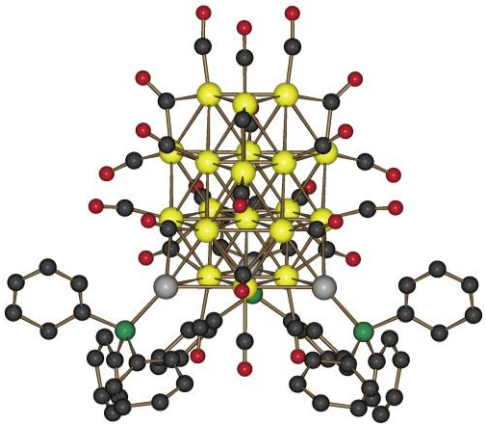

Figure 1 - XRD structure of $[Pt_{19}(CO)_{24}(AuPPh_3)_3]^-$ anion

- ✓ **$[Pt_{19}(CO)_{24}\{Au(PPh_3)_3\}]^-$**

The reaction is carried out starting from $[Pt_{19}(CO)_{22}]^{4-}$ in acetonitrile under carbon monoxide atmosphere with a molar ratio $[Pt_{19}]$: $ClAu(PPh_3)$ = 1 : 3. The product precipitates directly from the solution. Crystals suitable for X-ray analysis can be obtained by layering 2-propanol onto a THF

solution of the product. The molecular structure is shown in **Figure 1**.

We have studied the redox behaviour of this new derivative via electrochemistry (**Figure 2**) and IR spectro-electrochemistry (**Figure 3**). The product shows one oxidation and three reduction steps. The oxidation and the first reduction are chemically and electrochemicaly reversible. The second and third reduction steps are reversible as well, although complicated by chemical reactions following the electron transfer. Also the spectroelectrochemical investigation confirmed the electrochemical data, by showing isosbestic point when the monoanion is transformed into the dianion.

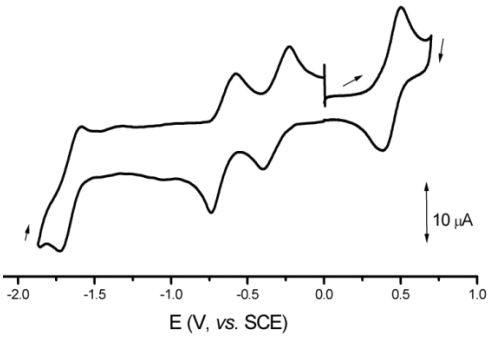

Figure 2 - Cyclovoltammetric profile of $[Pt_{19}(CO)_{24}(AuPPh_3)_3]^-$ in THF

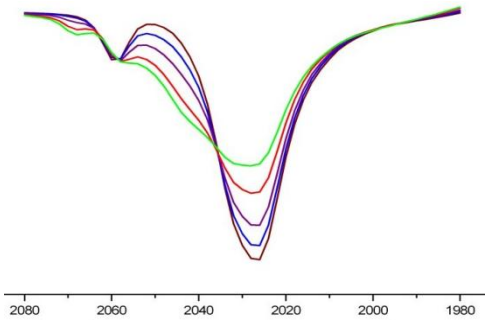

Figure 3 - IR spectroelectrochemistry of $[Pt_{19}(CO)_{24}(AuPPh_3)_3]^-$ in THF

- ✓ **$[Pt_{19}(CO)_{24}\{Au(PPh_3)_4\}]$**

The compound is prepared starting from $[Pt_{19}(CO)_{24}\{Au(PPh_3)_3\}]^-$ with one equivalent of $[AuPPh_3]^+$ in THF under carbon monoxide atmosphere. The molecular structure (**Figure 4**) has been obtained from X-ray diffraction analysis on single crystal grown by layering 2-propanol onto a THF solution of the product. The redox behaviour has been analyzed resulting to be analogous to the precursor's one.

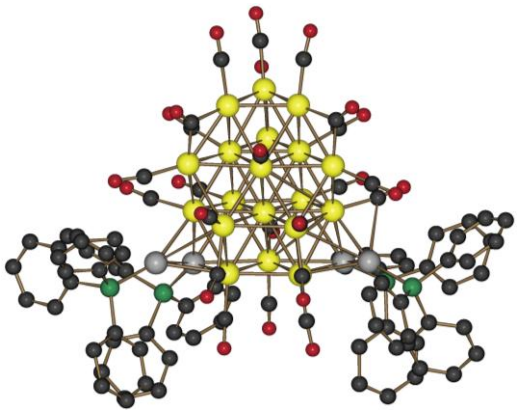

Figure 4 - XRD structure of $[Pt_{19}(CO)_{24}(AuPPh_3)_4]$

- ✓ **$[\{Pt_{19}Au(CO)_{22}\}_4(180tetraphos)]^{12-}$**

As previously shown, $[Pt_{19}(CO)_{22}]^{4-}$ reacts with one equivalent of $ClAu(PPh_3)$ forming the $[Pt_{19}(CO)_{22}\{Au(PPh_3)\}]^{3-}$ trianion. We used a multidentate gold-polyphosphane ligand to assemble several $[Pt_{19}]$ clusters. For this purpose we prepared the gold functionalized tetraphosphane (180tetraphos) ligand shown in the below scheme which cannot be a chelating agent for the cluster because of its rigid skeleton.

The gold-phosphane derivative synthesis is shown in the following scheme:

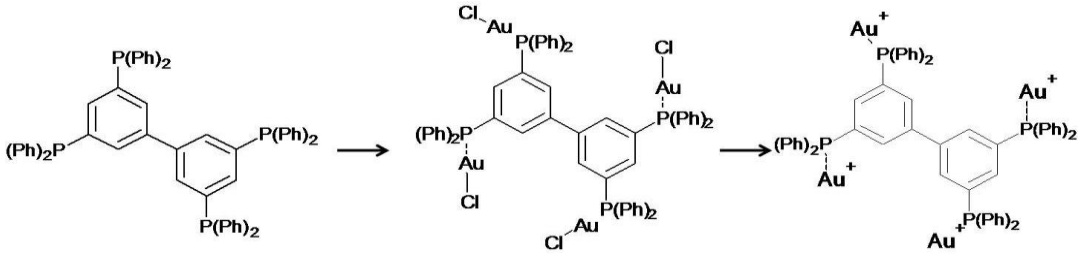

Synthesis of $[Au_4(180tetraphos)]^{4+}$

In fact we were able to obtain the desired product according to the stoichiometry:

$$4[Pt_{19}(CO)_{22}]^{4-} + [Au_4(180tetraphos)]^{4+} \longrightarrow [\{Pt_{19}Au(CO)_{22}\}_4(180tetraphos)]^{12-}$$

To perform the reaction a dehalogenation step of the gold complex is necessary. The product has been characterized by IR and elemental analysis while its electrochemical behaviour is currently under investigation. Because of the nanocapacitor behaviour of the $[Pt_{19}]$ cluster [1], this molecule could represent a sort of compartmental nanocapacitor where each cluster moiety behaves separately.

2- Assembly of Ir_6 carbonyl clusters using gold-phosphane complexes

We used the hexairidium carbonyl cluster $[Ir_6(CO)_{15}]^{2-}$ and gold-phosphane complexes in order to get cluster aggregates suitable for further studies (i.e. electrochemistry and fluorescence).

The tested ligands were 180tetraphos and 120hexaphos coordinated to Au^+ centres.

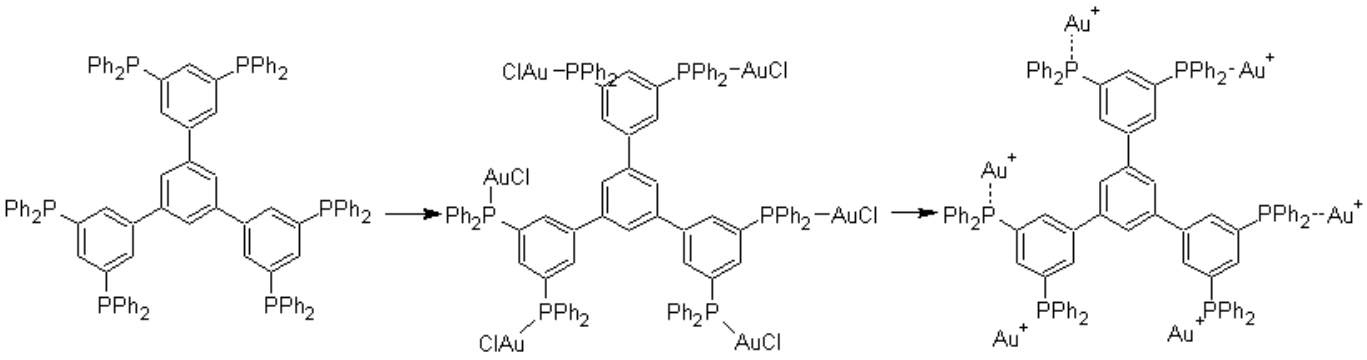

Synthesis of $[Au_4(120hexaphos)]^{6+}$

- ✓ **Reaction with 180tetraphos**

The reactions are conducted under CO atmosphere and they were similar for both ligands, so only one is here reported. A solution of 180tetraphos in THF is added in stoichiometric amount to a THF solution of the cluster:

$$4\ [Ir_6(CO)_{15}]^{2-} + [Au_4(180tetraphos)]^{4+} \xrightarrow{CO} [\{Ir_6Au(CO)_{15}\}_4(180tetraphos)]^{4-}$$

After one hour stirring the reaction is completed, as by IR checking, featuring carbonyl stretching bands at 2020(vs) and 1788(m) cm^{-1} .

Elemental analysis and ^{31}P-NMR spectroscopy agree with the proposed formulation $[\{Ir_6Au(CO)_{15}\}_4(180tetraphos)]^{4-}$. We performed the reaction under nitrogen atmosphere too. The resulting product is not as pure as in the case of CO atmosphere, as revealed by elemental analysis.

We compared our spectroscopic data with those ones reported in literature for the simpler analogous gold-monosubstituted species $[Ir_6(CO)_{15}(AuPPh_3)]^-$ and we found a strict similarity, as we would expected. The only substantial difference being that the reported species shows fluxionality at room temperature in the ^{31}P-NMR, whereas our molecule does not, showing two singlets at 97.70 and 23.64 ppm.

Redox behaviour of the compound has been investigated, undergoing four processes, two reductions cathodic peaks at -1,65 and -1,83 volt, and two oxidation anodic peaks at 0,64 and 0,87 volt.

The first cathodic process is electrochemically and chemically irreversible, whereas the second one (-1,83 volt) is partially reversible.

By varying the scansion speed of the second cathodic process, it is clear that reversibility decreases as the scansion speed increases (**Figure 5**).

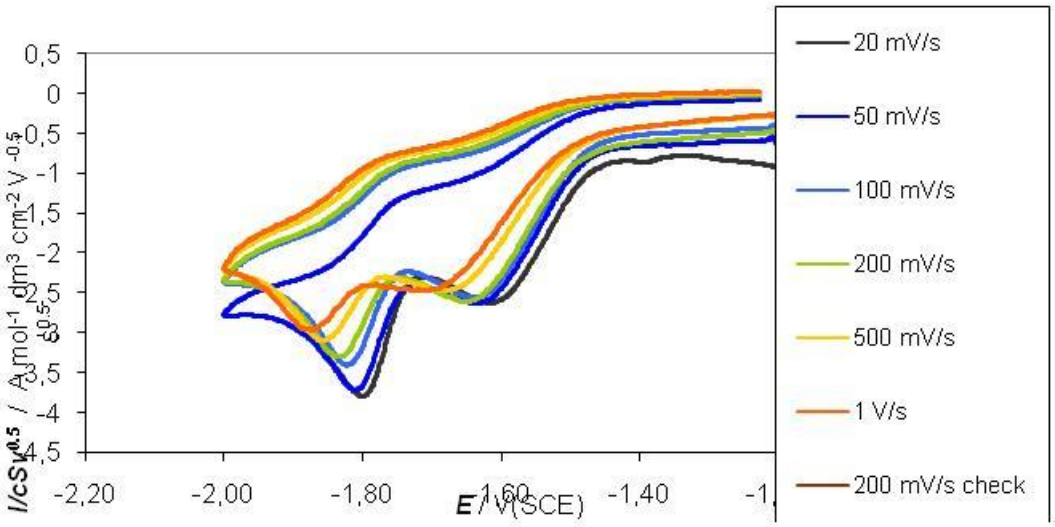

Figure 5 - Cyclic voltammograms of $[\{Ir_6Au(CO)_{15}\}_4(180tetraphos)]^{4-}$ (10^{-3} M) in THF. GC, T=298 K, at varied speed, supporting electrolyte $[Net_4][PF_6]$ (0,2 M)

- ✓ **Reaction with 120hexaphos**

The species $[\{Ir_6Au(CO)_{15}\}_6(120\text{-hexaphos})]^{6-}$ is formed according to the reaction:

$$6\ [Ir_6(CO)_{15}]^{2-} + [Au_6(120\text{-hexaphos})]^{6+} \xrightarrow{CO,\ THF} [\{Ir_6Au(CO)_{15}\}_6(120\text{-hexaphos})]^{6-}$$

The product shows in the IR spectrum, carbonyl stretching bands typical for a formal monoanionic hexairidium carbonyl cluster at 2019(vs), 1985(sh), 1781(m) cm^{-1}).

Then we performed a metathesis reaction in order to exchange the PPN^+ monocation (PPN=bis(triphenylphosphoranylidene)ammonium), with the fluorescent N,N'-dimethyl-9,9'-bisacridinium di-cation. The isolated product showed an up-shift in the carbonyl stretching bands at 2027(s), 1972(sh), 1818(b) and 1780(w) cm^{-1}.

Fluorescence measurements (**Figure 6**) have demonstrated that the obtained species emits at higher wavelengths both with respect to the phosphane ligand, the gold-phoshane complex and the acridinium (as di-cation or neutral form).

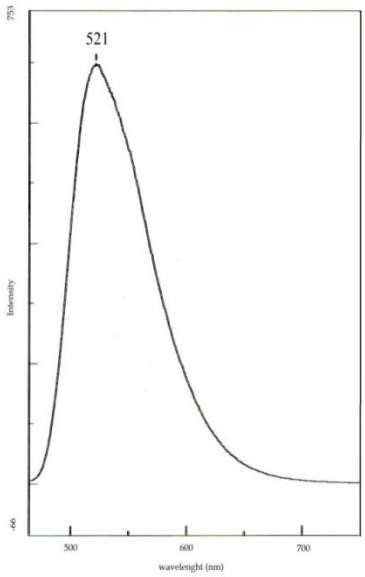

Figure 6 - Fluorescent spectrum of the metathesis product between $[PPN]_6[\{Ir_6Au(CO)_{15}\}_6(120\text{-hexaphos})]$ and $[Bis\text{-}acridinium][BPh_4]_2$

This red-shift reflects a decrease in the distance between ground state orbitals and outer orbitals where electrons are promoted after the absorption of exciting radiation.

3- Assembly of Ir_4 carbonyl clusters using diphosphane ligands

The reactivity of the neutral $[Ir_4(CO)_{12}]$ cluster and its halogenated $[Ir_4X(CO)_{11}]^-$ derivatives with P-donor ligands (i.e. PPh_3 , $PPh_2(CH_2CH_2)PPh_2$) has been deeply investigated in the past years. So, we have exploited the reaction between $[Ir_4Br(CO)_{11}]^-$ and multi-phosphane ligands in order to obtain cluster aggregation and to prepare molecular materials with a well definited structure and formula.

- ✓ **Reaction with bis(diphenylphosphano)acetylene (dppa) and 1,2-bis(diphenylphosphano) ethene (t-dppethe)**

The reaction of $[PPh_4][Ir_4Br(CO)_{11}]$ and bis(diphenylphosphano)acetylene (dppa) or 1,2-bis(diphenylphosphano)ethene (t-dppethe) in acetonitrile in 2:1 molar ratio afforded an almost immediate yellow microcrystalline precipitate of $[\{Ir_4(CO)_{11}\}_2(dppa)]$ or $[\{Ir_4(CO)_{11}\}_2(t\text{-dppethe})]$. These products are insoluble in all common organic solvents.

Crystals, suitable for X-ray diffraction analysis, have been obtained by slow diffusion of a n-heptane solution of the ligand into a dichloromethane solution of the cluster.
Solid state structures are reported in **Figure 7** and **Figure 8** respectively .

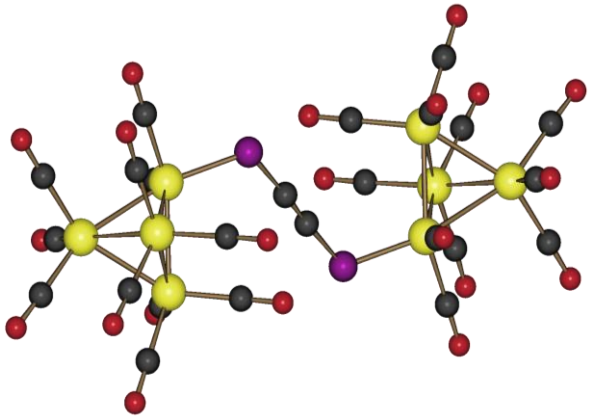

Figure 7 - XRD structure of [{$Ir_4(CO)_{11}$}$_2$(dppa)]

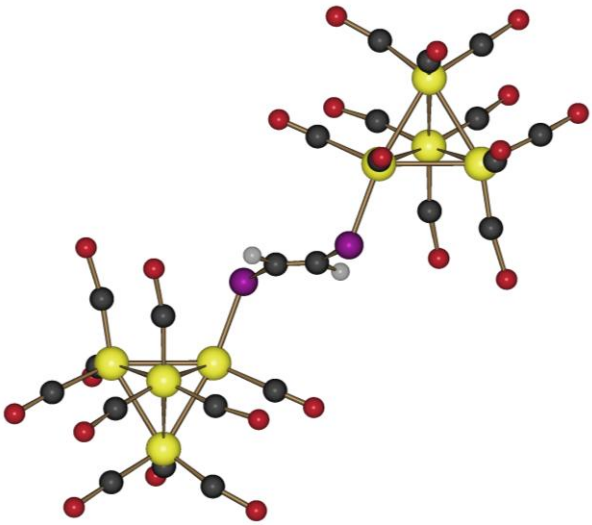

Figure 8- XRD structure of [{$Ir_4(CO)_{11}$}$_2$(t-

ATR-IR spectra of the new derivatives have been registered on a total attenuated reflectance spectrophotometer. The experiment consists in deposing a small amount of sample on a ZnSe crystal, and applying a pressure through a mechanic press. These IR spectra, registered on different crystals for which the elemental cell was checked, have given always the same result .

Two bands in the typical region of edge-bridging COs region are present, in disagreement with single crystal X-ray diffraction analysis , which showed the presence of terminal COs only. Actually Nujol IR spectra show only terminal COs stretching bands.

This phenomenom allows us to suppose that the pressure applied to register the first spectrum causes a structural re-arrangement and three carbonyl ligands would change their coordination mode, from terminal to edge-bridging. These species has a low solubility in CH_2Cl_2. Anyway, with 38000 scansions, it has been possible to obtain a satisfying ^{31}P-NMR spectrum for [{$Ir_4(CO)_{11}$}$_2$(t-dppethe)], showing a singlet at -18,8 ppm.

- ✓ **Reaction with 1,4bis(diphenylphosphano)butane(dppbut)**

In addition to the above discussed rigid diphosphane ligands, we tested flexible diphosphane ligands too. So 1,4bis(diphenylphosphano)butane(dppbut) and [$Ir_4(CO)_{12}$] have been reacted in solvothermal conditions. The reaction directly afforded orange crystals, which have been studied by X ray analysis. The molecular structure is reported in.**Figure 9**

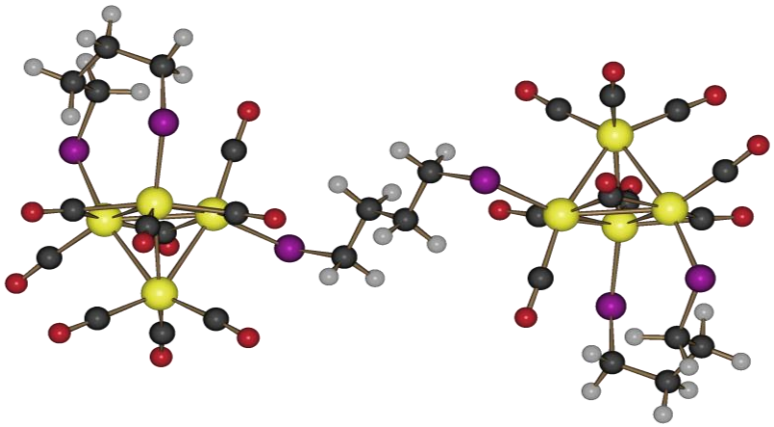

Figure 9 - XRD structure of [{$Ir_4(CO)_9$(□-dppbut)}$_2$(dppbut)]

Two Ir_4 clusters are joined by a radial-radial coordinated dppbut ligand. Each Ir_4 cluster is also chelated by another axial-axial coordinated diphosphane lying under the tetrahedron basal plane. ATR-IR spectrum shows carbonyl stretching bands at 2040(w), 1980(w), 1954(m) cm^{-1} (terminal COs) and 1789(s), 1771(vs) cm^{-1} (edge-bridged COs).

- ✓ **Reaction with 1,6-bis(diphenylphosphano)hexane (dpphex)**

Solvothermal reaction of $[Ir_4(CO)_{12}]$ with 1,6-bis(diphenylphosphano)hexane (dpphex) gave yellow crystals of $[\{Ir_4(CO)_9\}_2(dpphex)_3 \bullet (solv)]$. The molecular structure is reported in **Figure 10**.

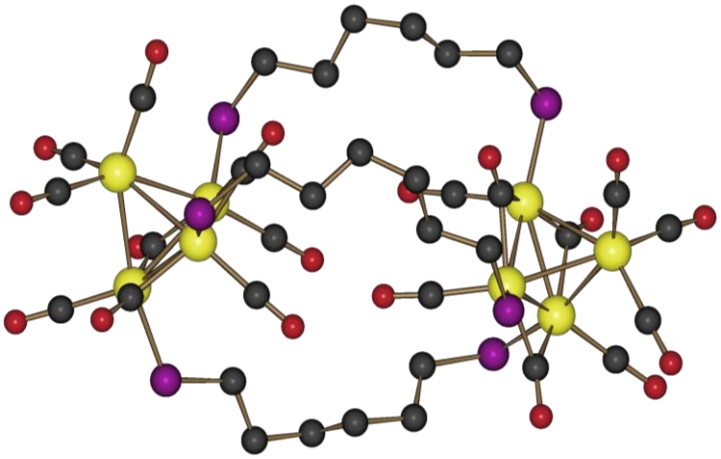

Figure 10 - XRD structure of $[\{Ir_4(CO)_9\}_2(dpphex)_3]$

Two $Ir_4(CO)_9$ cages are linked by three dpphex molecules, being two radial-radial coordinated, with a P-P distance of 7,718 and 7,975 Å, and one axial-axial coordinated , with a P-P distance of 8,631 Å.

Each Ir_4 tetrahedron has two radially and one axially coordinated P atoms. Nine COs, three edge-bridged and six terminal, complete the coordination sphere at each cluster; a dichloromethane molecule is also chlatrated.

ATR-IR spectrum shows carbonyl stretching bands at 2036(m), 1998(m), 1972(s), 1952(s) cm^{-1} (terminal COs) and 1774(s), 1760(vs) cm^{-1} (edge-bridged COs).

- ✓ **Reaction with 180tetraphos**

The reaction is performed in chloroform at room temperature and the product is obtained in good yield following the stoichiometry:

$$4[Ir_4Br(CO)_{11}]^- + 180tetraphos \longrightarrow [\{Ir_4(CO)_{11}\}_4(180tetraphos)] + 4\ Br^-$$

Crystals suitable for X-ray analysis can be grown by layering a chloroform solution of the product with 2-propanol. The molecular structure is shown in **Figure 11**. We have then performed an electrochemical study to investigate the redox behaviour of this material (**Figure 12**).

The compound exhibits an irreversible reduction at -1,37 V. After this process, the resulting species is adsorbed on the electrode and redox active breaking down products are formed. From the voltammetric profile it is evident that some of them give adsorption processes too. During the electrolysis the solution gradually changes color, moving from yellow to dark red and the process appears to be multielectronic.

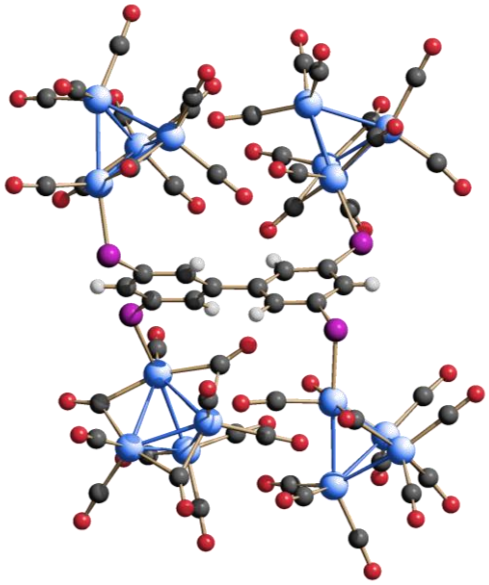

Figure 11 - XRD structure of [{$Ir_4(CO)_{11}$}$_4$(180tetraphos)]

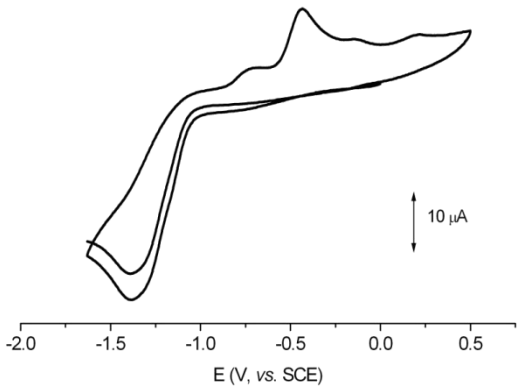

4-

Figure 12 - Voltammetric profile of [{$Ir_4(CO)_{11}$}$_4$(180tetraphos)] in THF

Synthesis and electrochemical studies of $[Pt_{26}(CO)_{32}]^{2-}$

The synthesis of the $[Pt_{26}(CO)_{32}]^{2-}$ anion was already reported, but not optimized.

With some slight modifications with respect to the past, in particular by using the weaker CF_3COOH acid instead of the strong H_2SO_4 as oxidizing agent on a preformed Pt carbonyl clusters mixture, we have been able to obtain a highly pure product. This allowed us to perform electrochemical and spectroelectrochemical studies. The species shows a redox behaviour poorer than its analogous $[Pt_{19}(CO)_{22}]^{4-}$, $[Pt_{24}(CO)_{30}]^{2-}$ and $[Pt_{38}(CO)_{44}]^{2-}$.[2] The cyclic voltammetry (**Figure 13**) of the product in THF shows three cathodic and one anodic processes, all reversible. The spectroelectrochemical trend for the oxidation step $[Pt_{26}]^{2-/-}$ displays an isosbestic point, which confirms the stability of the two related oxidation states (**Figure 14**). One isosbestic point is shown by the reduction step $[Pt_{26}]^{2-/3-}$ too.

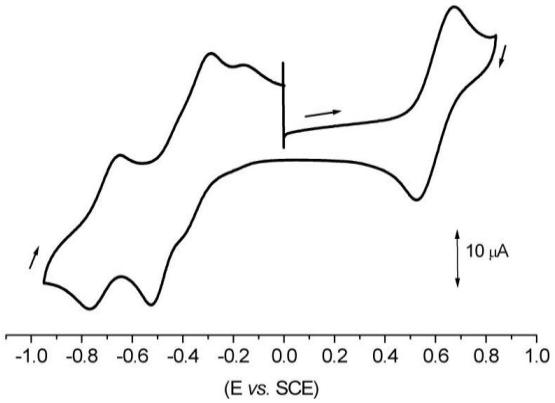

Figure 13 - Voltammetric profile of $[Pt_{26}(CO)_{32}]^{2-}$ in THF

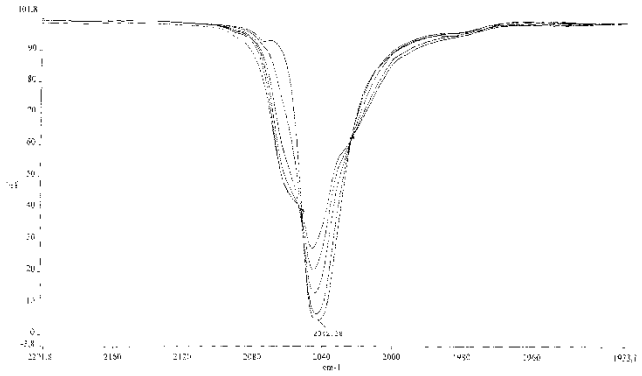

Figure 14 - IR spectroelectrochemistry of $[Pt_{26}(CO)_{32}]^{2-}$ in THF

5- Synthesis of mixed Pt-Sn carbonyl clusters

Heterometallic Pt-Sn systems are interesting as they show a good catalytic activity in hydrogenation, isomerisation, hydroformylation and water-gas-shift reactions.

We have optimized the syntheses of some platinum heteroleptic clusters, starting from $[Pt_{15}(CO)_{30}]^{2-}$, with ligands like carbon monoxide, phosphanes and SnX_n fragments (X= Cl, Br, n=2, 3).

In particular we have focused our attention on the reactivity of the derivative $[Pt_6(SnCl_2)_2(SnCl_3)_4(CO)_6]^{4-}$ cluster towards nucleophilic agents.

Under different condition and using PPh_3 as nucleophile, it has been possible to define the following cycle of reactions:

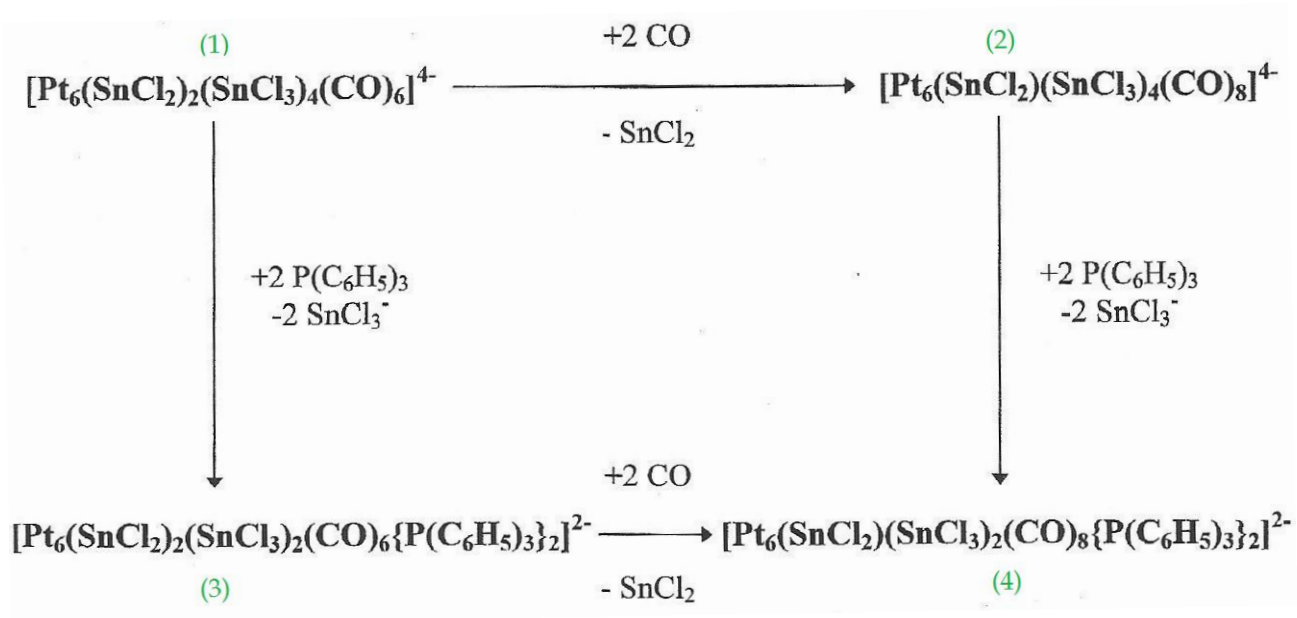

The parent cluster (1), under CO atmosphere, converts into (2) which in turn reacts with 2 equivalents of PPh_3 to form (4). The species (1), (2) and (4) have been all isolated an fully characterized. Derivative (4) can be also obtained by reversing the order of reagents (CO, PPh_3) as well and so passing through the hypothetical species (3).

We have observed that (1), (2) and (4), although they have an almost identical metal skeleton, have a different cluster valence electron number, according to the coordinated ligands. The possibility to modulate electronic and steric features of the clusters, by properly changing the phosphane ligand, can be used in view of possible applications in catalysis.

Another Pt-Sn cluster family is represented by the compounds having general formula $[Pt_5(CO)_5\{Cl_2Sn(\mu\text{-}OR)SnCl_2\}_3]^{3-}$ (R = H, Me, Et, i-Pr). We have studied these clusters in collaboration with the University of Bologna and ICCOM-CNR of Sesto Fiorentino,[3] finding that all the Pt cores have a trigonal bipyramidal geometry electronically stabilized by the Sn(II) fragments.

6- Use of bulky cations for growthing Pt carbonyl clusters

The 1,12-bis(triphenylphosphonium)dodecane dication has been employed as counter-ion of the platinum columnar cluster $[Pt_{15}(CO)_{30}]^{2-}$ during its oxidation reactions towards $[Pt_{3n}(CO)_{6n}]^{2-}$ (n =6-10) species. The goal was to increase the solubility of the oxidized species in order to favour the crystallization step and possibly the X-ray characterization step. The dication, as dibromide salt, has been obtained starting from 1,12-bis(diphenylphosphino)dodecane, bromobenzene and nickel bromide as catalyst. Furtherly the $[Ph_3P\text{-}(CH_2)_{12}\text{-}PPh_3][Pt_{15}(CO)_{30}]$ compound has been prepared by mean of a metathesis reaction on $Na_2[Pt_{15}(CO)_{30}]$.

The $[Ph_3P\text{-}(CH_2)_{12}\text{-}PPh_3][Pt_{15}(CO)_{30}]$ derivative, dissolved in THF, has been oxidized with H^+ deriving from CF_3COOH. The obtained product, dissolved in N,N-dimethylformamyde, showed IR carbonyl stretching bands at 2059(vs), 1902 (sh) 1875 (s), 1853(sh), 1840(sh) cm^{-1}, typical for the species $[Pt_{18}(CO)_{36}]^{2-}$.

Crystals, suitable for X-ray analysis, have been obtained by slow diffusion of 2-propanol into DMF solution of the product. Diffraction data have allowed to formulate the compound as $[Ph_3P\text{-}(CH_2)_{12}\text{-}PPh_3][Pt_{18}(CO)_{36}]$.

Crystal lattice is reported in **Figure 15**.

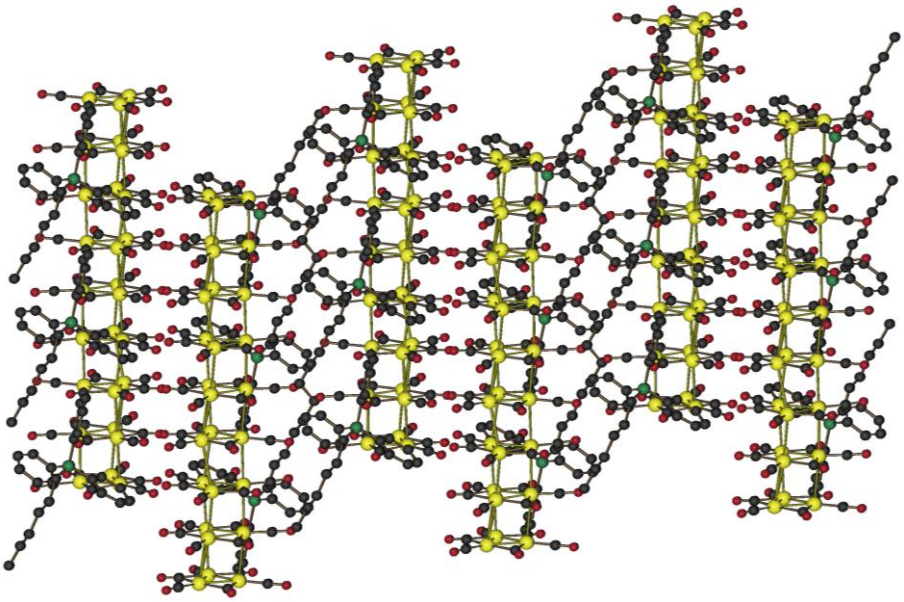

Figure 15 - View along 0, -1, 0 axis of $[Ph_3P\text{-}(CH_2)_{12}\text{-}PPh_3][Pt_{18}(CO)_{36}]$

The species $[PPh_3\text{-}(CH_2)_{12}\text{-}PPh_3][Pt_{18}(CO)_{36}]$, in the solid state, packs as an infinite anionic polymer, in which $[Pt_9(CO)_{18}]$ sub-units can be recognized. These sub-units are stacked at 3.21 Å, a distance lower than the double of the platinum Van der Waals radius (3.4 Å); this fact lets to suppose a weak metal-metal bond interaction among the sub-units.

Instead, the anionic polymer columns are stabilized in the elemental cell by long chain dication units (**Figure 16**). In fact, in the elemental cell one dication and two $[Pt_9(CO)_{18}]$ sub-units are present, the latter at 3.21 Å from the units belonging to contiguous cells.

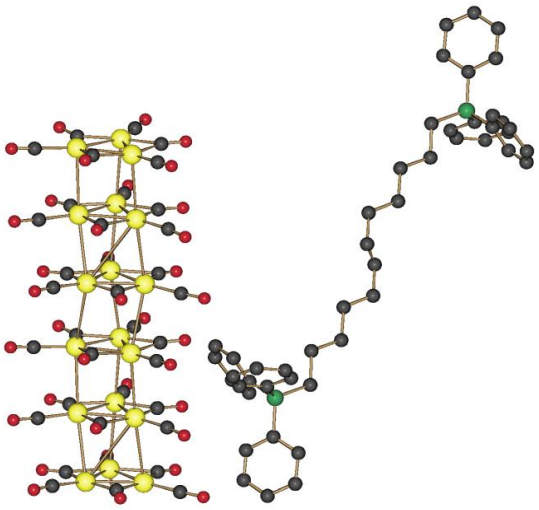

Figure 16 - Elemental cell of $[Ph_3P\text{-}(CH_2)_{12}\text{-}PPh_3][Pt_{18}(CO)_{36}]$

Introduction

1.1 Carbon Monoxide as ligand

In 1884 Ludwig Mond was studying the possibility to recover chlorine from ammonium chloride. His process involving carbon monoxide was conducted in a stainless steel reactor. Mond observed that the nickel valves were being eaten away by CO. To understand what was going on he tried to heat Ni powder in a CO stream. A volatile compound formed: the first metal carbonyl, $Ni(CO)_4$, was born. Subsequently Mond used this reaction to refine nickel because the metal carbonyl can be decomposed to give pure metal by further heating. Lord Kelvin was so impressed by this result that he stated "Mond has given wings to nickel."

Unlike a simple alkyl, CO is an unsaturated ligand, by virtue of the C−O multiple bond. Such ligands are soft because they are capable of accepting metal d_π electrons by back bonding; that is, these ligands are π-electron acceptors. In contrast hard ligands [e.g., H_2O, alkoxides] are σ-electron donors, and often π–electron donors too. CO can act as a spectator or an actor ligand.

Let us look first at the frontier orbitals of M and L because these usually dominate the M−L bonding. The electronic structure of free CO is shown in **Figure 17**. At the beginning, both the C and the O are *sp* hybridized. The singly occupied *sp* and p_z orbitals on each atom form a σ and a π bond, respectively.

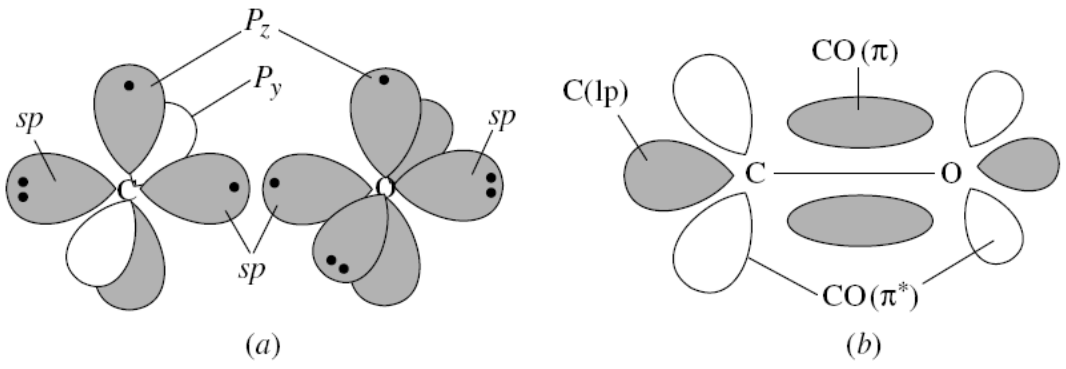

Figure 17 - Electronic structure of CO (occupied orbitals shaded)

This leaves the carbon π orbital empty, and the oxygen p_y orbital doubly occupied, and so the second π bond is formed only after we have formed a dative bond by transfer of the lone pair of O(π) electrons into the empty C(π) orbital. This transfer leads to a $C^-{-}O^+$ polarization of the molecule, which is almost exactly canceled out by a partial $C^+{-}O^-$ polarization of all three bonding orbitals because of the higher electronegativity of oxygen. The free CO molecule therefore has a net dipole moment very close to zero. In **Figure 18** the reason for the polarization of the π_z orbital is shown in MO terms.

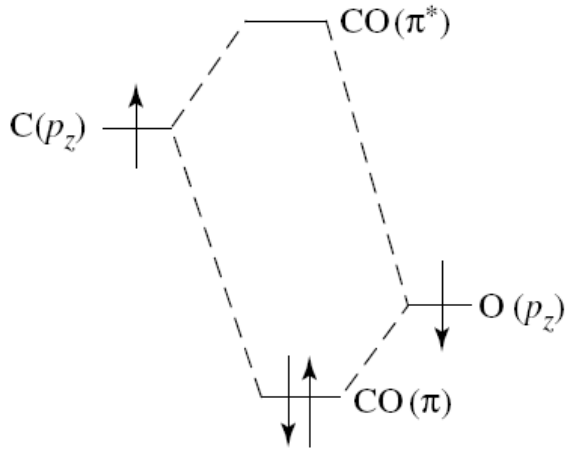

Figure 18 –π MOs of CO

An orbital is always polarized so as to favor the AO that is closest in energy and so the C−O π MO has more O than C character. The valence bond picture of CO and one form of the M-CO system are shown in **Figure 19**.

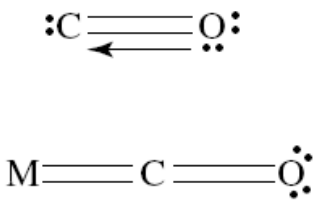

Figure 19 - Valence bond of CO molecule and M-CO fragment

It is not surprising that the metal binds to C, not O, because the ligand HOMO is the C, not the O lone pair; this is because O is more electronegative and so its orbitals have lower

energy. In addition, the CO(π^*) LUMO is polarized toward C, and so M−CO π overlap will also be optimal at C not O. **Figure 20** shows the electron donation from the CO HOMO, (the carbon lone pair) to the metal LUMO (the empty M(dσ) orbital), and the electron back-donation from the metal HOMO (the filled M(dπ) orbital) to the CO LUMO (the π* empty MO orbital).

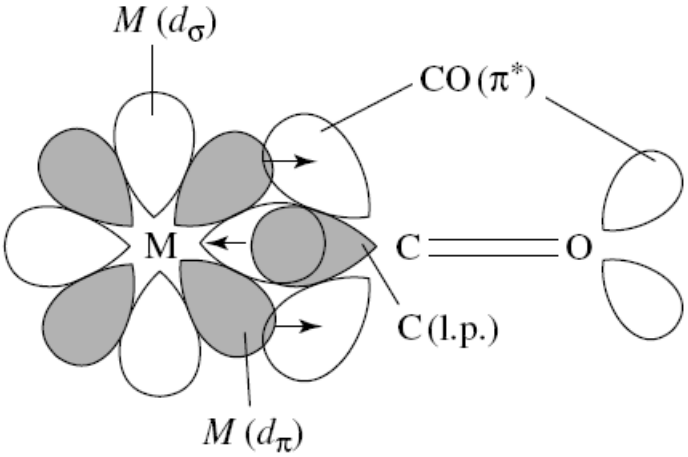

Figure 20 - Molecular orbitals of M-CO interaction

While the former removes electron density from C, the latter increases electron density at both C and O because CO(π^*) has both C and O character. The result is that C becomes more positive on coordination, and O becomes more negative. This translates into a polarization of the CO on binding.

This metal-induced polarization chemically activates the CO ligand. It makes the carbon more sensitive to nucleophilic and the oxygen more sensitive to electrophilic attack. The polarization will be modulated by the effect of the other ligands on the metal and by the net charge on the complex. In a complex of general formula $L_nM(CO)$, the CO carbon becomes particularly ∂^+ in character if the L groups are good π-acceptors or if the complex is cationic [e.g., $Mo(CO)_6$ or $[Mn(CO)_6]^+$], because the CO-to-metal σ-donor electron transfer will be enhanced at the expense of the metal to CO back donation. On the contrary if the L groups are good σ-donors or the complex is anionic [e.g., $Cp_2W(CO)$ or

$[W(CO)_5]^{2-}$], back donation will be encouraged, the CO carbon will lose its pronounced ∂^+ charge, but the CO oxygen will become significantly ∂^-.

The range can be represented in valence bond terms as the extreme in which CO acts as a pure σ-donor (**Figure 21a)**, through the extreme in which both the π_x^* and π_y^* are both fully engaged in back bonding (**Figure 21 b and c**).

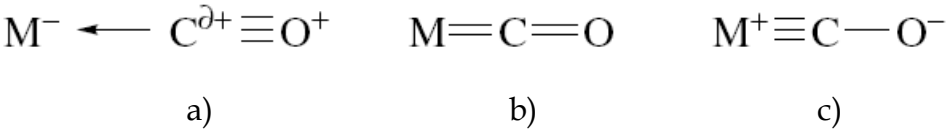

a) b) c)

Figure 21- Extreme representations of M-CO bond

Neither extreme is reached in practice, but each can be considered to contribute differently to the real structure according to the circumstances. In general, polarization effects are of great importance in determining the reactivity of unsaturated ligands.

Note that, on the covalent model, the electron count of CO in
Figure 21- a-c is $2e^-$. The same electron count applies to all true resonance forms.

We can tell where any particular CO lies on the continuum between the situation represented in Figure 5a and 5c, by looking at the IR spectrum.

Because in **21c CO** has a lower C=O bond order than in **21a**, the greater the contribution of **Figure 21c** to the real structure, the lower the observed C=O stretching frequency, $\nu_{CO,}$ being 2200-1600 cm^{-1} the normal range. The MO picture leads to a similar conclusion. As the metal to CO π* back bonding becomes more important, we populate an orbital that is antibonding with respect to the C=O bond, and so we lengthen and weaken the CO bond. In a metal carbonyl, the M−C π bond is made at the expense of the C=O π bond. The high intensity of the CO stretching bands, also partly a result of polarization on binding, means that IR spectroscopy is extremely useful. From the band position, we can tell how good the metal is as a π base. From the number and pattern of the bands, we can tell the number and stereochemistry of the COs present.

Carbonyl ligands bound to very poor π-donor metals, where **Figure 21a** is the predominant contributor to the bonding, have very high ν_{CO} bands as a result of weak

back donation. When these appear to frequency higher than 2143 cm^{-1} (band of free CO), the complexes are sometimes called *nonclassical carbonyls*. Even d^0 species can bind CO, for example, the nonclassical, formally d^0 Zr(IV) carbonyl complexes, $[Cp^*_2Zr(\kappa^2\text{-}S_2)(CO)]$, prepared from reaction of d^2 $[Cp^*_2Zr(CO)_2]$ with S_8 at 80°C, has a ν_{CO} stretching frequency of 2057 cm^{-1}. One of the most extreme weak π-donor examples is $[Ir(CO)_6]^{3+}$ with ν_{CO} bands at 2254, 2276, and 2295 cm^{-1}. The X-ray structure of the related complex $[IrCl(CO)_5]^{2+}$ shows the long M−C [2.02(2) Å] and short C−O [1.08(2) Å] distances expected from Figure 5a structure contribution.

The highest oxidation state carbonyl known is *trans*$[OsO_2(CO)_4]^{2+}$ with ν_{CO} = 2253 cm^{-1}.[4] Carbonyls with exceptionally low ν_{CO} frequencies are found for negative oxidation states (e.g., $[Ti(CO)_6]^{2-}$ ν_{CO} = 1747 cm^{-1}) or where a single CO is accompanied by non-π-acceptor ligands (e.g., $[ReCl(CO)(PMe_3)_4]$ ν_{CO} = 1820 cm^{-1}); these show short M−C and long C−O bonds.

Although Figures 5 represent three ideal structures in the bonding range possible for CO, no one structure can be said to perfectly represent the situation for any particular case. There is therefore considerable looseness in the way carbonyls are represented in organometallic structures. Often, M−CO or M−C=O are used. Whatever picture is chosen for graphical representation, the bonding picture discussed above still applies.

1.2 General considerations on metal carbonyl clusters

In 1964 Francis Albert Cotton defined metal atom cluster as "finite group of metal atoms which are held together mainly, or at least to a significant extent, by bonds between metal atoms, even though some nonmetal atoms may also be intimately associated with the cluster".[5,6] At that time, an exiguous number of compounds, which could satisfy this definition, was known and only a dozen of complexes were structurally characterized. Nowadays, it results quite difficult to suggest, even with some approximation, the number of compounds which agree with Cotton proposition. Moreover, different compound categories fitting with Cotton definition are known. During the last thirty years, the

growing interest in this field has been exponential, and the number of structurally characterized compounds is close to ten thousand. The preparation of the first carbonyl cluster, $[Fe_3(CO)_{12}]$, was performed many years ago.[7] Its molecular structure was uncertain for a long time until 1966 when, thank to the pioneer work of Larry Dahl, the nuclearity and the CO molecules distribution were definitively clarified.[8] Dahl determined many structures of carbonyl clusters, as those ones of the correlated derivatives $[Ru_3(CO)_{12}]$ and $[Os_3(CO)_{12}]$.[9] During the same period, Chini [10] and co-workers prepared on grams scale the first metal carbonyl cluster containing four metal atoms, $[Co_4(CO)_{12}]$, and then the syntheses of the analogous $[Rh_4(CO)_{12}]$ and $[Ir_4(CO)_{12}]$ were reported. In 1963 Dahl identified the real formula and the structure of the first hexametallic carbonyl cluster, $[Rh_6(CO)_{16}]$.[11]

Again in the Sixties, $[Re_3Cl_{12}]^{3-}$ was obtained, and the name cluster officially entered the chemical terminology.

At the beginning of Seventies, it was time for an explosive develop of the carbonyl cluster chemistry which has continued for more than thirty years. Nowadays, the field is so wide that an exhaustive collection of all data dealing with this issue is almost impossible.

In the last twenty years many advances have been made in the field of metal carbonyl clusters. Chemistry and Physics have as main goal the discovery how a catalytic process depends on the cluster dimension, how the metal chemistry changes with its aggregation state, how the structural, electronic, optical and magnetic properties are modulated by the cluster dimension and finally when they collimate with massive metal properties. For an organometallic Chemist some questions remain unresolved: which is the dimension of the highest nuclearity soluble cluster, which are the general rules governing the dimensions and the structures of the stable complexes and finally which is the metal nuclearity value for a cluster to show redox properties as for a massive metal.

1.2.1 Synthetic aspects of metal carbonyl clusters

Metal nanoparticles are one of the most widely studied topics, being the subject of thousands of papers every year. They play a fundamental role in both nanosciences and nanotechnology, with consequences and applications in chemistry, catalysis, optics, sensing, biology and medicine, among other.[12,13,14,15,16]

Within this framework, the interest of many scientists has moved during the years towards smaller and smaller metal nanoparticles; obtaining atomically monodisperse ultrasmall metal nanoparticles (smaller than 5 or even 3 nm) is one of the major current goals of nanochemistry.[17]

As well exemplified for Au nanoparticles, when the diameter approaches the de Broglie wavelength for conduction electrons (ca. 1 nm), the quasi-continuous electronic bands in bulk metals or large nanoparticles (ca. 5 nm) splits into discrete levels.[18] Thus, ultrasmall nanoparticles (ca. 3 nm) should display peculiar and unique physical properties. For instance, it has been demonstrated that Au nanoparticles become catalytically active in several processes when their diameter is below 5 nm, whereas above this threshold they are almost inert.[19] At the same time, within this size regime, the chemistry of ultrasmall metal nanoparticles overlaps with that of ligand-protected molecular metal clusters.[20] Actually, ultrasmall metal nanoparticles are nothing but mixtures of more or less polydisperse large molecular clusters. Alternatively, higher-nuclearity molecular clusters may be viewed as perfectly monodisperse and atomically defined metal nanoparticles. Thus, all the knowledge, experimental techniques and methods developed along the years for the preparation, purification and characterization of large molecular metal clusters may play a major role in a better understanding of ultrasmall metal nanoparticles and metal nanoparticles in general.

For instance, the general model adopted for many years for thiol-stabilised Au nanoparticles has been based on a close-packed core of Au atoms protected by an innocent shell of ligands. Then, after the structural characterisation of the molecular cluster Au_{102}(*p*-MBA)$_{44}$ (*p*-MBA = *para*mercaptobenzoic acid)[21] by means of single-crystal X-ray crystallography, a completely different model has been proposed, on the basis of icosahedral or poly-icosahedral metal cores decorated by $[Au_n(SR)_{n+1}]$– fragments (the so-called "staple motives" or "staples").[22,23,24] This point well exemplifies the great impact that molecular techniques, and X-ray crystallography in particular, may have in nanoscience chemistry. Different examples of nanometric molecular clusters are known, including semiconductor molecular nanoclusters such as $Ag_{490}S_{188}(SR)_{114}$,[25] metalloid molecular nanoclusters such as $[Al_{77}\{N(SiMe_3)_2\}_{20}]^{2-}$ [26]and $[Ga_{84}\{N\text{-}(SiMe_3)_2\}_{20}]^{4-}$,[27] as well as low-valent transition metal molecular nanoclusters such as $[Pd_{145}(PEt_3)_{30}(CO)_{60}]$.[28]

Within the last category, homoleptic molecular metal carbonyl clusters (MCCs) represent one of the most widely studied classes of molecular clusters.[20-29,30,31,32,33]

The topic of MCCs has been largely investigated throughout the 1970s and 1980s, with a marked decline in the literature during the 1990s. However, due to the recent explosion of interest in nanochemistry, there has been a gradual revival in this area over the past decade, as summarised in a few comprehensive reviews that appeared recently on the subject.[29,30]

1.2.2 Synthetic methods

Large MCCs display a rich variety of structures and even species with very similar compositions can adopt rather different geometries. This is, probably, the result of the fact that M–M interactions are not very strong and are nondirectional, as compared, for instance, to C–C bonds. Moreover, only occasionally does a given product represent a relatively deep potential well along the reaction coordinate, and therefore only supposedly minor changes in the reagents or in the experimental conditions can result in completely different products.[34] Thus, even though our knowledge on the synthesis of high-nuclearity MCCs has incredibly grown over the years, it is not yet possible to design *a priori* the preparation of a species with a predefined structure. Nonetheless, we can outline some general guidelines in order to induce the growth of MCCs. The yields of the reactions vary from case to case, but several large MCCs can nowadays be obtained in the scale of hundreds of milligrams or even grams. Experimental conditions must be carefully chosen in order to selectively obtain a single species as major product, and IR spectroscopic monitoring of the reactions were revealed to be very useful for seeking the best operative conditions. Side products may be other MCCs, small carbonyl species {e.g. $[Ni(CO)_4]$, $[Co(CO)_4]$–, $Ni(CO)_3(PPh_3)$, $[Rh(CO)_4]^-$}, bulk metals and metal salts. Purification is usually achieved on the basis of their different solubility in water and organic solvents, and, since most of the MCCs studied are anionic, further differentiation

of the solubility of the products may be achieved by using suitable tetraalkylammonium or phosphonium counterions.

The reader may notice that sometimes larger MCCs contain hydride ligands. These may arise from the solvent, from water (traces present in the solvents or added in the workup)

or may be directly added in the form of free acids. It must be remarked that hydrides in MCCs are usually slightly acidic and may thus be removed with bases or added as H^+. Further details on the syntheses are given below.

The possible methods for the preparation of large MCCs can be classified as follows: (1) direct (reductive) carbonylation; (2) thermal methods; (3) redox methods; (4) other chemically induced methods.

1.2.3 Direct reductive-carbonylation

Direct (reductive) carbonylation represents the main entry to the chemistry of metal carbonyls.[35] Actually, direct carbonylation (i.e. the reaction between a finely divided metal and CO) works only in the Ni and Fe cases, whereas all other binary metal carbonyls are obtained by reductive carbonylation (i.e. metal salt + CO + reducing agent). These reactions usually afford to the formation of low-nuclearity metal carbonyls, such as $[Ni(CO)_4]$, $[Fe(CO)_5]$, $[Cr(CO)_6]$, $[Mn_2(CO)_{10}]$, $[Ru_3(CO)_{12}]$, $[Co_2(CO)_8]$ and $[Rh_4(CO)_{12}]$, which can then be converted into higher-nuclearity species (see below).

A rather fascinating exception is represented by the reductive carbonylation of Pt(IV) salts developed by Chini and Longoni[36,37] (**Figure 22**), which operates at room temperature and ambient CO pressure. In this case, the reducing agent is CO itself under basic conditions according to the following equation:

$$CO + 2OH^- \rightarrow CO_2 + H_2O + 2e^-$$

In fact by employing methanol as solvent and CH_3COONa as weak base, Na_2PtCl_6 is quantitatively converted into the insoluble "platinum carbonyl" $Na_2[Pt_{3n}(CO)_{6n}]$ ($n \approx 10$) whose formula is based on elemental analysis. Increasing the CH_3COONa amount or using NaOH as stronger base, soluble $[Pt_{3n}(CO)_{6n}]^{2-}$ (n = 2–6) oligomers, the so-called "Chini clusters", are obtained. These clusters can also be prepared by the radiolysis of Pt salts in alcoholic media[38] or directly in water by room temperature carbonylation of M_2PtCl_6 (M = Na, K).[39] This latter procedure (operating with high yields also in the gram scale) represents a considerable simplification for the synthesis of Pt carbonyl clusters.

Moreover, by performing the carbonylation in water with different CO pressures, both $[Pt_{3n}(CO)_{6n}]^{2-}$ (n =6; 900 Torr CO) and $[Pt_{38}(CO)_{44}]^{2-}$ (760 Torr CO) can be obtained in a single step.

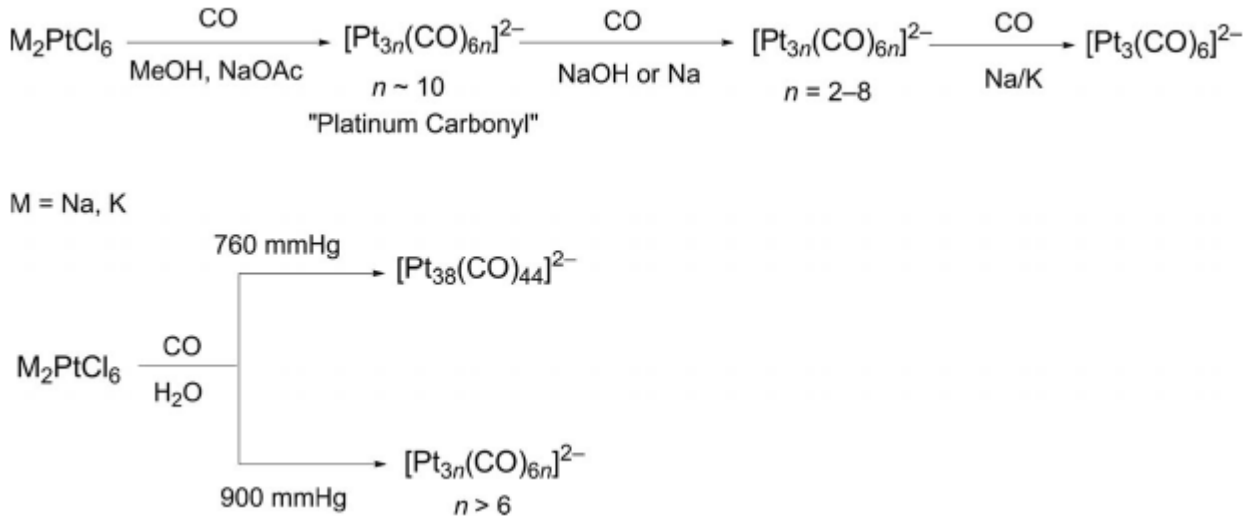

Figure 22 - Synthesis of Pt clusters by reductive carbonylation

Apart from solution procedures, reductive carbonylation can also be used in the solid state after impregnation of a suitable metal salt on supports such as metal oxides or zeolites.[40] In particular, the so-called "ship-in-a-bottle" technique has allowed the preparation of several homometallic Pt, Rh and Ir clusters, as well as heterobimetallic clusters, in the microporous cavities of zeolites.[40,41] Reductive carbonylation in the presence of PR_3 ligands has been extensively employed by Dahl and Mednikov for the preparation of phosphane-substituted Pd–CO clusters according to the following equation:[42]

$$n\mathrm{Pd(OAc)_2} + (x + n)\mathrm{CO} + y\mathrm{PR_3} + n\mathrm{H_2O} \rightarrow \mathrm{Pd}_n(\mathrm{CO})_x(\mathrm{PR_3})_y + n\mathrm{CO_2} + 2n\mathrm{HOAc}$$

1.2.4 Thermal methods

The simplest thermal reaction for the preparation of larger MCCs is based on partial decarbonylation of the precursor followed by condensation of the resulting unsaturated species with formation of new M–M bonds, as in the equation:[43]

$$3Rh_4(CO)_{12} \rightleftharpoons 2Rh_6(CO)_{16} + 4CO$$

In a few cases, removal of CO ligands from the precursor results only in an intramolecular rearrangement of the cluster cage without an increase in the metal nuclearity. For instance, thermal removal of two CO molecules from the trigonal prismatic $[Rh_6C(CO)_{15}]^{2-}$ yields the octahedral $[Rh_6C(CO)_{13}]^{2-}$ anion.[44] Recently, it was described a peculiar case in which the $[Rh_{12}Sn(CO)_{27}]^{4-}$ cluster undergoes sequential loss of two CO ligands without any major change in the icosahedral metal cage.[45]

Pyrolysis of neutral $[M_3(CO)_{12}]$ (M = Os, Ru) metal carbonyls was extensively used by Lewis and Johnson for the preparation of large MCCs (**Figure 23**).[46] Apart from decarbonylation followed by condensation to higher-nuclearity homometallic species such as $[Os_8(CO)_{23}]$, $[Os_{17}(CO)_{36}]^{2-}$ and $[Os_{20}(CO)_{40}]^{2-}$, carbido clusters, such as $[Os_8C(CO)_{21}]$, and hydrido-carbido clusters, such as $[H_2Os_7C(CO)_{19}]$, were formed after the dismutation of CO into to C and CO_2, due to the severe conditions adopted. The main drawback of thermal methods is their scarce selectivity.

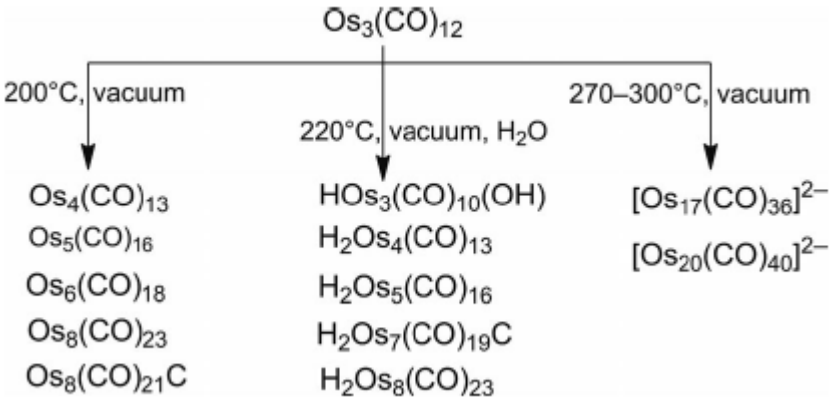

Figure 23 - Synthesis of Os clusters by thermal condensation

Nonetheless, Chini and Martinengo demonstrated that carefully monitoring the dosage of sodium hydroxide while performing the thermolysis of]$Rh_4(CO)_{12}$] under different atmospheres enables the more or less selective preparation of several high-nuclearity rhodium carbonyl clusters.[33a,33c,47] The enhancement of the anion selectivity can be nearly

quantitative, as in the preparation of $[Pt_{19}(CO)_{22}]^{4-}$ [48] and $[Pt_{15}(CO)_{19}]^{4-}$ [49] by heating appropriate mixtures of Chini clusters.

1.2.5 Redox methods

Several kinds of redox reactions (i.e. reduction, oxidation, redox condensation and disproportionation) can be used for the preparation of MCCs. In some cases MCCs are multivalent in the sense that they undergo reversible redox reactions without any major structural rearrangement. For these species, the stoichiometric addition of a reducing or oxidizing agent simply results in the formation of an isostructural cluster with increased or decreased negative charge, for example $[Ag_{13}Fe_8(CO)_{32}]^{n-}$ (n = 3–5),[50] $[Ni_{13}Sb_2(CO)_{24}]^{n-}$ (n = 2–4)[51] and $[Co_8Pt_4C(CO)_{24}]^{n-}$ (n = 1–4).[52] More often, the redox reaction is followed by irreversible processes yielding new MCCs or decomposition products. Reduction of a MCC often results in cleavage of M–M bonds as a consequence of electrons added to a metal antibonding orbital. For instance, reduction of Chini clusters $[Pt_{3n}(CO)_{6n}]^{2-}$ affords analogous species each having an n value lower than the previous one. The new product is obtained by Pt–Pt bonds breaking,[36,37] up to complete depolymerisation to $[Pt_3(CO)_6]^{2-}$ (n = 1). Alternatively, addition of reducing agents such as alkali metals can result in the replacement of a CO ligand with two negative charges with or without structural rearrangement, as in the reduction of $[Rh_{12}C_2(CO)_{25}]$ to $[Rh_{12}C_2(CO)_{24}]^{2-}$ and $[Rh_{12}C_2(CO)_{23}]^{4-}$.[53] Reduction with simultaneous CO loss can also be promoted by addition of OH^- ions; the resulting unsaturated species may undergo condensation processes to yield higher-nuclearity MCCs (**Figure 24**).

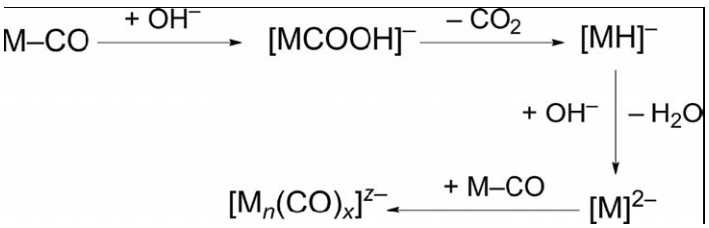

Figure 24 – Reduction-induced condensation

This approach was first developed by Hieber for the synthesis of Fe carbonyl anions after treatment of $[Fe(CO)_5]$ with bases such as NaOH or amines,[54] and then also applied to the

preparation of $[Ni_6(CO)_{12}]^{2-}$ and other Ni carbonylates starting from $[Ni(CO)_4]$.[35a,55] Oxidation of MCCs with innocent (noncoordinating) reagents, such as tropylium, tetrafluoroborate or ferricinium hexafluorophosphate, may result in the formation of new M–M bonds with or without CO loss, as in the dimerization of $[Ir_6(CO)_{15}]^{2-}$ to $[Ir_{12}(CO)_{26}]^{2}$,[56] or $[Pt_{19}(CO)_{22}]^{4-}$ to $[Pt_{38}(CO)_{44}]^{2-}$.[57] Conversely, when using coordinating oxidants such as H^+ or isolobal $[ML]^+$ fragment (M = Cu, Ag, Au; L= neutral ligand) and $[HgR]^+$, the reactions are more complex, since these reagents can act as oxidizing and/or coordinating agents. The latter process has been widely used to increase the nuclearity of clusters by stepwise addition of 1-2 eq.s of $[ML]^+$ fragments. The reaction of MCCs with metal salts or complexes can also afford heterobimetallic clusters by redox condensation (vide infra). In the case of acids, several MCCs can add H^+ ions reversibly, affording hydrido clusters. On the contrary, if the resulting hydride is not stable, it can condense to larger species with H_2 evolution, as shown in the following equation:

$$2[Rh_6C(CO)_{15}]^{2-} + 2H^+ \rightarrow [Rh_{12}C_2(CO)_{24}]^{2-} + 6CO + H_2$$

The H^+ ions necessary for these reactions can alternatively be provided by the hydrolysis of $[M(H_2O)_x]^{n+}$ ions.[58] Redox-condensation is probably the most useful procedure for the preparation of higher-nuclearity MCCs.[33a] It consists of the reaction between a reduced metal carbonyl anion and a more oxidized species, which can be another carbonyl species, a metal salt or complex, or even a main group compound. In this way homometallic, heterometallic and heteronuclear MCCs can be prepared (**Figure 25).**

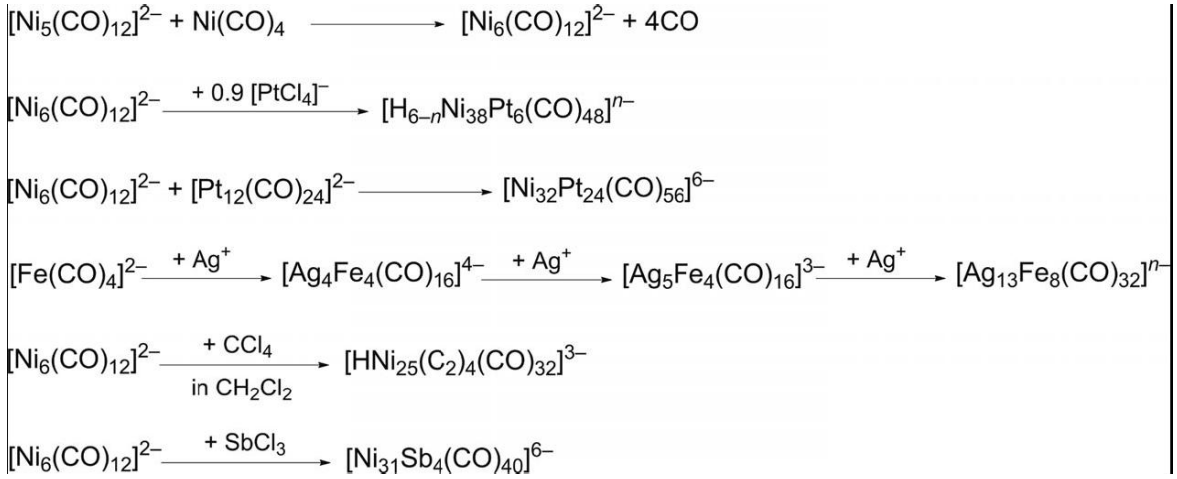

Figure 25 – Some examples of redox-condensation synthesis

Heterometallic Fe–Co, Rh–Pt, Ni–Co, Ni–Pt and so on can be easily prepared by starting from reduced carbonyls of either metal salts of the second element. Conversely, when one of the two metals does not form metal carbonyls, as, for example, in Fe–Au, Fe–Ag, Ni–Pd and Ni–Au systems, the choice of the reagents is more limited. By employing main group compounds such as CCl_4, $SbCl_3$, $SnCl_4$, $GaCl_3$ and $GeCl_4$, heteronuclear clusters such as $[Ni_9C(CO)_{17}]^{2-}$,[59] $[HNi_{25}(C_2)_4(CO)_{32}]^{3-}$,[60] $[Ni_{31}Sb_4(CO)_{40}]^{6-}$,[61] $[Rh_{12}Sn(CO)_{27}]^{4-}$,[62] $[Ni_{12}Ga(CO)_{22}]^{3-}$ [63] and $[Ni_{12}Ge(CO)_{22}]^{2-}$ [64] can be easily obtained from reduced homometallic anions such as $[Ni_6(CO)_{12}]^{2-}$ and $[Rh_7(CO)_{16}]^{3-}$. Similarly, heterobimetallic MCCs containing interstitial main group elements can be obtained by reacting a suitable heteronuclear anion with a metal salt; for example, $[Ni_{10}Rh_2C(CO)_{20}]^{2-}$ is obtained from $[Ni_9C(CO)_{17}]^{2-}$ and $[Rh(cod)Cl]_2$.[65] Inverse redox-condensation is favored in the case of neutral $[M_x(CO)_y]$ carbonyls in polar solvents. Depending on the reagents and experimental conditions, it can result in: (a) $[ML_6]^{2+}[M_a(CO)_b]^{2-}$ ionic couples, (b) isocarbonyl adducts or (c) xenophilic clusters. An example of (a) is represented by the formation of $[Fe(dmf)_6][Fe_4(CO)_{13}]$ after heating $[Fe(CO)_5]$ in dmf. Xenophilic clusters[66] contain a direct M–M bond between a metal centre in a formal negative oxidation state and a second metal in a positive oxidation state, for example $[Fe_4(CO)_8(py)_4]$[67] and $[Mn][Mn_7(thf)_6(CO)_{12}]_2$.[68]

1.2.6 Other chemically induced methods

Once formed, MCCs can be modified in several ways, and they can therefore be used for the preparation of new species. Apart from the use of acids, bases, oxidants and reducing agents that have been described above, both anionic (e.g. OH^-, I^-) and neutral (PR_3, CO, amines) nucleophiles can be employed. They can result in addition to the cluster, its degradation or even condensation to yield larger species. Nucleophilic addition, very often followed by removal of ML_x fragments, is the more usual reaction, as exemplified in the following equations:

$$[Ni_{12}Ge(CO)_{22}]^{2-} + 6CO \rightarrow [Ni_{10}Ge(CO)_{20}]^{2-} + 2Ni(CO)_4$$
$$[Ni_{38}C_6(CO)_{42}]^{6-} + 18CO \rightarrow [Ni_{32}C_6(CO)_{36}]^{6-} + 6Ni(CO)_4$$

In this way, higher-nuclearity MCCs are degraded to smaller species.[64,69]

In a few cases, nucleophilic attack promotes condensation and results in higher-nuclearity clusters instead of lower-nuclearity ones, as exemplified by the conversion of $[Ni_{10}C_2(CO)_{16}]2–$ into $[Ni_{16}(C_2)_2(CO)_{23}]^{4-}$ promoted by PPh_3,[70] the synthesis of $[Ni_{42}C_8(CO)_{44}(CdCl)]^{7-}$ after nucleophilic attack by OH^- on $[Ni_{36}C_8(CO)_{36}(Cd_2Cl_3)]^{5-}$ [71] and the CO-induced condensation of $[Ni_{10}Rh_2C(CO)_{20}]^{2-}$ to give $[Ni_6Rh_8(C_2)_2(CO)_{24}]^{4-}$.[65]

1.3 MCCs as nanocapacitors

From a formal point of view, a molecular MCC might be considered morphologically similar to a microscopic capacitor. As illustrated in **Figure 26** by the structures of $[Pt_{15}(CO)_{30}]^{2-}$ [72] and $[H_2Ni_{24}Pt_{14}(CO)_{44}]^{4-}$,[73] a MCC is generally based on a kernel of metal atoms surrounded by a shell of carbonyl ligands. Therefore, as a function of the geometry of its metal framework, it might be formally compared with either a cylindrical or spherical metal capacitor. However, apart from this morphological resemblance,

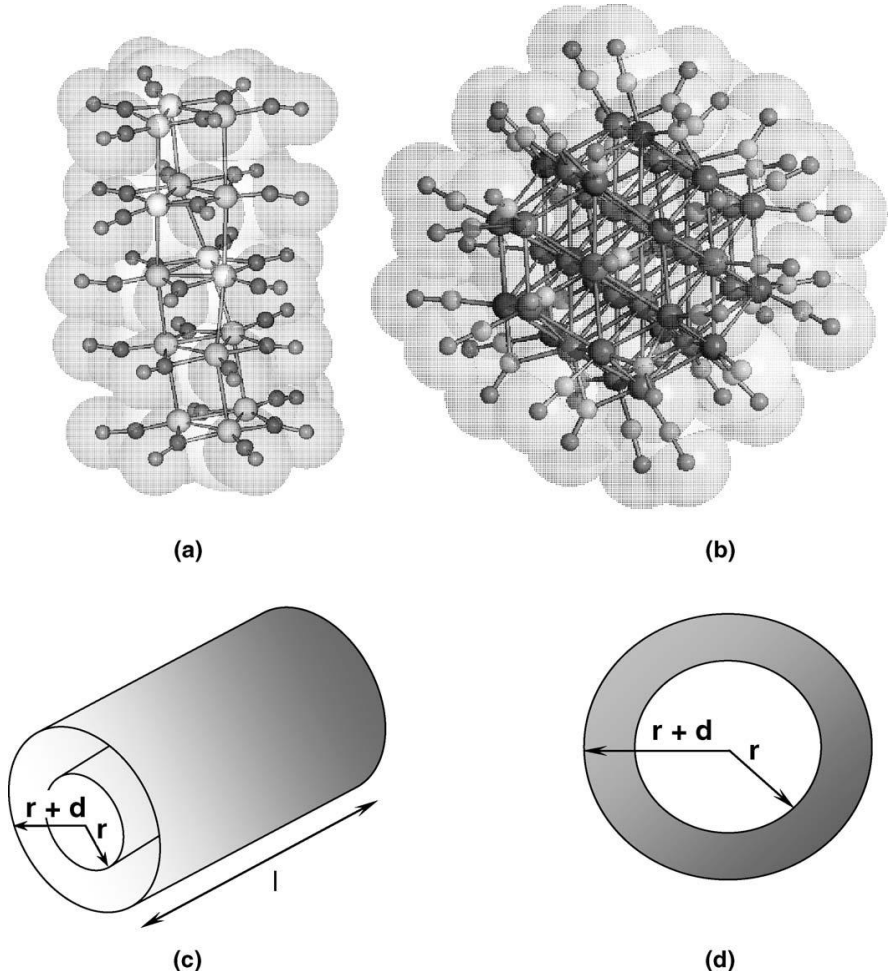

Figure 26 – Molecular structures of $[Pt_{15}(CO)_{30}]^{2-}$ (a) and $[H_2Ni_{24}Pt_{14}(CO)_{44}]^{4-}$ (b) as possible molecular counterparts of cylindrical (c) and spherical (d) capacitors, respectively.

a MCC must fulfils the following requirements:

(1) The MCC should have electron-sink behaviour (in other words, they should be able to reversibly accept and release electrons at given potentials while maintaining unaltered

their original structures. The MCC should, therefore, be multivalent or, at least, display reversible redox behaviour on the cyclic voltammetry time scale.

(2) The carbonyl ligand shell should effectively insulate the metallic core and hinder or, at least, hamper intermolecular exchange of electrons.

(3) The metallic core of the cluster should undergo transition from insulator-to-metal or be, at least, in a semiconductor regime.

(4) Finally, for practical purposes (see later), the metallic core should display dimensions falling in the nanometric field.

The capacity **C** of a molecular capacitor can be evaluated by the equation (1):

$$C = \frac{q}{\Delta E} \qquad (1)$$

where **q** is the electron charge (1.6 x 10^{-19} C) and ΔE is the potential separation of consecutive redox mono-electronic processes (V).

As calculations on some selected examples reported in Errore. L'origine riferimento non è stata trovata. show, the capacity of a metal carbonyl cluster molecule vary between 0.2 and 0.6 aF (attoFaraday, 1 aF =10^{-18} F) and grossly increases with the nuclearity and so the cluster dimension.

The capacity of a spherical metal capacitor ($C_{s.m.c.}$) depends from the radius and the thickness of the dielectric layer, according to the equation (2):

$$C_{s.m.c.} = \frac{4\pi\varepsilon_0\varepsilon\ r(r+d)}{d} \qquad (2)$$

where ε_0 is the dielectric constant in empty (8.85 x 10^{-12} F/m), ε is the dielectric constant of the isolating layer (here CO monolayer), ***r*** is the radius of the metal sphere and ***d*** is the thickness of the dielectric layer.

Analogously, the capacity of a cylindrical metal capacitor ($C_{c.m.c.}$) is given by the equation (3):

$$C_{c.m.c.} = \frac{2\pi\varepsilon_0\varepsilon\ l}{\ln[(r+d)/r]} \qquad (3)$$

Where ***l*** is the length of the cylinder.

After the calculation of the capacitor C of a cluster with equation (1), equations (2) and (3) allow to evaluate the dielectric constancy of the CO monolayer. The obtained $\varepsilon_{COmonolayer}$ is limited by the fact that a cluster is only grossly approximate to a cylinder or a sphere. The radius of the sphere which contains the whole metal core can be taken as value for ***r***, while the corresponding distances along the shortest and longest extensions in a cylindrical cluster can be taken as ***r*** and (½)***l*** respectively.

In both cases, thickness ***d*** of CO monolayer is evaluated by the equation (4):

$$d = d_{b-0} - r + r_0 \qquad (4)$$

where $d_{b\text{-}0}$ is the distance between the barycentre of the cluster and the most far oxygen atom, ***r*** is the radius of the metal core and e r_0 is the oxygen covalent radius.

Errore. L'origine riferimento non è stata trovata. reports the cited values for some selected clusters, with nuclearity between 11 and 44, which can be considered as cylindrical or spherical nanocapacitor.

$\varepsilon_{COmonolayer}$ are comprised in the quite a little range of 1.6-1.7. these values are slightly higher than the value of **ε** for gaseous carbon monoxide (1.003), liquid (ca. 1.5, calculated from its index of refraction at 78 K) and solid (1.5455 at 29.65 K).[74] Moreover, $\varepsilon_{COmonolayer}$ value is in good agreement with the dielectric constant measured for CO adsorbed on Cu and Ag surfaces.[29]

Metal carbonyl clusters	***C****(aF)*	***r****(nm)*	***d****(nm)*	***L****(nm)*	$\varepsilon_{COmonolayer}$
Cylindrical capacitors					
$[Pt_{19}(CO)_{22}]^{4-}$	*0.37*	*0.40*	*0.13*	*1.08*	*1.7*
Spherical capacitors					
$[Ni_{11}Sb_2(CO)_{18}]^{3-}$	*0.21*	*0.38*	*0.19*		*1.7*
$[HRh_{14}(CO)_{25}]^{3-}$	*0.25*	*0.47*	*0.23*		*1.6*
$[HNi_{24}Pt_{14}(CO)_{44}]^{5-}$	*0.40*	*0.57*	*0.19*		*1.6*
$[Ni_{38}Pt_6(CO)_{48}]^{6-}$	*0.57*	*0.67*	*0.19*		*1.7*

Table 1 - Capacity of cylindrical or spherical metal carbonyl clusters and dielectric constancy for the coordinated CO.

1.3.1 Electrochemistry of MCCs

A molecular cluster is defined as multivalent when it can undergo several reversible redox processes without any major structural rearrangement. It has been shown that redox properties of MCCs can be due either to ad hoc conditions or incipient metallization of the metal core. Ad hoc conditions are at the origin of the redox behavior of some low-nuclearity MCCs, which, in the absence of those conditions, are usually electron-precise and non redox- active.[29,75] Ad hoc conditions arise from the presence of a nonbonding or weakly antibonding molecular orbital (MO) within an otherwise large HOMO–LUMO gap. Usually, these electronic conditions are supported by steric protection from the ligands or the presence of interstitial main group elements reinforcing the metal cage, which hamper intermolecular reactions or fragmentation. Extended Hückel Molecular Orbital (EHMO) calculations clearly point out the presence of discrete energy levels in these clusters. As an example, the bimetallic dodecanuclear dicarbide $[Co_8Pt_4C_2(CO)_{24}]^{2-}$ undergoes one oxidation and two reduction processes, all displaying features of chemical reversibility (**Figure 27a**).

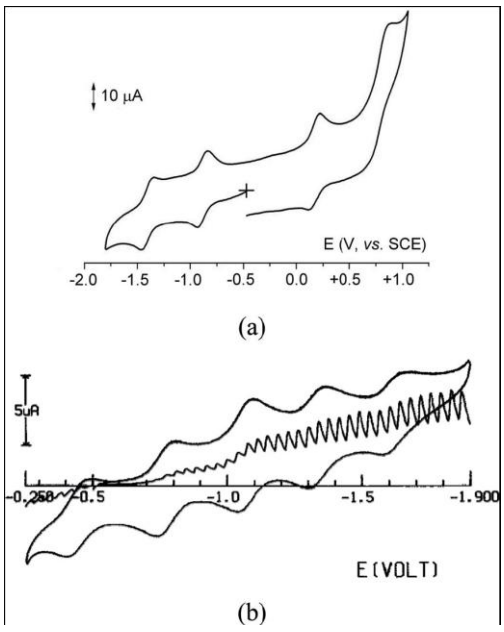

Figure 27 - Cyclic voltammetric profiles of (a) $[Co_8Pt_4C_2(CO)_{24}]^{n-}$ (n = 1–4) and (b) $[Ni_{32}C_6(CO)_{36}]^{n-}$ (n = 5–10).[52,69a]

Both of the isostructural mono and dianions have been structurally characterised.[52] As the nuclearity increases, multivalence becomes very common, and larger MCCs often display

a certain redox propensity. The structures of these large clusters usually include at least one metal atom with high connectivity, suggesting incipient metallization.[29] This is confirmed by EHMO calculations, which indicate that HOMO–LUMO gaps of high-nuclearity MCCs are considerably reduced relative to those of lower-nuclearity MCCs. Thus, larger MCCs very often display two or more reversible redox processes as a consequence of the fact that they can reversibly release or accept several electrons in their frontier orbitals. The incipient metallization of these high-nuclearity clusters is further corroborated by the fact that voltammetric profiles of the largest species display almost equally spaced redox waves, as in the case of $[Ni_{32}C_6(CO)_{36}]^{6-}$ (**Figure 27b**).[69] This means that in such high-nuclearity MCCs, the pairing energy within a single MO is very similar to the energy gap between two consecutive MOs. A systematic analysis of the electrochemical data available for several multivalent high-nuclearity MCCs has shown that the gap between the pairs of redox waves decreases as the MCC nuclearity increases and, by extrapolation, it should be almost zero at a nuclearity of approximately 70,[29] indicating that complete metallization should occur at this nuclearity. In doing this analysis, it is of paramount importance to consider the real nuclearity of the metal core and not the nominal one, which is sometimes affected by staple motives and conjuncto structures. Multivalence properties of larger MCCs makes them feasible candidates for molecular nanocapacitors, and applications can be envisioned in nanolithography and information storage.[29] In this regard, it is interesting to note that mixed Langmuir–Blodgett films consisting of an inert molecular stearic acid matrix and embedded MCCs, such as $[Pt_4(CO)_5(PEt_3)_4]$, $[Pt_5(CO)_6(PR_3)_4]$ (R=Et, Ph), $[Pt_{17}(CO)_{12}(PEt_3)_8]$ and $[Pd_{23}(CO)_{20}(PEt_3)_8]$, were prepared some years ago, and they were studied as possible high-temperature single-electron tunnelling (SET) devices.[76] More recently, a gold–cluster–gold junction has been fabricated by depositing a molecular Pt cluster on a gold surface and employing a Au STM tip.[77] With this approach, single-molecule MCCs can be electrically characterized. Multivalence may also have some important chemical consequences on the behavior of larger MCCs. For instance, we can speculate that, as the metallization limit is reached and the energy difference between consecutive redox couples approaches the order of the thermal energy, *RT*, such large MCCs should undergo spontaneous autodisproportionation equilibria in solution. Above this limit, even a single

atomically monodisperse molecular MCC would be "ionically" polydisperse, in the sense that in solution there would be a mixture of species with exactly the same size and structure but with different ionic charges. At the actual size (20–50 metal atoms), the charge of multivalent MCCs can be selected and controlled by means of chemical redox reactions or by electrochemical methods. This has allowed, in certain cases, the isolation and structural characterization of redox-related species. At the same time, complications may arise, because high-nuclearity MCCs sometimes display a polyhydride nature. Hydrides in MCCs are usually slightly acidic, and therefore hydride atoms can be added or removed by protonation–deprotonation (acid–base) reactions.[78,79] As a consequence, the charge in a molecular MCC might change as a result of a redox or acid–base reaction. By considering both multivalence and polyhydride behaviour in high-nuclearity MCCs, four cases may be distinguished: (a) MCCs with neither redox nor polyhydride nature (fixed charge); (b) multivalent MCCs without polyhydride nature; (c) polyhydride MCCs without redox properties; (d) MCCs with both multivalent and polyhydride properties. Below a nuclearity of 22–30, these four cases can be easily distinguished by ^{1}H NMR spectroscopic studies. Conversely, as discussed in the next section, larger MCCs become NMR-silent, and their polyhydride nature can thus be confirmed only by means of indirect chemical and electrochemical studies.[80,78,79]

1.3.2 Electron-sink behavior of MCCs

It is generally accepted that the metal carbonyl clusters, by adopting close shell electronic configurations, exhibit a closely perfect correspondence between cluster valence electrons (CVE) and metal cage geometry and *vice-versa*.

The rules for electron counting, developed with semi-empirical calculations,[81,82,83,84] rationalize the relationships between electron counting and metal cage geometries. Low nuclearity metal carbonyl cluster are in good agreement with electron counting rules. Anyhow, by increasing the nuclearity, significant deviations from those rules occur.

Closed shell metal carbonyl clusters feature quite poor redox behaviour,[100,85,86,87] showing not more than one reversible process.

If determined conditions are satisfied, this turns in the stabilization of sufficiently stable open shell configurations, which allows richer redox properties. This occurs when in the boundary HOMO-LUMO region one or more weakly anti-bonding or non-bonding orbitals are present. These orbitals can so be occupied or not without a deep effect on the cluster stability. These conditions may give rise to several reversible processes.[88]

As an example, the presence of one or more interstitial atoms owning to **p** group (B, C, N, Si, P, As, Bi, Sb, Sn, Ge), as in the case of $[H_{6-n}Ni_{30}C_4(CO)_{34}(CdCl)_2]^{n-}$ (n = 3–6), $[Ni_{34}C_4(CO)_{38}]^{6-}$, $[H_{5-n}Ni_{36}C_8(CO)_{36}(Cd_2Cl_3)]^{n-}$ (n=3-5) and $[HNi_{42+x}C_8(CO)_{44+x}(CdCl)]^{6-}$ makes available empty and low energy orbitals in the boundary region. Moreover, the interstitial p group atom can induce a steric pressure which promotes a metal skeleton enforcement.

It has been then proposed that the presence of an interstitial metal atom could be required for observing a reversible redox behaviour. Interstitial metal atom alters the number of cluster valence molecular orbitals (CVMO) in the HOMO-LUMO region, according to the relative energies of their valence atomic orbitals. This hypothesis is supported by the comparison among redox properties of $Ni_{12}E$-centred[89] (E = post transition element), icosahedric carbonyl clusters, $Ni_{10}E_2$ non-centred[90,91,92] and $Ni_{10}E_2$Ni-centred.[93,94]

$Ni_{12}E$-centred icosahedric clusters and $Ni_{10}E_2$ non-centred feature a conventional close-shell electron counting, showing only irreversible redox behaviour. On the contrary, $Ni_{10}E_2$Ni-centred species present an uncommon CVE number (8-10 electrons more than E-centred and non-centred clusters), being open-shell and showing a broad series of reversible redox processes.

Nowadays about eighty examples of clusters containing at least one interstitial metal atom are known.[29] Most of Co-, Ni-, Pt- and Ag centred carbonyl clusters show two to six (or more) reversible redox processes.

1.3.3 Modulation of MCCs electronic properties and tuning of their electronic potential

Chemical behavior of metal carbonyl clusters offers some opportunities for modulating the electronic properties and so redox potentials of a cluster.

Firstly, it is possible to progressively substitute π-acid carbonyl ligands with strong σ–donor ligands like phosphanes. A significant example is represented by the family cluster $[Co_{11}Te_7(CO)_{10-x}(PMe_2Ph)_x]^n$ (x=0-5; n= from +1 to -4).[95] Within such cluster series, each CO substitution by a phosphane shifts the equivalent reduction processes -Z/-(Z+1) to more negative potentials (E ≅ 200 mV). At the same time, the higher oxidation states become more stable.

A second possibility arises from the protonation of polianionic clusters, as in the case of $[H_{6-n}Ni_{30}C_4(CO)_{34}(CdCl)_2]^{n-}$ (n=3–6). The formal compensation of a negative charge with a proton in the parent polianion leads to two main effects. First, the corresponding redox processes (in terms of charge) are at a more negative potential in the hydride derivative than in the non-hydride precursor. This is due to the fact that the hydride and non-hydride derivatives with the same charge are not isoelectronic, the formers having one more valence electron. A further consequence is that hydride derivatives often feature less reductions and more oxidations than hydride species.

Strictly correlated to the protonation is the subsequent addition on polianionic clusters of $[AuPPh_3]^+$ fragments (which are isolobal to H^+), as observed for the series $[Pt_{19}(CO)_{24}(AuPPh_3\}_x]^{(4-x)-}$ (x=3, 4, *vide infra*). In this case it is observed that corresponding redox processes (in terms of charge) lie at more negative potentials for the gold-phosphane derivatives than for the parent cluster, while decomposition correlated to reductive elimination of the gold-phosphane fragment is not observed.

A third way for modulating the electronic properties and so the redox potentials of a cluster is the substitution of some surface metal atoms with others of a different transition element. As an example it is possible to cite the quasi-isostructural clusters $[Ni_{44-x}Pt_x(CO)_{48}]^{n-}$ (x=6,9).[96,97] The substitution of three nickel atoms on the surface of $[Ni_{38}Pt_6(CO)_{48}]^{6-}$, by three platinum atoms, leads to the cluster $[Ni_{35}Pt_9(CO)_{48}]^{6-}$. It has been found that the corresponding redox processes shift to more negative potentials. It is

reasonable suggest that this effect is due to a higher residual negative charge on the metal core due to a lower Pt-CO back-donation in respect to Ni-CO. At the same time, the presence of more platinum in the cluster seems to decrease the number of reversible reduction processing, promoting redox processes at more oxidized states.

1.3.4 Effectiveness of CO as insulating shielding

The importance of the second requirement highlighted at the beginning of this paragraph is based on the consideration that the intermolecular electron transfers, which are easy in solution but anyway possible in the solid state too, would hinder the efficient storage of electrons in metal carbonyl clusters. Among ionic clusters without ligands, for example fullerenide C_{60}^{n-} and their endoedric derivatives, Coulomb repulsion generates an energetic barrier to the intermolecular electron transfers. Such energetic barrier is not enough high for hindering intermolecular electron exchange in solution, which is fast in the ^{13}C-NMR timescale. In fact, mixtures of differently charged fullerenide, for example C_{60}/C_{60}^{-} and C_{60}^{2-}/C_{60}^{3-}, show a ^{13}C NMR chemical shift which is intermediate between the values of their pure anions. Moreover, intermolecular electron transfers in the solid state can not be excluded. So, a mere electrostatic repulsion could not to be really efficient in avoiding intermolecular electron transfer.

Although the effectiveness of CO as insulating agent is not completely known, EPR experiments suggest that intermolecular electron transfer among metal carbonyl clusters is not fast. In fact, EPR spectra of odd-electron clusters $[Fe_3Pt_3(CO)_{15}]^-$ and $[Ag_{13}Fe_8(CO)_{32}]^{4-}$ are not influenced by the presence of their respective even-electron congeners $[Fe_3Pt_3(CO)_{15}]^{0/2-}$ and $[Ag_{13}Fe_8(CO)_{32}]^{3-/5-}$ at any ratio and temperature, both in solution and in the solid state. It is worth to note that, due to the coupling of the unpaired electrons with ^{195}Pt and ^{107}Ag-^{109}Ag respectively, the hyperfine structure of $[Fe_3Pt_3(CO)_{15}]^-$ and $[Ag_{13}Fe_8(CO)_{32}]^{4-}$ spectrum should show a well defined profile. If intermolecular electron transfer among species with different charge were in the EPR timescale, the coupling with spin active nuclei should be influenced.

It is possible to conclude that metal core in metal carbonyl clusters behaves as a quantum dot in which electrons are confined.[98]

1.3.5 Size-induced insulator-to-metal transition of the metal core of MCCs

In order to individuate the size-value for the transition from insulator to metallic state a series from medium to high nuclearity clusters have been electrochemically analyzed: $Fe_3Pt_3(CO)_{15}]^{n-}$ (n = 0-2),[99] $[Co_8C(CO)_{18}]^{n-}$ (n = 1-4),[100] $[Ni_{11}Sb_2(CO)_{18}]^{n-}$ (n = 2-4),[101] $[Ni_{11}Bi_2(CO)_{18}]^{n-}$ (n = 2-4),[102] $[HFe_6Pd_6(CO)_{24}]^{n-}$ (n = 2-5),[103] $[Ni_{13}Sb_2(CO)_{24}]^{n-}$ (n = 2-4),[104] $[Co_{13}C_2(CO)_{24}]^{n-}$ (n = 3-6),[105] $[Ir_{14}(CO)_{27}]^{n-}$ (n = 0-2),[106] $[Pt_{19}(CO)_{22}]^{n-}$ (n = 3-7),[107] $[Ag_{13}Fe_8(CO)_{32}]^{n-}$ (n = 3-5),[108] $[Pt_{24}(CO)_{30}]^{n-}$ (n = 1-5),[109] $[Ni_{32}C_6(CO)_{36}]^{n-}$ (n = 5-10),[110] $[HNi_{38}C_6(CO)_{42}]^{n-}$ (n = 3-7),[111] $[Ni_{38}C_6(CO)_{42}]^{n-}$ (n = 5-9),[112] $[HNi_{36}P_{t4}(CO)_{45}]^{n-}$ (n = 4-7),[113] $[HNi_{38}Pt_6(CO)_{48}]^{n-}$ (n = 3-7), $[Ni_{38}Pt_6(CO)_{48}]^{n-}$ (n = 5-9).

Redox active carbonyl cluster voltammetric profiles vary as a function of the metal nuclearity. As the latter increases, consecutive redox processes progressively become almost equally spaced in potential values and more and more closer among them. [97]

Separation between consecutive redox potential (ΔE) grossly reflects the difference between consecutive ionizzation energies. So, ΔE can be used in order to approximately quantify the energetic separations between frontier energetic levels. ΔE values in low/medium nuclearity metal carbonyl clusters suggest a semiconductor behaviour instead of a conductor nature. While the carbonyl cluster grow in dimension its behaviour are closing to the massive metal and the transition from semiconductor to conductor is expected to happen.

Plotting the average separation between redox potentials of two consecutive oxidation state (*ordinate*), which is approximately proportional to the energy gap between electronic levels, versus the cluster nuclearity (*abscissa*), a value of about 65 can be estimated when the line meets the abscissa (**Figure 28**).

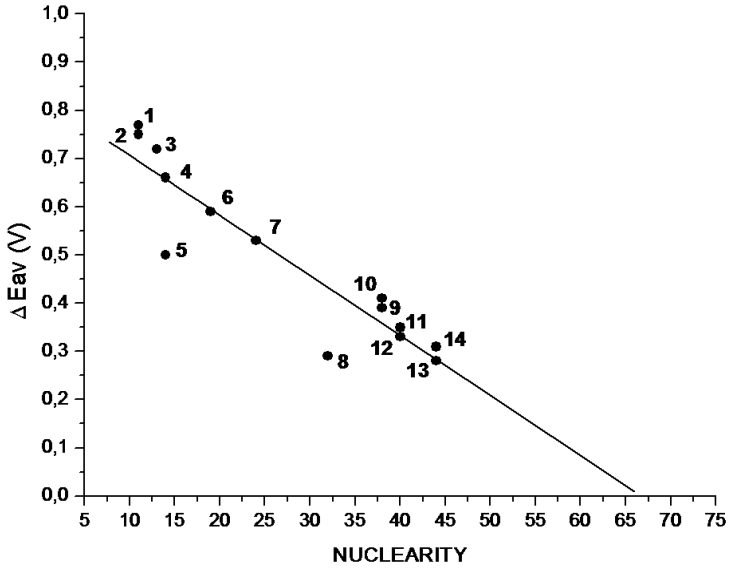

Figure 28 - Metal nuclearity *vs* ΔE_{av} of selected metal carbonyl clusters

A sixty-five atom core should turn, for a cluster, in the transition from semi-conducting to conducting behaviour, featuring metallic properties. Observing Errore. L'origine riferimento non è stata trovata.**...** graph it can be noted that the correlation coefficient is not very good as the examined clusters. Conversely, if only nickel or platinum containing clusters are considered, a correlation coefficient of about 0,996 is obtained.

1.3.6 Size of MCCs

The final requirement deals with the dimension of metal carbonyl clusters. The communication with a single molecule for transfer of a single electron could allow the storage of information in binary code at molecular level. The nanometric dimension is crucial for permitting to interact with a single molecule, instead of lot of molecules. This last requirement is satisfied by many metal carbonyl clusters reported in literature. Contrasting with metal nanoparticles, metal carbonyl clusters are monodispersed and perfectly defined in the structure. **Table 2** and **Table 3** report all the known metal carbonyl clusters with nuclearity higher than 30, both homo- and hetero-metallic up to 2009. Quasi spheric or ellipsoid clusters like $[Ni_{32}Pt_{24}(CO)_{56}]^{6-}$, $[Ni_{26}Pd_{20}(CO)_{54}]^{6-}$, $[Pd_{59}(CO)_{32}(PMe_3)_{21}]$, $[Pd_{69}(CO)_{36}(PEt_3)_{18}]$ and the triple shell giant $[Pd_{145}(CO)_x(PEt_3)_{30}]$ (x~60) feature metal core

diameters in the range of 1-2 nm.[29] In any case, the dimension look not to be a severe limitation respect to the possibility to assemble carbonyl clusters in different ways.

Table 2 -	
$[Co_{38}As_{12}(CO)_{50}]^{4-}$	$[Pd_{35}(CO)_{23}(PMe_3)_{15}]$
$[H_{6-n}Ni_{30}C_4(CO)_{34}(CdCl)_2]^{n-}$ (n=3-6)	$[Pd_{37}(CO)_{28}(P\textit{p}\text{-tolyl}_3)_{12}]$
$[H_2Ni_{30}C_4(CO)_{34}(CdI)_2]^{4-}$	$[Pd_{38}(CO)_{28}(PEt_3)_{12}]$
$[HNi_{30}C_4(CO)_{34}(CdBr)_2]^{5-}$	$[Pd_{39}(CO)_{23}(PMe_3)_{16}]$
$[Ni_{31}Sb_4(CO)_{40}]^{6-}$	$[Pd_{52}(CO)_{36}(PEt_3)_{14}]$
$[Ni_{32}C_6(CO)_{36}]^{6-}$	$[Pd_{54}(CO)_{40}(PEt_3)_{14}]$
$[H_2Ni_{32-x}C_4(CO)_{36-x}(CdBr)]^{5-}$ (x=0,22)	$[Pd_{59}(CO)_{32}(PMe_3)_{21}]$
$[HNi_{33-x}C_4(CO)_{37-x}(CdCl)]^{6-}$ (x=0,86)	$[Pd_{66}(CO)_{45}(PEt_3)_{16}]$
$[Ni_{34}C_4(CO)_{38}]^{6-}$	$[Pd_{69}(CO)_{36}(PEt_3)_{18}]$
$[HNi_{34}C_4(CO)_{38}]^{5-}$	$[Pd_{145}(CO)_{60}(PEt_3)_{30}]$
$[Ni_{35}C_4(CO)_{39}]^{6-}$	$[Pt_{31}(CO)_{40}]$
$[Ni_{36}C_8(CO)_{36}(Cd_2Cl_3)]^{5-}$	$[Pt_{35}(CO)_{40}]^{2-}$
$[HNi_{38}C_6(CO)_{42}]^{5-}$	$[Pt_{38}(CO)_{44}]^{-}$
$[Ni_{42+x}C_8(CO)_{44+x}(CdCl)]^{7-}$ (x=0,2)	$[Pt_{38}(CO)_{44}]^{2-}$
$[Pd_{30}(CO)_{26}(PEt_3)_{10}]$	$[Pt_{44}(CO)_{47}]^{4-}$
$[Pd_{34}(CO)_{24}(PEt_3)_{12}]$	$[Pt_{50}(CO)_x]^{2-}$

Table 2 - Homo-metallic carbonyl clusters with nuclearity higher than 30

Table 3 –	
$[Fe_{10}Au_{21}(CO)_{40}]^{5-}$	$[Ni_{36}Au_8(CO)_{42}]^{6-}$
$[Fe_{12}Au_{22}(CO)_{48}]^{6-}$	$[Ni_{36}Pt_4(CO)_{45}]^{6-}$
$[Fe_{14}Au_{28}(CO)_{52}]^{8-}$	$[Ni_{37}Pt_4(CO)_{46}]^{6-}$
$[Fe_{14}Au_{34}(CO)_{50}]^{8-}$	$[Ni_{38}Pt_6(CO)_{48}]^{6-}$
$[Ni_3Pd_{29}(CO)_{22}(PMe_3)_{13}]$	$[HNi_{38}Pt_6(CO)_{48}]^{5-}$
$[Ni_9Pd_{33}(CO)_{41}(PPh_3)_6]^{4-}$	$[H_2Ni_{38}Pt_6(CO)_{48}]^{4-}$
$[Ni_{14}Pd_{16}(CO)_{36}]^{4-}$	$[Ni_{32}Au_6(CO)_{44}]^{6-}$
$[Ni_{16}Pd_{16}(CO)_{40}]^{4-}$	$[Ni_{24}Ag_{16}(CO)_{40}]^{4-}$

$[Ni_{18}Pd_{24}(CO)_{42}(PPh_3)_2]^{6-}$	$[Ni_{24}Au_{16}(CO)_{40}]^{4-}$
$[Ni_{22}Pd_{20}(CO)_{46}]^{6-}$	$[(Ni_{35-x}Cu_x)(CO)_{40}]^{5-}$ (x=3)
$[Ni_{24}Pd_8(CO)_{40}]^{4-}$	$[Pd_6(Pd_{6-x}Ni_x)Ni_{20}Au_6(CO)_{44}]^{6-}$ (2<x<5,5)
$[Ni_{26}Pd_{20}(CO)_{54}]^{6-}$	$[H_{12}Pd_{28}Pt_{13}(CO)_{27}(PMe_3)(PPh_3)_{12}]$
$[Ni_{30}(Ni_{8-x}Pd_x)Pd_6(CO)_{48}]^{6-}$ (x=2)	$[Pd_{41}Au_2(CO)_{27}(PEt_3)_{15}]$
$[H_2Ni_{24}Pt_{14}(CO)_{44}]^{4-}$	$[Pd_{28}Au_4(CO)_{22}(PMe_3)_{16}]$
$[HNi_{24}Pt_{17}(CO)_{46}]^{5-}$	$[Pd_{32}Au_4(CO)_{28}(PMe_3)_{14}]$
$[Ni_{24}(Ni_{12-x}Pt_x)Pt_{20}(CO)_{56}]^{6-}$ (x=4)	$[Pt(Pd_{164-x}Pt_x)(CO)_{72}(PPh_3)_{20}]$ (x=7)
$[Ni_{24}(Ni_{14-x}Pt_x)Pt_6(CO)_{48}]^{6-}$ (x=3)	

Table 3 - Hetero-metallic carbonyl clusters with nuclearity higher than 30

The largest homoleptic MCC characterised up to now is $[Ni_{24}(Ni_{12-x}Pt_x)Pt_{20}(CO)_{56}]^{6-}$ (x=4) or $[Ni_{32}Pt_{24}(CO)_{56}]^{6-}$ (with a maximum length of ca. 2.1 nm), which already enters the domain of ultrasmall metal nanoparticles (**Figure 29**).[114]

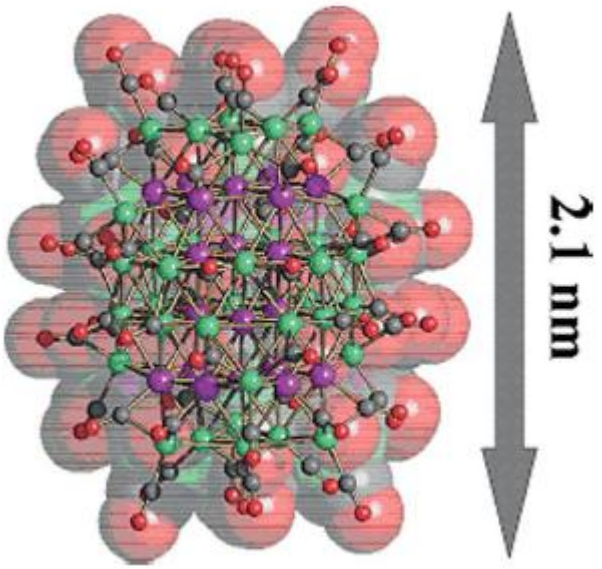

Figure 29 – Molecular structure of $[Ni_{32}Pt_{24}(CO)_{56}]^{6-}$ (Ni, green; Pt, purple; C, grey; O, red).

1.4 Assembling MCCs

Synthesis of high nuclearity clusters and molecules containing clusters with high molecular weight and well defined structure and composition is a challenge attracting continuous interest. This is stimulated both by purely academic and practical reason. The peculiar structures of transition metal cluster and their potential behavior as electronic capacitors suggest their use as versatile building block to synthesize molecular networks, macromolecules and nanomaterials in general. These materials could find application in nanoelectronic, non linear optics, sensoristic and so on.[115,116,117,118] The molecule and desired materials architecture is in principle predictable and their properties could be point up by varying the substituents of the clusters. In this context, a key role is played by polyfunctionalized bridging ligands, that can connect cluster fragments acting as spacers at the same time. Their spacer role is fundamental in determining the electronic connection (or not connection) within the network.

Bridge-linked cluster have received considerable attention for the last 15 years. Most of the structures contain various functionalized organic molecules[119,120,121,122,123] or phosphanes as linking group among metallic subunits.[124,125,126,127,128,129,130] It should be stressed that the number of complexes where three or more carbonyl clusters are linked by phosphanes are still very limited.[60,64,65,66,131] The relatively slow advances in this field are likely caused by the rarity of suitable and easily accessible ligands, that could be used in the design of supramolecular aggregates.

Anyway, functionalized 4,4'-bipyridile and related ligands can be used for the synthesis of different supramolecular organometallic complexes. Use of rigid aromatic N-donor ligands favours in most cases their complexation to positive oxidation state metal centres.[132,133,134] Non labile N-heteroaryl groups containing carbonyl clusters normally show additional metal-ligand interaction as, for example, ortometallic bond C-M[135,136,137,138] and dative bond M-N[139,140,141] or M-P.[142,143, 144,145]

So, functionalization of 4,4'-bipyridile (with the introduction of additional coordinating groups that could strongly bind to metal core) could considerably amplify coordination chemistry of these ligands.

Condensation of metal carbonyl clusters have been obtained in several ways. Some of these methods are the following:

(1) oxidation of anionic MCCs with formation of new direct homometallic M-M bonds (for example oxidation of $[Pt_6(CO)_{12}]^{2-}$ to $[Pt_{12}(CO)_{24}]^{2-}$ or to $[Pt_{18}(CO)_{36}]^{2-}$),[146]

(2) condensation of anionic MCCs with $[M']^{z+}$ (z=1-3) cations, through the complete elimination of counterion and, in some cases, carbon monoxide. This process results in the formation of heterometallic M-M'-M bonds (for example $\{Ag[Rh_6C(CO)_{15}]_2\}^{3-}$,[147] $\{Hg[Os_{10}C(CO)_{24}]_2\}^{2-}$,[148] $[M_2Ru_{12}C_2(CO)_{30}]^{2-}$ (M = Pd, Ag),[149,150] $[Pd_3Os_{18}C_2(CO)_{42}]^{2-}$,[151] and $[Ni_{12}(\mu_6\text{-}In)(\eta_2\text{-}\mu_6\text{-}In_2Br_4OH)(CO)_{22}]^{4-}$),[152]

(3) condensation of anionic MCCs with Groups 11-13 metal salts ($M'X_n$), and partial or no elimination of X counterions and formation of M-M'X_{n-1}-M or M-M'$_nX_m$-M metal heterometallic interactions (for example $[H_2Ru_{12}Cu_6Cl_2(CO)_{34}]^{2-}$,[153] $[H_4Ru_{20}Cu_6Cl_2(CO)_{48}]^{4-}$,[154] and $[Ag_3Ru_{10}C_2(CO)_{28}Cl])^{2-}$),[155]

4) condensation of anionic MCCs with Groups 11-13 metal salts ($M'X_n$), with limited or no elimination of X counter ions and formation of heterometallic M-M' interactions and M'-X-M' bridges (for example $\{Cd_2Cl_3[Ni_6(CO)_{12}]_2\}^{3-}$),[156]

5) condensation of anionic, neutral or cationic MCCs with neutral or anionic bridging ligands as diamines, diphosphanes, ditiolates, and formation of M-L-L-M bonds (for example $\{H_2N\text{–}(CH_2)_4\text{–}NH_2)\text{-}[Rh_5(CO)_{14}]_2\}^{2-}$,[157] $\{[Rh_6(CO)_{14}]_2(dpbp)\}$ and $\{[Ru_6C(CO)_{15}(dpbp)_3]Ir_4(CO)_8\}$ (dpbp=2,2'-bis(diphenylphosphano)-4,4'-bipyridine), (**Figure 30**).[158]

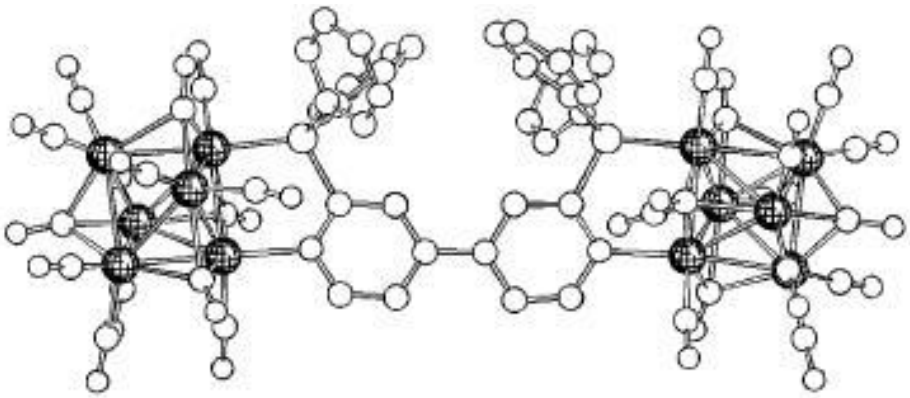

Figure 30 – Molecular structure of $\{[Ru_6C(CO)_{15}(dpbp)_3]Ir_4(CO)_8\}$ (dpbp = 2,2'- bis(diphenylphosphano)-4,4'-bipyridine)

Procedures 1-3 lead to the formation of new bigger MCCs, meaning architectures supported only (or nearly only) by M-M or M'-M metallic bonds.

Procedures 4, 5 lead to species where metal carbonyl clusters are not jointed by direct M-M or M'-M bonds but bridging ligands that could be conducting or isolating.

Predicted properties of some of these aggregates, obtained by assembling redox active MCCs, are a better electrons sink behaviour and the mixing valence. As an example, bis fullerene (C_{60}-C_{60}) shows a weak electronic communication within the space and exhibits 2 electrons reductions with a ΔEs of about 0.45V, practically equal to those ones of C_{60}.[159,160,161] On the contrary, MCC bridges in $[Rh_6(CO)_5(dppm)_2(CNCH_2Ph)(C_{60})_2]$ enormously improve communication between C_{60} groups. This species exhibits 1 electron reduction and shows a ΔEs between two consecutive redox couples decreased at 0.19-0.29V.[162] So that species, depending on the conducting behavior of the bridge, could allow studies on intramolecular electronic transfer processes between two MCC units and more.

In principle, all the procedures 1-5 can also make possible the self-assembly of a variety of 1D molecular wires. Both Physics and Chemists are fascinating by 1D and pseudo 1D materials. As this subject covers both organic, inorganic and organometallic chemistry, an impressive mole of literature is yet available.

These are some historical example:

- 1D stacked square planar d^8 coordination compounds have short M-M contacts along the axes perpendicular to the planes due to a doping (for example $K_2[Pt(CN)_4]X_{0.3} \cdot 3H_2O$),[163]
- organic molecules based compounds with almost parallel array (for example [TTF][M(dmit)$_2$] (M= Ni, Pd; dmit = 4,5-dimercapto-1,3-dityole-2-tione)[164], α-[EDTTTF][Ni(dmit)$_2$] (EDT-TTF = ethilenditiotetratia fulvalene[165]),
- compounds with mixed valence planes of donor – acceptor organic molecules as [TTF][TCNQ] (TTF = tetratiafulvalene, TCNQ= 7,7',8,8'-tetracianoquinodimetano)[166]) or [TMTSF]$_2$[ClO_4] (TMTSF = tetrametiltetraselenafulvalene),[167]
- conducting organic polymers like polyacetylene, pirrols and tiophens[168,169].

The discovery of their conducting and superconducting behavior, combined with Physics theories anticipating 1D high T_C superconductors,[170,171] have fed the interest for this research field.

An example of metallic molecular wire coming from coordination chemistry is $\{[Rh(CH_3CN)_4][BF_4]_{1.5}\}_\infty$, obtained through electro-crystallization of $[Rh_2(CH_3CN)_{10}][BF_4]_4$ on Pt electrode[172,173]. Anyway, despite the presence of an infinite sequence of alternated Rh-Rh contacts (2.84 and 2.93 Å) and mixed valence Rh centres, those molecular wires show a semiconducting behavior.[109]

1.4.1 Molecular 1D e 2D aggregates from self-assembly of MCCs

Metallic molecular wires involving positive oxidation state metal centres and CO are known for a long time. For example many halo-carbonyls like $[Ir(CO)X_3]$ (X=Cl, Br),[102] $[Rh(CO)_2(acac)]$[174] or $[Pt(CO)_2Cl_2]$[175] crystallize as an infinite stacks with a M-M 10-20% longer with respect to the massive metal. Some of them show metallic conductivity under doping.[100] A more recent example regarding M-M bonds supported by ligands is $\{[Rh_2(CF_3COO)_4][Rh_2(CF_3COO)_2(CO)_4]_2\}_\infty$.[176,177]

Metallic molecular wires based on zero or negative charged metal centres and COs are more rare. The first structurally characterized example has been $[CuCo(CO)_4]_\infty$.[178] This compound derives from the self-assembly of $[Co(CO)_4]^-$ with Cu^+ cations, that can lead both to a tetrameric cycle, $[Cu_4\{Co(CO)_4\}_4]$, and to an infinite 1D polymer, $[CuCo(CO)_4]_\infty$ showing a zig-zag chain of metal atoms, as a result of crystallization process.

The structure of a linear polymer of formula $[Ru(CO)_4]_\infty$, obtained starting from $Ru_3(CO)_{12}$,[179] has been determined by X-ray powder diffraction.

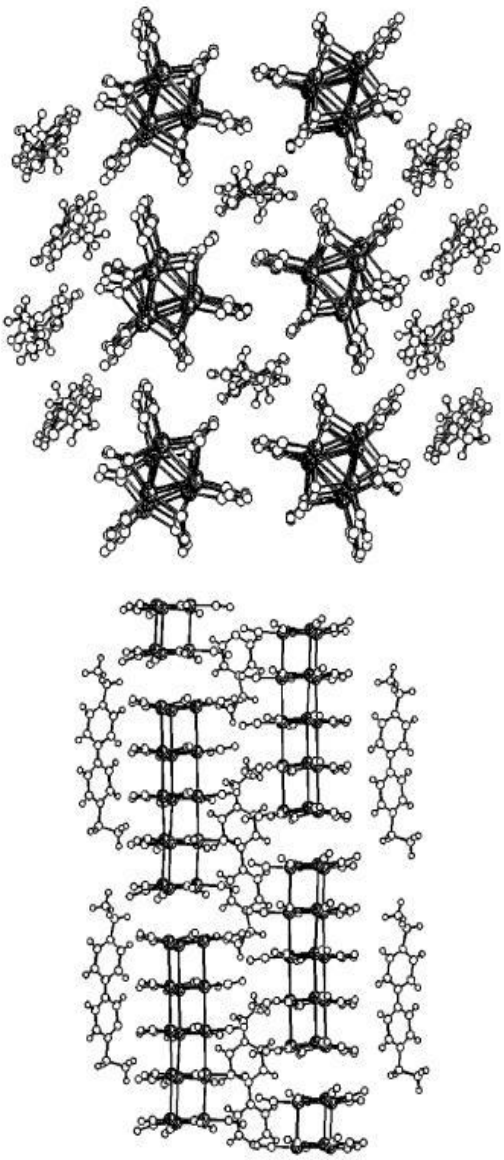

Anyhow, in 1D aggregates, the most pertinent example is the superwire $\{[AgRu_6C(CO)_{16}]^-\}_\infty$.[87] It has been obtained with quantitative yield from the reaction between $[Ru_6C(CO)_{16}]^{2-}$ cluster and Ag^+ ions. So it can be considered an example of the condensation procedure 2. The formation of infinite ruthenium cluster – silver atoms chain in crystalline phase is supposed to be favored by the suitable size of $[N(PPh_3)_2]^+$ or $[PPh_4]^+$ cations with respect to the cluster.

Both the salts are soluble in acetone, probably because polymer breaks into oligomers. The product can be re-obtained by precipitation.[87] This de-assembly and re-assembly is an important characteristic for possible future applications.

An incipient self-assembly of MCC units is shown by the salt $[NMe_4]_2[Ni_6(CO)_{12}]$.[180,181]

Figure 31 - Two images of crystal packing in $[EtV^{2+}][EtV^{\bullet+}]_2\{[Pt_{15}(CO)_{30}]^{2-}\}_2$

$[Ni_6(CO)_{12}]^{2-}$ cluster ions are stacked in ordered columns, so there is an infinite sequence of staggered and eclipsed $Ni_3(CO)_6$ groups, alternatively separated by bonding contacts of about 2.5Å and non-bonding contacts of about 4.5Å. A further evidence that not completely shielded clusters like $[M_{3n}(CO)_{6n}]^{2-}$ (M = Ni, Pt) and $[Pt_{26}(CO)_{32}]^{2-}$ can aggregate into oligomers containing up to twenty or thirty units come from mass spectroscopy.[182]

Longoni and co-workers have first suggested the use of redox active and not coordinating dications to build up inorganic polymers. Remarkable examples are 4,4′-bipyridils dications (viologens),[183] showing a formal redox potential comparable with MCC and tunable by changing 1,1′ substituents. $[PPh_4]_2[Pt_{3n}(CO)_{6n}]$ metathesis with 4,4′-diethyl-

bipyridile (EtV^{2+}) leads to the formation of mixed salt $[EtV^{2+}][EtV^{\bullet+}]_2\{[Pt_{15}(CO)_{30}]^{2-}\}_2$, containing both initial EtV^{2+} and monocationic radical $EtV^{\bullet+}$.[184] Two images of the crystal packing of $[EtV^{2+}][EtV^{\bullet+}]_2\{[Pt_{15}(CO)_{30}]^{2-}\}_2$ are shown in **Figure 31**.

The two different diethylviologen dications are clearly distinguishable for their frequence in the structure and because EtV^{2+} is bent, while $EtV^{\bullet+}$ is nearly planar. The most interesting feature of this structure is that dianionic groups $[Pt_{15}(CO)_{30}]^{2-}$, although maintaining their molecular identity, are assembled into infinite columns. Inside each molecular ion, distance between $Pt_3(CO)_6$ planes is slightly lower than 3.1Å, whereas intermolecular distance (circa 3.9Å) is shorter than in $[NMe_4]_2[Ni_6(CO)_{12}]$ (4.5 ° Å) and near to the double of usually van der Waals radius usual for platinum(0).

1.5 Magnetic properties of homo- and hetero-leptic metal clusters

Odd-electron MCCs displaying one or more unpaired electrons are paramagnetic species, as confirmed experimentally in several cases.[29] A notable case is $[Ag_{13}Fe_8(CO)_{32}]^{4-}$,[50] where coupling of the unpaired electron in its ESR spectrum with the different Ag atoms of the centred Ag_{13} cube-octahedral cage allowed an experimental mapping of electron density within the cluster by performing "experimental quantum mechanics" as originally envisioned by Dahl. Conversely, the magnetic behavior of even-electron MCCs is rather controversial.[185]The appearance of a temperature-dependent (Curie) paramagnetism resulting from quantum size effects was predicted as soon as the HOMO–LUMO gap was reduced to values close to kT.[186] In this sense, magnetic measurements might be helpful to unravel metallization of the metal core of the cluster. Magnetism was first discovered in osmium carbonyl clusters,[187] and then followed by studies of magnetism in other MCCs, both by EPR spectroscopy[188] and magnetic susceptibility measurements.[185,189] Microcrystalline samples of several homometallic carbonyl clusters of Ru, Os, Ni, Pt, as well as bimetallic Ni–Pt carbonyl clusters[185,188,189] revealed weak Curie-type temperature-dependent paramagnetism (TDP) corresponding to magnetic moments in the range of 0.1–4 μ_B (Bohr magnetons) per cluster ion, in some cases also associated with a van Vleck temperature-independent paramagnetism (TIP), which was found to increase with cluster size.

However, SQUID measurements on a single crystal of $[HNi_{38}Pt_6(CO)_{48}]^{5-}$ failed to confirm the Curie-type TDP.[190] Moreover, combined magnetic susceptibility and EPR spectroscopic studies on single crystals of $[Fe_3Pt_3(CO)_{15}]^{2-}$ and $[Ag_{13}Fe_8(CO)_{32}]^{3-}$ salts unambiguously showed that their TDP was due to impurities of the oxidized and reduced $[Fe_3Pt_3(CO)_{15}]^{-\cdot}$ and $[Ag_{13}Fe_8(CO)_{32}]^{4-\cdot}$ species, respectively. This finding emphasized the necessity to investigate such behavior by at least two complementary techniques.[191] Furthermore, DFT calculations on optimized model structures of highest-nuclearity Ni and Ni–Pt carbonyl clusters suggested that the surface carbonyl ligands should completely quench the magnetic moments of their corresponding bare metal kernels.[192] The above experimental and theoretical observations led to the conclusion that TDP, as well as TIP, of even-electron MCCs systematically arises from adventitious contamination with odd-electron species or the presence of unidentified magnetic impurities. Consequently, studies aimed at proving that large MCCs could feature progressively vanishing HOMO–LUMO gaps and high-spin ground states as a function of size came to a rest for a while.

A somehow related controversy regarding the magnetic properties of ligand-stabilized gold nanoparticles and thiolated gold surfaces or thin films was raised later in the literature.[193] Assessment of the intrinsic magnetic properties of gold nanoparticles, rather than molecular MCCs, would be further complicated by their non molecular nature and ill-defined composition and structure. As for electrochemical properties, the magnetic behavior of even-electron MCCs may arise either from ad hoc conditions, stabilizing two or more almost degenerate MOs, or from incipient metallization of the metal core, reducing the energy gap of MOs to close to kT. For instance, recent DFT calculations suggested that even low-nuclearity MCCs such as $[Fe_6Ni_6N_2(CO)_{24}]^{n-}$ (n =2, 4),[194] $[Co_{11}RhN_2(CO)_{24}]^{2-}$ and $[Co_{10}Rh_2N_2(CO)_{24}]^{2-}$ [195] could feature a triplet ground state, which was partially substantiated in the latter by EPR spectroscopic studies, as a result of the stabilizing effect of the interstitial nitrogen atoms (ad hoc condition). This point was further corroborated by joined structural, NMR spectroscopic, electrochemical, variable-temperature EPR spectroscopic and SQUID studies on the structurally related dicarbides $[Co_8Pt_4C_2(CO)_{24}]^{n-}$ (n = 1,2) (**Figure 32**).[52]

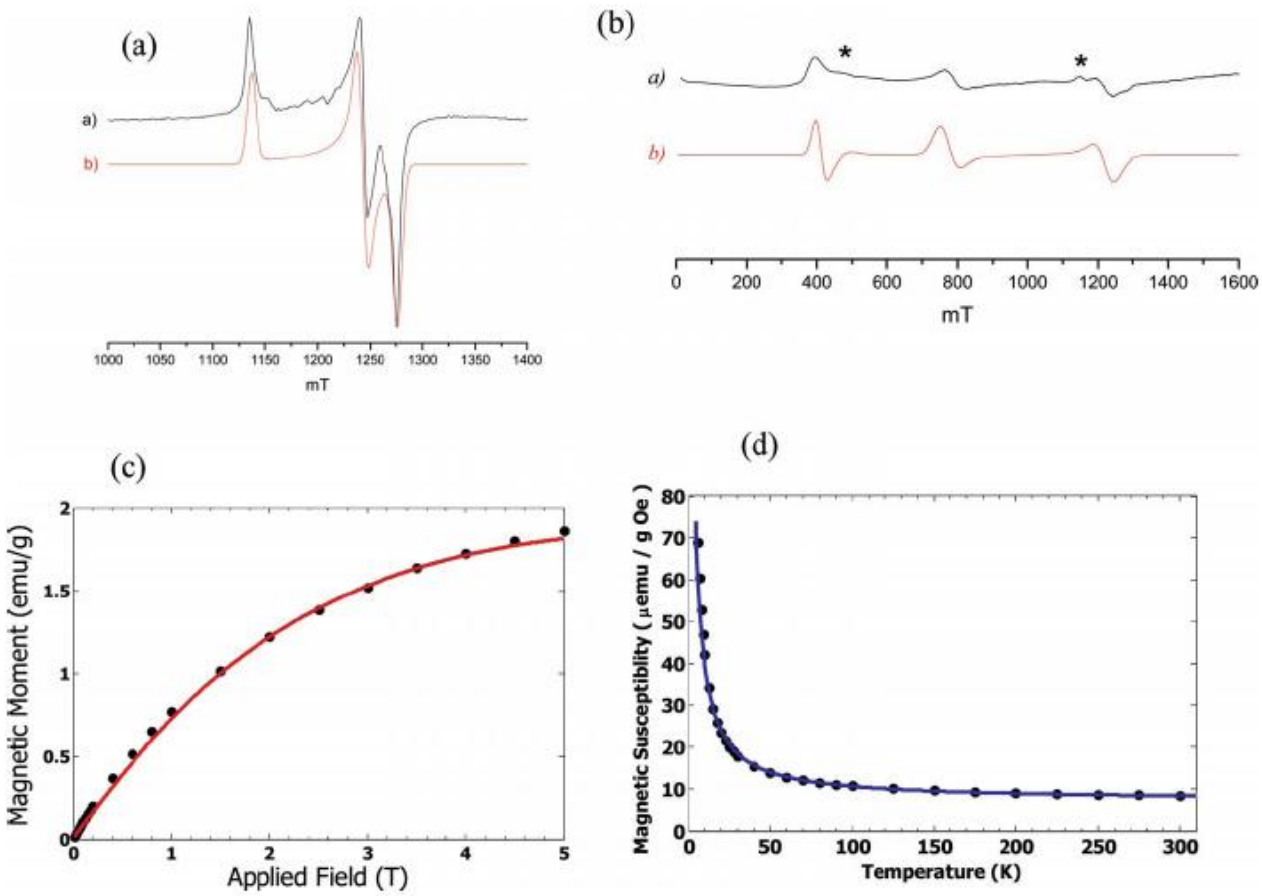

Figure 32 - EPR spectra of solid $[Co_8Pt_4C_2(CO)_{24}]^{n-}$ at 5 K: (a) $n = 1$, $S = 1/2$; (b) $n = 2$, $S = 1$ (* background impurity). (c) First magnetisation curve and (d) temperature dependence of magnetisation of $[Co_8Pt_4C_2(CO)_{24}]^{2-}$.[52]

The paramagnetism of the odd-electron monoanion ($n = 1$) is due to the presence of one unpaired electron in the SOMO, resulting in a doublet state ($S = 1/2$). Conversely, the paramagnetic behaviour displayed by the even-electron species $[Co_8Pt_4C_2(CO)_{24}]^{2-}$ arises from triplet states ($S = 1$), as indisputably pointed out by its EPR spectrum. These examples of intrinsic magnetism of an even-electron MCC may support the authenticity of some previously ascertained magnetic behavior found in highest-nuclearity MCCs and in gold colloidal particles. At the same time, it points out that magnetic data on larger molecules must be carefully considered and cross-checked with at least two independent techniques. This applies to $[Ni_{16}Pd_{16}(CO)_{40}]^{4-}$, whose magnetism has been confirmed by both SQUID magnetometry and muon spin rotation/relaxation (μSR) spectroscopy.[196] The susceptibility measurements show an exceptionally high magnetic moment corresponding

to a total spin value of $J = 2$, suggesting a Hund filling of a quadruplet ground state and indicating incipient metallization of the metal core of the cluster, as also confirmed by EHMO calculations. It may be conjectured that a progressive tightening of the frontier energy levels by further increasing the size of the cluster could trigger magnetism in an increasing number of MCCs, regardless of even or odd numbers of electrons.

Novel magnetic behavior could be at hand, since the unpaired electrons reside in molecular orbitals delocalized over most atoms of the molecule, rather than being localized in atomic orbitals, as for polynuclear compounds.[29,52,196] The development of electronic and magnetic properties in MCCs make them candidates for applications in nanosciences and nanotechnologies as molecular nanocapacitors, superparamagnetic quantum dots and nanomagnets,[29] as well as precursors of narrowly dispersed magnetic alloy and metal oxide nanoparticles of corresponding composition.[197]

1.6 Analytical techniques

Several techniques are used for characterizing metal carbonyl cluster and more generally organometallic compounds. Among these we can enumerate:

1) Nuclear Magnetic Resonance (NMR)
2) Electron Spin Resonance (ESR)
3) Infrared Spectroscopy
4) Microwave Spectroscopy on small molecules in the gaseous state
5) X-ray and Neutron single crystal Diffraction
6) X-ray Powder Diffraction
7) Mass Spectroscopy
8) Electrochemical Techniques
9) UV-Vis Spectroscopy
10) SQUID Magnetometry

Usually the identification of a novel organometallic compound requires for the contemporaneous use of almost all these techniques, even if the most common ones are NMR and IR.

A definitive evidence on the structure of a metal carbonyl cluster is necessarily obtained by X-ray diffraction analysis on single crystal accompanied by elemental analysis.

X-ray diffraction is truly powerful tool which is able to clarify the interaction among atoms, their reciprocal bond distances and angles. Anyhow, X-ray does not provide for information about dynamic behaviour of molecules in solution and it requires for the use of single crystals, which are sometimes really difficult to obtain.

Neutron diffraction is useful when hydrogen atom has to specifically localize in a crystal structure. For a standard experiment, larger crystals than those used for X-ray diffraction are required. Moreover few laboratories around the world are able to conduct such a kind of experiment.

Electrochemical studies and UV-Vis spectra are useful for specific applications, even if these techniques are not systematically applied for the identification of new complexes.

Mass spectroscopy is a very important technique for the determination of molecular weight of an organometallic compound and the knowledge of the fragmentation process can contribute in the assignment of the structure to a new compound.

Detailed information about the molecular structure can be obtained by NMR spectroscopy. Since the primordial of this spectroscopy enormous advances have been done and nowadays high field (usually 300-600 MHz) multinuclear NMR are available.

Finally infrared spectrophotometer are available since long time due to their constructive simplicity and the relatively cheapness.

1.6.1 Isolation

The characterization of a metal carbonyl cluster starts with its isolation as a pure compound. Isolation and separation methods resemble organic chemistry ones. Most of carbonyl complexes are non-volatile microcrystalline solids, even if some of them, in standard conditions, are liquid, like as $[CH_3C_5H_4Mn(CO)_3]$ and $[Fe(CO)_5]$, or easily vaporizable substances like $[Ni(CO)_4]$. Metal carbonyl clusters usually feature solubility similar to that of organic derivatives. Neutral species can be soluble in aromatic or halogenated solvents, in tetrahydrofurane (THF) and acetone, while anionic clusters are soluble in THF, acetone and acetonitrile.

Unlike organic compounds, the majority of metal carbonyl clusters are air sensible, being reactive with oxygen and moisture. Usually crystalline material is more stable than its solution but in most cases both solid and solutions are manipulated under inert atmosphere (nitrogen, argon) or carbon monoxide by standard Schlenk techniques.

Metal carbonyl clusters are neutral or anionic species and bulky organic salts, often alkyl/aryl ammonium or phosphonium, are used as counter ions. Both in solutions and in the solid state very low interactions exists among anionic clusters and cations. Although usually the structure, spectroscopic properties and the reactivity of the cluster do not depend from the cation nature, some examples are known which contradict this statement. For example $[Rh_{11}(CO)_{23}]^{3-}$ obtained as tetramethylammonium salt has been isolated in two pseudo-isomeric forms which differ in the CO distribution. This different CO distribution is due to the clathrated solvent molecules, which is acetone in one case and toluene in another. A second example is $[Ir_4(CO)_{11}(SCN)]^-$: again it has been found a different distribution of the CO ligands: the first one shows the usual distribution found in the substitution products of $[Ir_4(CO)_{12}]$ while the second one only contains terminally coordinated ligands. This different distribution is due to the counter ions, which are $[N(PPh_3)_2]^+$ in the first case and $[N(CH_3)_2(CH_2C_6H_5)_2]^+$ in the second case.
Sometimes, the cation plays a key role in modifying the salt solubility and so its solution equilibrium. The proper choice of the cation can often modify the crystal packing, contributing to the stabilization of the compound in the solid state when X-ray irradiated.

1.6.2 Infrared Spectroscopy

Infrared spectroscopy is a fast, sensible technique, suitable for metal carbonyl investigation since few other bonds adsorb in this region. ν(CO) stretching bands are usually sharp and intense, lying in 2150-1550 cm^{-1}. Such wide window is correlated to the nature of M-CO bond, which is influenced by:

i. the cluster charge,
ii. the nature of the metal to which CO is coordinated,
iii. the presence of other ligands,
iv. the coordination mode adopted by CO.

CO stretching band intensity depend from the square of the M-CO dipole variation. Dipole variation can be induced both by bond polarity and by changes in the electronic structure of the bond.

Regarding to carbon monoxide and metal carbonyls, CO bond polarity is weak. So the high intensity of ν(CO) bands is due to the nature of M-CO bond, which gives rise to significant variations on the electronic structure, apart from a change in the carbon oxygen distance. C-O vibration width is about 6 pm for the first excited vibrational state. This results into a decrease of 2π orbital energy of 20000 cm^{-1}. Moreover M←CO back-bonding donation is increased and the electronic distribution in the M-C≡O system is varied. These facts account for the value of the oscillating dipole and the high intensity of CO stretching bands. Sometimes these intensities are weak or even forbidden, if oscillating dipoles of particular CO groups are directed one upon the other. Bands attributable to

M-C vibration are weaker than CO vibration but generally stronger than δ(MCO). So, M-C bond length variations are less affected by M-C bond character than C-O distance changes. The most useful application of IR spectroscopy in the investigation of metal carbonyl cluster chemistry is the monitoring of a reaction proceed.

This operation can be conducted classically, by sampling and collecting the IR spectrum or, by using optical fibres joined to a spectrophotometer and poured in the reacting solution, it is possible to constantly monitoring the reaction.

1.6.3 Nuclear Magnetic Resonance (NMR)

Nuclear Magnetic Resonance (NMR) is the most versatile technique for the determination of molecular structures in solution. NMR provides with information about the atom connectivity (through the chemical shift, δ), the relative number of equal nuclei (through peak integer) and the presence of near groups (through the coupling constancies).

Many magnetically active nuclei are conveniently used in organometallic chemistry, particularly for studying the species in the solution.

1.6.3.1 Dynamic Varied Temperature NMR Spectroscopy

NMR timescale is intrinsically long, typically 10^{-4} s, while for example IR spectroscopy occurs 10^{-13} s. This fact is useful as many dynamic processes are faster than NMR timescale and the observed signal is an average peak which accounts for ligands exchanges. This phenomenon is exploited in Varied Temperature NMR experiments. The sample is cooled until the dynamic process becomes slower than NMR timescale, Different exchange processes, especially in the case of carbonyl scrambling and hydride migration around the metal cage, can be observed. A detailed analysis on half-height peak broadness can provide with an estimation of the energies involved during fluxional process.

Organic ligands too can undergo to dynamic process. For example, ^{1}H-NMR of $[Os_3(CO)_8(\mu^3\text{-}C_6H_6)(\eta^2\text{-}C_2H_4)]$ at -85°C shows ten resonances, meaning that each proton has a unique environment and the ligands are not fluxional.

Many carbonyl compounds feature less NMR resonances than the expected ones on the basis of their static structure. This is usual because molecule are not rigid and the observing nuclei are exchanging their position faster than the NMR timescale. Sometimes the exchange occurs at a velocity which is comparable with the timescale. In these cases, it is possible to cool down the sample until raising a static spectrum.

1.6.3.2 ^{13}C NMR spectroscopy

Terminal COs show resonances between +160 ppm and +250 ppm, while edge-bridged and triple bridged COs typically fall at higher frequencies. If a metal carbonyl cluster contains all these coordinated COs, then the resonance sequence CO_t, μ-CO, μ_3-CO can be observed. A carbide C atom, namely completely incapsulated in the metal cage falls at higher frequencies than COs, typically its resonance is found between +250 ppm and +400 ppm. Usually ^{13}CO enrichment of the sample is required in order to get sufficiently intense peaks.

CO scrambling is a typical example of fluxionality, a phenomenon which occurs whenever a molecules has a number of accessible structures separated by relatively low energy barriers. The CO coordination mode varies during the exchange: for example a fluxional process can convert a terminal CO into a edge bridging or triple bridging CO and during

this process metal centres do not gain or loose electrons. As a CO donates two electrons independently on its coordination mode, this concerted migration does not require for additional electrons by the ligand.

1.6.3.3 Multinuclear NMR spectroscopy

Besides ^{1}H and ^{13}C, other nuclei can be investigated through NMR spectroscopy. For example, P-containing ligands can be easily characterized as ^{31}P nucleus has:

i. Natural abundance = 100%,
ii. Sensivity = 0,06,
iii. Nuclear spin = ½

These characteristics make easy and fast the collection of a spectrum. So, reactions of species containing P-ligands can be followed through ^{31}P NMR spectroscopy.

Other NMR-active nuclei are ^{10}B, ^{11}B, ^{14}N, ^{15}N, ^{19}F and ^{29}Si which are often found in organometallic ligands. Metallic elements which have provided good NMR spectra are ^{103}Rh, ^{183}W, ^{187}Os and ^{195}Pt. NMR spectroscopy has been used to demonstrate that in some cases the metallic core is fluxional.

The first study toward this direction has dealt with the behavior of the oligomeric series $[Pt_n(CO)_{2n}]^{2-}$ (n = 3, 6, 9, 12, 15) in solution.[198] ^{195}Pt-NMR spectra are very complicated especially by considering Pt_{12} and Pt_{15} clusters. This complexity is due to the presence of isotopomers which are reported in **Figure 33** in the case of a triangular platinum unit.

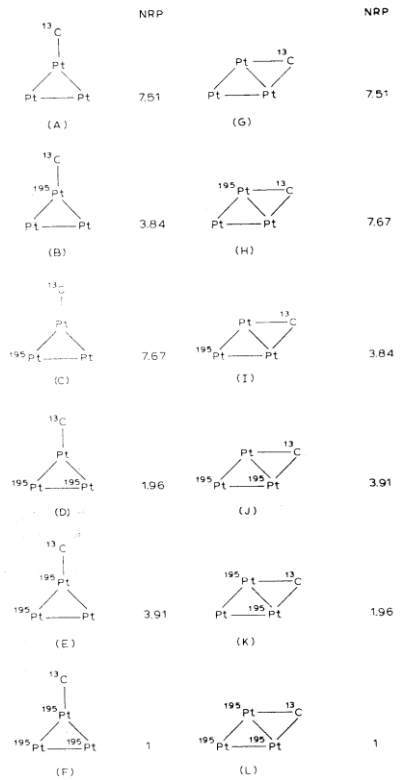

Figure 33 - Isotopomers of $[^{195}Pt_zPt_{3-z}(^{13}CO)(^{12}CO)_5]$ (z = 0-3)

^{195}Pt-NMR studies carried out over a broad range of temperatures have given the following conclusions:

i. There is an intra-molecular Pt_3 triangles rotation about the main axis
ii. There is an inter-molecular Pt_3 triangle exchange between anions
iii. There is not exchange between terminal and edge-bridging COs in the triangular unit $[Pt_3(CO)_6]$
iv. The above described processes occur within a determined range of temperatures.

1.6.4 X-ray crystallography

X-ray crystallography has contributed more than any other analytical technique in the characterization and study of metal carbonyl cluster. The possibility, provided by crystallography, of giving detailed structural information has allowed the characterization of many metal cage and the individuation of uncommon coordination modes.

X-ray crystallography is so the most effective method for the determination of solid structure.

1.6.4.1 X-ray structure representation

Representation of X-ray structures can be variable. The conventional stick-and-ball style uses spheres whose radius are proportional to the element atomic weight. Space filling style shows van der Waals radius of each atom and is useful for emphasizing the topography of the molecule outer sphere. For example, stick-and-ball model of $[Fe_5C(CO)_{15}]$ seems to suggest that the carbide atom is quite exposed, **Figure 34**.

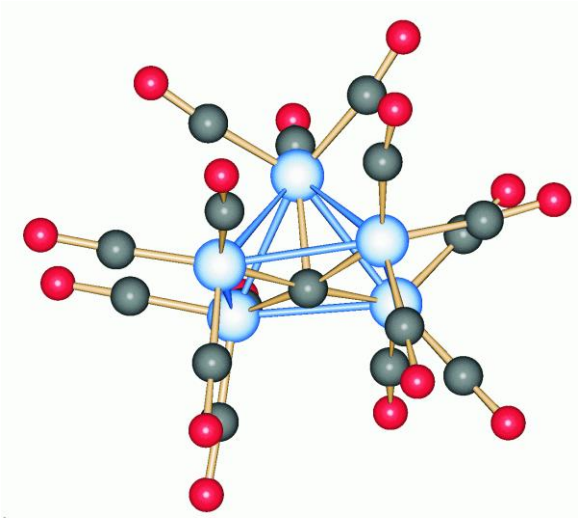

Figure 34 – Molecular structure (stick-and-ball model) of $[Fe_5C(CO)_{15}]$

Actually space filling model clearly shows that carbide atom is well protected by CO ligands, **Figure 35**.

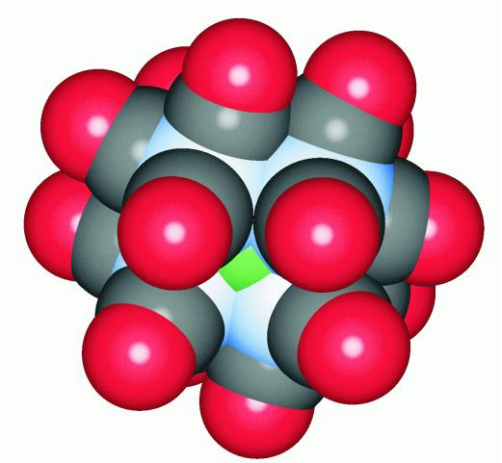

Figure 35 – Molecular structure (space filling model) of $[Fe_5C(CO)_{15}]$

Atoms can be then drawn as ellipsoids and this shape is the best representation of the actual electron density distribution of the atom. Thermal ellipsoids show atom vibrations: as atom vibration turns into a longer shifting than a stretching deformation, ellipsoid are rarely spherical. Edge-bridged COs have larger thermal ellipsoids and this is due to the pronounced ligand moving, **Figure 36**.

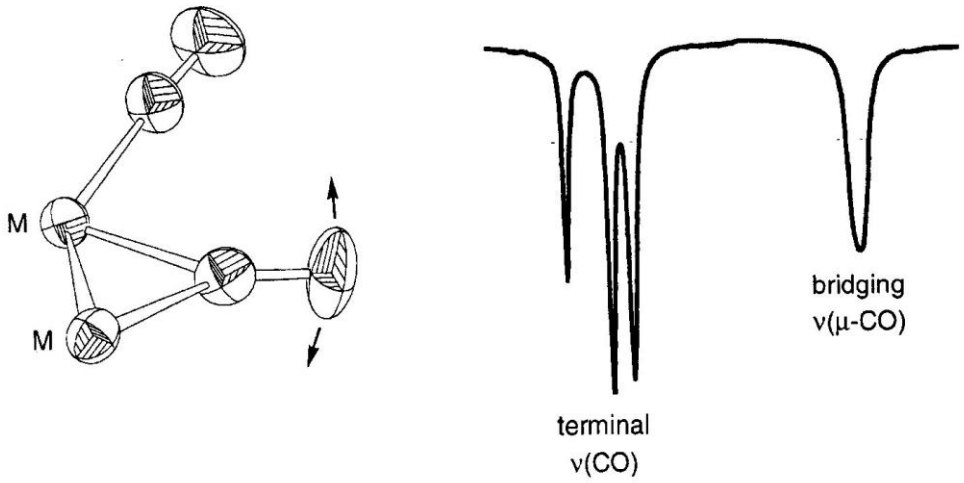

Figure 36 - Different thermal ellipsoids give rise to different band broadness

This phenomenon has been used to justify why infrared ν(CO) bands of edge-bridging COs are significantly broader than terminal bridging COs.

1.6.4.2 Disorder

Disorder arises from a casual distribution of a single atom or a group of atoms in two or more sites of the unit cell and it causes an important problem for crystallographers.
Static disorder leads to an average structure which includes fractions of atoms. A typical example is represented by $[Fe_3(CO)_{12}]$ structure where the iron atom triangle, shelled by a distorted icosahedron constituted by CO ligands, is disordered about two sites in a star of David-like pattern. The structure of $[Fe_3(CO)_{12}]$ together with the non disordered structure of $[Ru_3(CO)_{12}]$ are shown in **Figure 37a** and **b.**

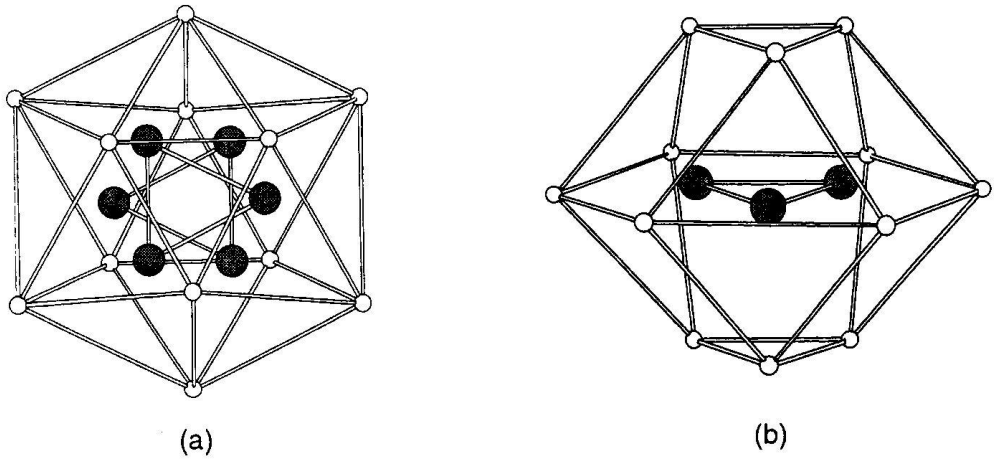

Figure 37 – Structural: a) disorder in $[Fe_3(CO_{12}]$ and b) order in $[Ru_3(CO_{12}]$

Another kind of static disorder is the substitution disorder where different atoms can be found place in some sites in any ratio. A worth example of bimetallic substitution which turns into disorder in some crystallographic sites is represented by the high nuclearity metal carbonyl cluster $[Au_6Pd_6(Pd_{6-x}Ni_x)Ni_{20}(CO)_{44}]^{6-}$. Its XRD structure was determined starting from seven different crystals and always six sites have been found occupied both by nickel and palladium. The x value of $Pd_{6-x}Ni_x$ is in between from 2,1 (65 % Pd, 35 % Ni) and 5,5 (8 % Pd, 92 % Ni).

Dynamic disorder is slightly a different phenomenon and it involves the quick rotation of part of a structure in the solid state. By collecting the structure at low temperature, this motion can be stopped, decreasing the disorder.

1.7 Voltammetric techniques

1.7.1 Cyclic voltammetry

Redox activity of any chemical species can be investigated by cyclic voltammetry. By this techniques it is possible to measure the current passing through an electrochemical cell by varying the voltage applied to a working electrode (versus an unpolarizable referring electrode) as a function of times. After a determined time, the potential is inverted. By doing this, the electronic transfer products, induced by the first scanning, can be analyzed

during the returning scanning. The shape of the potential-time impulse is shown in **Figure 38**.

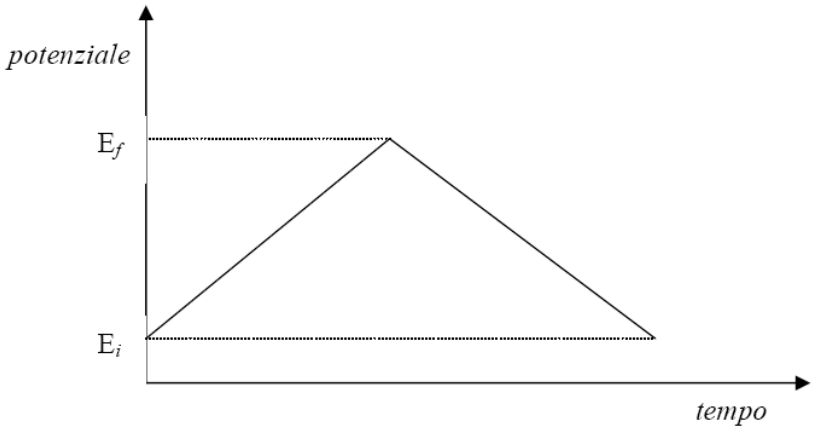

Figure 38 - Potential-time profile in cyclic voltammetry.

The curves obtained by reporting the current as a function of the applied potential are defined cyclic voltammogram. These curves not only reveal the redox potential of the process, but also allow the individuation of possible chemical complications accompanying the electronic transfer, as their shape is function of the potential scan rate. In the voltammetric analysis scanning rates are usually varied between 0.02 V/s and 50 V/s.

So cyclic voltammetry is able to offer information about the electrochemical potential, about the presence, or not, of chemical reactions occurring before or after the electron transfer and, finally about the kinetic of these complications.

1.7.1.1 Reversible processes

In the case of a reversible charge transfer, the cyclic voltammetry experiment can be described as followed. If it is supposed to have a chemical species which is able to assume two different and stable oxidation states (Ox and Red one), the reaction undergoing at the electrode can be schematized as:

$$Ox + ne^- \rightleftharpoons Red$$

At the starting point, only the Ox species is present in solution. Starting from a more positive potential than the formal E°′ potential of the ox/red couple (which generally corresponds to the standard E° potential) and scanning with a certain rate towards more negative potential, a curve like one reported in **Figure 39** (ABC) can be expected.

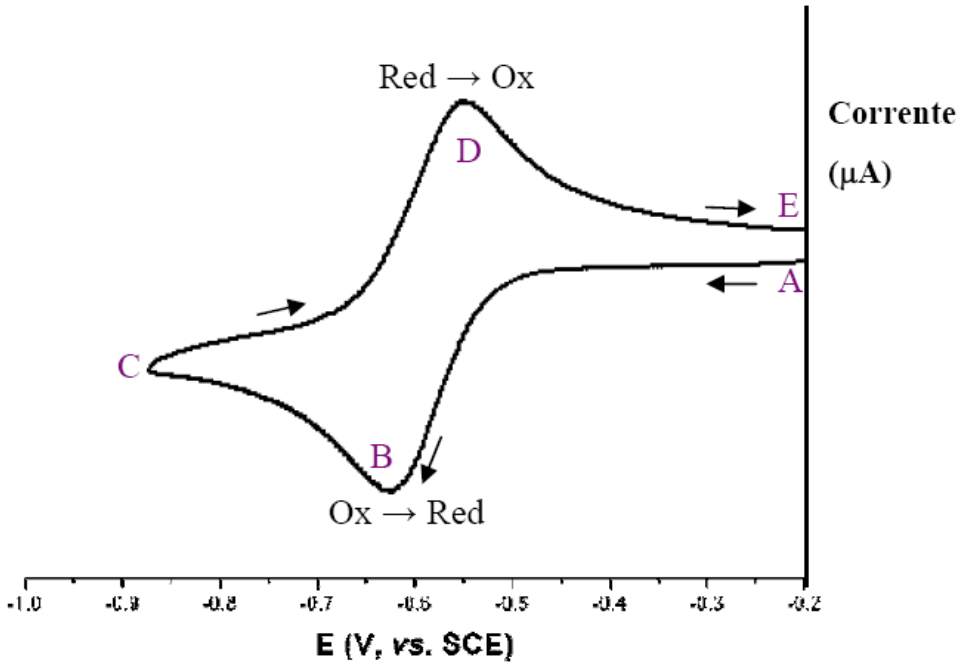

Figure 39 - Typical cyclic voltammogram for a redox reversible process

The shape of this curve can be justified by considering the concentration profiles in **Figure 40**

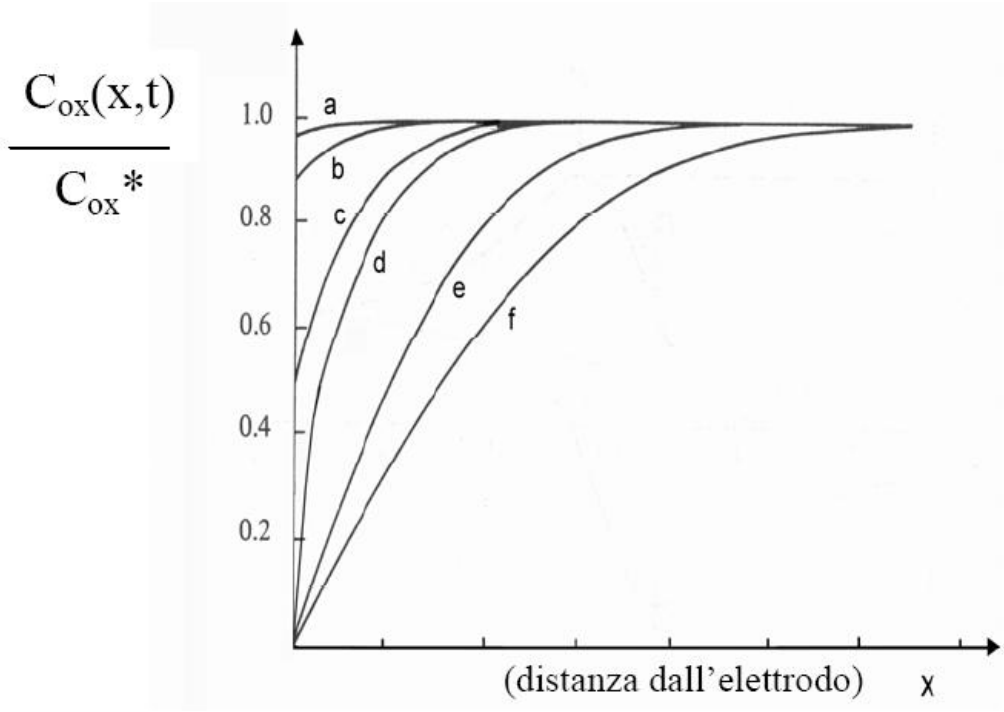

Figure 40 - Concentration profiles of Ox species during the semi-reaction Ox + ne^- → Red

At the starting point A there is not conversion of Ox to Red. While the potential is approaching E°′ value, the reduction current progressively increases. This occurs because the electrode surface concentration of Ox is decreasing respect to that one present in the massive solution (C_{Ox}*), so creating a concentration gradient whit a consequent current passage ("a" curve). Whit the proceeding of the potential scanning, in order to satisfied Nernst equation, an increasing amount of Ox is reduced making larger the concentration gradient ("b", "c", "d", "e" curves). When the potential scanning have reached the value corresponding to B all the Ox species is reduced to Red and the gradient concentration have reached its maximum value ("f"). Than the gradient doesn't not grow up anymore. Indeed, due to physical reason (the amplification of the diffusion layer with the time) it tends to decrease and consequently the current too decreases until the point C.

After the inversion of potential, the voltammetric curve assumes the shape of CDE segment because inverse phenomena occur to the Red electrogenerated.

IUPAC convention establishes to consider positive currents for anodic processes end negative currents for cathodic processes.

A process is defined "electrochemically reversible" when the electron transfer rate between the electrode and the active species is higher than the mass transport rate of the active species from the massive solution to the electrode surface.

The cyclic voltammogram for a reversible process assumes a profile whose diagnostic parameters are shown in **Figure 41**.

If *n* electrons *per* molecule are exchanged by the active species then:

a) the forward peak potential is independent from the potential scan rate;

b) the separation between the forward and the reverse peak, ΔE_p, is $59/n$ mV at 25°C and at any scan rate;

c) the ratio between the reverse current and the forward current i_{pa}/i_{pc}, is always equal to 1 at any scan rate.

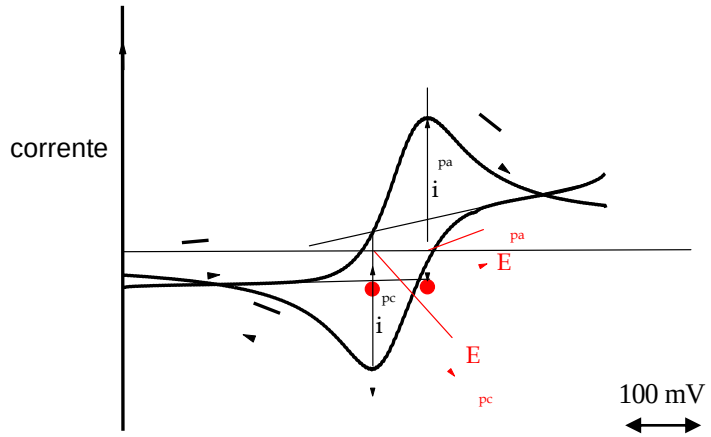

Figure 41 - Typical parameters of a cyclic voltammogram for a electrochemically reversible process

Chemical meaning of reversibility in an electrochemical process

One of the main factor increasing the activation barrier of an electron exchange process is the geometrical reorganization of the active species which accompanies this transfer. The fact that a *reversible* electrochemical process occurs means that a marginal structural reorganization is involved.

1.7.1.2 Irreversible processes

When the electron transfer rate is lower than the mass transport rate, the process is defined "*irreversible*".

During a reduction:

$$Ox + ne^- \rightleftharpoons Red$$

if the peak potential is more cathodic than the formal Ox/Red couple potential E°′ , ΔE_p could be so high that the reverse peak is not detectable.

Chemical meaning of irreversibility in an electrochemical process

Occurring for an electrochemically *irreversible* process implies for so high activation barrier during the electron transfer that the molecule undergoes to fragmentation and consequently a new species are formed.

1.7.1.3 Quasi-reversible processes

A *quasi-reversible* process occurs when the electron transfer rate is comparable to the mass transport rate.

The first effect of quasi-reversibility on voltammetric profile is a deeper peak separation respect to a reversible process, **Figure 42**.

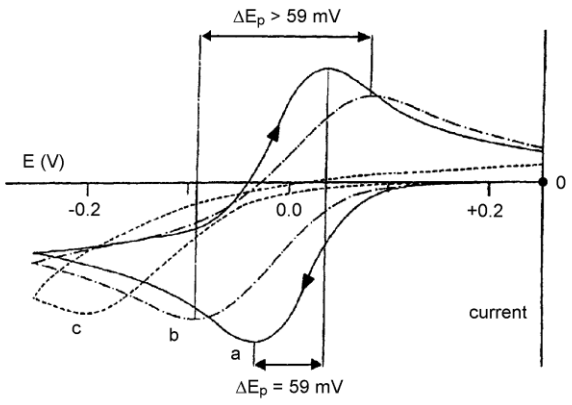

Figure 42 – Cyclic voltammetric profiles of monoelectron reduction process characterized by electrochemical feature of: (a) reversibility; (b) quasi-reversibility (c) irreversibility. E°′ = 0.00V, T = 25°C.

Diagnostic criteria of a quasi-reversible process are:

a) the forward peak potential shifts with the increasing of scan rate;
b) generally ΔE_p is higher than $59/n$ mV at 25°C, and increases with the scan rate;
c) the forward peak current grows with $v^{1/2}$, but not always the growth is directly proportional.

Chemical meaning of quasi-reversibility in an electrochemical process

Electrochemical quasi-reversibility implies for a significant structural reorganization concomitant with the electron transfer without any molecular fragmentation. As a first approximation, it is possible to assume that the higher the process peak-peak separation difference is respect to the theoretical value of $59/n$ mV, the more significant is the geometrical reorganization following the *redox step*.

1.7.1.4 Chemical reaction coupled with a charge transfer

Homogeneous chemical reactions can *precede* or *follow* the charge transfer. They can involve the Ox species or Red and, if occur with a rate comparable with cyclic voltammetry times, they can interfere with the typical voltammogram parameters.
Diagnostic criteria for the more commun electrodic mechanisms accompanied by chemical reactions are reported in **Table 4**, where E represents an electronic transfer, while C stays for a chemical complication.

Diagnostic parameter	Mechanism ^{b,c} C_rE^d	Mechanism EC_r^d	Mechanism ^{c,e} EC_i^d
	$A \underset{K_b}{\overset{K_f}{\rightleftharpoons}} Ox$ $Ox + ne^- \rightleftharpoons Red$ $K=K_f/K_b$	$Ox + ne^- \rightleftharpoons Red$ $Red \underset{K_b}{\overset{K_f}{\rightleftharpoons}} A$ $K=K_f/K_b$	$Ox + ne^- \rightleftharpoons Red$ $Red \longrightarrow A$
Peak potential E_p	Anodic shift with scan rate increase (for a reduction process)	Cathodic shift with the scan rate increase (for a reduction process)	Cathodic shift with scan rate increase (for a reduction process)

Current function $i_{pc}/v^{1/2}$	It decreases by increasing the scan rate	Practically constant	Practically constant
Ratio i_{pa}/i_{pc}	It is ≥ 1 and it increases with the scan rate	It is ≤ 1, it decreses by increasing by the scan rate	It increases with the scan rate up to 1

Diagnostic parameter	Mechanism EC (Catalytic regeneration)	Mechanism EC_i (dimerization)	Mechanism EC_i[a] (disproportion)
	$Ox + ne^- \rightleftharpoons Red$	$Ox + ne^- \rightleftharpoons Red$	$Ox + ne^- \rightleftharpoons Red$
	$Red + A \longrightarrow Ox$	$2Red \longrightarrow A$	$2Red \longrightarrow Ox + A$
Peak potential E_p	Anodic shift (for a reduction process) with the increase of the scan rate	Cathodic shift both with scan rate increase and [Ox] decrease	Cathodic shift both with scan rate increase and [Ox] decrease
Current function $i_{pc}/v^{1/2}$	Significantly increase with scane rate decrease un to a maximum value	Slightly decrease with scan rate increase	Quickly decrease with scan rate increase
Ratio i_{pa}/i_{pc}	It is ≥ 1	It increases with the scan rate and it decreases by increasing [Ox]	It increases with the scan rate and it decreases by increasing [Ox]

[a] sigmoidal curve with v [b] for K >> 1 and when reaction kinetic is slow respect to the CV timescale, the diagnostic parameters are the same of those for a simple reversible/irreversible process; [c] for K << 1 voltammogram sigmoidal curve is diagnostic at S; [d] electrochemical reversible/irreversible.

Table 4- Diagnostic criteria for the characterization of the possible reaction accompanying the redox process.

1.7.2 Differential pulsed voltammetry

As shown in **Figure 43** for a species, differential pulsed voltammetry (DPV) results to be particularly useful for determining redox potentials of two or more processes which occur at potential values separated by less than 100 mV.

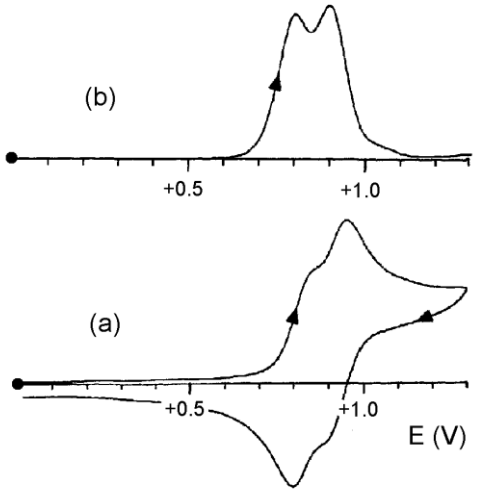

Figure 43 - a) Cyclic voltammetry (0.2 V/s) and b) DPV (0.02 V/s) for a species undergoing to two vicinal oxidative processes.

According to this technique, the potential is varied over the time by means of periodic application of little peak step which are superimposed to modulated and more consistent potential impulse. **Figure 44**.

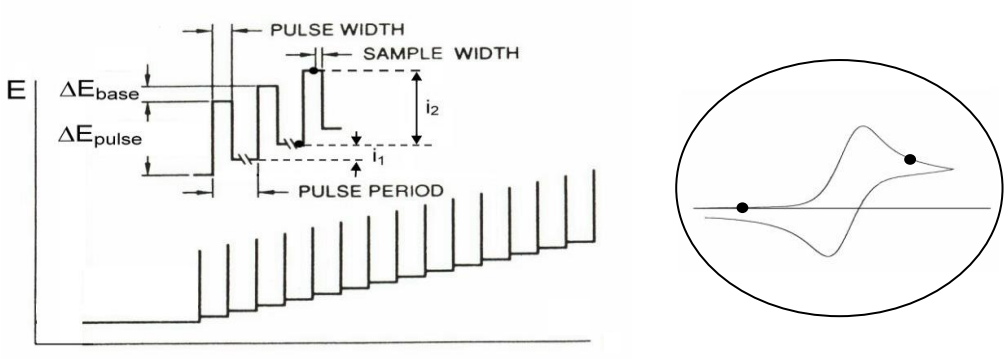

Figure 44 - Potential-time pulse shape in DPV and extrapolation of the potential value to which the current of each pulse is monitored respect to a cyclic voltammogram

As **Figure 43 b** shows DPV outputs are symmetrical peaks which start from and arrive to zero current.

As a first approximation, DPV peak potential can be assumed to be the formal potential of the redox process under investigation. Actually this peak potential is less cathodic (for reduction processes) than the formal potential by a factor:

$$E_p = E^{o\prime} - (\Delta E/2)$$

1.7.3 Square wave voltammetry

As shown by **Figure 45**, the potential in square wave voltammetry (Osteryoung, OSWV) is varied during time by means of the periodic combination of little and constant peak step wave shape ($1 \leq \Delta E_{base} \leq 40mV$) with a share wave perturbation ($1 \leq \Delta E_{sw} \leq 250mV$). The latter consists of alternate direction cycles, namely forward (reduction or oxidation) and reverse (oxidation or reduction) (1≤*frequence* SW ≤*2000 Hz*). This results into a sequence of equally spaced steps: the forward step $2\Delta E_{sw} + \Delta E_{base}$ in height; the reverse $-2\Delta E_{sw}$ in height.

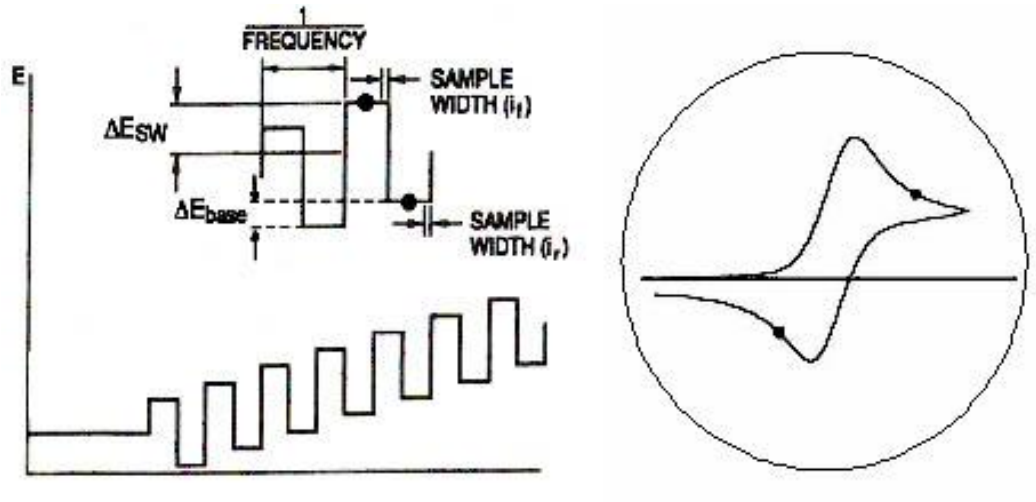

Figure 45 - OSWV Potential-time pulse and extrapolation of potential values to which the current is monitored at each pulse respect to a cyclic voltammogram.

As illustrated by **Figure 46,** the final result is a differential curve between the registered current during the forward hemi-cycle and that of reverse hemi-cycle. As the forward and reverse current have opposite sign, their difference results in a sum as absolute value.

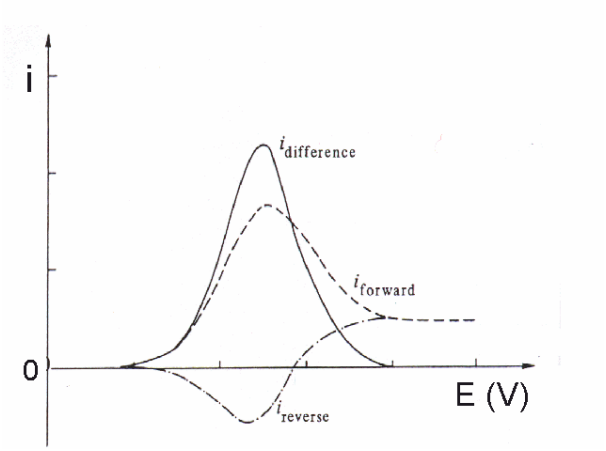

Figure 46 - Typical voltammogram obtained with OSWV.

For a reversible process the half height peak broadness $\Delta E_{p/2}$, is given by:

$$\Delta E_{p/2} = 4.90\ RT/nF$$

and

$$\Delta E_{p/2} = \frac{126}{n} \quad (mV)$$

at 25°C.

The advantages of OSWV technique with respect to DPV are:

a) a higher analysis rate. In fact scan rate in the order of 0.2 V/s are possible in OSWV, while this rate is 10-20 mV/s for DPV;
b) a higher sensibility, which increases with the scan rate.

1.7.4 Voltammetry with periodic renew of the electrodic diffusion layer

One of the method for applying this technique consists in the periodic shaking (3-5 sec) of the external summit of the working electrode in order to stir and renew the solution nearby the electrode surface during the potential scan. The result is similar to a polarographic curve.

1.7.5 Controlled potential electrolysis

In order to quantified the number of electrons exchange during an electrodic process, the controlled potential electrolysis is the most useful method. This technique employs Faraday law on electrolysis:

$$n_{app} = \frac{Q}{Fm}$$

where:

n_{app} = number of electrons apparently involved in a electrodic semi-reaction;

Q = electricity quantity (Coulomb);

m = number of moles;

F = Faraday constant (equal to 96500 Coulomb/mol e^-).

In order to measure the number of electrons involved during a reduction, a known concentration solution of a substance is prepared, then it is put in electrolysis cell and a tension is applied, whose value being 0.1 V more negative respect to the reduction peak collected in cyclic voltammetry. With the proceeding of the electrolysis the current asymptotically slow down. The process is considered as concluded when the current is 1/10 than the initial one.

This technique is fundamental also for the statement of the chemical stability of the electrogenerated species, otherwise the reversibility of a redox process. After the collection of a cyclic voltammogram on the exhaustive electrolyzed solution, the chemical reversibility involved for this output is complementary to the initial one.

Results and Discussion

Many Pt-Au mixed metal clusters have been obtained in the past and many of them contain 3-6 metal atoms. These compounds have assumed particular relevance, because of their peculiar bonding properties. [199] In the field of high nuclearity clusters (Pt + Au > 6) less examples are known, either rich in Pt [200] or with a high Au content. [201] A few trimetallic clusters, mainly containing other metals of group 11-12 (Cu, Ag, Hg) were also described [202] and they are typically based on icosahedral structures. Beside theoretical and structural aspects, the combination of Pt and Au in molecular compounds of well defined composition may be relevant to the preparation of bimetallic nanoparticles, which are known to possess peculiar electrocatalytic activity[203].

The anion $[Pt_{19}(CO)_{22}]^{4-}$ played a special role in the field of carbonyl clusters, since it remained for a long time as the largest structurally characterized compound of this kind. Moreover, it is still one of the rare examples of high nuclearity carbonyl clusters possessing a framework of pentagonal symmetry. [204] Despite these peculiarities, the studies on its reactivity were hampered by the difficult characterization of fairly unstable products. For example, it is known that the reactions of $[Pt_{19}(CO)_{22}]^{4-}$ (**1**) with NO^+ and H^+ eventually lead to the formation of $[Pt_{38}(CO)_{44}]^{2-}$, but only $[Pt_{19}(CO)_{21}NO]^{3-}$ could be isolated as an intermediate.[205] Conversely, the formation of hydridic species could be confirmed by neither crystallographic nor spectroscopic methods. Nevertheless, some electrochemical investigations have been described, showing that the cluster undergoes several couples of redox processes, spanning reversibly the -8/0 oxidation states. [206]

The behavior of the cluster under CO atmosphere has been deeply studied observing a clean, quantitative and rapid reaction, but also in this case the real nature of the product could never be ascertained. In contrast to what normally observed,[207] the infrared bands of the carbonylated product shift to *lower* wavenumbers, indicating an increased Metal-to-Ligand backdonation and suggesting that this uncharacterized species would be a better electron donor toward electrophiles.

1 - Reaction between $[Pt_{19}(CO)_{22}]^{4-}$ and gold phosphane fragments

1.1 $[Pt_{19}(CO)_{22}\{Au(PPh_3)\}]^{3-}$

The anion $[Pt_{19}(CO)_{22}]^{4-}$ **(1)** played a special role in the field of carbonyl clusters, since it remained for a long time as the largest structurally characterized compound of this kind. Moreover, it is still one of the rare examples of high nuclearity carbonyl clusters possessing a framework of pentagonal symmetry. Despite these peculiarities, the studies on its reactivity were hampered by the difficult characterization of fairly unstable products. For example, it is known that the reaction of (**1**) with NO^+ and H^+ eventually lead to the formation of $[Pt_{38}(CO)_{44}]^{2-}$, but only $[Pt_{19}(CO)_{21}NO]^{3-}$ could be isolated as an intermediate.

Conversely, the formation of hydric species $[Pt_{19}(CO)_{22}H]^{3-}$ could be confirmed by neither crystallographic nor spectroscopic methods.

In the attempt to prove the intermediate formation of the hydridic species, we performed a similar reaction by using the isolobal fragment $Au(PPh_3)$ whit the hope that the gold-fragment could give greater stability to the cluster.

1.1.1 Synthesis

It has been observed that $[Pt_{19}(CO)_{22}]^{4-}$ tetranion very slowly reacts with PPh_3AuCl under nitrogen atmosphere in CH_3CN as solvent. This is probably due to the spare solubility of the gold-phosphane derivative in CH_3CN and to the insufficient nucleophility of the cluster. Instead, by using CO atmosphere the reaction is faster. This fact is not surprising if we consider that $[Pt_{19}(CO)_{22}]^{4-}$ converts, under CO atmosphere, into the hypothetical anion $[Pt_{19}(CO)_{24}]^{4-}$ which, having four valence electrons more, assumes a more nucleophilic character.

I have further investigated the reaction between $[Pt_{19}(CO)_{22}]^{4-}$ and PPh_3AuCl in 1:1 molar ratio and nitrogen atmosphere by using acetone as solvent which allows the gold-phosphane solvent to be dissolved, so eventually favouring the reaction kinetics.

The adopted synthetic procedure was as follow.

The reactants $[TBA]_4[Pt_{19}(CO)_{22}]$ and PPh_3ClAu were dissolved in acetone and constantly stirred under nitrogen atmosphere for 24 hours, during which the reaction was checked by IR spectroscopy. Then 2-propanol was added until a solid precipitated. The compound was then isolated in the solid state, re-dissolved in acetone and re-precipitated with 2-propanol. After filtration and desiccation, the product was crystallized from acetone / 2-propanol. Needle-like crystals were obtained which were analyzed by elemental analysis and IR spectroscopy, which were in agreement with the formulation $[TBA]_3[Pt_{19}(CO)_{22}(AuPPh_3)]$. Carbonyl stretching bands were presents at 2012(s), 1953(w) and 1807(m) cm^{-1} (**Figure 47**)

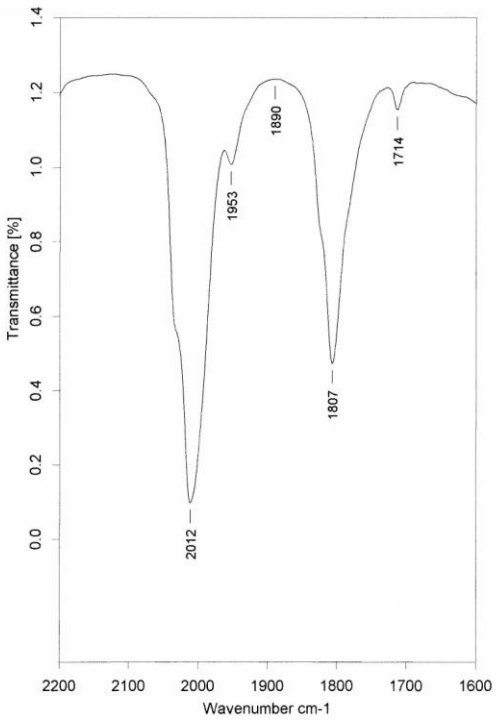

Figure 47- IR spectrum in CH_3CN of the hypothetic anion $[Pt_{19}(CO)_{22}(AuPPh_3)]^{3-}$

This spectrum resembles that of the compound obtained by reacting $[Pt_{19}(CO)_{22}]^{4-}$ with H^+ in acetonitrile as solvent under nitrogen atmosphere. The compound was formulated as $[HPt_{19}(CO)_{22}]^{3-}$ but never isolated due to high acidic character of the H atom which

induces an instant deprotonation in ordinary solvents. Isolobality between H^+ and $AuPPh_3^+$ suggested to use this one in order to overcome the deproonation problem.

1.2 $[Pt_{19}(CO)_{24}\{Au(PPh_3)\}_3]^-$ (2) and $[Pt_{19}(CO)_{24}\{Au(PPh_3)\}_4]$ (3)

1.2.1 Synthesis and reactivity

The reaction of $[Pt_{19}(CO)_{22}]^{4-}$ (**1**) with PPh_3AuCl was carried out in acetonitrile at room temperature, under inert atmosphere or under CO: in both cases, infrared monitoring of the reaction mixture showed a progressive shift of the CO bands to higher wavenumbers. Spectra of the products collected under CO and under inert atmosphere are constantly different, with the formers always showing maxima shifted about 10 cm^{-1}.

Under CO, when the Pt_{19}:Au molar ratio is 1:3, a brown precipitate forms, which can be easily isolated by filtration, and dissolved in THF for characterization and crystallization. The product is stable under inert atmosphere and does not need to be handled under CO. Thus, crystals of $[NBu_4][Pt_{19}(CO)_{24}(AuPPh_3)_3]$ ($[NBu_4]$**2**) suitable for X-ray determination were obtained by layering these THF solution with 2-propanol.

The poor solubility of the salts of **2** in acetonitrile hampered its further reactions with excess of PPh_3AuCl. Therefore, to obtain clusters with higher gold content, we reacted THF solutions of pure **2** with the solvated cationic complex $[PPh_3AuTHF]^+$, obtained *in situ* by dehalogenation of PPh_3AuCl with Ag^+.

This reaction induced a definite shift of the infrared spectrum and allowed the isolation of the neutral $[Pt_{19}(CO)_{24}\{Au(PPh_3)\}_4]$ cluster by precipitation from THF with 2-propanol.

^{31}P-NMR spectra have been recorded for both clusters but only for $[PPh_4][Pt_{19}(CO)_{24}(AuPPh_3)_3]$ we could detect a signal, consisting of a singlet ($[PPh_4]^+$) and a multiplet at 61.79 ppm. Since the $AuPPh_3$ group binds to non equivalent Pt atoms, belonging to different layers of the cluster (see later), the number of lines of the multiplet and the value of the $^2J(^{31}P\text{-}^{195}Pt)$ can give some clues on the amount of Au-Pt interactions. If the ^{31}P couples equally with all Au-bound Pt atoms, a non binomial nonet can be anticipated (resulting by the superposition of five subspectra, corresponding to the

different molecules with 0-4 NMR active ^{195}Pt (S = ½, natural abundance 33 %); however a non binomial quintet of quintets would result if phosphorous couples differently with the two pairs of structurally unequivalent Pt atoms. As a matter of fact the intensities of the five observed central lines are in the 0.39:0.62:1:0.53:0.09 ratio, in keeping with a nonet (calculated intensities of the central lines 0.18:0.62:1:0.62:0.18). Therefore all the coupling constants must be very similar. Very few examples of $^{2}J(^{31}P\text{-}^{195}Pt)$ are reported for Au-PPh_3 bridging in carbonyl clusters, and these values are in the range 500-300 Hz;,**Errore. Il segnalibro non è definito.**,[208] in the present case the coupling constant is lower (206 Hz), which may be the result of a less localized Pt-Au interaction. Attempts to obtain the same spectrum with samples of **2** prepared in the NMR tube showed a very broad band, suggesting a fast exchange with the solvated $[THF\text{-}Au\text{-}PPh_3]^+$ cation. The absence of any signal in the ^{31}P spectrum of **3** can be the consequence of its limited solubility, or of dynamic processes involving the four Au-PPh_3 groups. Beside the dissociation of $AuPPh_3$ groups, two additional processes can be envisaged, involving exchange of nonequivalent gold sites within the two Au_2 units, and scrambling of the di-gold entities over the three square faces available. Indeed $Au_2(PR_3)_2$ moieties in carbonyl clusters are known to be highly fluxional.[209]

1.2.2 Solid state structures

The solid state structures of **2** and **3** are shown in **Figure 48** and **Figure 49** , respectively.

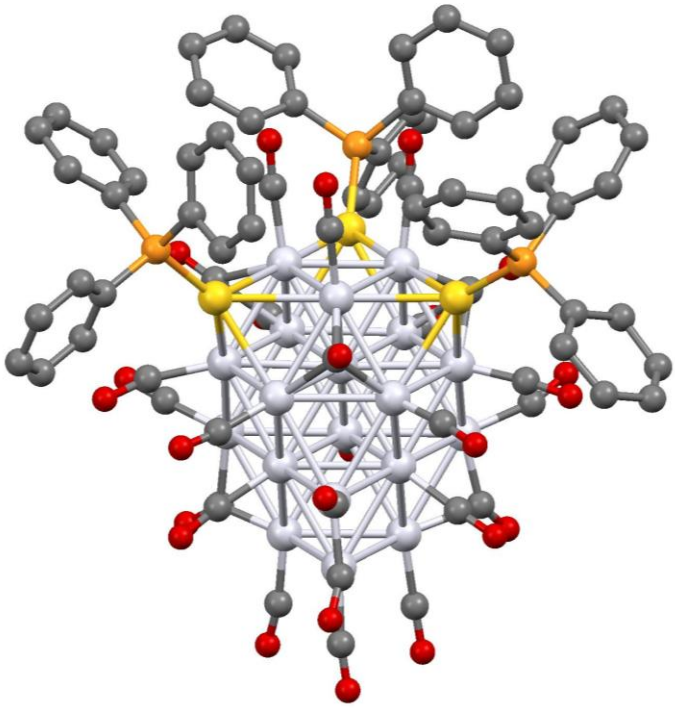

Figure 48 - The solid state structure of $[Pt_{19}(CO)_{24}(AuPPh_3)_3]^-$, (**2**) from X-ray diffraction data

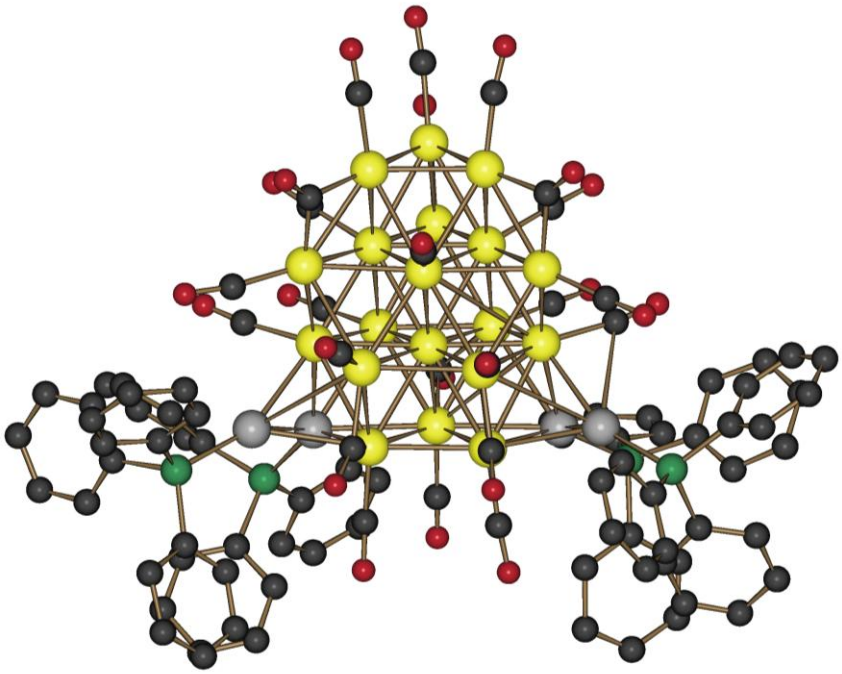

Figure 49 - The solid state structure of $[Pt_{19}(CO)_{24}(AuPPh_3)_4]$, (**3**) from X-ray diffraction data

The platinum framework is identical in the two compounds, being composed by a cubic-closed core, and four layers of 3, 7, 6 and 3 Pt atoms, respectively. All Pt atoms lay on the surface and bears at least one carbonyl ligand, but one which is fully interstitial at the center of the second layer. The cluster can be idealized as a cuboctahedron, with three square faces capped by other 3 Pt atoms and face-fused with an octahedron (**Figure 50**). The upper part of the cluster is therefore exposing three square faces and four triangular faces as a cube-octahedron. The two structures differ, however, in the coordination of $AuPPh_3$: in **2** the three $AuPPh_3$ fragments are capping all three square faces, whereas the four $AuPPh_3$ fragments in **3** form a $(AuPPh_3)_2$ dumbbell, capping asymmetrically square faces of the cluster. The distribution of the carbonyl ligands is similar in **2** and **3**. Thus, the ideal symmetry is C_s in **3** and C_{3v} in **2** (reduced to C_1 and C_3, respectively, if the out-of-plane rotation of the phenyl rings is considered). In the crystal structures, **2** is mirror symmetric, whereas **3** is not sitting on any symmetry element.

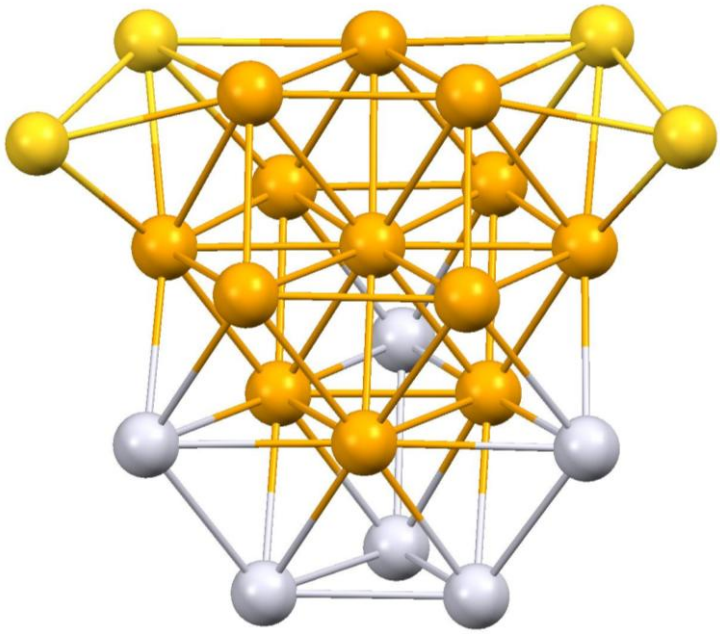

Figure 50 - The metallic framework of $[Pt_{19}(CO)_{24}\{(AuPPh_3)_2\}_2]$, (3). The cube-octahedron core of Pt_{13} is highlighted in orange. The remaining Pt atoms are in light gray and the four Au atoms in yellow.

The Pt-Au bond distances in **2** span the range 2.80-2.93 Å and average 2.86 Å. They are systematically longer for the three Pt atoms of the outer triangle (>2.85 Å) and shorter for the Pt atoms of the inner hexagon (< 2.85 Å), suggesting a slightly stronger interaction. In **3**

the Pt-Au distances are more scattered, being included in the range 2.64 -2.97 Å, but the average (2.84 Å) is almost unchanged. The shorter distances are those connecting the two more external Au atoms, bound to only two Pt (**Figure 50**).

In both crystal structures, the clusters leave large voids to host solvent molecules and cations (in **3**) which are not visible, given the relative scarce diffraction and the likely disordered arrangement around the clusters.

1.2.3 Electrochemical studies

As illustrated in **Figure 51**, the $[PPh_4]^+$ salt of the anion **2** undergoes one anodic processes at +0.45 V, complicated by subsequent chemical reactions. In fact, we are in the presence of an ECE mechanism with the formation of a by-product undergoing two new oxidation processes at +0.73 V and +0.88 V. By analogy with was has been observed for the series of $[Pt_{19}(CO)_{22}]^{4-}$, $[Pt_{24}(CO)_{30}]^{2-}$ and $[Pt_{38}(CO)_{44}]^{2-}$ clusters, two pairs of cathodic processes, separated by ~300 mV are also visible at -0.31 V, -0.65 V, -1.66 V and -1.90 V, only the first of which manifesting features of chemical reversibility in the time scale of cyclic voltammetry. In fact, at lower scan rates the departure from the current ratio $i_{p(reverse)}/i_{p(forward)}$ =1 expected for a chemical reversible process, is observed for all the reduction processes, except for the first. A fifth reduction process at -2.25 V is also detected, while the possible partner of this pair could be beyond the experimental window, limited by the solvent discharge. Controlled potential coulometric tests in correspondence of the first reduction (Ew=−0.4 V) proved that it involves one electron per molecule, while the cyclic voltammetry on the exhaustively reduced solution indicates that also the addition of one electron, in facts, makes the cluster to partially decompose, as suggested by the appearance of new small peaks and by the general decrease of the current intensity.

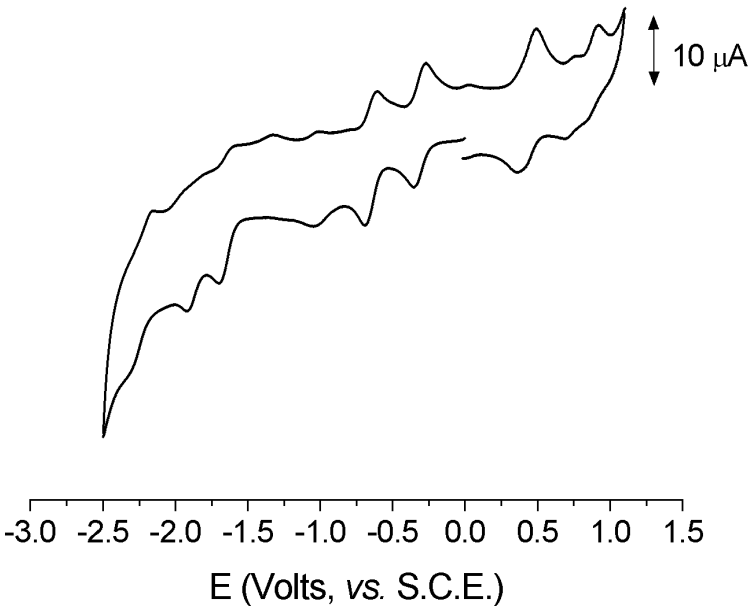

Figure 51 - Cyclic voltammetric profile of $[PPh_4][Pt_{19}(CO)_{24}(AuPPh_3)_3]$, recorded at a platinum electrode in THF solution of 2 (0.5×10^{-3} M). $[NBu_4][PF_6]$ supporting electrolyte (0.2 M). Scan rate 0.2 V s^{-1}.

In spite of the incomplete stability of the electrogenerated neutral and dianionic species, we have monitored by IR spectroelectrochemistry the variation of ν_{CO} of both the terminal and the bridging groups of this cluster. The experiment has been conducted *in-situ* step-by-step, in way to maintain the isosbestic points, so that the electrolysis was, in fact, not completed. As expected, in both cases the original spectrum is only partially recovered on the backscan. Figure 52 illustrates the IR spectral trend recorded in the $^{0}/^{-}$ and $^{-}/^{2-}$ passage. The original spectrum shows two main absorptions: at 2027 cm^{-1}, which is assigned to the stretching vibration of the carbonyl groups terminally bound at the metal core, and at 1803 cm^{-1}, which is assigned to the stretching vibration of the bridged carbonyl groups. Upon oxidation, both bands are blue-shifted by ~15-20 cm^{-1} and appear at 2042 and 1821 cm^{-1}, while the contrary happens upon reduction, with two new bands appearing at 2009 and 1780 cm^{-1}. This is a common trend in the case of carbonyl clusters and indicates the decrease or increase of the dπ-Pt→π^*-CO back-bonding induced by the removal or addition of electrons, respectively. It is interesting to note the agreement between the trend of the ν_{CO} and the first oxidation or first reduction redox potential values of the pristine sample of **2** when compared to the analogous values observed for

$[Pt_{19}(CO)_{22}]^{4-}$ (2001 cm^{-1} and -0.15 V and -1.13 V, for the first oxidation and the first reduction, respectively), in fact these values all clearly indicated how the metallic core $\{Pt_{19}\}^{4-}$ is much less electron-rich in **2** than in the parent **1**.

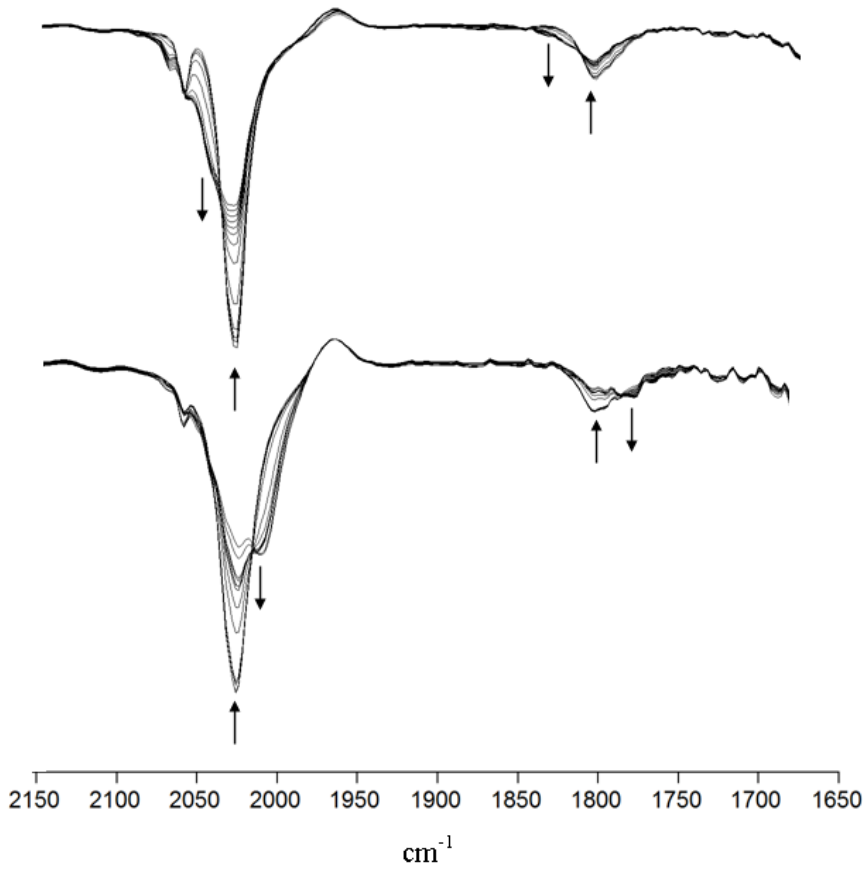

Figure 52 - IR spectral changes recorded in an OTTLE cell upon the progressive oxidation (top) and reduction (bottom) of 2. THF solution; $[NBu_4][PF_6]$ supporting electrolyte (0.2 M).

As illustrated in **Figure 53,** the redox behaviour of the neutral cluster **3** seems apparently somehow reminiscent of that of **2**, since an oxidation (E°=+0.33 V) and a couple of reductions (at E°=-0.34 V and -0.67 V) are observed. A clear trait of the illustrated cyclic voltammogramm is the general lower chemical reversibility of all these redox processes ($i_{p(reverse)}/i_{p(forward)}$ at v=0.2 Vs^{-1} is 0.1 for the oxidation and 0.5 and 0.2 for the first and second reductions, respectively). Anyway, a closest inspection of the redox pattern of **3,** obtained by using a potential step technique, like for example the differential pulse voltammetry (DPV) shown in **Figure 54**, reveals a more complicated situation. In fact, the presence of a mixture of **2** and **3** is clearly revealed. A new couple of anodic processes is visibly detectable at -1.21 and – 1.41 V, while the doubt now emerges that the true first

couple of anodic processes of **3** is partially hidden by the correspondent couple of anodic processes of **2**. As a matter of fact, two shoulders at -0.53 and -0.78 V are visible behind the first couple of **2** reductions, which could be possibly ascribed to **3**. Admittedly, at this stage this latter can not be more than a pure conjecture but the low solubility and the redox instability of **3** probably exclude a more distinct description. To conclude we can put in evidence how, as a general trend, the addition of heterometallic fragments reduces the electron content of these Pt clusters and, at the same time makes them much less prone to the electron-sink behaviour observed for the homometallic related family of clusters.

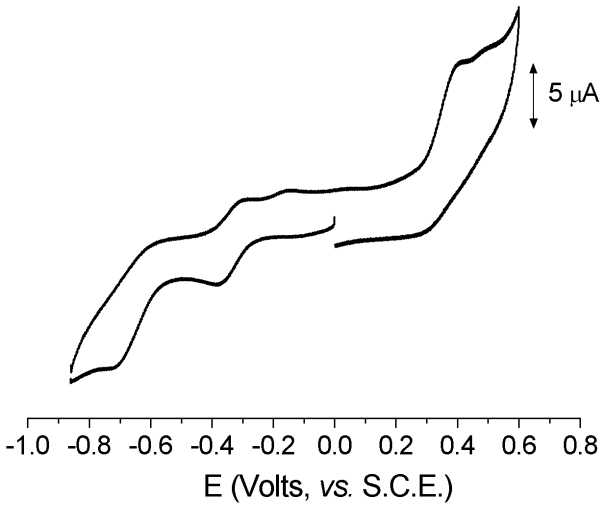

Figure 53 - Cyclic voltammetric profile of $Pt_{19}(CO)_{24}\{(AuPPh_3)_2\}_2]$, recorded at a platinum electrode in THF solution of 3 ($0.4x\ 10^{-3}$ M). $[NBu_4][PF_6]$ supporting electrolyte (0.2 M). Scan rate 0.2 V s^{-1}.

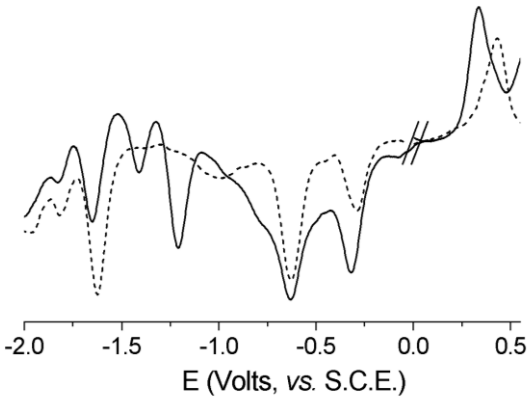

Figure 54 - Differential pulse voltammetric responses recorded at a platinum electrode in THF solution of 2 ($0.5x\ 10^{-3}$ M, dashed line) and 3 ($0.4x\ 10^{-3}$ M, full line). $[NBu_4][PF_6]$ supporting electrolyte (0.2 M).

1.3 $[\{Pt_{19}Au(CO)_{22}\}_4(180tetraphos)]^{12-}$

1.3.1 3,3-5,5′-tetrakis(diphenylphosphano)biphenyl(180tetraphos) and $[\{AuCl\}_4(180tetraphos)]$

This tetradentate phosphane ligand (180tetraphos) is obtained by substitution reaction between the corresponding tetrafluorobiphenyl derivative and $KPPh_2$ in THF.

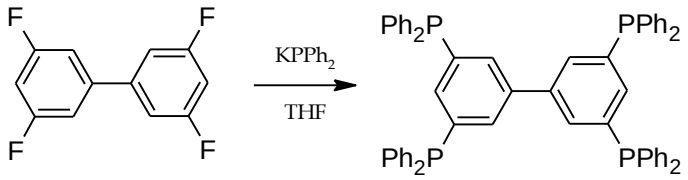

The name refers to the presence of four phosphane groups in the molecule and to the 180° angle (respect to the symmetry centre) between the two benzene rings.

Then four [AuCl] fragments were coordinated to the PPh_2 groups, in order to exploit the reactivity of gold(I) centres, eventually dehalogenated, towards nucleophilic anionic clusters.

The tetraphosphane ligand was dissolved in chloroform and four equivalents of [AuCl(THT)] (THT = tetrahydrothiophene) were added to the obtained solution. We chose this gold species as THT is a labile ligand and it can be easily substituted by an incoming ligand. This operation is conducted under nitrogen atmosphere and far from light, as the starting gold complex easily undergoes to photo-oxidation. After about half an hour the reaction was completed and the solvent was evaporated by a vacuum pump. The remaining solid was washed with ethanol and diethyl ether affording a white powder which was stable to air and light. The reaction undergoes according to the following stoichiometry:

$$4\ [AuCl(THT)] + 180tetraphos \longrightarrow [\{AuCl\}_4(180tetraphos)] + 4\ THT$$

^{31}P-NMR peak shifts to lower field respect to the free ligand, moving from -3,9 ppm to 34,3 ppm (**Figure 55** and **Figure 56**).

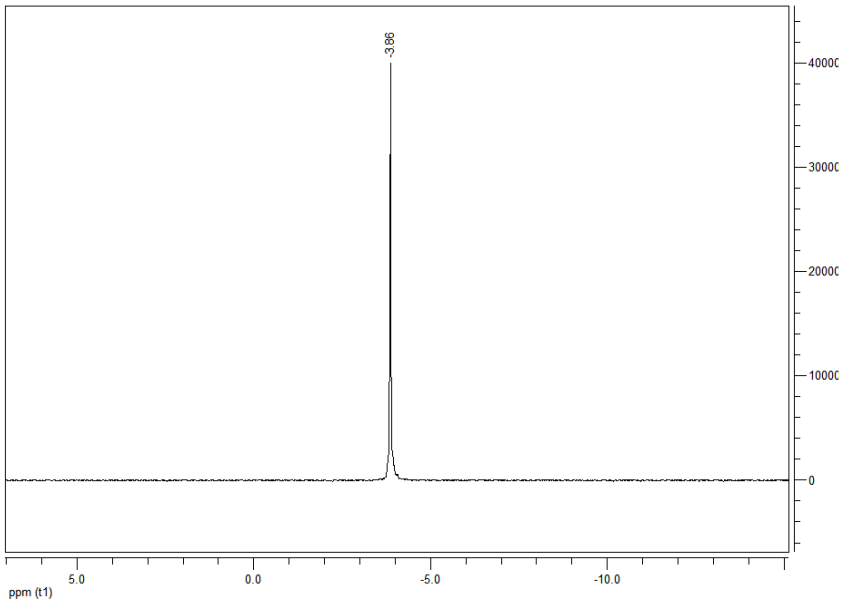

Figure 55 - ^{31}P-NMR spectrum of 180tetraphos in $CDCl_3$

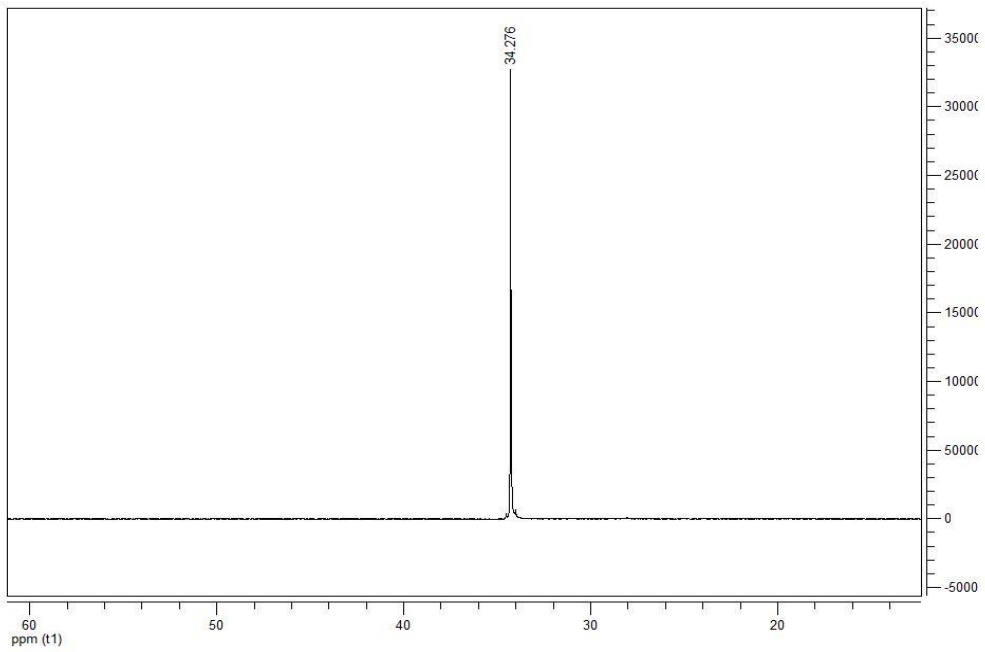

Figure 56 - ^{31}P-NMR spectrum of $[\{AuCl\}_4$(180tetraphos)] in $CDCl_3$

The 180tetraphos ligand is fluorescent showing, in the emission spectrum, a maximum at 515 nm, under an excitation wavelength of 330 nm (**Figure 57**). The phenomenon is likely due to n → p* charge transfer between phosphorous non bonding doublets and the anti ligand orbitals of biphenyl fragment.

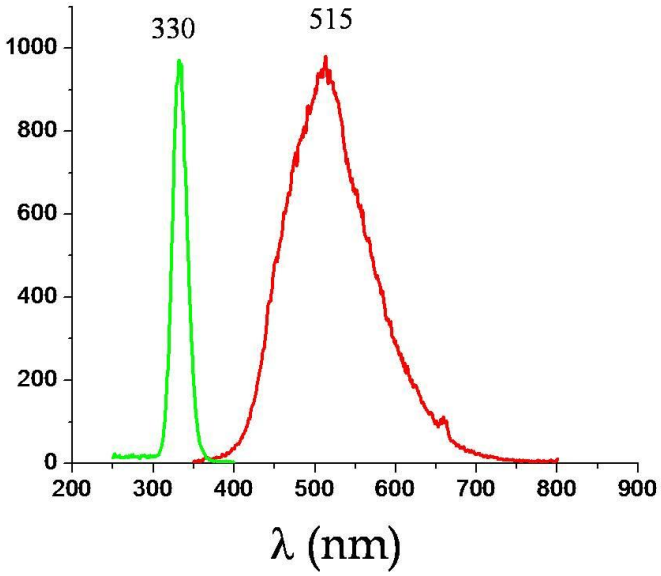

Figure 57 - Excitation (green) and emission (red) spectra of 180tetraphos. Spectra collected in degassed dichloromethane.

Gold phosphane complex too is luminescent, as shown by the emission spectrum (**Figure 58**). The emission maximum (364 nm) has a blue shift with respect to the free ligand.

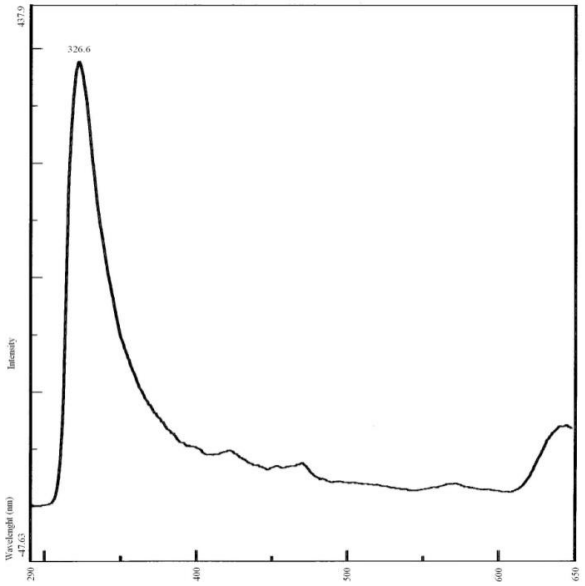

Figure 58 - Fluorescence spectrum of [{AuCl}$_4$(180tetraphos)] collected in dichloromethane. Excitation wavelenght 310 nm.

1.3.2 Reactivity of [{AuCl}$_4$(180tetraphos)] with [Pt$_{19}$(CO)$_{22}$]$^{4-}$

After the characterization of 2 and 3, we decided to use the new tetradentate gold-phosphane fragment in order to bond one Pt19 on each AuPPh2 group.

By doing so, the resulting species will show four metal clusters separated by an organic, electrically isolating scaffold. This results in a so-called *compartmental nanocapacitor*, a molecule having:

1) a nanometric size,

2) a capacitor-like behaviour, thanks to the reversible redox activity,

3) four different isolated active regions of the molecule.

The reaction between $[Pt_{19}(CO)_{22}]^{4-}$ and 180tetraphos gold complex has been conducted under CO atmosphere according to the following stoichiometry:

$$4\ [Pt_{19}(CO)_{22}]^{4-} + [Au_4(180tetraphos]^{4+} \xrightarrow{CO} [\{Pt_{19}Au(CO)_{24}\}_4(180tetraphos)]^{12-}$$

We found that a dehalogenation step of the gold-phosphanes (made with Ag^+) has been necessary as the reaction occurred.

A solution of the gold phosphane complex in THF has been added to a solution of $[Pt_{19}(CO)_{22}]^{4-}$ in acetone and the resulting solution has been put in CO atmosphere and stirred for some hours.

Crystals of the reaction product have beew grown by layering the solution with 2-propanol. Unfortunately they were geminate or, in another attempt, their unit cell was too big and so it was not possible to get the structure. Actually the crystallization of such a big species as $[NBu_4]_{12}[\{Pt_{19}Au(CO)_{24}\}_4(180tetraphos)]$ can be really challenging.

In **Figure 59** is reported the IR spectrum (in acetone) of the isolated product which shows a sharp absorption band in the terminal carbonyl region at 2020 cm^{-1}. The frequency value is in good agreement with the value shown in the corresponding spectrum of the anion $[Pt_{19}(CO)_{24}\{Au(PPh_3)\}]^{3-}$ formally its parent monomeric species.

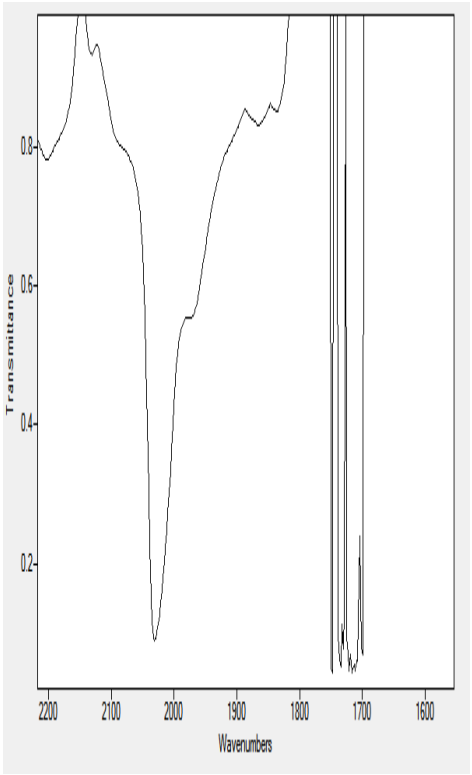

Figure 59 - IR spectrum in acetone of the hypothetic $\{Pt_{19}Au(CO)_{24}\}_4$(180tetraphos)]$^{12-}$ cluster

2 - Reaction between $[Ir_6(CO)_{15}]^{2-}$ and gold phosphane fragments

An intrinsic advantage using gold(I) complexes for the synthesis of macrocycles, oligomers and polymers consists in the tendency of Au(I) of giving linear dicoordinated complexes which can present further gold-gold interaction. Both theoretical and experimental studies show that in the presence of a Au–Au distance of 2,5-4 Å, the aurophilic interaction is about 30 kJ mol^{-1} in energy, a comparable value with a typical hydrogen bond. This can pushes towards a particular crystal packing and a single conformation or molecular stereochemistry, besides influencing the physical properties of the species.

The dianionic cluster $[Ir_6(CO)_{15}]^{2-}$ is a good nucleophile and its $^{2-}/^{-}$ and $^{-}/^{0}$ redox couples are known. In the past our group has synthesized and characterized the $[Ir_6(CO)_{15}(AuPPh_3)]^{-}$ species[12] where the phosphorous ligand is the simple triphenylphosphine.

So we have extended the reactivity of the iridium cluster to the rigid more complex 180tetraphos.

2.1 $[\{Ir_6Au(CO)_{15}\}_4(180tetraphos)]^{4-}$

2.1.1 Reactivity of $[\{AuCl\}_4(180tetraphos)]$ with $[Ir_6(CO)_{15}]^{2-}$

At first we have tested the reactivity of $[(AuCl)_4(180tetraphos)]$ with the dianionic cluster $[Ir_6(CO)_{15}]^{2-}$. The latter was dissolved in THF with a concentration of about 10^{-2} M under nitrogen atmosphere. The gold-phosphane complex $[(AuCl)_4(180tetraphos)]$ was added in solid, with a 4:1 stoichiometric ratio cluster to ligand.

The reaction was followed by IR spectroscopy but no changes in the carbonyl stretching bands were observed, meaning that the carbonyl cluster is not enought electron-rich to be able to dehalogenate the gold(I) complex and so bonding with it.

A dehalogenation step was so necessary, in order to obtain the much more electrophile cationic form of the gold(I) complex.

[{AuCl}4(180tetraphos)] was dissolved in THF, under nitrogen atmosphere and in the dark, and AgTf (silver trifluoromethanesulfonate) was added to the resulting solution.

Few minutes later a AgCl precipitated was observed and allowed to deposit. The stoiochiometry of the reaction is the following:

$$[\{AuCl\}_4(180tetraphos)] + 4\ AgTf \longrightarrow [Au_4(180tetraphos)][Tf]_4 + 4\ AgCl$$

Then the resulting uncoloured solution was added to a THF solution of $[Ir_6(CO)_{15}]^{2-}$ under CO atmosphere, by using a cluster to ligand 4:1 molar ratio.

$$4\ [Ir_6(CO)_{15}]^{2-} + [Au_4(180tetraphos)]^{4+} \xrightarrow{CO} [\{Ir_6Au(CO)_{15}\}_4(180tetraphos)]^{4-}$$

The reaction is complete in about 1 hour. In fact, the carbonyl stretching bands of the starting material were substituted by other bands at 2020(s) and 1778(m) cm^{-1} (**Figure 60**). ^{31}P-NMR spectrum showed two singlets having same intensity at 97.70 ppm and 23.64 ppm. The first one is attributed to the phosphorous directly bonded to Au atoms, while the second one is due to the cation (**Figure 61**). Elemental analysis and spectroscopic data agree with the proposed formulation.

The reaction was repeated under nitrogen atmosphere but it was slower. Moreover, the product was less pure, as revealed by its elemental analysis.

We compared our spectroscopic data with those ones reported in literature for the analogous but simplier species $[Ir_6(CO)_{15}(AuPPh_3)]^-$, finding a strict similarity, as we would expect. The only substantial difference consists in the different molecular rigidity of the two species. The above reported species shows fluxionality in ^{31}P-NMR spectrum, a phenomenon which is absent in our case.

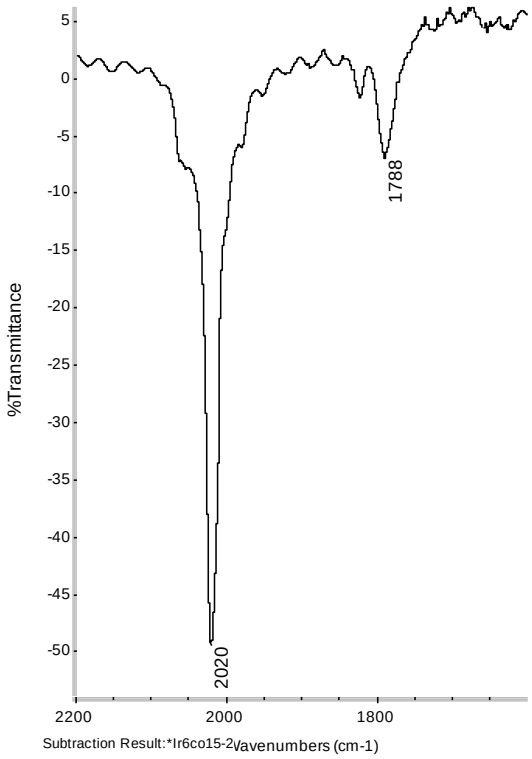

Figure 60 - IR spectrum in THF of the hypothetic $[\{Ir_6Au(CO)_{15}\}_4(180tetraphos)]^{4-}$ cluster

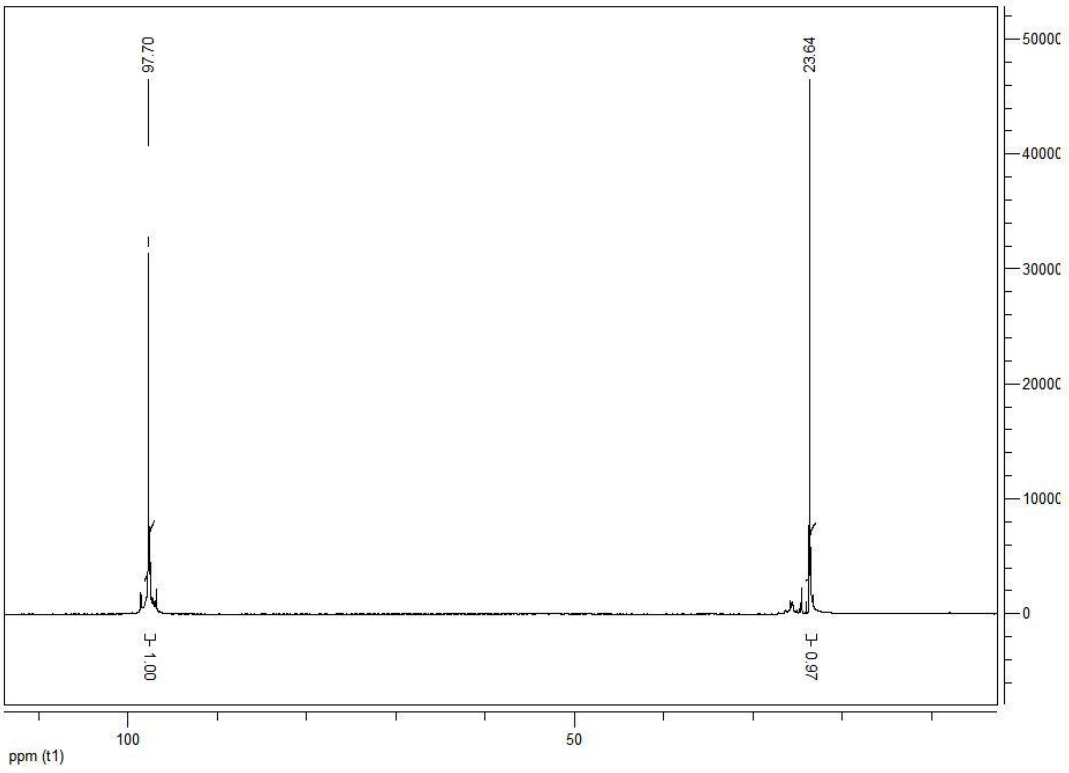

Figure 61 - ^{31}P-NMR spectrum in THF-d^4 of $[PPh_4]_4[\{Ir_6Au(CO)_{15}\}_4(180tetraphos)]$

2.1.2 Voltammetric study on $[PPh_4]_4[\{Ir_6Au(CO)_{15}\}_4(180tetraphos)]$

Redox behaviour study was performed by using cyclovoltammetric techniques in collaboration with Prof. Patrizia Mussini (University of Milan). The aim was making a comparison with the parent $[Ir_6(CO)_{15}]^{2-}$ cluster, whose redox activity is reported in literature.[210]

This 86 valence-electrons cluster undergoes in THF to two oxidative monoelectronic processes, both chemically reversible (**Figure 62**). It is worth to note that, in spite of the analogous isoelectromic $[Co_6(CO)_{15}]^{2-}$ and $[Rh_6(CO)_{15}]^{2-}$ clusters , not only the $[Ir_6(CO)_{15}]^{2-/-}$ couple, but also the second $[Ir_6(CO)_{15}]^{-/0}$ couple is completely reversible. Particularly the species $[Ir_6(CO)_{15}]^0$, although instable, (being the stable neutral cluster $[Ir_6(CO)_{16}]$), shows a relatively long hemilife time ($t_{1/2} \sim 2$ sec.).

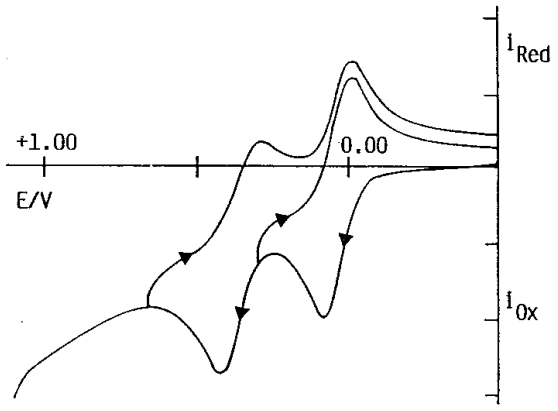

Figure 62 - Cyclic voltammetry profile of $[Ir_6(CO)_{15}]^{2-}$, collected on a Pt electrode in THF solution. Scanning rate 0,2 Vs^{-1}

The cluster $[Ir_6(CO_{15})]^{2-}$ is known for reacting with molecules like $HgCl_2$ and $Au(PPh_3)Cl$, yielding to the corresponding capped cluster, see for example $[Ir_6(CO_{15})Au(PPh_3)]^-$.

So, we have investigated the redox behaviour of the species obtained by assembling four iridium hexanuclear cluster with the tetradentate gold-phosphane fragment.

The compound has been studied in THF solution (10^{-3} M) under nitrogen atmosphere at 298 K and undergoes to four redox processes, two reductions and two oxidations (**Figure 63)**. The two cathodic peaks are centred at -1,65 and -1,83 volt, while the anodic ones at 0,64 and 0,87 volt.

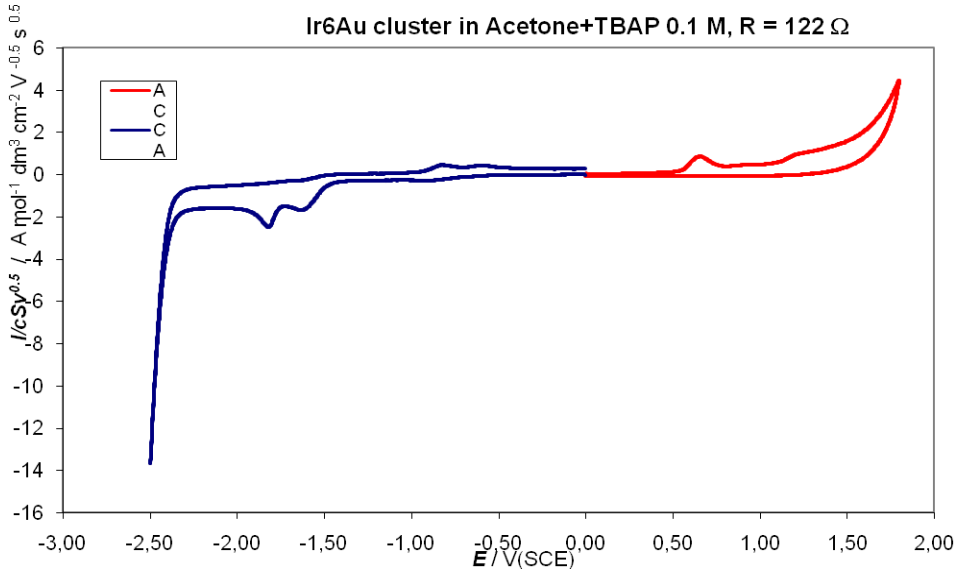

Figure 63 - Cyclic voltammogram of $[PPh_4]_4[\{Ir_6Au(CO)_{15}\}_4(180tetraphos)]$ (10^{-3} M THF) collected on glassy carbon electrode at 298 K. Scansion rate 0,2 V/s, supporting electrolyte $[NEt_4][PF_6]$ (0,2 M)

The first cathodic process is electrochemically and chemically irreversible, while the second one, at -1,84 volt, is partially reversible: in fact, the forward peak potential moves to more positive values increasing the scansion rate (**Figure 64**).

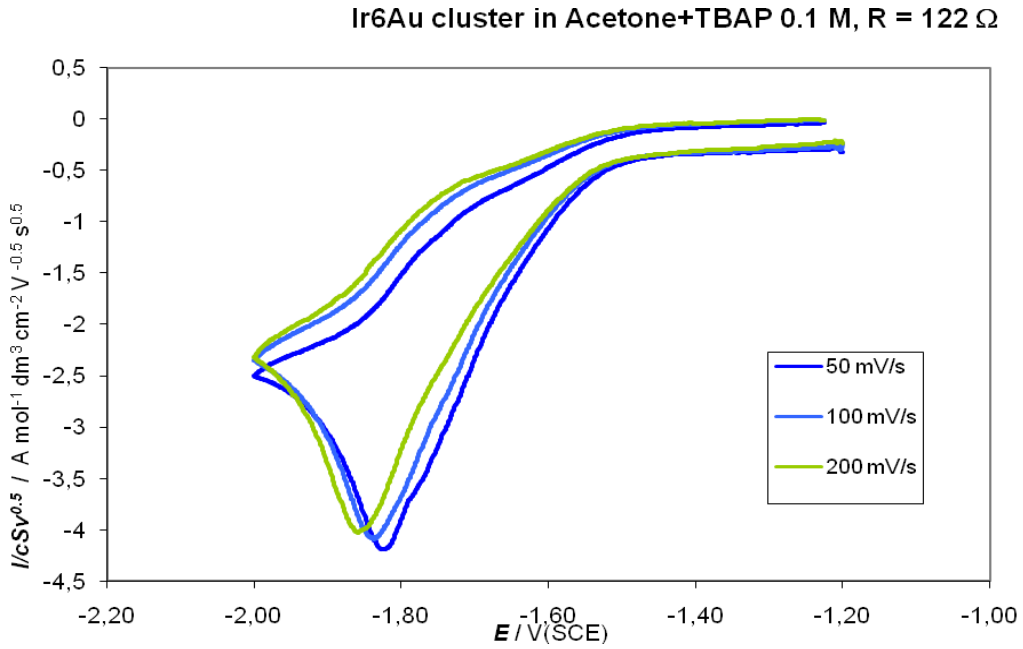

Figure 64 - First cathodic peak at variable scansion rate

By conducting the same experiment on the second cathodic process, it is clear that by increasing the scansion rate the reversibility behaviour tends to be lost (**Figure 65)**.

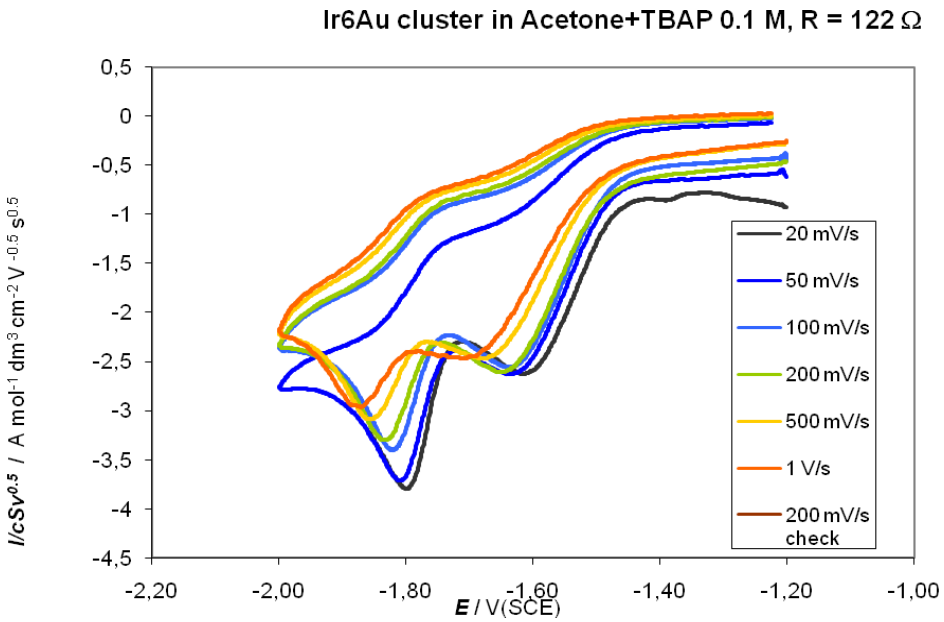

Figure 65 - Second cathodic peak at variable scansion rate

In order to verify if the species produced during the reduction processes are adsorbed onto the electrode, five consecutive cycles were conducted avoiding to clean up the electrode. As it is possible to see from **Figure 66**, cycle II-V are substantially superimposable. So, there is not any deposition on the electrode, but the species generated are dissolved in the solution.

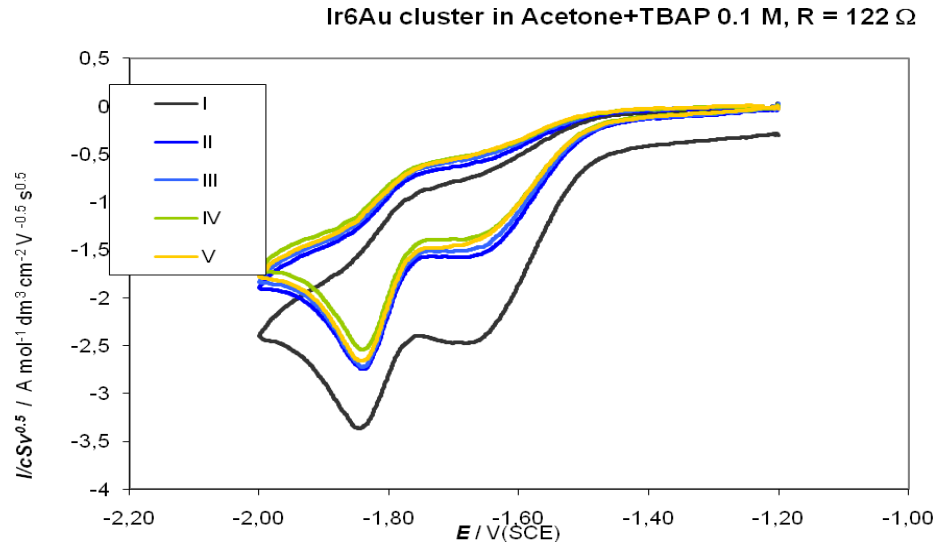

Figure 66 - Subsequent cycles without electrode cleaning

In order to verify if the species generated during the anodic processes are adsorbed onto the electrode, another experiment was conducted by varying the scansion rate.

By increasing the scansion rate the peaks are not superimposable anymore but they are progressively moving to more anodic potentials (**Figure 67**). The forward current peak is not proportional to the square of the rate but to the rate itself.

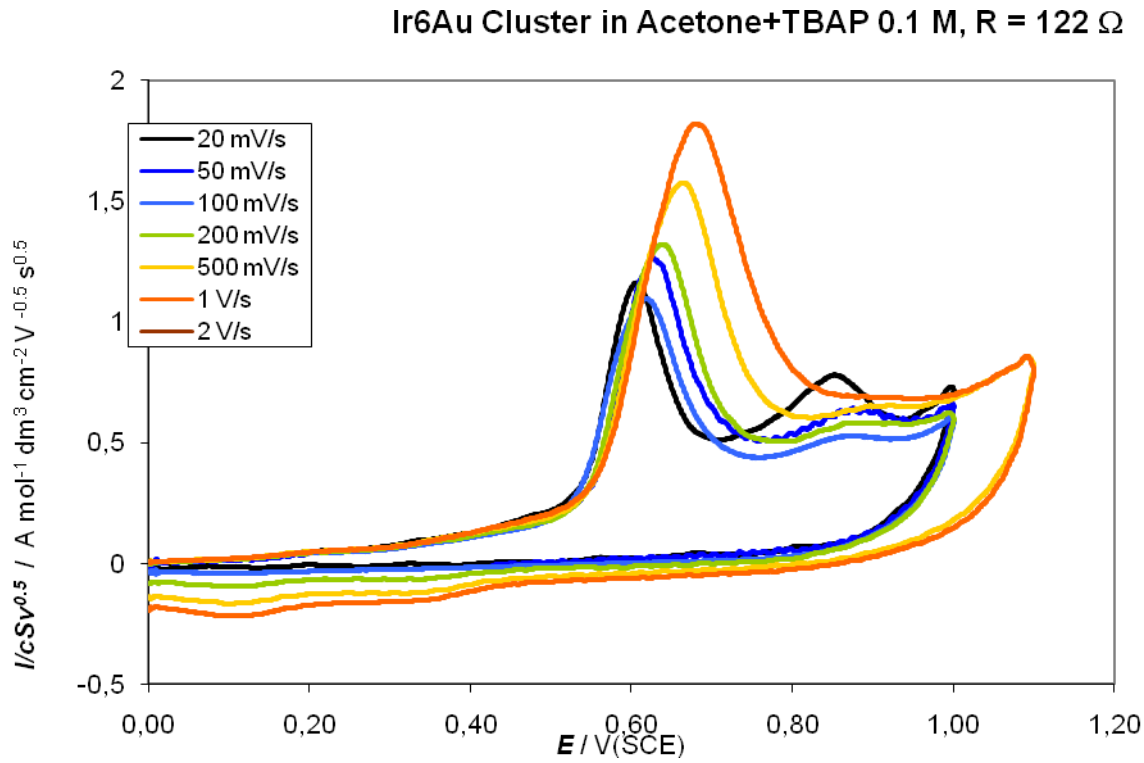

Figure 67 – First anodic peak at variable scansion rate

2.2 $[\{Ir_6Au(CO)_{15}\}_6(120hexaphos)]^{6-}$

2.2.1 1,3,5-tris[3'-5'-bis(diphenylphosphano)phenyl]benzene (120hexaphos) and $[\{AuCl\}_6(120hexaphos)]$

The hexaphosphane ligand (120heaxaphos) was recently obtained in our laboratories by reaction between the corresponding hexafluorotetraphenyl derivative and $KPPh_2$ in refluxing THF.

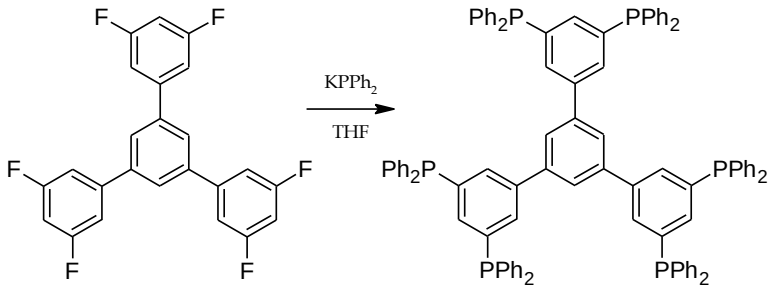

The ligand shows, in ^{31}P-NMR spectrum, a singlet at -4 ppm (**Figure 68**).

The current name refers to the presence of six phosphane groups in the molecule (hexaphos) and to the 120° angle existing among the central benzene ring and the aryl substituents in the position 1,3,5.

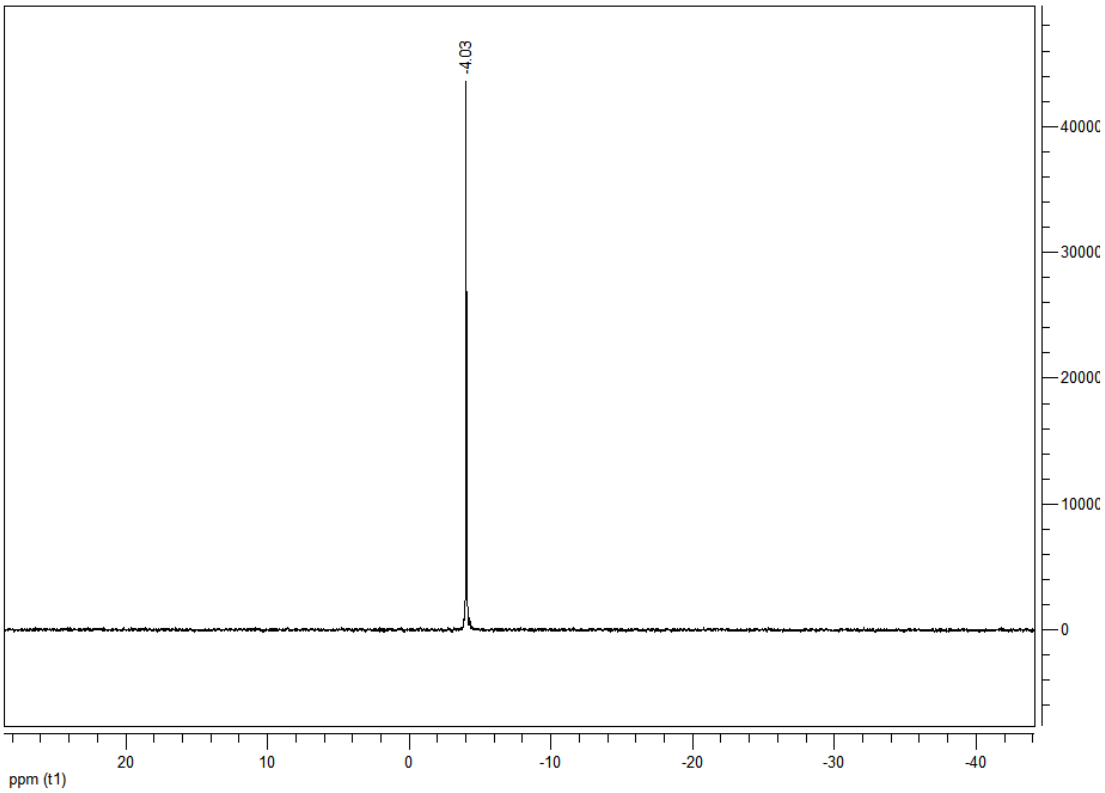

Figure 68 - ^{31}P-NMR spectrum of 120hexaphos in $CDCl_3$

The reaction with six equivalents of [AuCl(THT)] in chloroform yields to the formation of the complex [{AuCl}$_6$(120hexaphos)], which shows in ^{31}P-NMR one singlet at 33.7 ppm, shifted to lower fields with respect to the free ligand (**Figure 69**).

$$6\ [AuCl(THT)] + 120tetraphos \longrightarrow [\{AuCl\}_6(120tetraphos)] + 6\ THT$$

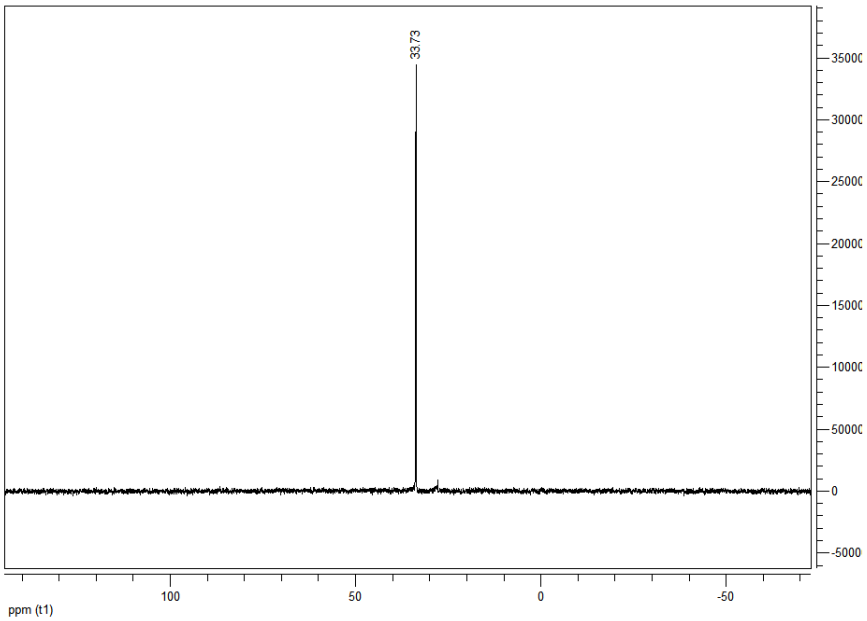

Figure 69 - ^{31}P-NMR spectrum of $[\{AuCl\}_6(120tetraphos)]$ in $CDCl_3$

The 120hexaphos ligand is fluorescent. **Figure 70** shows the emission spectrum collected in dichloromethane solution. As for 180tetraphos, the fluorescent phenomenon is expected to be due to the n → π* charge transfer among P lone pairs and antiligand π orbitals of the aromatic system.

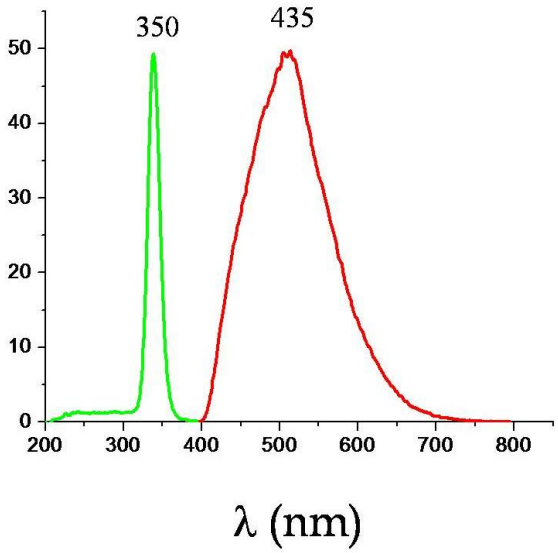

Figure 70 Excitation (green) and emission (red) spectra of 120hexaphos.

Spectra collected in degassed dichloromethane.

Gold-phosphane complex is fluorescent too and the emission peak shows a blue shift respect to the free ligand (**Figure 71**).

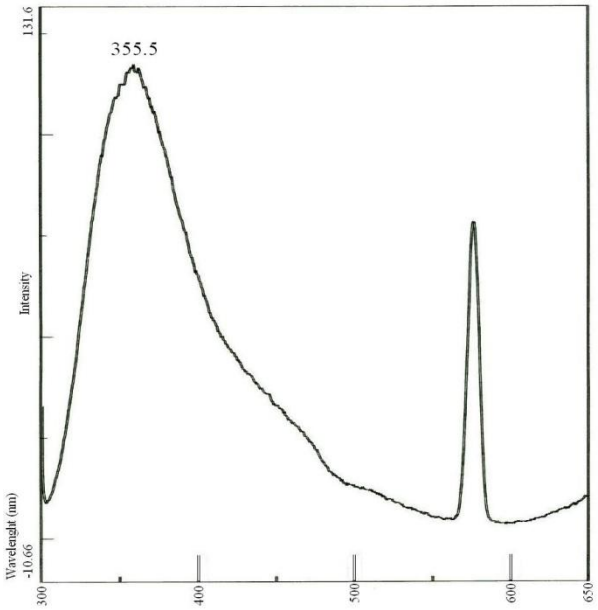

Figure 71 - Fluorescence spectrum of [{AuCl}$_6$(120hexaphos)] collected in dichloromethane. Excitation wavelength 310 nm.

2.2.2 *Reactivity of [{AuCl}$_6$(120hexaphos)] with [Ir$_6$(CO)$_{15}$]$^{2-}$*

The reactivity of 120hexaphos gold complex towards $[Ir_6(CO)_{15}]^{2-}$ was explored by using THF as solvent.

The reaction was conducted under CO atmosphere and the gold-phosphane complex undergoes to a dehalogenation pre-step by using Ag^+. A THF solution of such prepared ligand was added to a THF solution of the carbonyl cluster, by using a 6:1 cluster to ligand molar ratio.

$$6\ [Ir_6(CO)_{15}]^{2-} + [Au_6(120hexaphos)]^{6+} \xrightarrow{CO} [\{Ir_6Au(CO)_{15}\}_6(120hexaphos)]^{6-}$$

The resulting solution was allowed to stir and after about half an hour the reaction was completed. In fact, the carbonyl stretching band showed a shift to higher wave numbers, according to a formal charge reduction on the clusters. IR spectrum (**Figure 72)** exhibits

carbonyl stretching bands at 2062(w), 2019(s), 1985(m) cm^{-1} for terminal coordinated COs, and 1782(m) cm^{-1} for edge-bridging COs. Elemental analysis and spectroscopical data are in agreement with the proposal formulation.

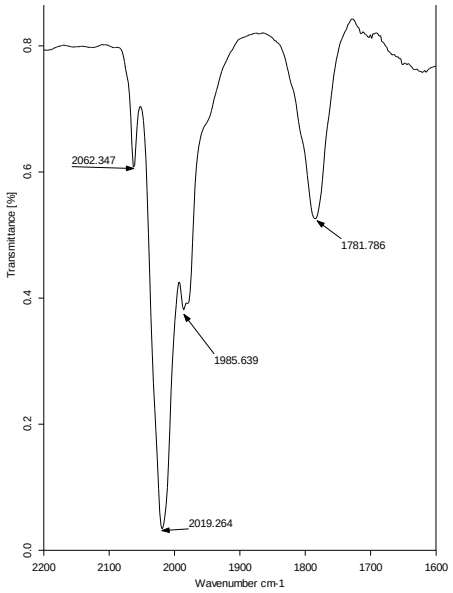

Figure 72 - IR spectrum in THF of the hypothetic $[\{Ir_6Au(CO)_{15}\}_6(120hexaphos)]^{6-}$ cluster

3 - Assembly of tetrairidium carbonyl clusters using multidentate phosphane ligands

With the aim to aggregate metal carbonyl clusters by using poliphosphane ligands, I have continued to exploit tetrahedral iridium cluster.

Our research group developed considerable expertise in the synthesis, characterization and reactivity of these metal carbonyl cluster.

The first of this compound family is $[Ir_4(CO)_{12}]$ (Figure 73), which has been presented in the introduction.

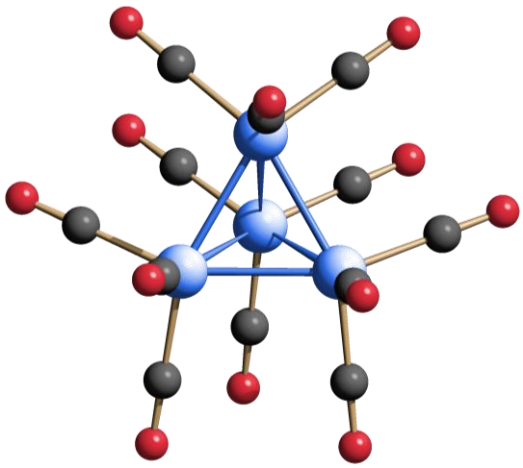

Figure 73 – The solid state structure of $[Ir_4(CO)_{12}]$

The compound is a yellow air-stable powder and it is prepared by reductive carbonylation in an autoclave starting from $IrCl_3 \cdot 3H_2O$ and formic acid.[211]

Its almost complete insolubility in all common organic solvent represents an hindrance in its reactivity which is possible to overcome only in drastic conditions (refluxing in high boiling solvents). It is known, from kinetics studies, that CO substitution rate increases with increasing the substitution degree.[212] With P-donor ligands and isonitriles tri- and tetra-substituted products have been mainly obtained[213] in place of mono-substituted products.[214] The introduction of an halide or a pseudohalide (Cl^-, Br^-, I^-, CN^-, SCN^-) radically changes the situation: it is possible to isolate products that are soluble in basic solvents easily giving substitution reactions.

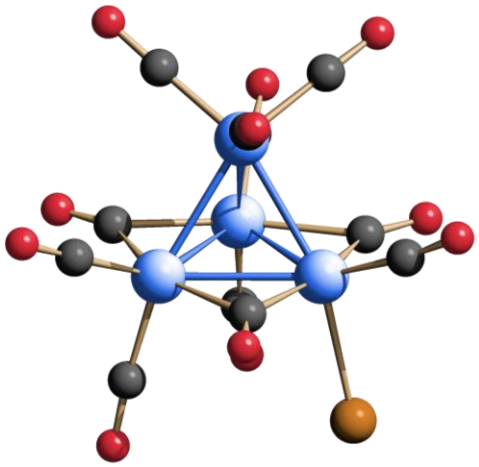

Figure 74 – The solid state structure of $[Ir_4Br(CO)_{11}]^-$

Therefore we used $[Ir_4Br(CO)_{11}]^-$ (Figure 74) as starting material, which can be isolated with different ammonium or phosphonium counterions, by treating $[Ir_4(CO)_{12}]$ with excess of LiBr in refluxing THF for some days. The product is precipitated adding an aqueous (or alcoholic) solution of the desired cation.

The reaction between $[Ir_4Br(CO)_{11}]^-$ and rigid 180tetraphos (vide infra) leaded to polymetallic dendrimers which are soluble in solvents like chloroform, tetrahydrofuran and toluene.

In particular, their dimensions above the nanometer, their behaviour to undergo to redox processes and the segregation of the metal clusters made by the organic ligand scaffold, leads to define these molecules as "compartmental nanocapacitors".

Nanometric metal carbonyl clusters showing the ability to reversibly acquire or give electrons maintaining the metal cage unbroken, can be defined as nanocapacitors. Some remarkable examples from the Ceriotti's, Longoni's and Zanello's research groups have been recently reported.[215]

Nowadays, only few examples of self-assembled materials containing metal carbonyl clusters are known.[216,217] Generally, self-assembly is mainly obtained through the formation of M-M bonds (for example $[Pt_{24}(CO)_{48}]^{2-}{}_\infty$ and $[Pt_{18}(CO)_{36}]^{2-}{}_\infty$)[218,219] or M-M' (for example $\{Ag^+[Rh_6C(CO)_{15}]^{2-}\}_n$ and $\{Ag^+[Ru_6C(CO)_{15}]^{2-}\}_\infty$).[220,221]

So far, the use of multidentate ligands to connect clusters together have received less attention and only few example of oligomers $(\{[Rh_5(CO)_{15}]_2(H_2N(CH_2)_4NH_2)\}^{2-}$,[222]

{$[Rh_6(CO)_{14}]_2$(dpbp)} and {$[Ru_6C(CO)_{15}$(dpbp)$]_3[Ir_4(CO)_8]$}[223] (dpbp = 2,2'-bis(diphenylphosphano)-4,4'-bipyridine)) and only one 1D polymer, containing $[Fe_4Cu_2(\mu_6\text{-}C)(CO)_{12}]$ cluster units linked by N donor ligands are known.[224]

So far the use of poliphosphane ligands was not explored, although many phosphane-substituted clusters are known and the CO substitution reactions have been studied since '70 and '80 of the XX Century.

3.1 Reactions of bis(diphenylphosphano)acetylene (dppa) and trans-1,2-bis(diphenylphosphano)ethane (t-dppethe) with $[Ir_4Br(CO)_{11}]^-$

As rigid diphosphanes bis(diphenylphosphano)acetylene (dppa, **Figure 75**) and *trans*-1,2-bis(diphenylphosphano)ethane (t-dppethe, **Figure 76**) have been tested.

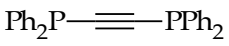

Figure 75 – dppa

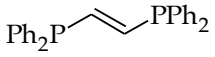

Figure 76 - t-dppethe

By conducting the reaction in dichloromethane at room temperature with a 2:1 cluster/phosphane molar ratio, and monitoring the reaction proceed by IR spectroscopy, an upshift of the carbonyl stretching bands, after adding ligand to the cluster solution, is noted. This is what we would expect moving from anionic to neutral species (Figure 77). Shape and position of the CO bands, according to literature data, show the formation of a monosubstituted species in which bromine is substituted by a phosphorous donor.

After about two hours a neutral compound precipitates from the solution. It has been fully characterized as $[\{Ir_4(CO)_{11}\}_2$(P-P)], following the stoichiometry:

$$2\,[Ir_4Br(CO)_{11}]^- + P\text{-}P \longrightarrow [\{Ir_4(CO)_{11}\}_2(P\text{-}P)] + 2\,Br^-$$

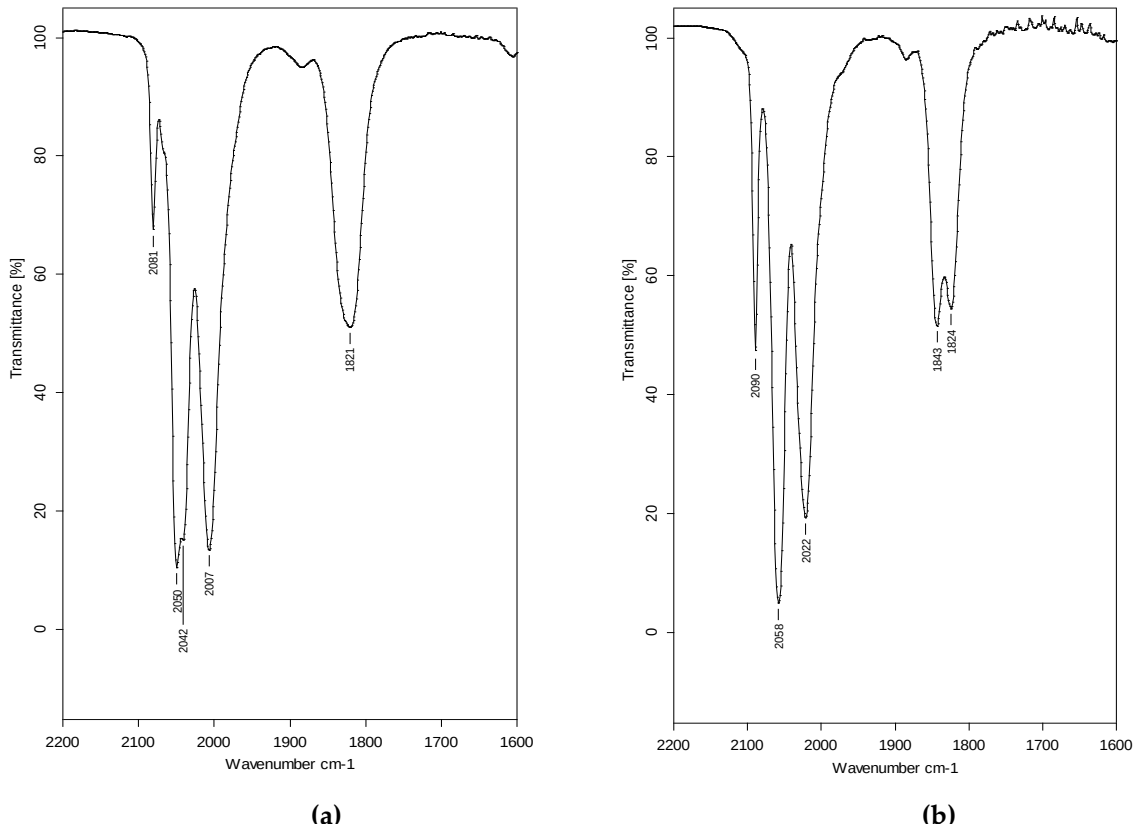

Figure 77 - IR spectra in dichloromethane of a) $[Ir_4Br(CO)_{11}]^-$ and b) $[\{Ir_4(CO)_{11}\}_2(P\text{-}P)]$

By conducting the reaction in dichloromethane at room temperature with a 1:1 cluster/phosphane molar ratio, it has not been possible to characterize a 1D coordination polymer or derivative where the tetrahedral cluster coordinates a pendant diphosphane. As in the previous case, formation of $[Ir_4(CO)_{11}(P\text{-}P)]$ (ν_{CO}= 2087, 2055, 2018 cm^{-1} terminal COs and 1843, 1819 cm^{-1} bridging COs) is observed. This species has not been yet structurally characterized.

In the case of dppa, after about 2 hours, some $[\{Ir_4(CO)_{11}\}_2(dppa)]$ precipitates, while the IR spectra is roughly unvaried. Then a low downshift of the CO stretching bands is observed, (ν_{CO}= 2075, 2049, 2014 cm^{-1} terminal COs and 1825, 1802 cm^{-1} bridging COs), suggesting a further substitution. These values are in agreement with the formation of a $[Ir_4(CO)_{12}]$ disubstituted species (Figure 78, after 3 days stirring).

It is possible to assume a three steps mechanism affording to the observed result:

$$3\,[Ir_4(CO)_{11}Br]^- + 3\,dppa \longrightarrow 3\,[Ir_4(CO)_{11}(dppa)] + 3Br^-$$

$$2\,[Ir_4(CO)_{11}(dppa)] \longrightarrow [\{Ir_4(CO)_{11}\}_2(dppa)] + dppa$$

$$dppa + [Ir_4(CO)_{11}(dppa)] \longrightarrow [Ir_4(CO)_{10}(dppa)_2] + CO$$

$$3\,[Ir_4(CO)_{11}Br]^- + 3\,dppa \longrightarrow [\{Ir_4(CO)_{11}\}_2(dppa)] + [Ir_4(CO)_{10}(dppa)_2] + CO + 3Br^-$$

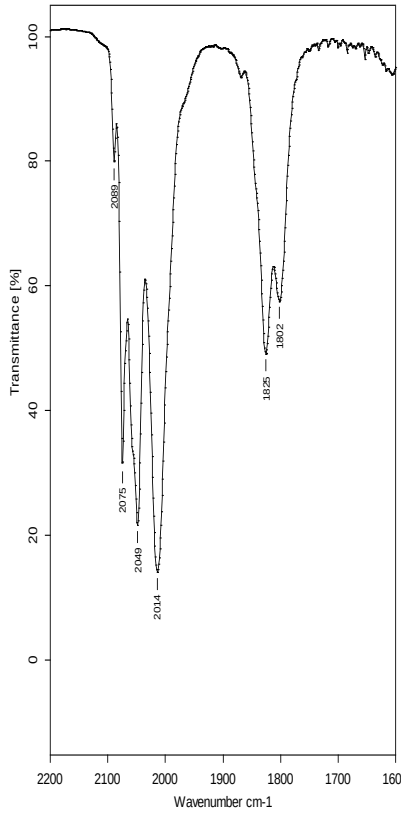

Figure 78 - IR spectrum in dichloromethane of $[Ir_4(CO)_{10}(dppa)_2]$

On the contrary, with t-dppethe ligand precipitation of $[\{Ir_4(CO)_{11}\}_2(t\text{-dppethe})]$ was not observed but anyway in the IR spectrum slowly appears a weak band at 1796 cm^{-1}, which can be attributed to the presence of a small amount of disubstituted species.

Finally, by conducting the reaction in dichloromethane with a 1:2 cluster/phosphane molar ratio, formation of the monosubstituted derivative $[Ir_4(CO)_{11}(P\text{-}P)]$ (ν_{CO}= 2087, 2055, 2018 cm^{-1} terminal COs and 1843, 1819 cm^{-1} bridging COs) is first observed. Then COs stretching bands slowly downshift, indicating a second substitution (ν_{CO}= 2065, 2038, 2002 cm^{-1} terminal CO and 1817, 1792 cm^{-1} bridging COs)(Figure 79).

$$[Ir_4(CO)_{11}Br]^- + 2\ P\text{-}P \longrightarrow [Ir_4(CO)_{10}(P\text{-}P)_2] + Br^- + CO$$

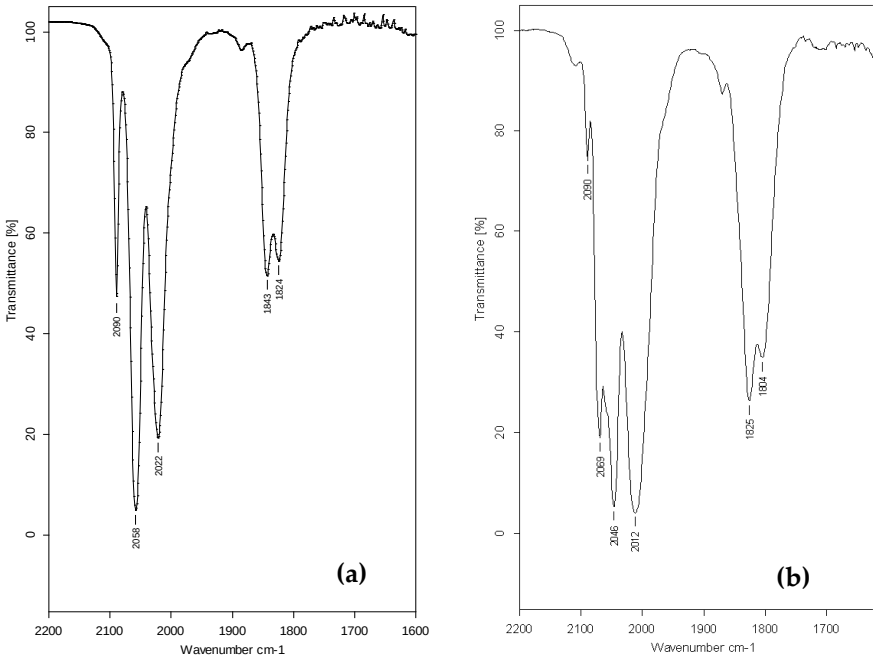

Figure 79 - IR spectra in dichloromethane of a) $[Ir_4(CO)_{11}(PP)]$ and b) $[Ir_4(CO)_{10}(PP)_2]$

3.1.1 Synthesis and characterization of [{Ir$_4$(CO)$_{11}$}$_2$(dppa)]

During the reaction of $[PPh_4][Ir_4Br(CO)_{11}]$ and dppa in acetonitrile 2:1 molar ratio an almost immediate precipitation of yellow microcrystalline powder of $[\{Ir_4(CO)_{11}\}_2(dppa)]$ occurs, insoluble in all the common organic solvents.

$$2[PPh_4][Ir_4Br(CO)_{11}] + dppa \longrightarrow [\{Ir_4(CO)_{11}\}_2(dppa)] + 2[PPh_4]Br$$

Crystals, suitable for X-ray diffraction, have been obtained for slow diffusion of a n-heptane solution of the ligand into a dichloromethane solution of the cluster.

3.1.2 Solid state structure of [{$Ir_4(CO)_{11}$}$_2$(dppa)]

The molecule consists of two $Ir_4(CO)_{11}$ tetrahedral cages linked by a dppa molecule. The conformation of the two clusters at the P-C≡C-P axis is *trans,* as the molecule lies on a crystallographic inversion centre.

Each cluster moiety terminally coordinates eleven CO molecules, Figure 80.

In the following **Table 5** some significant bond lengths are reported.

Bond	Å
Ir-Ir (average)	2,696
C-O (average)	1,136
Ir-P	2,299
C≡C	1,171

Table 5

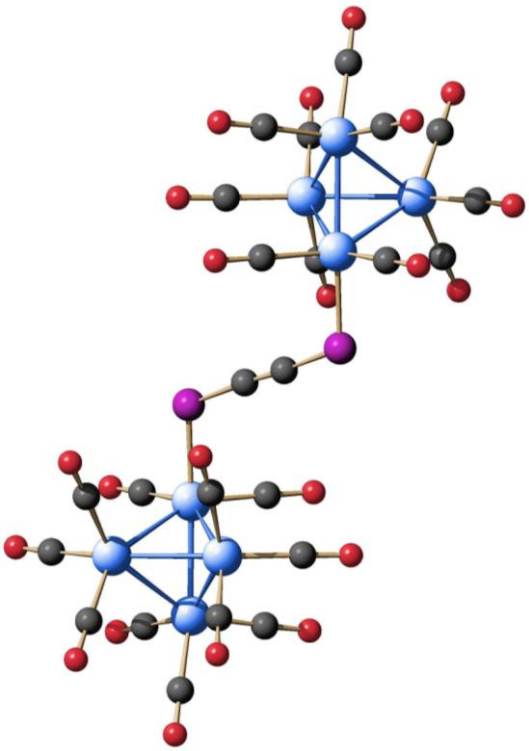

Figure 80 – The solid state structure of [{$Ir_4(CO)_{11}$}$_2$(dppa)]. Phenyl rings are omitted for clarity

ATR-IR spectra of the new derivative has been registered on a total attenuated reflectance spectrophotometer (Thermonicolet- Avatar 360 FT-IR- with Smart Endurance accesory). The experiment consists in deposing a small amount of sample on a ZnSe crystal, and applying a pression through a mechanic press. This IR spectra, more and more times registered on different crystals for which the elemental cell was checked, have given always the same result (Figure 81a). In this spectra two bands in the typical region of edge-bridging COs are present. Anyway, XRD analysis determined only the presence of terminal coordinated COs. Actually Nujol IR spectra shows only terminal COs stretching bands, Figure 81b).

This phenomenom allows us to suppose that the pressure applied to register the first spectrum causes a structural re-arrangment and some carbonyl ligands would change their coordination mode, from terminal to edge-bridging.

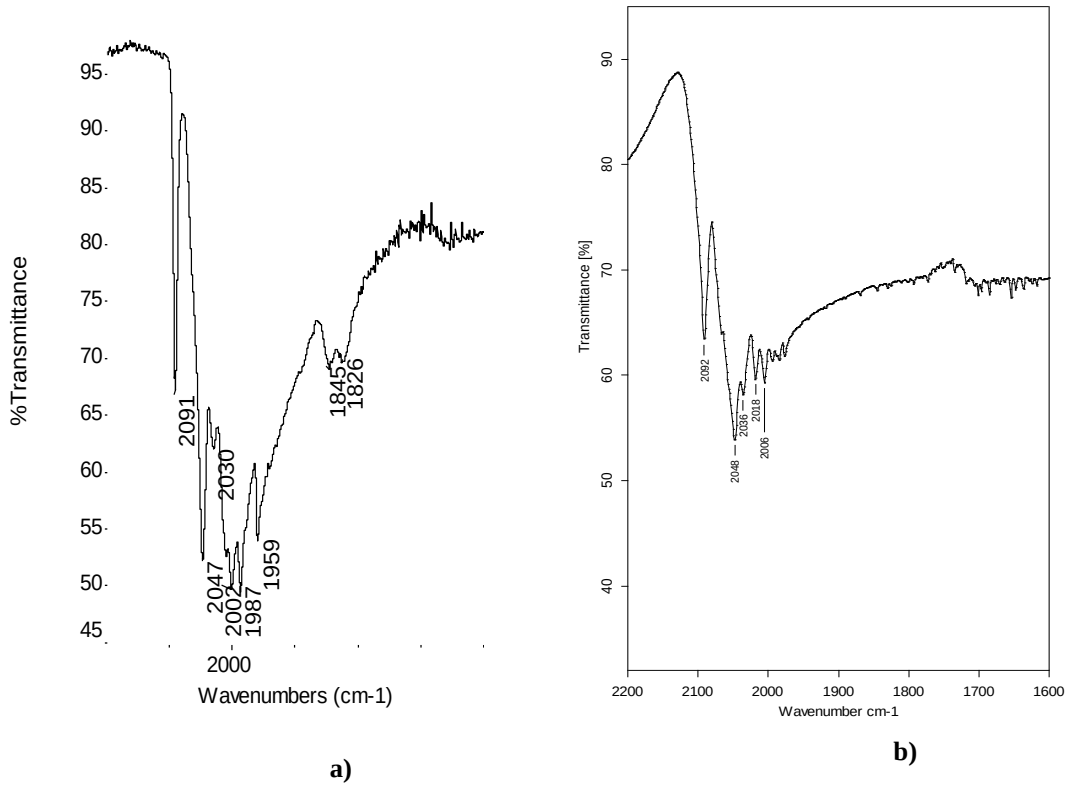

Figure 81 - a) ATR-IR spectrum and b) Nujol-IR of $[\{Ir_4(CO)_{11}\}_2(dppa)]$

3.1.3 Synthesis and characterization of [{Ir$_4$(CO)$_{11}$}$_2$(t-dppethe)]

By reacting [PPh$_4$][Ir$_4$Br(CO)$_{11}$] and *t*-dppethe in acetonitrile in 2:1 molar ratio a yellow microcristalline powder of [{Ir$_4$(CO)$_{11}$}$_2$(*t*-dppethe)] precipitates very quickly (yield 70%). This solid is insoluble in all common organic solvents.

$$2[PPh_4][Ir_4Br(CO)_{11}] + t\text{-dppethe} \longrightarrow [\{Ir_4(CO)_{11}\}_2(t\text{-dppethe})] + 2[PPh_4]Br$$

Crystals suitable for X.ray analysis have been obtained by reaction in dichloromethane and cooling the resulting solution at 4°C for some days.

This species has a low solubility in CH_2Cl_2. Anyway, with 38000 scansions, it has been possible to obtain a satisfaying ^{31}P-NMR spectrum (Figure 82) showing a singlet at -18,8 ppm.

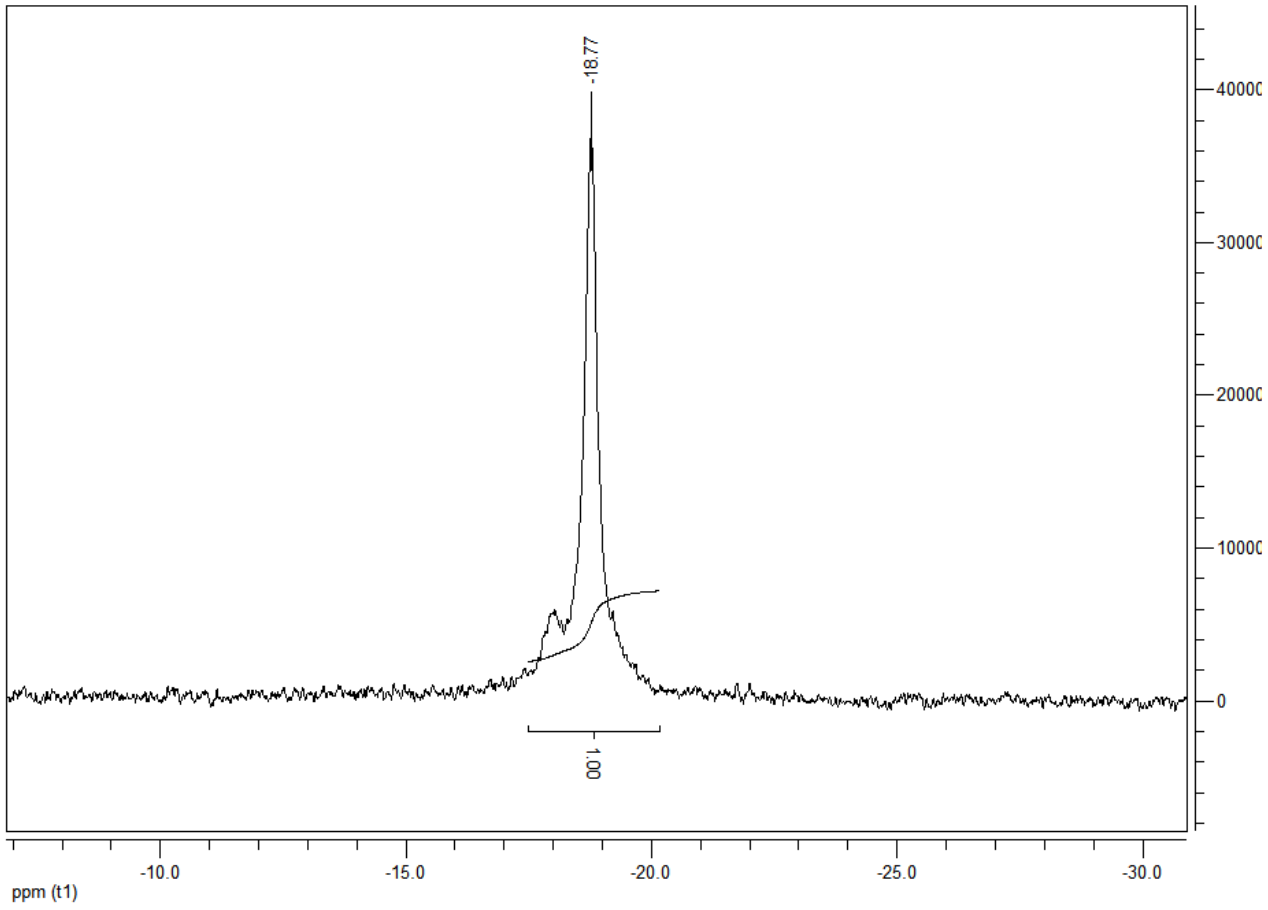

Figure 82 - ^{31}P-NMR in $CD_2Cl_2$of [{Ir$_4$(CO)$_{11}$}$_2$(*t*-dppethe)]

3.1.4 Solid state structure of [{Ir$_4$(CO)$_{11}$}$_2$(t-dppethe)]

The structure is analogous to that of [{Ir$_4$(CO)$_{11}$}$_2$(dppa)]: the molecule is constituted by two Ir$_4$(CO)$_{11}$ tetrahedral cages linked by a diphosphanoethylenic bridge. The conformation of the cages at the axe of the two phosphorous atoms is trans because the molecule lies on a inversion crystallographic centre. Each cluster unit coordinates eleven terminal COs: two for the iridium atom bonding the phosphorous and three for the others (Figure 83).

In the following **Table 6** some significant bond lenghts are reported:

Bond	[{Ir$_4$(CO)$_{11}$}$_2$(dppa)] Å	[{Ir$_4$(CO)$_{11}$}$_2$(*t*-dppethe)] Å
Ir-Ir (average)	2,696	2,691
C-O (average)	1,136	1,097
Ir-P	2,299	2,336
C≡C	1,171	-
C=C	-	1,319

Table 6

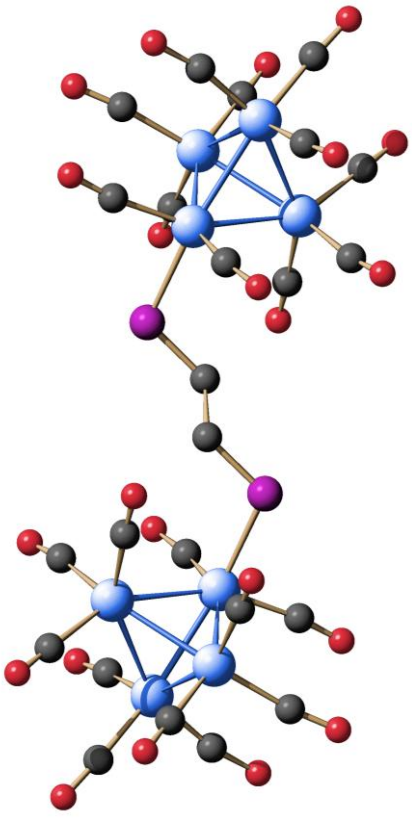

Figure 83 – The solid state structure of [{Ir$_4$(CO)11}$_2$(t-dppethe)]. Phenyl rings omitted for clarity

By collecting the IR spectra it has been observed the same phenomenon described for [{$Ir_4(CO)_{11}$}$_2$(dppa)]: in nujol-IR there are not bands for edge-bridging COs (**Figure 84a**), which are present in the ATR-IR registered under pressure (**Figure 84b**).

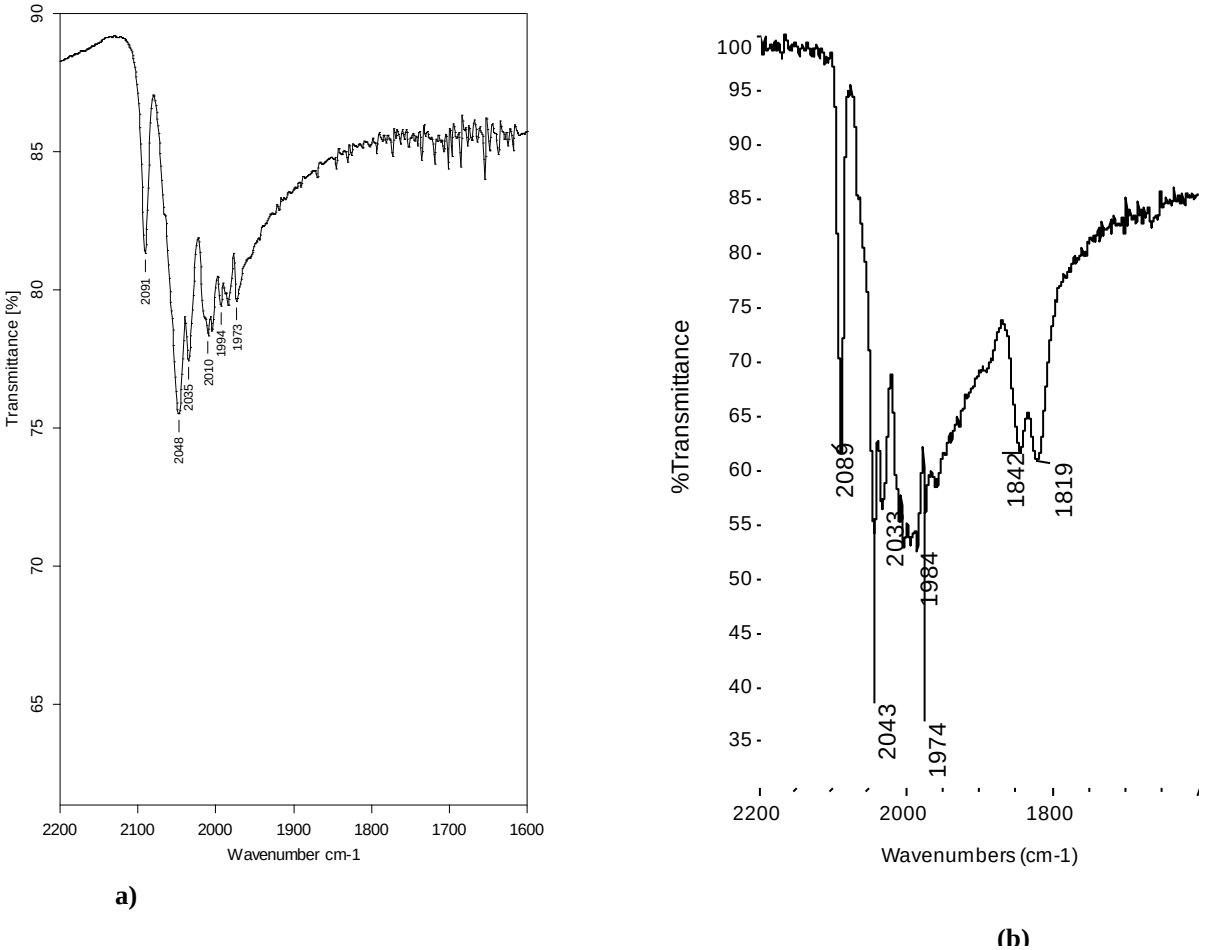

Figure 84 - a) Nujol-IR and b) ATR-IR of [{$Ir_4(CO)_{11}$}$_2$(*t*-dppethe)]

3.2 Reactivity of 1,4-bis(diphenylphosphano)butane (dppbut) and 1,6-bis(diphenylphosphano)hexane (dpphex) with $[Ir_4(CO)_{12}]$

3.2.1 Synthesis and solid state characterization of $[\{Ir_4(CO)_9(\mu\text{-dppbut})\}_2(dppbut)]$

This commercially available diphosphane (**Figure 85**) is flexible and rather short to be able both to chelate on the edge of a cluster and to link two cluster molecules.

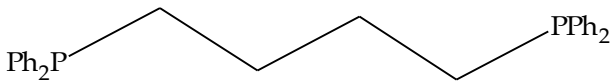

Figure 85 - dppbut

In literature the formation of a cyclic dimer starting from $[Rh_2Cl_2(CO)_2]$[225] is reported.
We used dppbut with $[Ir_4(CO)_{12}]$ in solvothermal condition and orange crystals of $[\{Ir_4(CO)_9(\mu\text{-dppbut})\}_2(dppbut)]$ were obtained (**Figure 86**).
Two Ir_4 clusters are joined by a radial-radial coordinated dppbut ligand. Each Ir_4 cluster is also chelated by another axial-axial coordinated diphosphane lying under the tetrahedron basal plane.

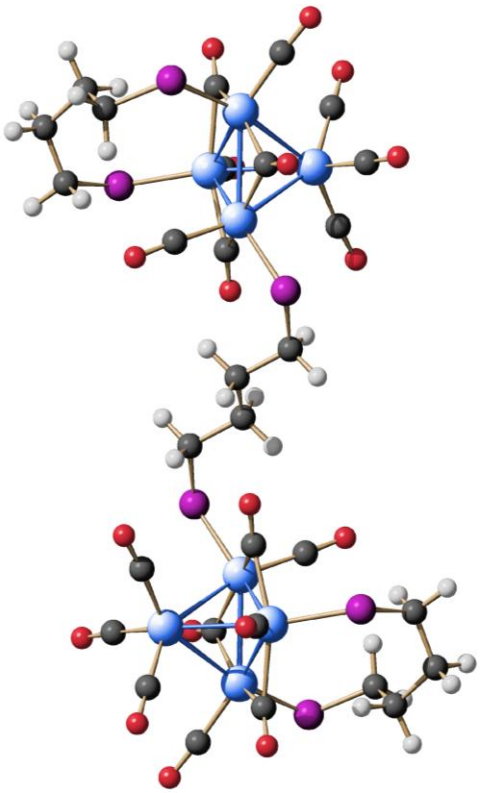

Figure 86 – The solid state structure of $[\{Ir_4(CO)_9(\mu\text{-dppbut})\}_2(dppbut)]$. Phenyl rings are omitted for clarity

3.2.2 Synthesis and solid state characterization of [{Ir4(CO)9}2(dpphex)3]

Solvothermal reaction of $[Ir_4(CO)_{12}]$ with dpphex (CH_2Cl_2/ n-heptane 1:2, T = 403 K, t = 16 h) gave yellow crystals of $[\{Ir_4(CO)_9\}_2(dpphex)_3 \bullet (CH_2Cl_2)]$, 51% yield.

ATR-IR spectrum shows carbonyl stretching bands at 2036(m), 1998(m), 1972(s), 1952(s) cm^{-1} (terminal COs) and 1774(s), 1760(vs) cm^{-1} (edge-bridged COs) (Figure 87).

Two $Ir_4(CO)_9$ cages are linked by three dpphex molecules, two radial-radial coordinated, with a P-P distance of 7,718 and 7,975 Å, and one axial-axial, with a P-P distance of 8,631 Å (Figure 88). So, each Ir_4 tetrahedron has two radially and one axially coordinated P atoms. Nine COs, three edge-bridged and six terminal, complete the coordination sphere at each cluster; a dichloromethane molecule is also chlatrated.

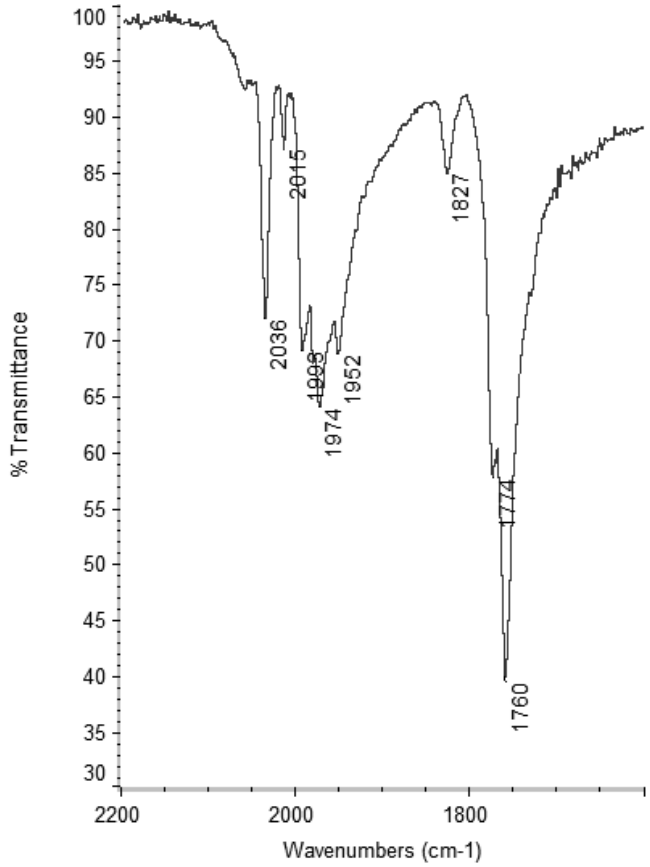

Figure 87 - ATR-IR spectrum of $[\{Ir_4(CO)_9\}_2(dpphex)_3]$

This new compound is closely related with the two others previously reported,[226] $\{[Ir_4(CO)_{11}]_2(dpphex)\}$ and $[Ir_4(CO)_{10}(dpphex)]_2$.

They can be considered as a series in which two Ir_4 cluster are linked by one, two, or three dpphex ligands. As the double linked cyclic dimer compound, also $[\{Ir_4(CO)_9\}_2(dpphex)_3 \bullet (CH_2Cl_2)]$ is sparingly soluble in all common solvents, preventing NMR or other in-solution studies.

In the following Table 7 some significant bond lengths are reported.

Bond	$[\{Ir_4(CO)_9\}_2(dpphex)_3]$ Å
Ir-Ir (average)	2,728
C-O (average)	1,153
Ir-P (average)	2,304

Table 7

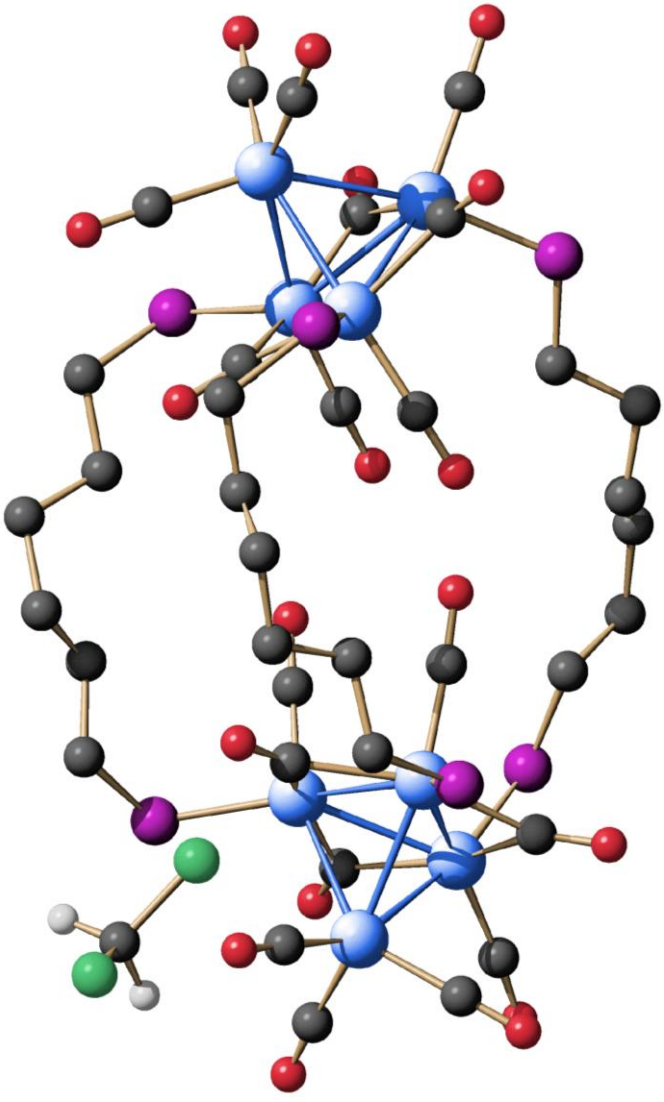

Figure 88 – The solid state structure of $[\{Ir_4(CO)_9\}_2(dpphex)_3 \bullet (CH_2Cl_2)]$. Phenyl groups are omitted for clarity.

3.3 Reactivity of 180tetraphos with $[Ir_4Br(CO)_{11}]^-$

3.3.1 Synthesis and characterization of [{Ir4(CO)11}4(180tetraphos)]

The reaction is performed dissolving the ligand in chloroform and adding to the resulting solution four equivalents of $[PPh_4][Ir_4Br(CO)_{11}]$. The starting orange solution turns to yellow as the reaction is completing.

$$4\ [PPh_4][Ir_4Br(CO)_{11}] + 180tetraphos \longrightarrow [\{Ir_4(CO)_{11}\}_4(180tetraphos)] + 4PPh_4Br$$

The reaction is followed by IR spectroscopy: in **Figure 89a** the carbonylic region of $[PPh_4][Ir_4Br(CO)_{11}]$ IR spectrum is reported, while in **Figure 89b** there is the final spectrum. A shift to higher wave numbers occurred, as we expect moving from an anionic to a neutral species.

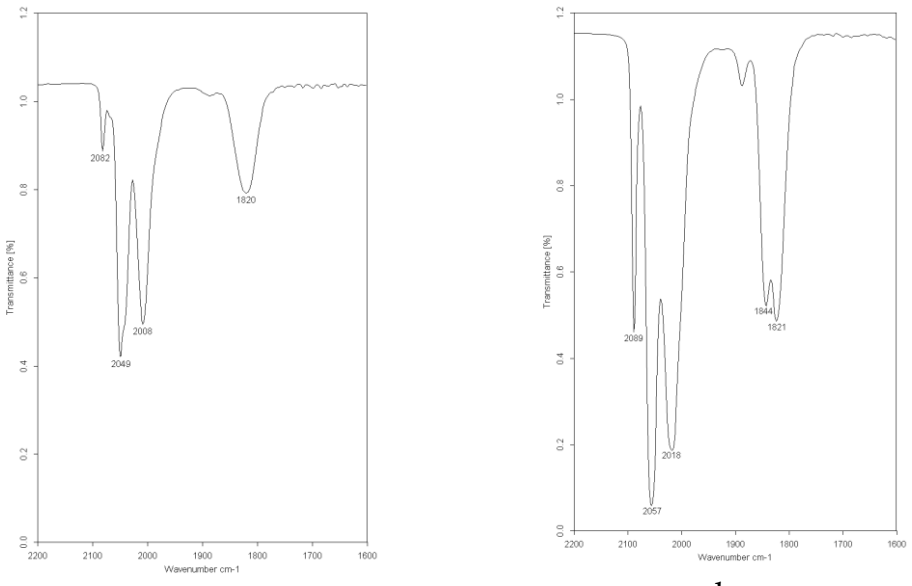

a b

Figure 89 - IR spectra in chloroform of a) $[PPh_4][Ir_4Br(CO)_{11}]^-$ and b) $[\{Ir_4(CO)_{11}\}_4(180tetraphos)]$

RT ^{31}P-NMR, registered in $CDCl_3$, is shown in Figure 90.

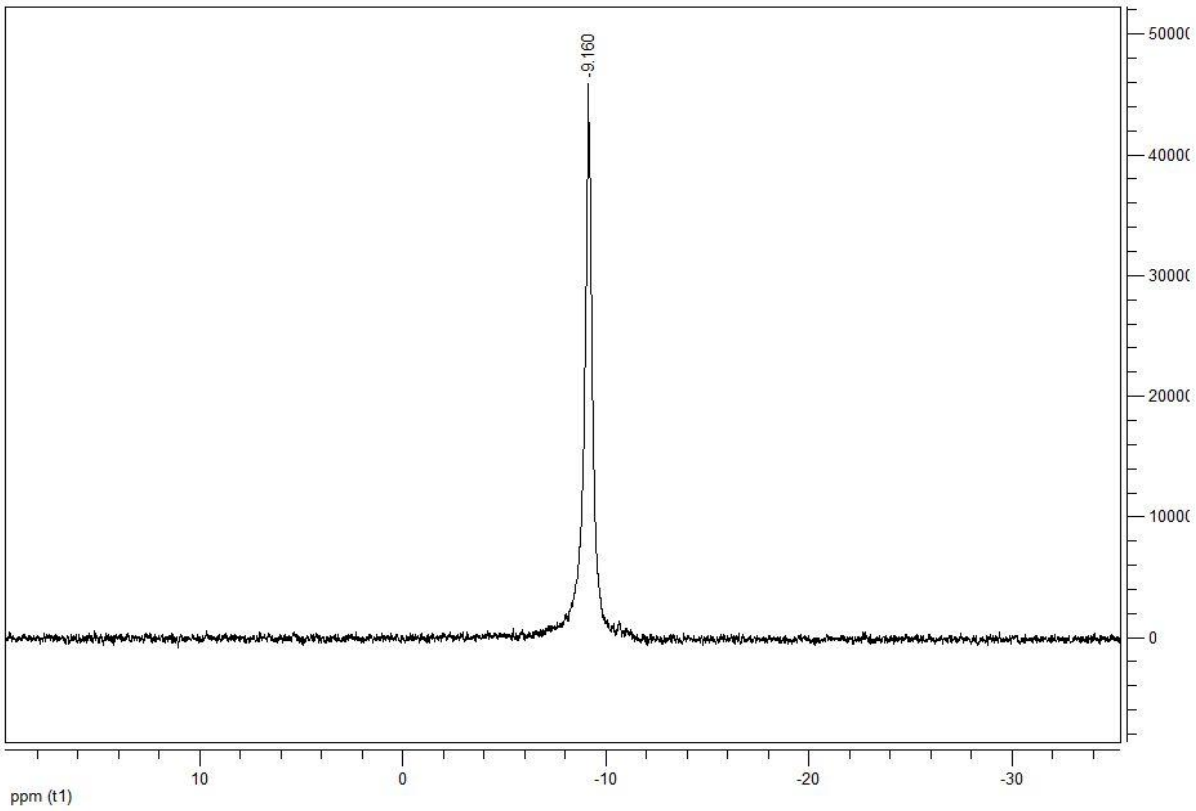

Figure 90 - ^{31}P-NMR in $CDCl_3$ of [{$Ir_4(CO)_{11}$}$_4$(180tetraphos)]

There is only one singlet at -9,16 ppm, while the free ligand chemical shift is -3,85 ppm. This means that all the phosphorus atoms have the same chemical environment. The chemical shift is in agreement with an axial coordination of the phosphane groups.

3.3.2 Solid state structure of [{$Ir_4(CO)_{11}$}$_4$(180tetraphos)]

The solid state structure was obtained from single crystals X-ray diffraction, Figure 91. The crystals were grown by layering a chloroform solution of the product with 2-propanol. It consists of four [$Ir_4(CO)_{11}$] fragments assembled through a 180tetraphos molecule. All the phosphane groups are axially coordinated and this is consistent with the ^{31}P-NMR spectrum, confirming that the structure in solution is the same than in solid.

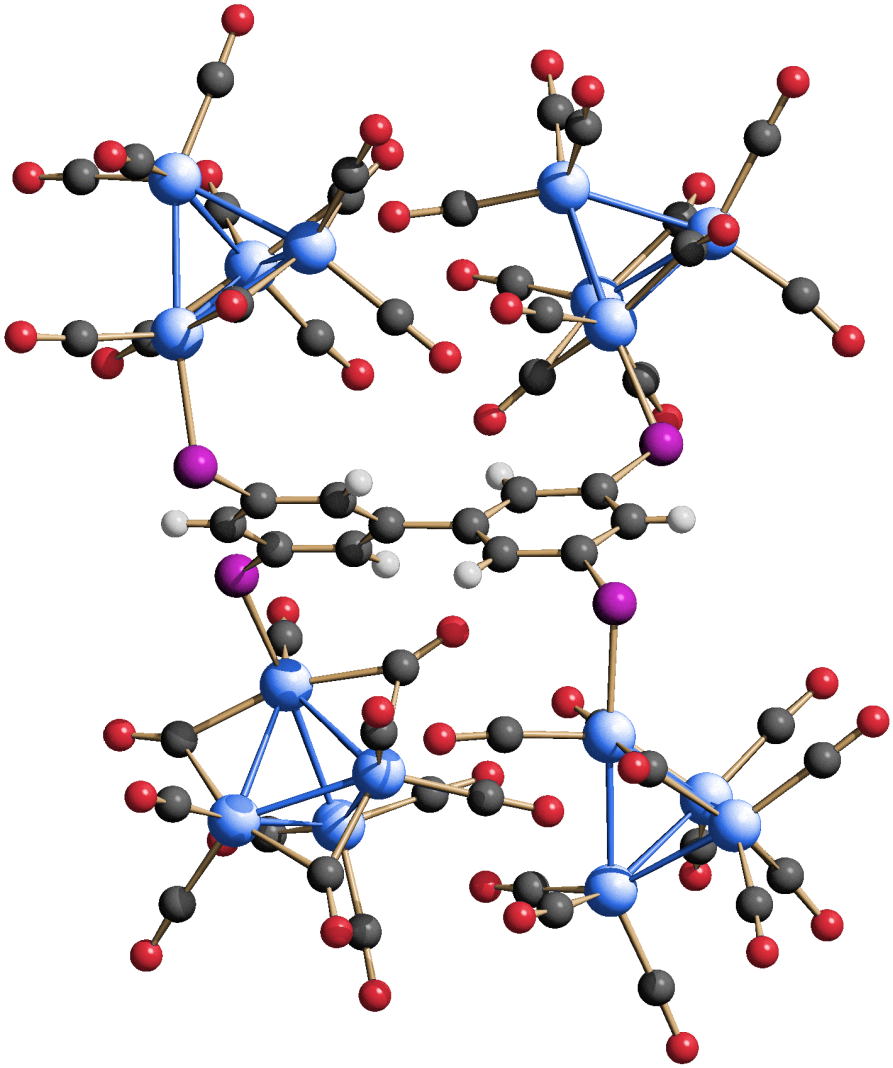

Figure 91 – The solid state structure of [{$Ir_4(CO)_{11}$}$_4$(180tetraphos)]

From Figure 92 it is possible to see how the four clusters are on the vertex of an irregular tetrahedrom. The distances among the metal atoms, excluding the coordinated CO spheres are included between 10,819 and 14,986 Å, so the molecule has nanometric size.

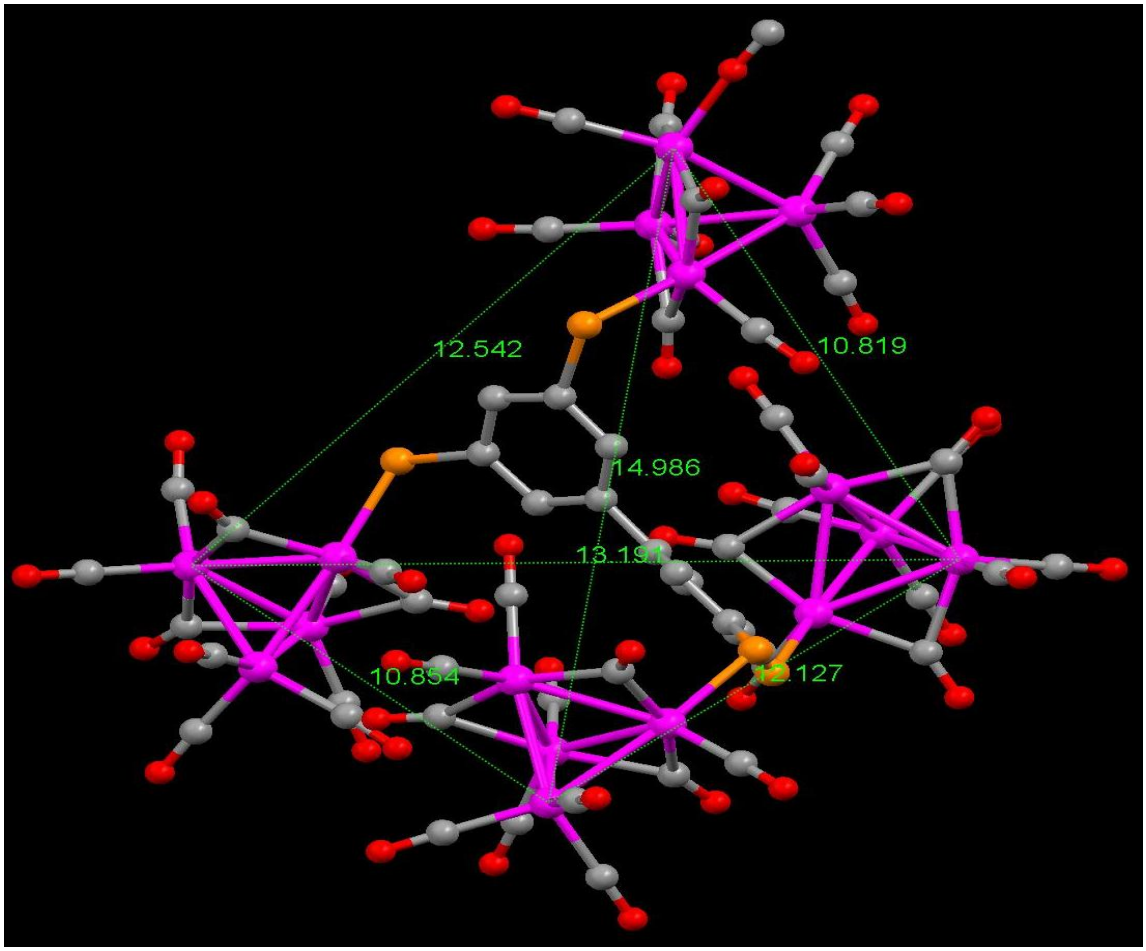

Figure 92 - Another view of [{$Ir_4(CO)_{11}$}$_4$(180tetraphos)]

3.3.3 Electrochemistry of [{$Ir_4(CO)_{11}$}$_4$(180tetraphos)]

An electrochemical study has been conducted on [{$Ir_4(CO)_{11}$}$_4$(180tetraphos)] (Figure 93). The compound exhibits an irreversible reduction at -1,37 V. After this process, the resulting species is adsorbed on the electrode and redox active breaking down products are formed. From the voltammetric profile it is evident that some of them give adsorbtion processes too.

During the electrolysis the solution gradually changes color, moving from yellow to dark red and the process appears to be multielectronic.

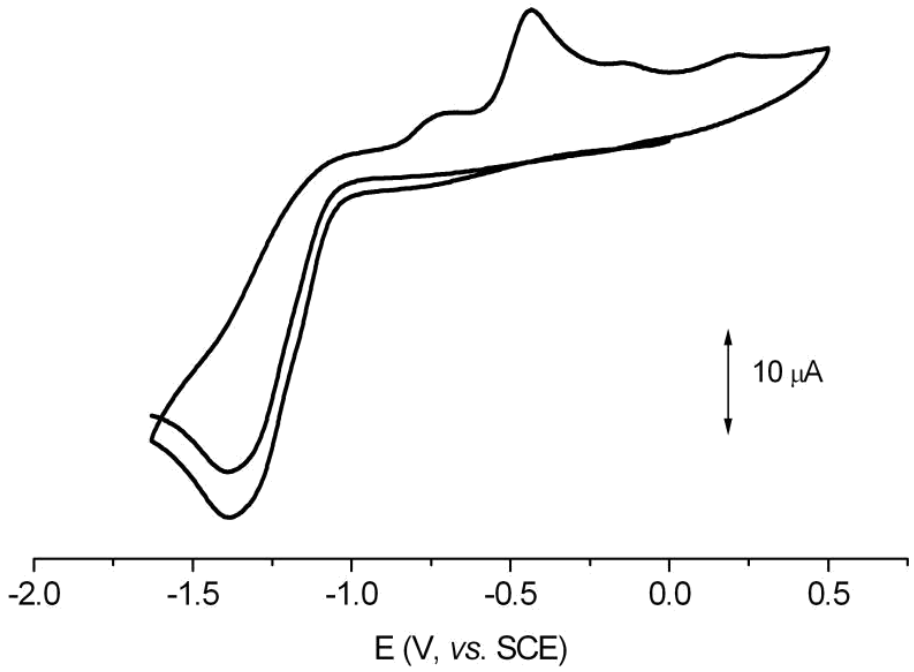

Figure 93 - Cyclic voltammetric responses recorded at a Pt electrode in THF solution of [{$Ir_4(CO)_{11}$}$_4$(180tetraphos)]. NBu_4PF_6 as supporting electrolyte.

4 - Reactions involving SnX_2 and SnX_3^- (X = Cl, Br)

4.0.1 Pt-Sn systems in catalysis

It is widespread known that an heterometallic system exhibits an higher catalytic activity and selectivity with respect to homometallic system containing a single metallic component. Catalysts having a single active component are quite an exception in industrial application, as usually more active different components are exploited.

Heterogeneous catalysis allows a better control of the particle intermetallic composition by using, as precursors, compounds which contain both the metals, like salts or heterometallic clusters.

A second advantage in using metal carbonyl clusters supported over inert carriers like as alumina, silica or magnesia derives from the possibility of preparing metal catalyst with an high dispersion grade. In fact it has been demonstrated that metal particles prepared starting from cluster compounds are smaller in size than ones prepared starting from inorganic salt solutions, offering an higher surface area. Finally, thanks to clusters, it is possible to produce particles with a thermodynamic forbidden intermetallic composition.

Pt-Sn based catalysts have given interesting results in oil reforming. Particularly, catalysts supported over Al_2O_3 have shown an high catalytic activity and stability, the former probably due to Pt, the latter to Sn. Different techniques (EXAFS, XPS, AES) are used in understanding if Pt and Sn are effectively present as alloy and which is its composition. An interesting study has been conducted on a Pt-Sn catalyst supported over $A1_2O_3$. It was prepared starting from the cluster $[Pt_3Sn_8Cl_{20}]^{4-}$, which contained both the metals (**Figure 94**).[227] Catalyst analyses reveal the presence of a Pt-Sn alloy.

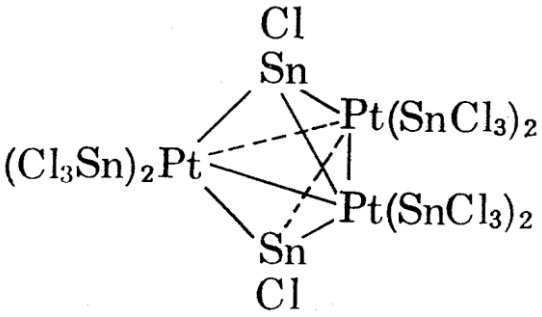

Figure 94 – Schematic structure of the cluster $[Pt_3Sn_8Cl_{20}]^{4-}$

In a previous work it has been studied the intermetallic composition of supported catalysts samples prepared starting from inorganic salts, by varying the preparation method, the supporting agent and the Pt:Sn ratio. Most of the phases have been Pt_3Sn for high Pt:Sn ratios, PtSn and Pt_2Sn_3 for intermediate ratios and $PtSn_4$ for low Pt:Sn ratios.[228] These results were the basis for a subsequent work. In fact, anionic clusters like $[Pt_8(SnX_2)_4(CO)_{10}]^{2-}$ (X = Br, Cl), $[Pt_{10}\{(SnCl_2)_2(OH)\}_2(CO)_{14}]^{2-}$ and $[Pt_6(SnX_2)_2(SnX_3)_4(CO)_6]^{4-}$ (X = Br, Cl) (*vide infra*) have an intermetallic Pt:Sn ratio equal to 1:0,5; 1:0,4; 1:1, lying in the intermetallic interval ratio previously shown. This make them particularly interesting as precursors for catalysts.

In the field of homogeneous catalysis, Pt-Sn system has been used in the selective hydrogenation reaction of conjugate dienes, of polyenes and activated mono-enes.

A typical example is represented by the compound *trans*-$[Pt(SnCl_3)H(PPh_3)_2]$ which catalyses the hydrogenation of hepta-1,5-dyene to 1-heptene with 91% selectivity.[229]

Pt-Sn system has found large application in hydroformilation reaction as well. In the absence of $SnC1_2$, Pt complexes containing tertiary phosphanes do not show any catalytic activity. On the contrary, when $SnC1_2$ is added to the system, a very active and selective catalyst is obtained. For a 1:5 $PtCl_2/SnCl_2$ molar ratio mixture, (T= 70°C, P= 100 atm, CO/H_2 = 1/1), a 100% conversion of 1-heptene is obtained, while the selectivity to octanale is 85%.[230] $[PtH(SnCl_3)(CO)(PPh_3)]$ or $[PtCl(SnCl_3)(PPh_3)_2]$ are supposed to be the catalytic active species.[231] An hydroformilation catalytic cycle, involving this complex, is shown in **Figure 95**.

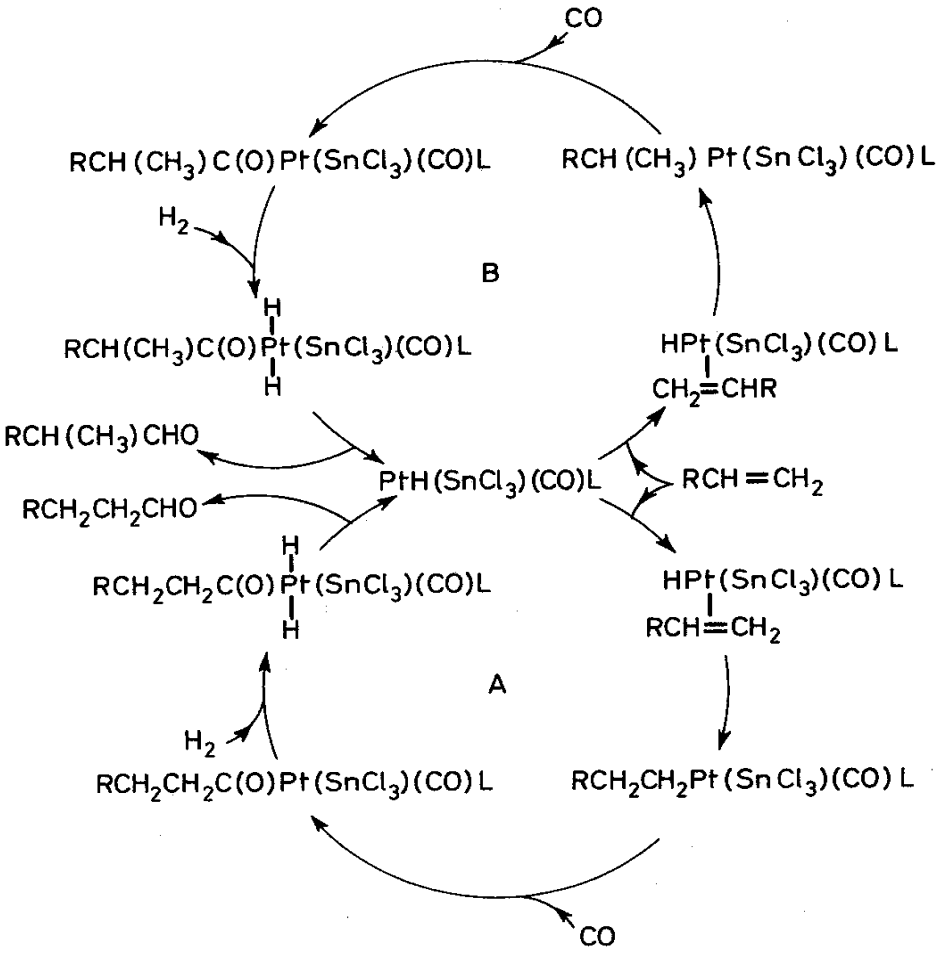

Figure 95 - Hydroformilation catalytic cycle involving $[PtH(SnCl_3)(CO)(PPh_3)]$

A very active system for catalysing the water-gas-shift reaction

$$CO + H_2O \rightarrow CO_2 + H_2$$

is constituted by K_2PtCl_4 and $SnCl_4$ in acetic acid as solvent. In such conditions different active species have been detected, like as $[PtCl(CO)(SnCl_3)_2]^-$ and $[PtCl_2(CO)(SnCl_3)]$.[232]

4.0.2 SnX_n (X = Cl, Br , I; n = 1-3) ligands in coordination chemistry

During the studies on platinum carbonyl clusters stabilized by tin based ligands, it has been observed that the reaction between carbonyl clusters of general formula $[Pt_3(CO)_6]_n^{2-}$ (n=2-5) and Sn halide leads to the formation of different compounds like:
$[Pt_8(SnCl_2)_4(CO)_{10}]^{2-}$, $[Pt_{10}\{(SnCl_2)_2(OH)\}_2(CO)_{14}]^{2-}$, $[Pt_6(SnCl_2)_2(SnCl_3)_4(CO)_6]^{4-}$, $[Pt_5\{(SnCl_2)_2(O\text{-}i\text{-}C_3H_7)\}_3(CO)_5]^{3-}$.
Within them the platinum metal core is stabilized by COs and monodentate ligands η^1–μ_4-$SnCl_2$ and η^1–μ_n-$SnCl_3$ (n = 2, 3), or by bidentate ligands like η^2–μ_6-$(SnCl_2)_2(OR)$ (R=H, *i*-C_3H_7). In the latter case the ligands chelates triangle faces of the Pt cluster.
It is worth observing that ligands like SnX_n (X=Cl, Br, I; n = 1, 2, 3) are well known in the field of coordination chemistry. They play an important role in catalytic reaction, as their high trans-labilizing effect promotes migrating insertion reactions besides the formation of vacant coordination sites, a basic stadium in all catalytic cycles.
Sn(II) compounds, alkyl/aryl Sn(II) (SnR_2, R = alkyl, aryl) or dihalo-Sn(II) (SnX_2, X = halide) are all carbene-like ligands, having a non-bonding electron pair. So they could act both as σ donors and, at the same time, as π acceptors, having empty *p* or *d* orbitals at low energy with an appropriate geometry. The fragile balance between these two limit situation is governed by the electronegativity of the Sn substituent (R, X) and by the donor-acceptor capability of the transition metal where the tin fragment is coordinated.
SnX_2 compopunds are Lewis acid, but they are able to easily convert in the corresponding Lewis base $[SnX_3]^-$ by adding X^- ion, according to the equilibrium reaction:

$$SnX_2 + X^- \rightleftharpoons [SnX_3]^-$$

A subsequent acid-base condensation between two different tin compounds may occurs, see for example:

$$SnX_2 + [SnX_3]^- \rightarrow [Sn_2X_5]^-$$

The resulting anion is a potential three electron-bidentate ligand which, under particular conditions, is able to chelate. Anyhow this anion, which may be present in solution, it has been never observed in our isolated and characterized Pt-Sn clusters. For example, in the

case of the anions $[Pt_6(SnX_2)_2(SnX_3)_4(CO)_6]^{4-}$ (X = Br, Cl), SnX_2 e $[SnX_3]^-$ are simultaneously present and their condensation giving the chelant $[Sn_2X_5]^-$ does not occur.

The use of ligands like SnX_n (X=Cl, Br, I; n = 1, 2, 3) in the cluster chemistry also allows to study of the mechanism of M-SnX_3 ligand formation. This mechanism could at first involve the insertion of SnX_2 fragment inside a M-M ligand with the consequent formation of a M-Sn(X_2)-M interaction. This is followed by an X transfer, yet coordinated on the cluster, forming the M-SnX_3 bond.

The insertion of $SnCl_2$ groups inside M-M bonds of low metal nuclearity is well known. Significant examples are the adducts $[(Ph_3P)(CO)_3Co\text{-}Sn(Cl_2)\text{-}Co(CO)_3(PPh_3)]$ [233] and $[(Me_3P)_3ClRh\text{-}Sn(Cl_2)\text{-}RhCl(PMe_3)_3]$.[234]

In the Rh compound $SnCl_2$ group inserts into the M-M bond instead of M-Cl bond.

The insertion of $SnCl_2$ inside M-M bond has been found in the Pt carbonyl clusters too. A chlorine atoms rearrangement according to the scheme:

$$2\,SnCl_2 \rightarrow [SnCl_3]^- + [SnCl]^+$$

has been found in the compound $[Os_3Pt(SnClOEt_2)(\mu\text{-}H)_2(SnCl_3)(PCy_3)(CO)_{10}]$, where one $SnCl_3$ group is terminally bonded and one SnCl groups is quadruple bridging.[235]

Such a kind of halide atoms rearrangement has not been yet found in Pt-Sn carbonyl clusters, as there is no evidence of the contemporaneous presence of SnX and SnX_3^- fragments on the cluster surface.

4.1 $[Pt_6(SnCl_2)_2(SnCl_3)_4(CO)_6]^{4-}$

4.1.1 - Synthesis of the tetranion $[Pt_6(SnCl_2)_2(SnCl_3)_4(CO)_6]^{4-}$

It was deeply investigated the reactivity of the anion $[Pt_6(SnCl_2)_2(SnCl_3)_4(CO)_6]^{4-}$ towards nucleophile agents with the aim of:

a) Observing possible structural rearrangements of the metal skeleton, as a consequence of ligand substitution or addition,

b) Finding preferential attack points on the metal cluster,

c) Studying possible coordination variations of the yet bonded ligands.

At first the synthesis of the tetranion has been optimized.
This anion has been prepared in high yield (79 % based on Pt) starting from an acetone solution of $[PPh_4]_2[Pt_{15}(CO)_{30}]$ and $SnCl_2$ with $[PPh_4]Cl$ added at the same time. The molar ratios were Pt_{15} : $SnCl_2$: $[PPh_4]Cl$ = 1 : 15 : 10, in order to reproduce the same Pt : Sn : Cl molar ratio present in the tetranion. The reaction occurs at room temperature and needs for some hours to complete. The $[PPh_4]_4[Pt_6(SnCl_2)_2(SnCl_3)_4(CO)_6]$ salt is present as an abundant precipitate, whereas the surnatant brown solution contains an unknown products showing a single IR carbonyl stretching band at 2025(s) cm^{-1}.
The different Pt oxidation states in the starting dianion (-0,133) and in the final tetranion (0) are very likely the origin of a concomitant reduction from Sn(II) to Sn(0), suggesting the following stoichiometry:

$$[Pt_{15}(CO)_{30}]^{2-} + 16\,SnCl_2 + 8\,Cl^- \rightarrow 2{,}5\,[Pt_6(SnCl_2)_2(SnCl_3)_4(CO)_6]^{4-} + Sn + 15\,CO$$

The tetranion salts are well soluble in acetonitrile, with a shining green colour and a single IR carbonyl stretching band at 2037(s) cm^{-1} **(Figure 96).** Crystals suitable for X-ray analysis can be obtained by slow diffusion of di-isopropylic ether layered on an acetonitrile solution of the product.

The high yield permitted the synthesis of enough sample for a carefull reactivity study of the species. ^{195}Pt NMR spectrum, collected in CD_3CN solution at – 30°C shows a single peak at δ_{Pt}= - 4514 ppm, where any spin coupling were identified.
It is worth underlining that, with the same synthetic strategy, is possible to obtain the anion $[Pt_6(SnBr_2)_2(SnBr_3)_4(CO)_6]^{4-}$ in high yield.

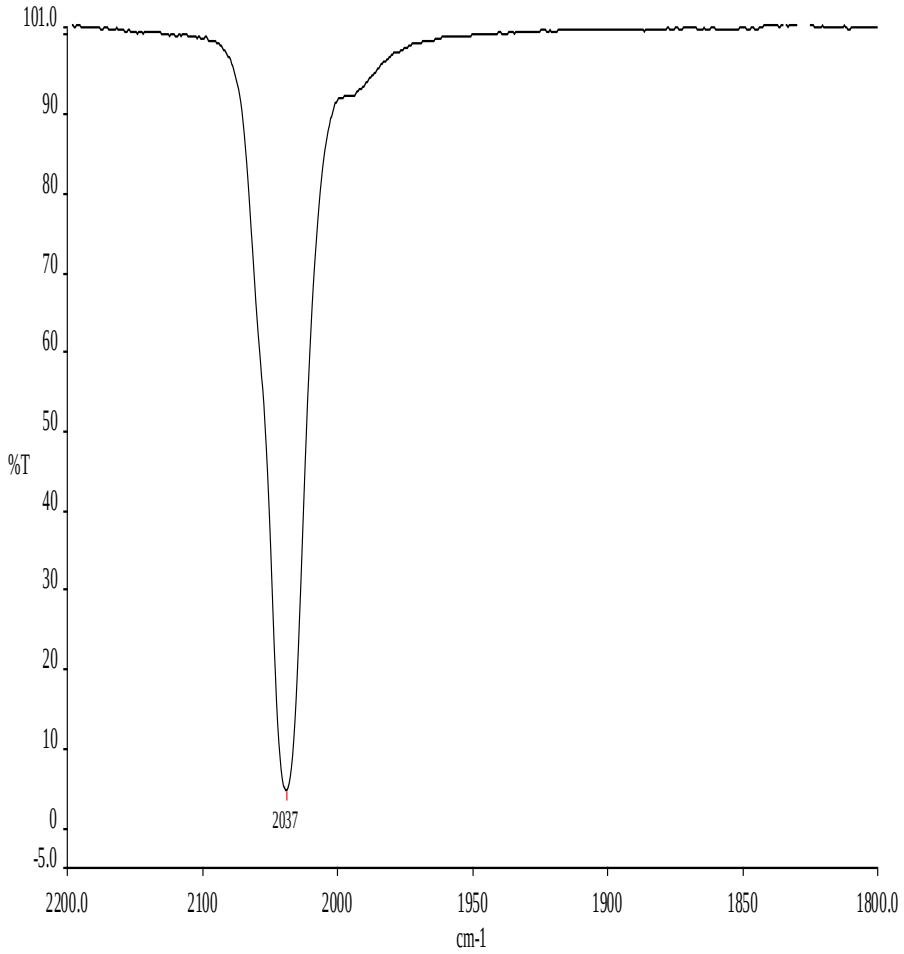

Figure 96 - IR spectrum in acetonitrile of $[Pt_6(SnCl_2)_2(SnCl_3)_4(CO)_6]^{4-}$

The structure of the tetranion is shown in **Figure 97.**
The 84 CVE cluster shows a metallic skeleton formed by two edge-shared tetrahedra and it is stabilized by terminal or edge-bridging carbonyls and by halo-tin fragments of different kinds. Two μ_4-$SnCl_2$ monodentate ligands find place in two butterfly concave surfaces of the cluster, while four μ_2-$SnCl_3$ ligands complete the coordination sphere edge- or triple-bridging Pt-Pt bonds or faces.

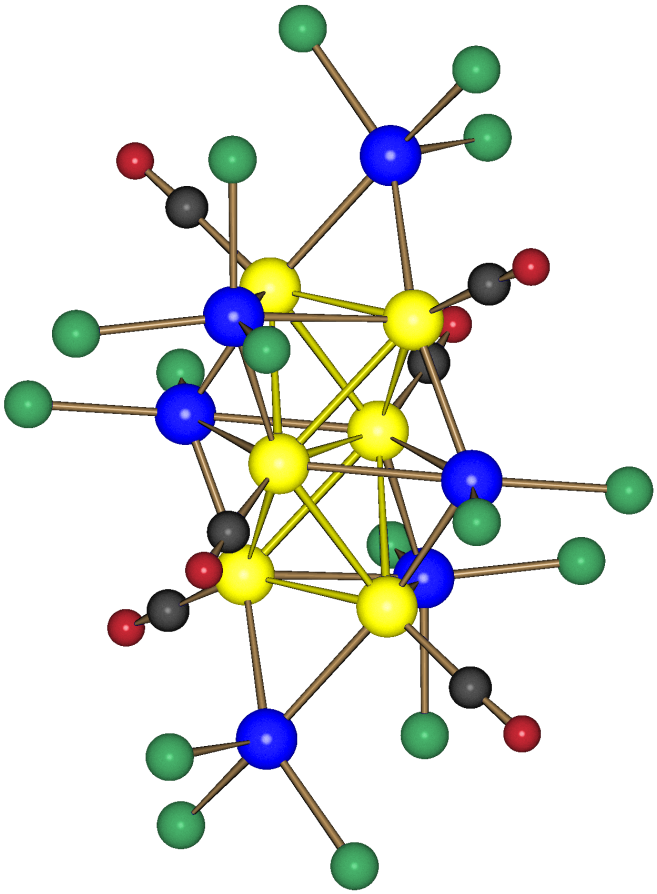

Figure 97 The solid state structure of $[Pt_6(SnCl_2)_2(SnCl_3)_4(CO)_6]^{4-}$

4.1.2 - Reactivity of the tetranion $[Pt_6(SnCl_2)_2(SnCl_3)_4(CO)_6]^{4-}$

At first it was investigated the anion coordinating capability towards functionalized alkenes and alkines. The compound is substantially inert with diphenylacetylene, while it showed a scarse reactivity with chloride or bromide allyl.

More interesting results were obtained during reactivity studies with CO and $P(C_6H_5)_3$, and a relevant series of compounds have been identified, leading to the synthesis and characterization of new platinum heteroleptyc carbonyl clusters.

4.1.3 - Synthesis and spectroscopic characterization of the hyphotethic anion $[Pt_6(SnCl_2)_2(SnCl_3)_2(CO)_6\{P(C_6H_5)_3\}_2]^{2-}$

The anion $[Pt_6(SnCl_2)_2(SnCl_3)_4(CO)_6]^{4-}$, dissolved in acetonitrile as $[PPh_4]^+$ salt, showed to be reactive towards CO and other nucleophiles, inducing substitution reaction of the coordinated ligands.

Particularly, the reaction between $[Pt_6(SnCl_2)_2(SnCl_3)_4(CO)_6]^{4-}$ and $P(C_6H_5)_3$ in Pt_6 : P = 1 : 2 molar ratio gave rise to a new compound which was isolated and partially characterized by elemental analysis (

Table 8), IR and NMR spectroscopy**.** Analytical data suggest the substitution of two $SnCl_3^-$ ligands by two phosphane ligands, with the consequent decreasing of the negative charge on the cluster by two units. This anion, under CO atmosphere converts into the anion $[Pt_6(SnCl_2)(SnCl_3)_2(CO)_8\{P(C_6H_5)_3\}_2]^{2-}$; the latter can be prepared by inverting the order of the reagents, so first carbonylation and then $P(C_6H_5)_3$ addition , passing through the anion $[Pt_6(SnCl_2)(SnCl_3)_4(CO)_8]^{4-}$. All these facts make possible to formulate the species as $[Pt_6(SnCl_2)_2(SnCl_3)_2(CO)_6\{P(C_6H_5)_3\}_2]^{2-}$.

So, the probable stoichiometry of the reaction is the following:

$$[Pt_6(SnCl_2)_2(SnCl_3)_4(CO)_6]^{4-} + 2\,P(C_6H_5)_3 \rightarrow [Pt_6(SnCl_2)_2(SnCl_3)_2(CO)_6\{P(C_6H_5)_3\}_2]^{2-} + 2\,SnCl_3^-$$

	Calculated	**Found**
C %	32,08	33,78
H %	2,08	2,59

Table 8 - Elemental analysis of $[PPh_4]_2[Pt_6(SnCl_2)_2(SnCl_3)_2(CO)_6\{P(C_6H_5)_3\}_2]$

Different efforts for growing crystals suitable for X-ray analysis were unsuccessfull. It has been used the classical technique of the slow diffusion of a precipitating solvent in a solution of the compound. Acetonitrile and acetone as solvents with diisopropylic ether and 2-propanol as precipitating agents were tried.

IR spectrum of the compound dissolved in acetonitrile shows carbonyl stretching bands at 2031(s), 2013(m), 1813(m) cm^{-1}, so the anion bears both terminal and edge bridging COs (**Figure 98**).

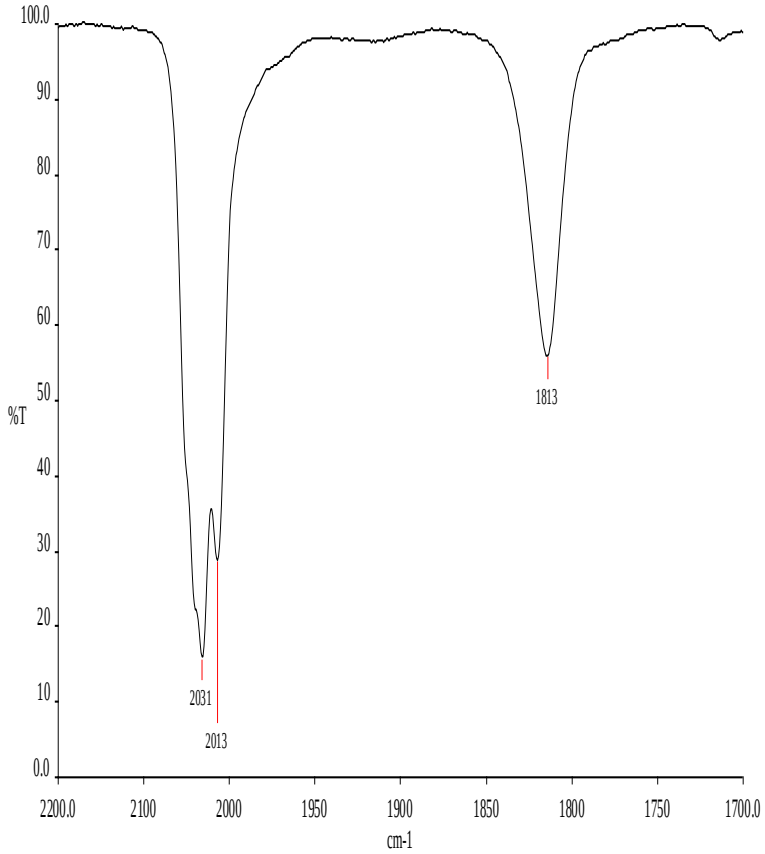

Figure 98 - IR spectrum in acetonitrile of $[Pt_6(SnCl_2)_2(SnCl_3)_2(CO)_6\{P(C_6H_5)_3\}_2]^{2-}$

^{195}Pt NMR spectrum, collected in CD_3CN solution at a – 30 °C, shows a single peak at δ_{Pt} = - 4100 ppm, without any spin coupling. ^{31}P NMR spectrum, collected in the same condition, shows a single peak at δ_P = 38,41 ppm, where spin coupling are present between heteronucleous: $^1J(^{31}P - ^{195}Pt)$ = 5564Hz, $^2J(^{31}P - ^{195}Pt)$ = 259Hz. Instead, in solution of C_3D_6O at – 30° C, two signals have been identified: δ_P = 38,41 ppm, $^1J(^{31}P - ^{195}Pt)$ = 5564 Hz, $^2J(^{31}P - ^{195}Pt)$=259Hz; δ_p = 28,53 ppm, $^1J(^{31}P - ^{195}Pt)$=3020Hz.

4.1.4 - Synthesis and spectroscopic characterization of the anion $[Pt_6(SnCl_2)(SnCl_3)_2(CO)_8\{P(C_6H_5)_3\}_2]^{2-}$

The anion discussed in the previous paragraph, dissolved in acetonitrile as $[PPh_4]^+$ salt, coverted in a new compound when exposed to CO atmosphere (P = 1 atm), which was isolated and completely characterized.

Single crystal X-ray diffraction permitted to formulate the compound as $[PPh_4]_2[Pt_6(SnCl_2)(SnCl_3)_2(CO)_8\{P(C_6H_5)_3\}_2]$.

The synthesis of this anion is supposed to happen through the elimination of one $SnCl_2$ ligand and the contemporaneous addition of two CO ligands, according to the following scheme:

$$[Pt_6(SnCl_2)_2(SnCl_3)_2(CO)_6\{P(C_6H_5)_3\}_2]^{2-} + 2\,CO \rightarrow [Pt_6(SnCl_2)(SnCl_3)_2(CO)_8\{P(C_6H_5)_3\}_2]^{2-} + SnCl_2$$

The global stoichiometry starting from the anion $[Pt_6(SnCl_2)_2(SnCl_3)_4(CO)_6]^{4-}$ becomes:

$$[Pt_6(SnCl_2)_2(SnCl_3)_4(CO)_6]^{4-} + 2\,P(C_6H_5)_3 + 2\,CO \rightarrow [Pt_6(SnCl_2)(SnCl_3)_2(CO)_8\{P(C_6H_5)_3\}_2]^{2-} + 2\,SnCl_3^- + SnCl_2$$

The whole reaction can be divided into two steps:

- a first stadium in which the substitution of two $SnCl_3^-$ ligands by two $P(C_6H_5)_3$ ligands occurs. The resulting cluster is isoelectronic with the starting tetranion, but the negative charge is decreased by two units;
- a second stadium in which one $SnCl_2$ ligand is eliminated and at the same time two COs are added, so obtaining a cluster with 2 valence electrons more and same negative charge.

The cluster $[Pt_6(SnCl_2)(SnCl_3)_2(CO)_8\{P(C_6H_5)_3\}_2]^{2-}$ was isolated in the solid state and characterized by elemental analysis (

Table 9), IR and NMR spectroscopy.

	Calculated	**Found**
C %	34,13	31,71
H %	2,16	2,61

Table 9 - Elemental analysis of $[PPh_4]_2[Pt_6(SnCl_2)(SnCl_3)_2(CO)_8\{P(C_6H_5)_3\}_2]$

Crystals suitable for X-ray diffraction were obtained by slow diffusion of 2-propanol layered on an acetone solution of $[PPh_4]_2[Pt_6(SnCl_2)(SnCl_3)_2(CO)_8\{P(C_6H_5)_3\}_2]$.

Also in this case IR spectrum in acetonitrile as solvent shows in the carbonyl stretching region the presence of both terminal COs, at 2042(s) cm^{-1} and edge-bridged COs at 1881(w), 1829(m) cm^{-1} (**Figure 99**).

^{195}Pt NMR spectrum, collected in CD_3CN solution at -30 °C, shows one peak at δ_{Pt} = - 4208 ppm, while ^{31}P NMR spectrum, collected in C_3D_6O solution at – 30° C, shows two signals at δ_P = 31,44 ppm, $^1J(^{31}P - ^{195}Pt)$ = 5362 Hz, $^2J(^{31}P - ^{195}Pt)$ = 343 Hz and δ_P = 19,62 ppm, $^1J(^{31}P-^{195}Pt)$ = 2051 Hz.

It is interesting to emphasize that this anion can be prepared in one step, dissolving the $[Pt_6(SnCl_2)_2(SnCl_3)_4(CO)_6]^{4-}$ anion in acetonitrile under CO atmosphere (P = 1 atm) and adding $P(C_6H_5)_3$ in 1:2 molar ratio. So, this synthesis does not require for the isolation of the intermediate anion $[Pt_6(SnCl_2)_2(SnCl_3)_2(CO)_6\{P(C_6H_5)_3\}_2]^{2-}$.

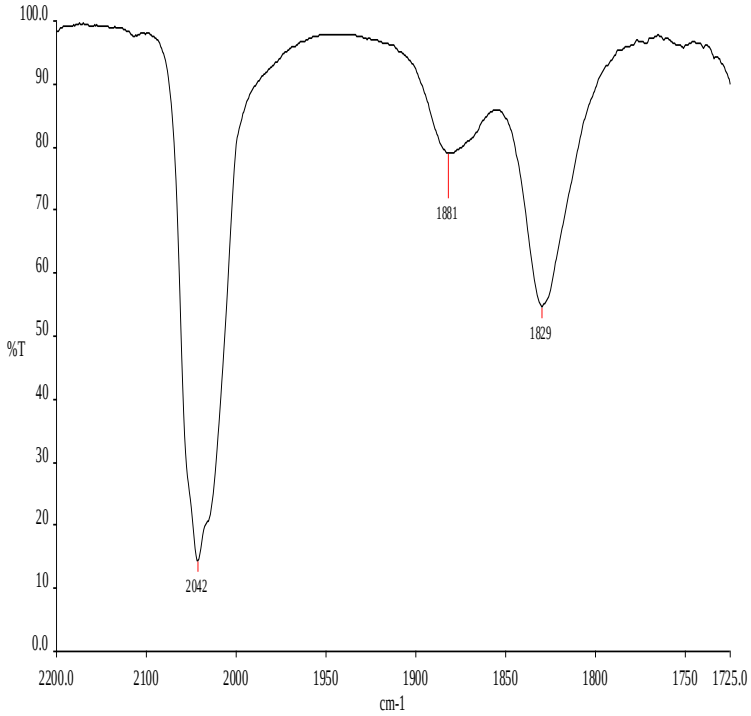

Figure 99 - IR spectrum inacetonitrile of $[Pt_6(SnCl_2)(SnCl_3)_2(CO)_8\{P(C_6H_5)_3\}_2]^{2-}$

4.1.5– Solid state structure of the anion $[Pt_6(SnCl_2)(SnCl_3)_2(CO)_8\{P(C_6H_5)_3\}_2]^{2-}$

The molecular geometry of the anion $[Pt_6(SnCl_2)(SnCl_3)_2(CO)_8\{P(C_6H_5)_3\}_2]^{2-}$ was determined by single crystal X-ray diffraction of the species as PPh_4^+ salt.

Figure 100 shows the whole structure of the anion, while the metallic skeleton formed by six platinum atoms is shown in **Figure 101**.

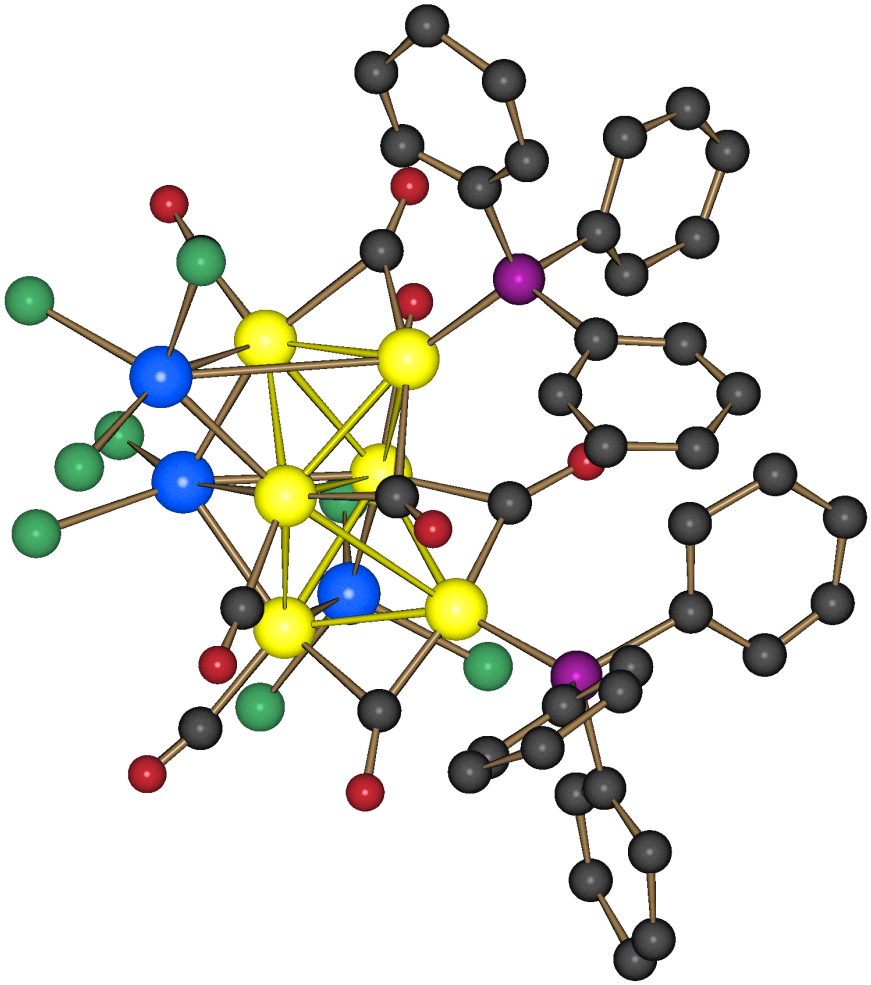

Figure 100 – The solid state structure of the anion $[Pt_6(SnCl_2)(SnCl_3)_2(CO)_8\{P(C_6H_5)_3\}_2]^{2-}$

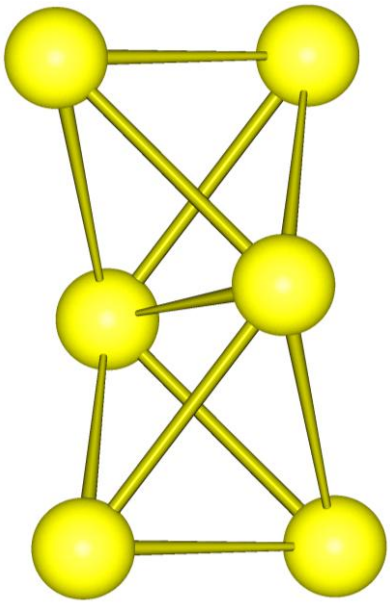

Figure 101 - Metallic skeleton of the anion $[Pt_6(SnCl_2)(SnCl_3)_2(CO)_8\{P(C_6H_5)_3\}_2]^{2-}$

It is possible to observe that the metallic skeleton is the same of the tetranion $[Pt_6(SnCl_2)_2(SnCl_3)_4(CO)_6]^{4-}$, so constituted by two platinum tetrahedrons condensated by an edge. The condensation generates two butterfly concavities on the surface of the cluster. Regarding the molecular geometry instead, remarkable differences exist respect to the disposition and the type of ligands.

In the tetranion, as previously seen, the two butterfly concavities are occupied by two quadruple coordinated μ_4-$SnCl_2$, while in the dianion only one butterfly concavity is occupied by one μ_4-$SnCl_2$ group.

μ_4-$SnCl_2$ coordination mode often occurs in the chemistry of Pt-Sn carbonyl clusters, as it has been found also in the clusters $[Pt_6(SnCl_2)(SnCl_3)_4(CO)_8]^{4-}$ and $[Pt_8(SnCl_2)_4(CO)_{10}]^{2-}$.

In the tetranion $[Pt_6(SnCl_2)_2(SnCl_3)_4(CO)_6]^{4-}$ two $SnCl_3$ groups are edge bridging coordinated, and two others are triple bridging. Moreover six COs are terminally coordinated, one for each platinum atom.

In the anion $[Pt_6(SnCl_2)(SnCl_3)_2(CO)_8\{P(C_6H_5)_3\}_2]^{2-}$ only two triple-bridged $SnCl_3$ groups are present, as the two edge-bridging $SnCl_3$ groups, present in the parent cluster, have been formally substituted by two phosphane groups.

The two phosphane groups are coordinated to Pt atoms in wingtip positions of the free butterfly concavity and, probably due to their steric hindrance, hamper the access of other ligands to the same concavity.

Eight carbonyl molecules complete the coordination sphere of the cluster. Four of them are terminally bonded, one for each Pt atom of the occupied butterfly concavity and four are edge-bridging coordinated.

This anion constitutes a rare example of heteroleptyc platinum cluster, so a cluster stabilized by four different ligands: CO, $SnCl_2$, $SnCl_3$ and $P(C_6H_5)_3$.

The formula of this new compound explicitating the different coordination modes is the following: $[Pt_6(\mu_4\text{-}SnCl_2)(\mu_2\text{-}SnCl_3)_2(\mu_2\text{-}CO)_4(CO)_4\{P(C_6H_5)_3\}_2]^{4-}$.

4.1.6 - Synthesis and spectroscopic characterization of the anion $[Pt_6(SnCl_2)(SnCl_3)_4(CO)_8]^{4-}$

The anion $[Pt_6(SnCl_2)_2(SnCl_3)_4(CO)_6]^{4-}$, dissolved in acetonitrile under CO atmosphere (P = 1 atm), converts into the cluster $[Pt_6(SnCl_2)(SnCl_3)_4(CO)_8]^{4-}$.

The solution changes rapidly colour on passing from shining green to brown-orange, while in the IR spectrum, only $[Pt_6(SnCl_2)(SnCl_3)_4(CO)_8]^{4-}$ anion is present. The salt $[PPh_4]_4[Pt_6(SnCl_2)(SnCl_3)_4(CO)_8]$ was obtained in high yield (85 % based on Pt) and crystals suitable for X-ray analysis were obtained by layering cyclohexane onto an acetonitrile solution of the species. All the solvents were previously saturated with carbon monoxide.

The anion is so prepared by following the stoichiometry:

$$[Pt_6(SnCl_2)_2(SnCl_3)_4(CO)_6]^{4-} + 2\ CO \rightarrow [Pt_6(SnCl_2)(SnCl_3)_4(CO)_8]^{4-} + SnCl_2$$

The reaction proceeds more fastly in the presence of chloride ions. The mechanism reaction is unknown but it is possible to suppose that one $SnCl_3^-$ group, originated on the custer surface by the reaction between Cl^- and $SnCl_2$, is easily replaced by CO, due to the high negative charge accumulated on the cluster.

Also in this case, IR spectrum shows, in the carbonyl stretching band region, both the presence of terminal and edge-bridged CO groups, at 2042 (s) and 1840 (m) cm^{-1} **(Figure 102)**

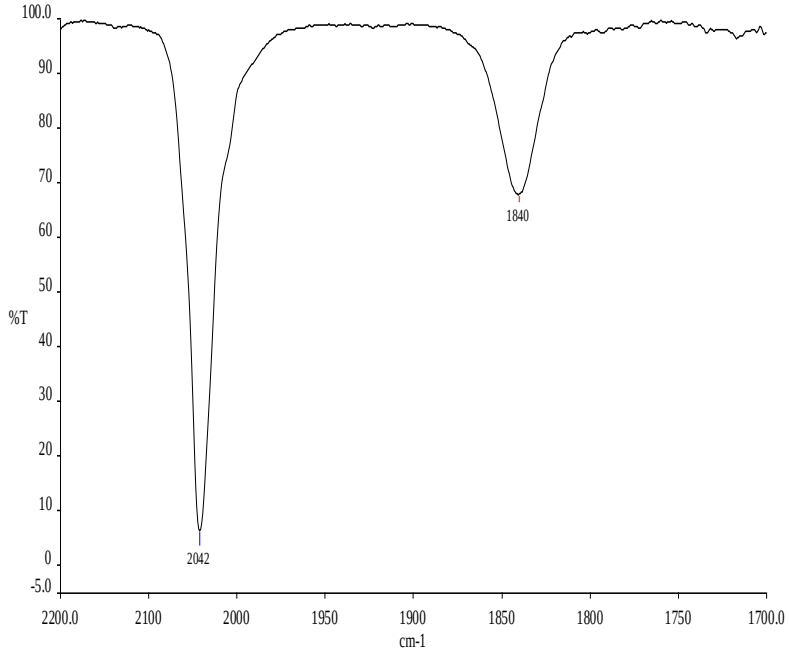

Figure 102 - IR spectrum in acetonitrile of $[Pt_6(SnCl_2)(SnCl_3)_4(CO)_8]^{4-}$

$[Pt_6(SnCl_2)(SnCl_3)_4(CO)_8]^{4-}$ can be conveniently stored in solution under CO atmosphere. The obtainment of the anion $[Pt_6(SnCl_2)(SnCl_3)_4(CO)_8]^{4-}$ in high yield and high purity degree allowed the study, even partially, of its behaviour in solution. For example ^{195}Pt-NMR spectrum, collected in CD_3CN solution at – 30°C (**Figure 103**) shows two singlets (δ_{Pt} = - 4455 ppm; δ_{Pt}= - 5003ppm), and any spin couplings are present.

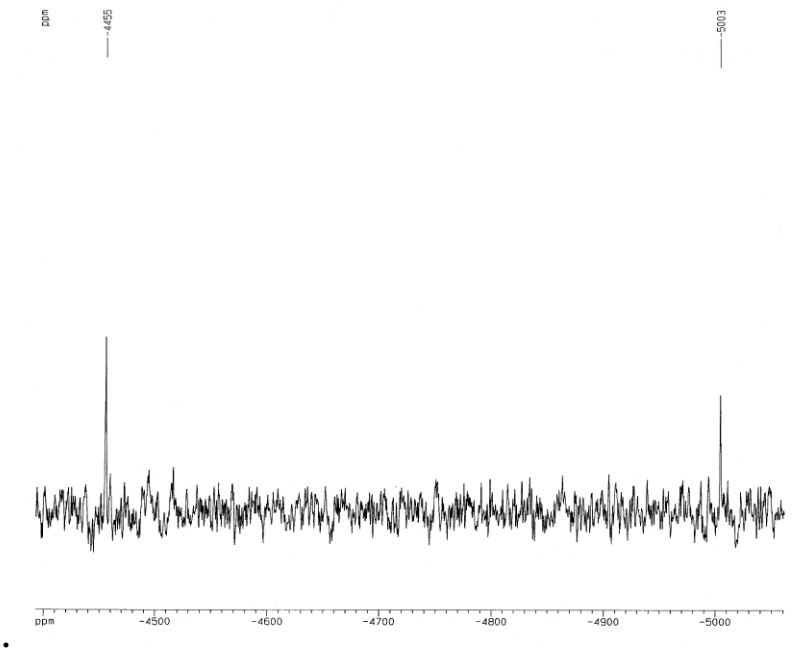

Figure 103 - ^{195}Pt NMR spectrum in CD_3CN of $[Pt_6(SnCl_2)(SnCl_3)_4(CO)_8]^{4-}$

It has been finally observed that, by subsequent reaction of $[Pt_6(SnCl_2)(SnCl_3)_4(CO)_8]^{4-}$ with triphenylphosphane, the dianion $[Pt_6(SnCl_2)(SnCl_3)_2(CO)_8\{P(C_6H_5)_3\}_2]^{2-}$ is obtained, by substitution of two $SnCl_3^-$ groups with two $P(C_6H_5)_3$ ligands. As previously stated, the second anion can be prepared by exchanging the reagents order so adding $P(C_6H_5)_3$ first and then CO.

As a consequence, the whole reactivity of $[Pt_6(SnCl_2)_2(SnCl_3)_4(CO)_6]^{4-}$, above discussed, can be summarized in the following reaction scheme:

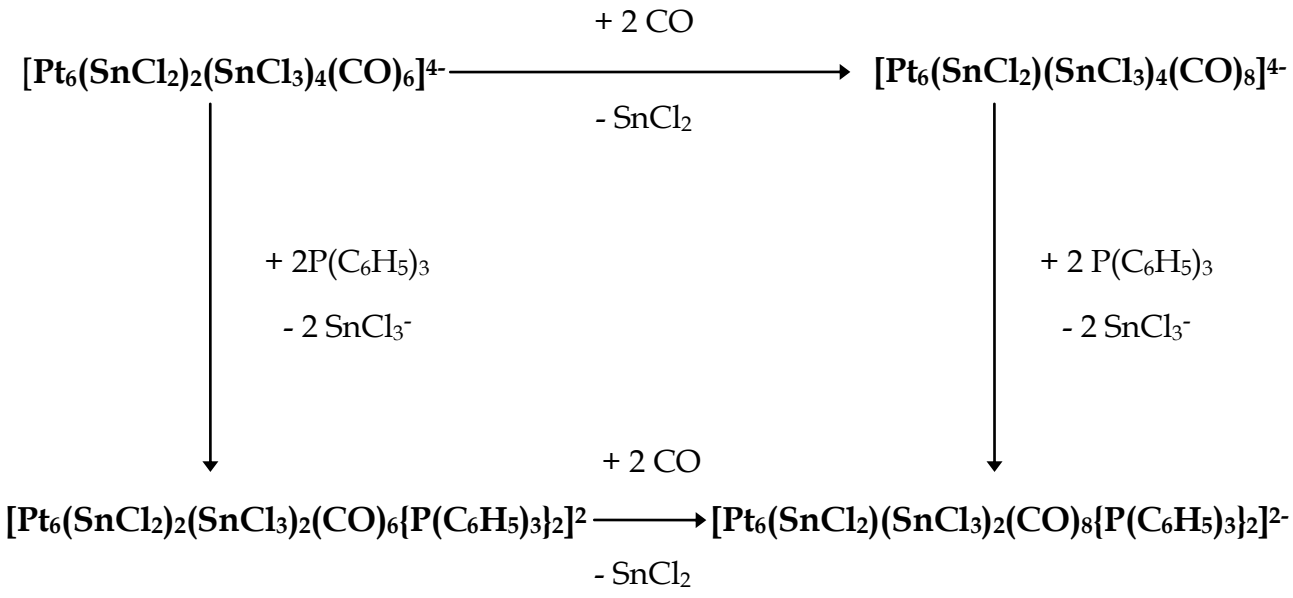

4.1.7 – Solid state structure of the anion $[Pt_6(SnCl_2)(SnCl_3)_4(CO)_8]^{4-}$

The structure of the anion $[Pt_6(SnCl_2)(SnCl_3)_4(CO)_8]^{4-}$ was determined by single crystal X-ray diffraction analysis on the species $[PPh_4]_4[Pt_6(SnCl_2)(SnCl_3)_4(CO)_8]$.

Figure 104 reports the whole structure of the anion, while **Figure 105** shows only the metallic skeleton, constituted by six platinum atoms.

The structure can be seen as deriving from three tetrahedron units sharing three faces. The resulting polyhedron features one concave face on the surface, where μ_4-$SnCl_2$ group is quadruple bridging coordinated. Such a coordination was found also in the previously discussed $[Pt_6(SnCl_2)(SnCl_3)_2(CO)_8\{P(C_6H_5)_3\}_2]^{2-}$ and in other Pt-Sn carbonyl clusters.

In the $[Pt_6(SnCl_2)(SnCl_3)_4(CO)_8]^{4-}$ tetranion two different kinds of tin based ligands are present, showing three different coordination modes. In fact, besides one $SnCl_2$ group, four $SnCl_3$ groups are bonded, two triple bridging on opposite faces of the central tetrahedron and two double bridging on opposite and alternate edges of the triangles individuating the concave face.

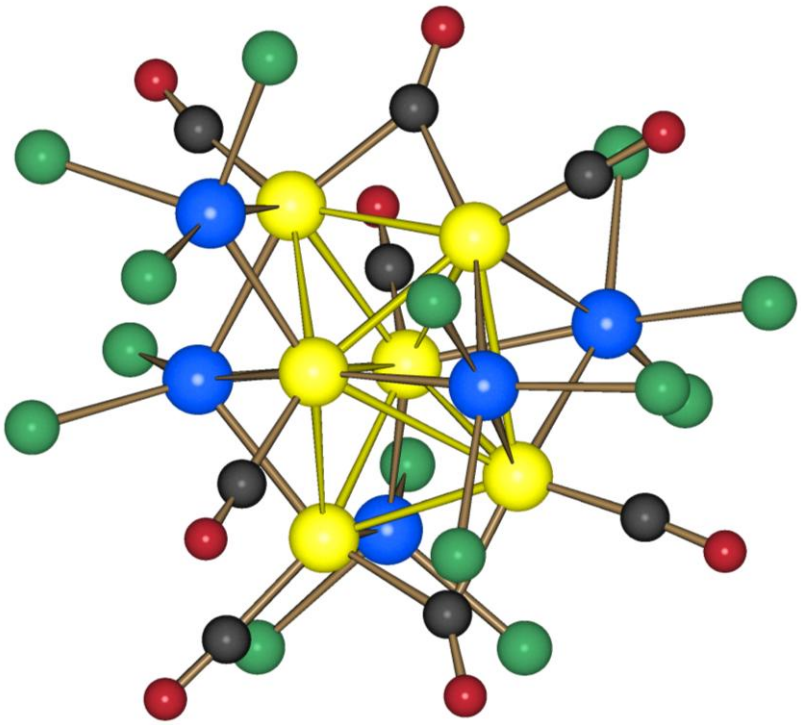

Figure 104 – The solid state structure of the anion $[Pt_6(SnCl_2)(SnCl_3)_4(CO)_8]^{4-}$

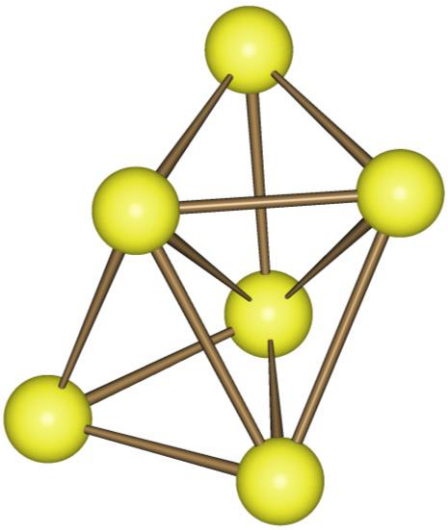

Figure 105 - Metallic skeleton of the anion $[Pt_6SnCl_2)(SnCl_3)_4(CO)_8]^{4-}$

Six carbonyl molecules are terminally bonded, one for each Pt atom, while two more CO groups are double bridged on edges of tetrahedrons not belonging to the concave face.

The formula of the new compound, explicitating the different coordination mode, is the following: $[Pt_6(\mu_4\text{-}SnCl_2)(\mu_2\text{-}SnCl_3)_2(\mu_3\text{-}SnCl_3)_2(\mu_2\text{-}CO)_2(CO)_6]^{4-}$.

The metallic skeleton deriving from three tetrahedron condensated by two faces is expected to have 84 cluster valence electrons, according to the PSEPT rule elaborated for complex polyhedra formed by formal condensation of simple polyhedra.

According to this rule, complex polyhedra belong a number of valence electrons equal to the sum of simple polyhedra valence electron, minus the compartecipating unit electron contribution. Anyhow, in the anion $[Pt_6(SnCl_2)(SnCl_3)_4(CO)_8]^{4-}$ 86 CVE are observed, instead of 84 predicted by PSEPT rule. This disprepancy between calculated and observed CVEs allows to think about the Pt atom polyhedra as deriving from tetrahedral condensed by an edge. By this way, one Pt-Pt bond lacks and so there are two more valence electrons. For supporting this second hypothesis it is worth observing that, in the solid structure, four Pt-Pt bonds are very longer (3,3 Å) than the remaining eight Pt-Pt bonds (2,8 Å). Moreover, two Pt-Sn bonds involving two triple bridging $SnCl_3$ groups, are longer (3,04 Å) than the other four Pt-Sn bonds (2,72 Å) of the same groups.

So it is reasonable supposing that the structure of the anion $[Pt_6(SnCl_2)(SnCl_3)_4(CO)_8]^{4-}$ derives from the one of $[Pt_6(SnCl_2)_2(SnCl_3)_4(CO)_6]^{4-}$ by rotation around the axis of the central Pt atom handlebars. Such rotation results in the approach of the two tetrahedrons until a weak ligand interaction occurs. This second description of the metallic skeleton in $[Pt_6(SnCl_2)(SnCl_3)_4(CO)_8]^{4-}$ anion requires for an electron counting in agreement with the observed CVEs.

4.2 $[Pt_5\{(SnCl_2)_2(OCH_3)\}_3(CO)_5]^{3-}$

4.2.1 Synthesis and spectroscopic characterization of the anion $[Pt_5\{(SnCl_2)_2(OCH_3)\}_3(CO)_5]^{3-}$

The trianions $[Pt_5(CO)_5\{Cl_2Sn(\mu\text{-}OR)SnCl_2\}_3]^{3-}$ (R = Me, Et, ^{i}Pr;) were obtained in good yields (55−62% based on Pt) from reactions of $[NBu_4]_2[Pt_{15}(CO)_{30}]$ with $SnCl_2$ (Sn/Pt = 1.2) in CH_3OH or mixtures of ROH/acetone (R = Et, iPr) in the presence of Na_2CO_3. In particular, R=CH_3 has been studied in Milan, whereas species with R = Et and iPr have been obtained by Longoni and co-workers at University of Bologna, so here we focus the attention on the metoxy derivative. The role of the base is to eliminate the acidity formed upon deprotonation of the alcohol molecules according to the following equation:

$$[Pt_{15}(CO)_{30}]^{2-} + 18\ SnCl_2 + 9\ ROH \rightarrow 3\ [Pt_5(CO)_5\{Cl_2Sn(\mu\text{-}OR)SnCl_2\}_3]^{3-} + 7\ H^+ + H_2 + 15\ CO$$

The anions were purified by precipitation with excess $[PPh_4]Cl$ and crystallization from acetone/methanol.

Crystals suitable for X-ray analyses have been obtained only for the salt $[PPh_4]_3[Pt_5(CO)_5\{Cl_2Sn(\mu\text{-}OiPr)SnCl_2\}_3]\cdot 3CH_3COCH_3$ from acetone/Pr^iOH.

All clusters display very similar ν(CO) [e.g., 2031(s) and 2006(s) cm^{-1} for metoxy species in acetone].

The μ-OH analogue $[Pt_5(CO)_5\{Cl_2Sn(\mu\text{-}OH)SnCl_2\}_3]^{3-}$ is also known and it has been more conveniently obtained from the reaction of $[NBu_4]_2[Pt_{12}(CO)_{24}]$ with $SnCl_2\cdot 2H_2O$ (Sn/Pt = 1.2) in acetone in the presence of $[NBu_4]Cl$ and Na_2CO_3. Also in this case, the base must neutralize the acidity, which develops according to the equation:

$$5\ [Pt_{12}(CO)_{24}]^{2-} + 72\ SnCl_2 + 36\ H_2O \rightarrow 12\ [Pt_5(CO)_5\{Cl_2Sn(\mu\text{-}OH)SnCl_2\}_3]^{3-} + 26\ H^+ + 5\ H_2 + 60\ CO$$

The $[Pt_5(CO)_5\{Cl_2Sn(\mu\text{-}OH)SnCl_2\}_3]^{3-}$ anion displays ν(CO) at 2033(s) and 2006(ms) cm^{-1} in acetone solution. All these compounds are stable under CO (1 atm), with the coordinated CO ligands slowly exchanging with free carbon monoxide.

This allowed the preparation of ^{13}C enriched sample, suitable for NMR studies.

As an example, is discussed the NMR behaviour of the cluster with R = Pr_i.

The ^{13}C NMR spectrum in deuterated acetone, which does not change in the temperature range 223−298 K, consists of two nonbinomial triplets at 205.0 ppm ($^1J_{C-Pt}$ = 2539 Hz) and 184.5 ppm ($^1J_{C-Pt}$ = 2621 Hz) with relative intensities 2:3 in agreement with a trigonal bypyramidal structure of the $Pt_5(CO)_5$ core of the cluster. Similarly, ^{195}Pt NMR at 243 K displays two multiplets at δ_{Pt} −4390 and −3949 ppm (relative intensities 2:3), that are attributable to the axial and equatorial Pt-atoms, respectively.

4.2.2 Structure of the anions $[Pt_5\{(SnCl_2)_2(OR)\}_3(CO)_5]^{3-}$ (R = H, CH_3, ^iPr)

Attempts for growing crystals of $[Pt_5\{(SnCl_2)_2(OCH_3)\}_3(CO)_5]^{3-}$ suitable for X-ray diffraction were unfortunately unsuccessfull. On the contrary, in the case of R = H (**1**) and ^{i}Pr (**4**) crystals were obtained and so the single crystal X-ray diffraction structures are available (**Figure 106**), which are expected to have same metal core and the same ligand distribution of the metoxy derivative.

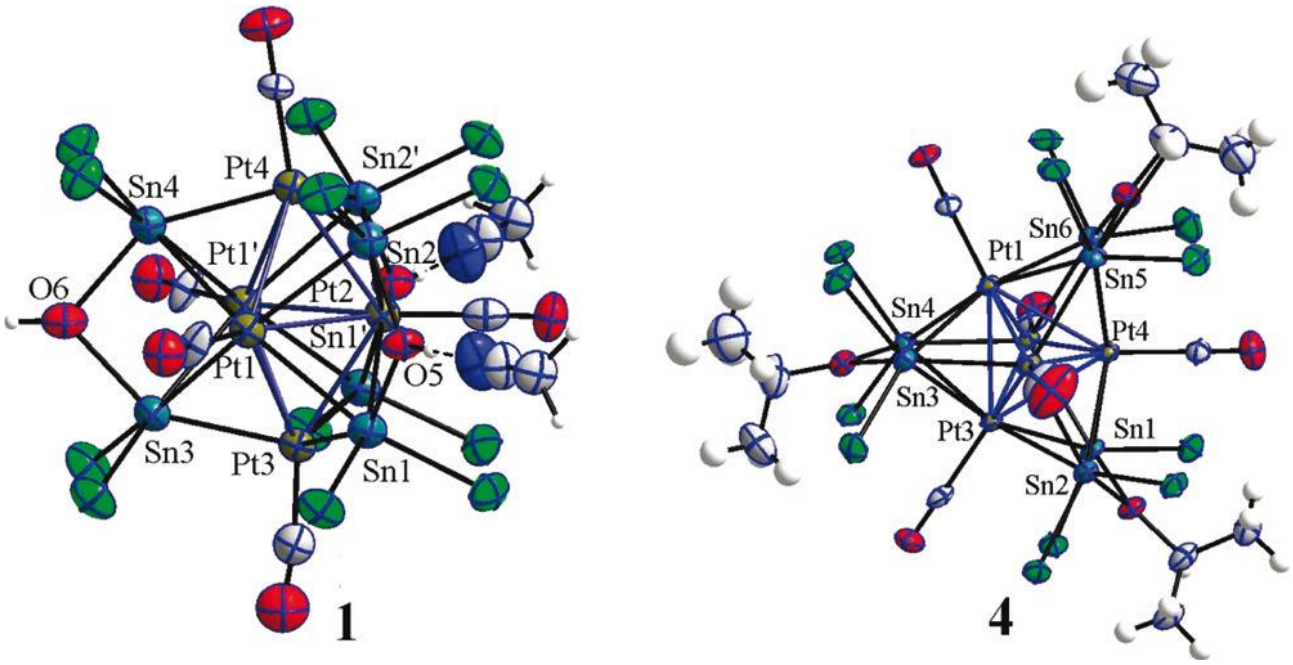

Figure 106 – The solid state structures of $[Pt_5\{(SnCl_2)_2(OR)\}_3(CO)_5]^{3-}$ (R = H for 1 and ^{i}Pr for 4)

Both clusters 1 and 4 approach pseudo-*D*3*h* symmetry and have a Pt_5 TBP core with a single terminal CO ligand per Pt atom, while the six face-capping Sn atoms from three $Cl_2Sn(\mu\text{-}OR)SnCl_2$ moieties form an ideal trigonal prism but remain unbound between themselves (Sn−Sn distances >3.4 Å).

Exact conformation of 1 and 4 to *D*3*h* symmetry is likely prevented by crystalline packing effects and H-bonding in 1.

In particular, the unengaged OH group is less strongly bound to Sn atoms than its analogues [2.317(18) and 2.296(19) Å versus 2.096(11)−2.102(12) Å]. In contrast, the presence of ^{i}Pr substituents instead of H atoms in 4, is inconsistent with H-bonding, such that all Sn−O distances are equivalent [2.136(6)-2.151(5) Å]. The $[Cl_2Sn{-}O(R){-}SnCl_2]^{-}$ fragment, analogously to a diphosphine ligand, may use the electron pairs of the three -coordinated Sn(II) ions for metal coordination.[236] As a matter of fact, a tetra-coordinated (hypervalent) Sn(II) ion can act as donor toward a single metal (Ru16 or Re17) or a Pt3 face, as found in 1−4. In 1 and 4, the Sn is apparently hexa-coordinated and the Sn(II) electrons are important for Pt_5 bonding. On the other hand, shorter Pt_{ax}−Sn than Pt_{eq}−Sn distances indicate Pt_{ax} donations, which satisfy the residual acidity of the main group atoms consistently with an uncommon but well documented[237] hypervalency.

5 - Use of redox active and/or bulky cations as counterions of MCCs

5.1 - N,N'-dimethyl-9,9'-bis-acridinium (Acr^{2+})

5.1.1 - Fluorescence behaviour

Aza-arenes are chemical compounds containing one or more heterocyclic N atoms. Among them it is possible to cite pyridin, quinoline, acridinium, N,N'-dialkyl-9,9'-bis-acridinium. They show low energy n →π* transitions and this accounts for their quite low fluorescence quantum yield in hydrocarbons. Nevertheless, fluorescence behaviour for these compounds strictly depend from the solvent. Hydrogen bonds can be formed among nitrogen atoms and solvent molecules in protic solvents like alcohols. This turns out in to an energetic inversion between n → π* e π → π* transition. As the latter is the lowest in energy fluorescence quantum yield becomes higher than in hydrocarbon solvents.

It is remarkable that electronic density on nitrogen atom is reduced during excitation; so the ability in forming hydrogen bonds is lower in the excited state. Ground state is so more stabilized by hydrogen bonds than excited state. As a consequence, a red-shift in the spectrum occurs moving from non polar hydrocarbon solvents to polar protic solvents. For same heterocyclic compound like as acridinium, n → π* absorption band is hardly distinguishable from the more π → π* adsorption bands. **Figure 107** reports the fluorescence spectrum of N,N'-dimethyl-9,9'-bis-acridinium dissolved in THF.

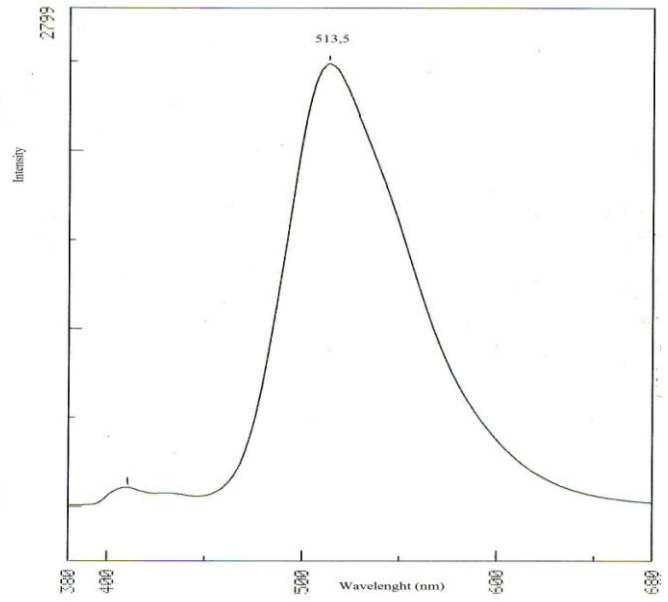

Figure 107 - Fluorescence spectrum of N,N′-dimethyl-9,9′-bis-acridinium in THF

5.1.2 - Redox behaviour

Cyclic voltammogram of Acr^{2+} in aqueous solution generally shows irreversible reductive processes. This fact is due to the insolubility of the Acr^0 species in water and to the slow conformational exchange following the reduction from $Acr^{\cdot+}$ to Acr^0. The two tricyclic acrydinium systems are linked by a single bond in Acr^{2+} and $Acr^{\cdot+}$ and by a double bond in Acr^0 (**Figure 108**)

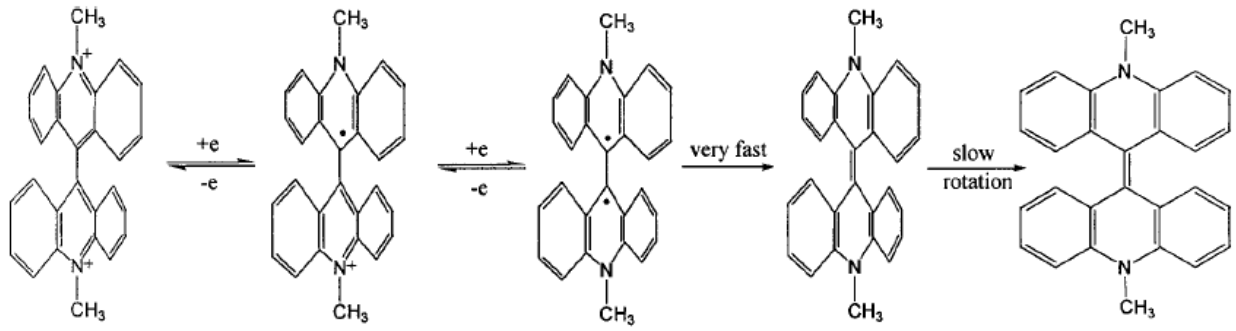

Figure 108 - Redox processes and conformational exchange in bis-acrydinium

This allows Acr^{2+} and $Acr^{\cdot+}$ to minimize the steric hindrance between the planes of the rings, raising an optimal torsion angle. On the contrary, the double bond in Acr^{0} forces to a quasi co-planar arrangement. As illustrated by Figure 108, the first monoelectronic reduction is followed by a second reduction leading to the biradical species specie $Acr^{\cdot\cdot}$ which slowly re-arranges forming the double bond and the quasi co-planar conformation of Acr^{0}.

This problem can be avoided by using high scansion rate so the reduction and the re-oxidation occur before the conformational exchange. **Figure 109** reports the cyclic voltammogram of bis-acrydinium collected in acetonitrile solution.

It can be noted a first bielectronic reduction process at –0,70 V and a bielectron oxidative process at –0,05 V. The high anodic potential is likely due to the conformational stabilization obtained by the neutral species, which makes more difficult the oxidative process.

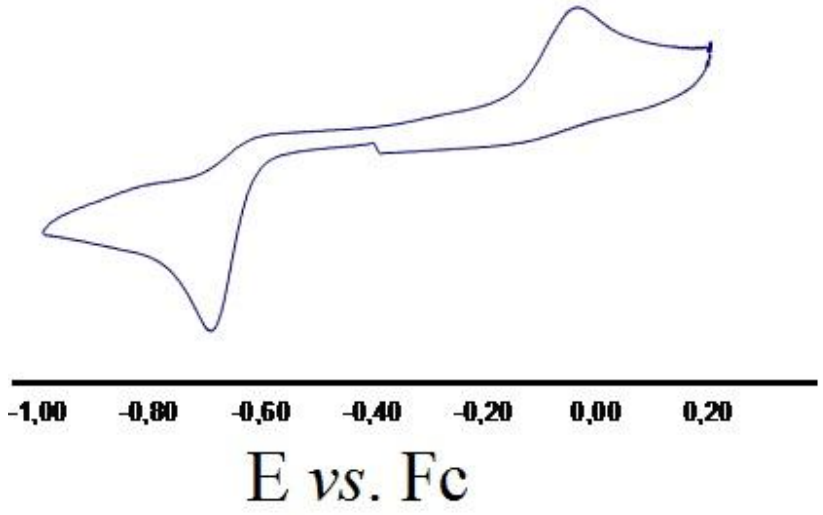

Figure 109 - Cyclic voltammogram of bis-acrydinium in acetonitrile

5.1.3 - Reactivity of $[Ir_6(CO)_{15}]^{2-}$ with $[Au_6$(120hexaphos)] and Acr^{2+}

One of the cluster aggregation methods or, more generally, of the metal particles, requires for the use of organic ligands where different atoms (i.e. N,O,P) are able to donate an electron pair to the metal forming a coordination bond.

Multidentate phosphane ligands like 180tetraphos and 120hexaphos have been previously presented. The structure of 120hexaphos is shown in **Figure 110.**

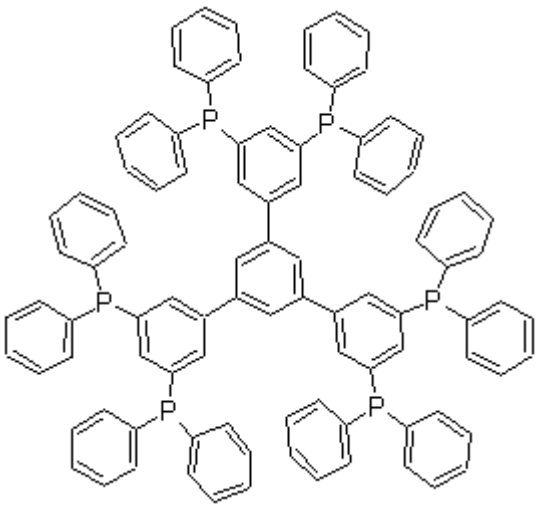

Figure 110 - Schematic structure of 120-hexaphos

The reaction between $[Ir_6(CO)_{15}]^{2-}$ and this hexa-phosphane did not lead to significant results. This fact is in agreement with what one would expect: in fact the cluster is too electron-rich to accept further electron density by the phosphane.

In order to overcome this problem we decided to use, as otherwise seen, a modified version of 120-hexaphos where each PPh_2 groups is coordinated by one Au-Cl fragment.

A THF solution of the dehalogenated gold-phosphane complex were added to a solution of $[PPN]_2[Ir_6(CO)_{15}]$ in THF, by using a Ir_6 : Au 6: 1 molar ratio. The reaction were conducted under CO atmosphere and it was monitored by IR spectroscopy.

IR spectrum of the starting carbonyl cluster is shown in **Figure 111**, having carbonyl stretching bands at 2009(s), 1981(vs), 1923(sh), 1772(m) cm^{-1}. After the addition of the solution of $[Au_6(120hexaphos)]^{6+}$, the IR spectrum quickly changes and the carbonyl stretching bands shift to higher wavenumbers (**Figure 112**), 2062(w), 2019(vs), 1985(s), 1781(m) cm^{-1}.

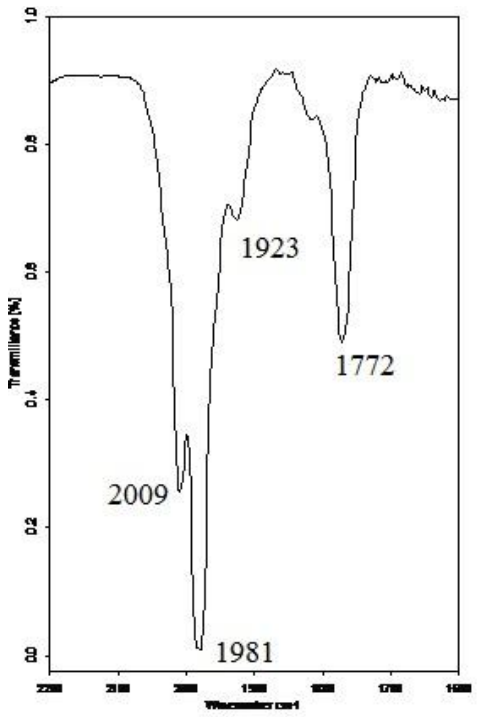

Figure 111 - IR spectrum in THF of $[Ir_6(CO)_{15}]^{2-}$

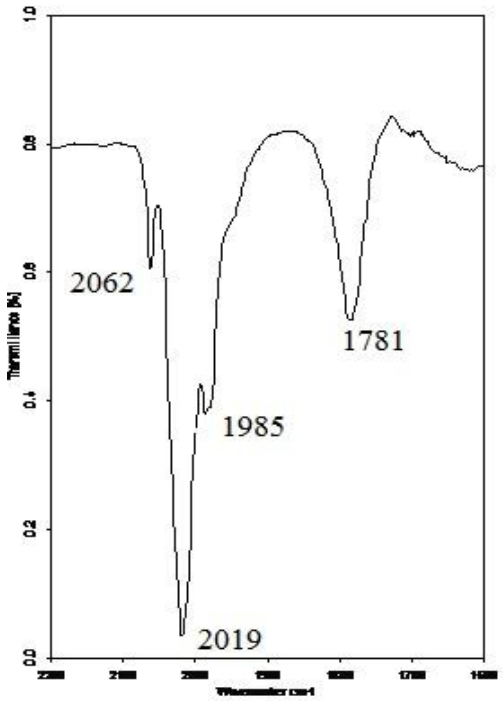

Figure 112 - IR spectrum inTHF of $[\{Ir_6Au(CO)_{15}\}_6(120\text{-hexaphos})]^{6-}$

According to the spectroscopical data reported in literature it is possible to think that the following reaction occurred:

$$6\,[Ir_6(CO)_{15}]^{2-} + [Au_6(120\text{-hexaphos})]^{6+} \xrightarrow{CO} [\{Ir_6Au(CO)_{15}\}_6(120\text{-hexaphos})]^{6-}$$

The carbonyl stretching bands of the reaction product, shifted to higher wavenumbers respect to the starting material, are in agreement with a decrease of electrical charge on the cluster and similar to those reported for the analogous $[Ir_6(CO)_{15}\{Au(PPh_3)\}]^-$.

The new molecule formally presents one negative charge for each Ir_6 cluster, for a total amount of six negative charges. Anyway, these electrons can not be considered unpaired, so generating paramagnetism phenomena. In fact $AuPPh_2R^+$ fragment, where R indicates the organic scaffold of 120-hexaphos, even bonding by capping a triangular face of the cluster, does not modify cluster valence electrons, leaving substantially paired the electrons of the dianion.

In a second stage we tried a methathesis reaction, with the aim to exchange the cation of the obtained product, PPN (PPN=bis(triphenylphosphoranilydene)ammonium), with the luminescent redox-active dication N,N'-dimethyl-9,9'-bisacridinium. So acridinium was added to a THF solution of the product with a product : acridinium 1:3 molar ratio, in order to satisfy the stoichiometric ratio between positive and negative charges.

After the addition of bisacridinium a little amount of an unknown product precipitated, while the carbonyl stretching bands shift to higher wavenumers, 2027(s), 1780(w) cm^{-1} (**Figure 113**)..

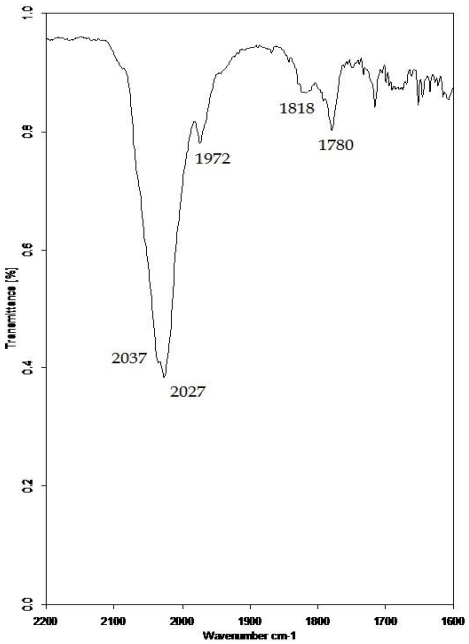

Figure 113 - IR spectrum in THF of [Bisacridinium]$_3$[{$Ir_6Au(CO)_{15}$}$_6$(120-hexaphos)]

After separation of the unknown precipitate, the product was isolated by recrystallization from 2-propanol. The species, dissolved in DMF, shows more definite carbonyl stretching bands at 2024(vs), 1974(m), 1778(s) cm^{-1} (**Figure 114**).

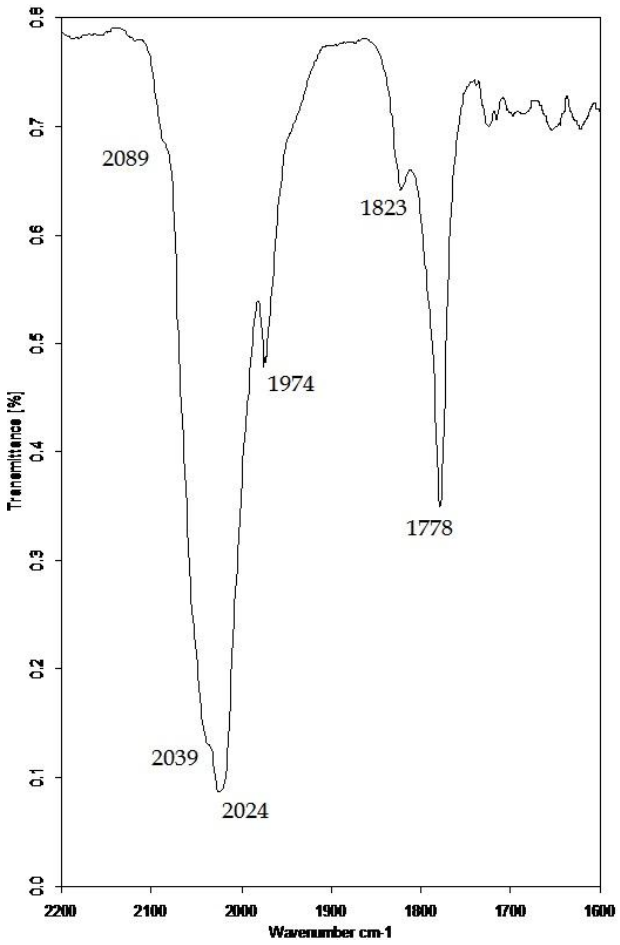

Figure 114- IR spectrum inDMF of [Bisacridinium]$_3$[{$Ir_6Au(CO)_{15}$}$_6$(120-hexaphos)]

As both bisacridinium and the gold phosphane complex are luminescent, the fluorescence of the product was investigated, in order to verify possible shifts of the emission bands due to presence of iridium carbonyl cluster. The spectra were collected on THF solution in inert atmosphere.

The gold-phosphane complex itself, dissolved in dichloromethane, exhibits an emission band at 355 nm (**Figure 115**).

Bisacridinium, dissolved in THF as tetraphenylborate salt, shows one emission band at 513 nm (λ_{exc}=306 nm) (Figure 116). The reduction of the compound with $NaBH_4$ leads to a change of the emission and the presence of two emission bands with almost the same intensity at 476 and 505 nm (λ_{exc}=360 nm) attributed to a mixture of $Acr^{\cdot+}/Acr^0$ (**Figure 117**).

Finally [Bisacridinium]$_3$[{$Ir_6Au(CO)_{15}$}$_6$(120-hexaphos)] shows one emission band centred at 562 nm when dissolved in THF (**Figure 118**) and at 521 nm when dissolved in DMF (λ_{ecc}= 444 nm) (**Figure 119**).

So the emission of the product has a red shift both respect to oxidized or reduced bisacridinium and to gold phosphane complex. **Table 10** summarizes the obtained results.

Species	λ_{exc} (nm)	λ_{em} (nm)	Figure
$[Acr]^{2+}$ (in THF)	306	513	**Errore. L'origine riferimento non è stata trovata.**
$[Acr]^{+}$ / [Acr] (in THF)	360	476-505	**Figure 117**
Reaction product (in THF)	444	562	**Figure 118**
Reaction Product (in DMF)	444	521	**Figure 119**
[{AuCl}$_6$(120hexaphos)] (in CH_2Cl_2)	310	355	**Figure 115**

Table 10 Fluorescence data of the discussed products

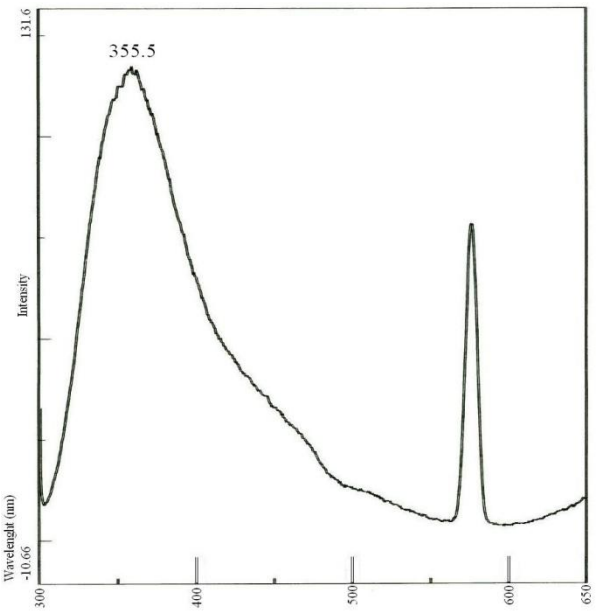

Figure 115 - Fluorescence spectrum in CH_2Cl_2 of [{AuCl}$_6$(120hexaphos)]

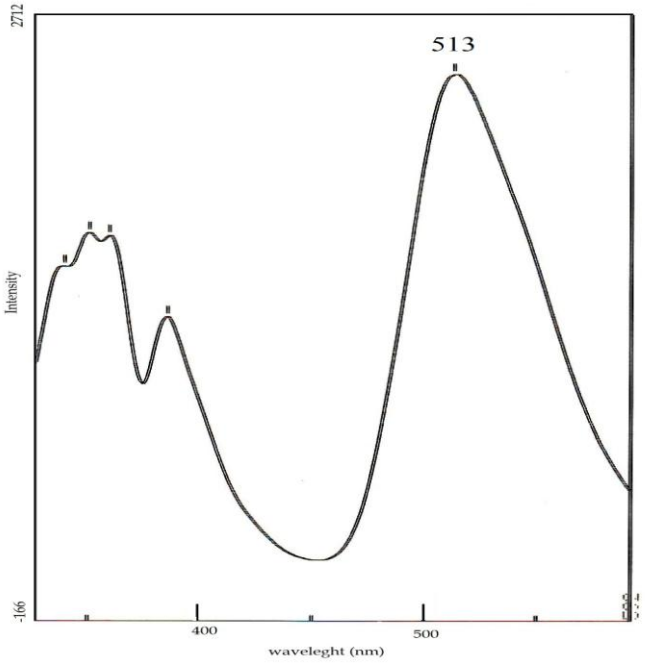

Figure 116 - Fluorescence spectrum inTHF of $[Acr][BPh_4]_2$

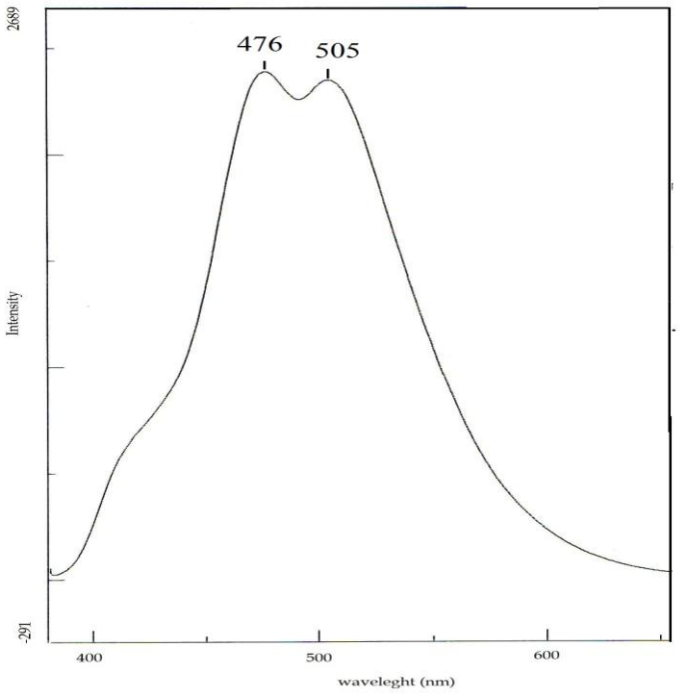

Figure 117 - Fluorescence spectrum in THF of $[Acr]^+/[Acr]$

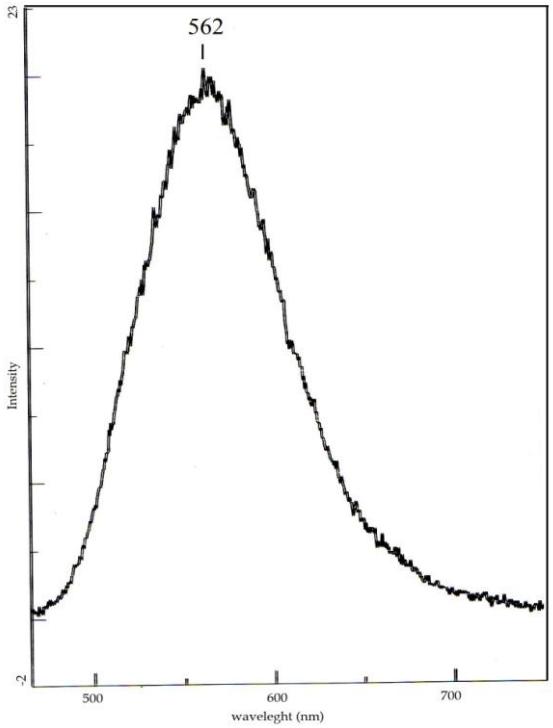

Figure 118 - Fluorescence spectrum inTHF of the reaction product

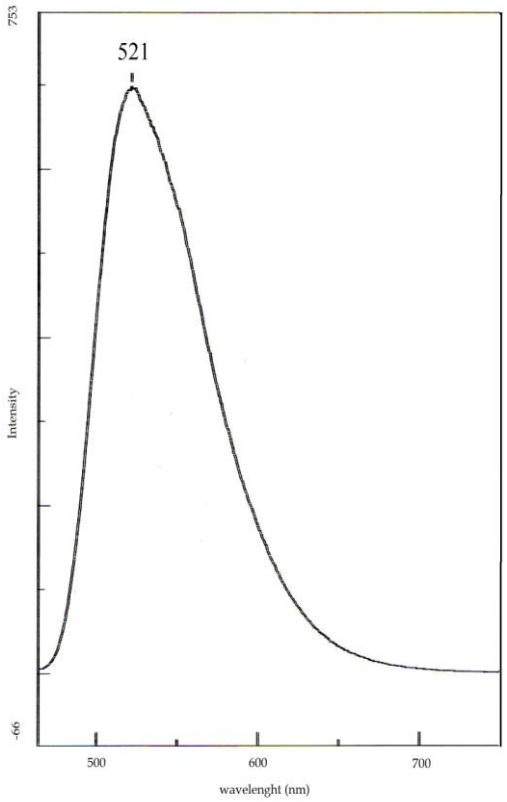

Figure 119 - Fluorescent spectrum in DMF of the reaction product

5.1.4 - Reactivity of $[Ir_6(CO)_{15}]^{2-}$ with N,N'-dimethyl-9,9'-bis-acridinium (Acr^{2+})

In order to investigate the reaction between these species it was at first necessary obtaining a salt of acridinium soluble in the same organic solvents (THF, acetone, DMF) suitable for the anionic cluster. In fact, the commercially available N,N'-dimethyl-9,9'-bis-acridinium of bis-nitrate is only water soluble. So, the nitrate was substituted by the more organophilic tetraphenylborate with a methathesis reaction, according to the following stoichiometry:

$$[Acr][NO_3]_2 + 2\,Na[B(C_6H_5)_4] \rightarrow [Acr][B(C_6H_5)_4]_2 + 2\,NaNO_3$$

Different reactions were conducted between $[Acr][B(C_6H_5)_4]_2$ and $[PPN]_2[Ir_6(CO)_{15}]$ (PPN=bis(triphenylphosphoranylidene)ammonium), varying the solvent and the operative conditions.

5.1.4.1 - Reaction in acetone

In this case the ionic cluster $[PPN]_2[Ir_6(CO)_{15}]$ was dissolved in acetone, collecting a starting IR spectrum. (**Figure 120**). Four portions of an acetone solution of bis-acridinium tetraphenylborate were then added step by step, containing 0,25 equivalents of bisacridinium respect to the cluster. IR spectra were collected after each addition, but after all, the carbonyl stetrching bands were nearly unchanged in the position and relative intensity (**Figure 121**).

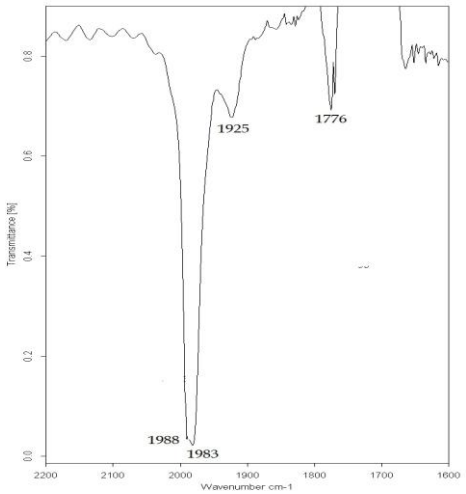

Figure 120- IR spectrum in acetone of $[Ir_6(CO)_{15}]^{2-}$

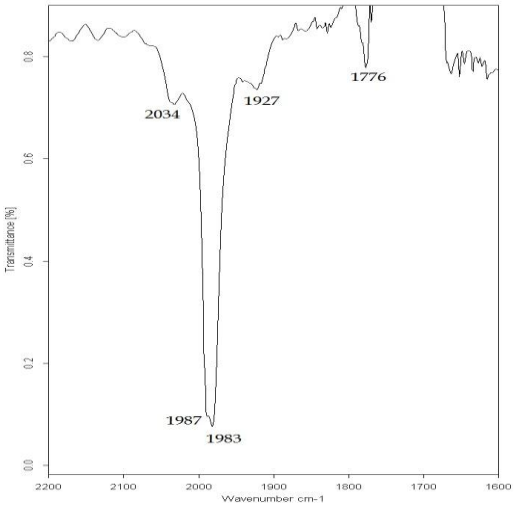

Figure 121 - IR spectrum in acetone with a $[Ir_6(CO)_{15}]^{2-}$: bisacridinium 1:1 molar ratio

The solvent was so removed by vacuum pump and the remaining solid was dissolved in THF. The IR spectrum collected just after this operation revealed that a reaction occurred. (**Figure 122**).

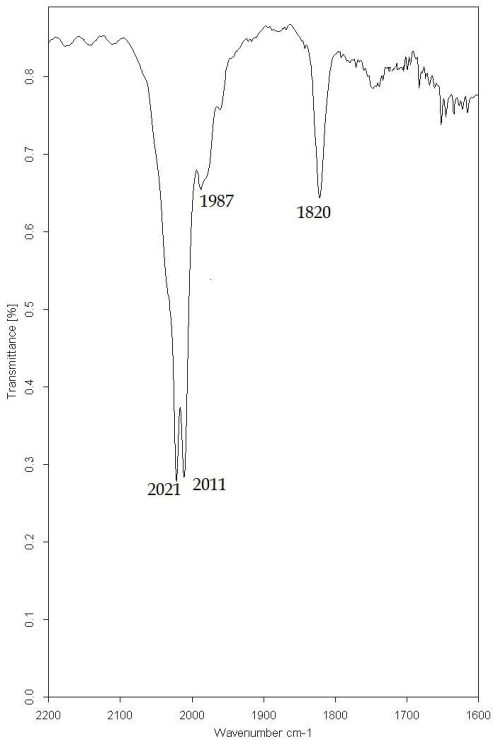

Figure 122 - IR spectrum in THF of the reaction solid

Such a spectrum is attributable to the species $[Ir_6(CO)_{15}]^-$. In order to confirm this result, the reaction was repeated by using THF as solvent.

5.1.4.2 - Reaction in THF

A THF solution of $[PPN]_2[Ir_6(CO)_{15}]$ was prepared (concentration about $7{,}5x10^{-3}$ M), and a starting IR spectrum was collected (**Figure 123**).

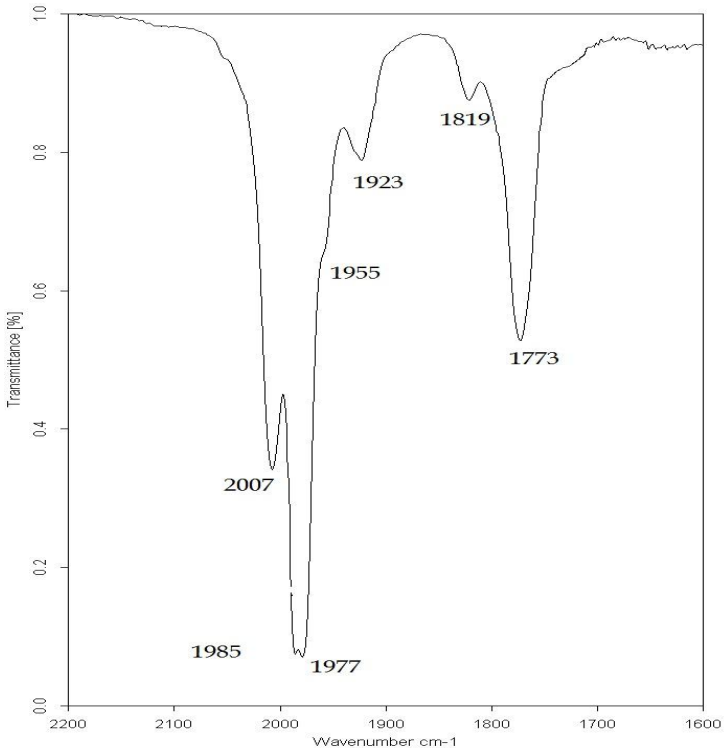

Figure 123 - IR spectrum in THF of $[Ir_6(CO)_{15}]^{2-}$

One equivalent of $[Acr][B(C_6H_5)_4]_2$ was added as solid to this solution, resulting in a quicky precipitation of a white solid, very likely $[PPN][B(C_6H_5)_4]$.

The IR spectrum of the solution (**Figure 124**) exhibits, in the carbonyl stretching region, a shift of the cluster ν_{CO} to higher frequencies (2033(s), 2020(vs), 2010(vs), 1987(m), 1821(m), 1778(m) cm^{-1}) respect to the starting dianion (1985(s), 1978(s), 1771(m) cm^{-1}).

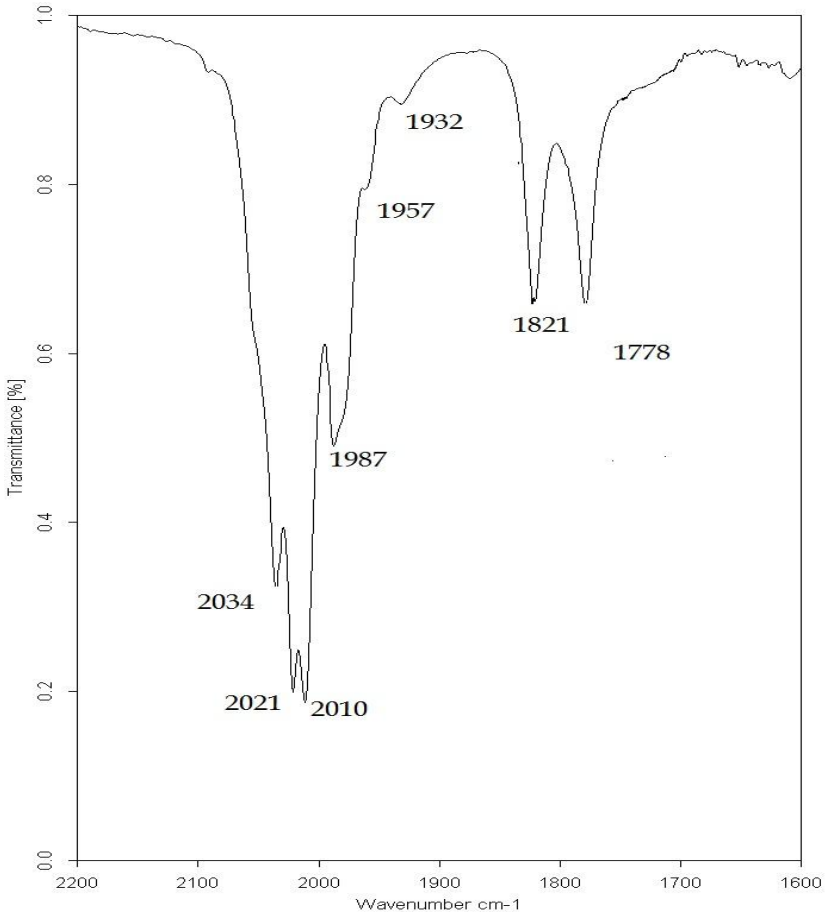

Figure 124 - IR spectrum in THF of $[Acr]^{\cdot+}[Ir_6(CO)_{15}]^-$

The band shift, shape and relative intensity agree with a monoelectronic oxidation of the cluster, without any change in the stereochemistry of the cluster itself, suggesting the following stoichiometry:

$$[Ir_6(CO)_{15}]^{2-} + Acr^{2+} \rightarrow [Ir_6(CO)_{15}]^- + Acr^{\cdot+}$$

where the cluster undergoes to an oxidation and bisacridinium to a reduction.

The product was isolated by precipitation with n-heptane. Elemental analysis (C, H, N) is in good agreement with the formulation requiring one bisacridinium *per* cluster. Acetone and DMF (**Figure 125**) IR spectra of the isolated product show very similar carbonyl stretching bands respect to THF solution. The edge-bridged CO region was hardly valuable as covered by high solvent absorbments.

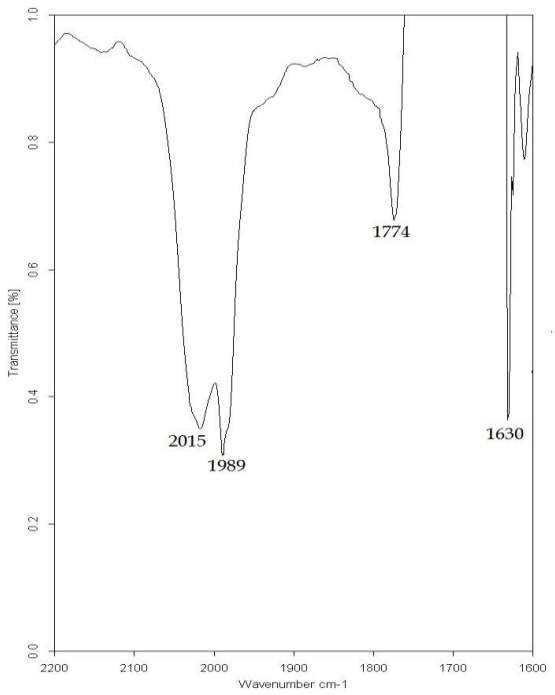

Figure 125 - IR spectrum in DMF of $[Acr]^{\cdot+}$ $[Ir_6(CO)_{15}]^-$

5.1.4.3 – Reaction in CH_3CN and DMF

The reaction was then repeated in both these solvents. In the case of acetonitrile (**Figure 126**) a whitish solid precipitated from the solution, while with DMF (**Figure 127**) all remained dissolved. In both cases, basing on IR spectra, the redox reaction raises an equilibrium, even after the addition of an excess of bisacridinium.

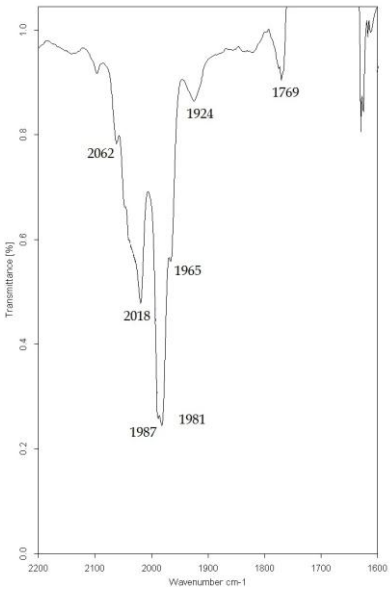

Figure 126 - IR spectrum in CH_3CN after addition of bisacridinium

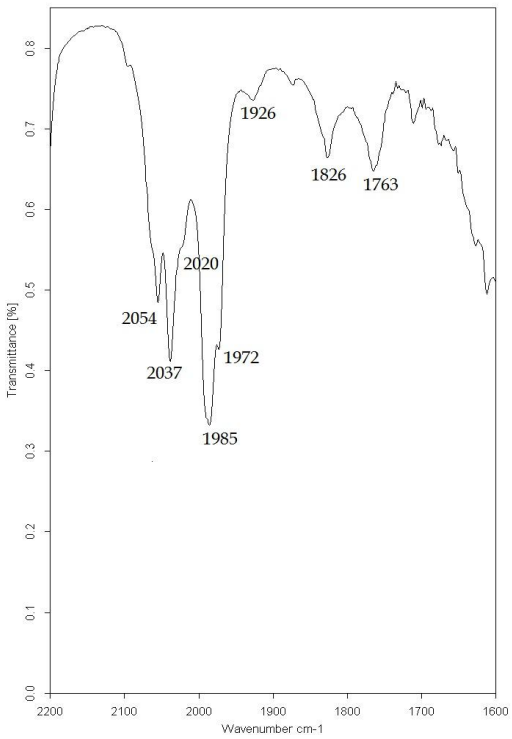

Figure 127 - IR spectrum in DMF after addition of bisacridinium

It is so likely that, in these cases, reduction potentials of the couples Ir_6^{2-}/Ir_6^{-} and Acr^{2+}/Acr^{+} are very close and the equilibrium moves towards the reagents.

5.1.5 - Magnetism measurements on $[Acr]^{\cdot+}[Ir_6(CO)_{15}]^{-}$

The formulation of the obtained species as $[Acr]^{\cdot+}[Ir_6(CO)_{15}]^{-}$ would provide for the presence of a double-radicalic species with one unpaired electron on the anion and one unpaired electron on the cation.

This would lead to a paramagnetic behaviour of the material. The magnetism measurements were conducted by the Department of Physic of University of Parma in collaboration with Prof. Mauro Riccò and Dr. Marcello Mazzani. Anyway the obtained results did not completely confirmed the proposed formulation, as a weak paramagnetism was measured, in disagreement the the predicted one.

Figure 128 shows the mass susceptibility as a function of temperature for the product.

The susceptibility was collected down to 2 Tesla, in order to be well after the saturation field due to the presence of ferromagnetic impurities, which would introduce signal distorptions.

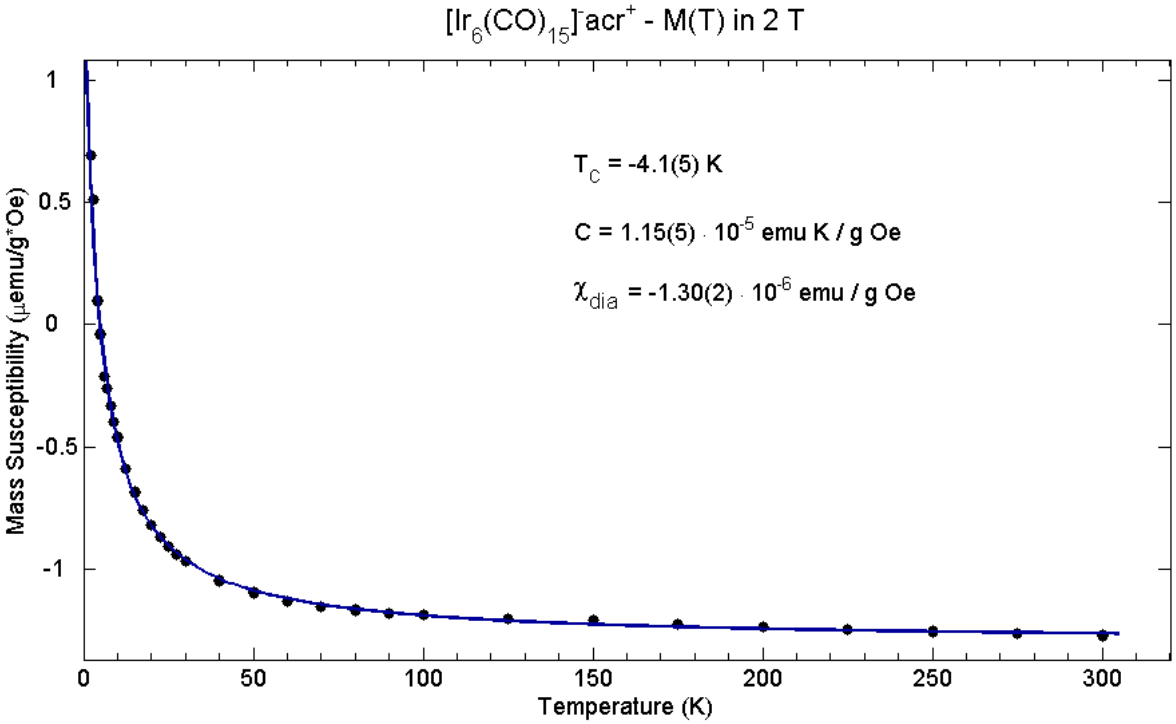

Figure 128- Mass susceptibility *vs* temperature

The experimental curve follows a Curie-Weiss behaviour, $\chi = \chi_{dia} + C/(T-T_{CW})$.

The negative Curie-Weiss temperature (T_{CW} = -4,1(5) K) indicates the presence of weak antiferromagnetic fluctuations.

From the signal width, so from the Curie constant, C = 1,15 x 10^{-5} emuK/g Oe, the number of ½ spin *per* gram, N_{sg}, was calculated, through the formula:

$$C = N_{sg}\ \mu_B^2\ g_e^2\ [S(S+1)]\ /\ 3\ k_B$$

where:

μ_B = 9,27 x 10^{-21} erg/G (Bohr magneton constant)

g_e = 2,0023 (factor g ratio for electron)

k_B = 1,38 x 10^{-16} erg/K (Boltzmann constant)

S = ½

So, applying the formula we found: $N_{sg} = 1.85 \times 10^{19}$ spin/g,

deriving the number of molecule *per* gram from the ratio between the Avogadro constant and the molecular weight, $N_{molec.g} = N_{Av} / P.M. = 3.07 \times 10^{20}$ molecole/g and calculating the ratio $[N_{sg} / N_{molec.g}] = 0,06$, results that 6 ½ spin contributions are present each 100 molecules.

This means that the solid state isolation of the compound causes a nearly complete stabilization of the starting situation with a dianion and a dication. The precipitation procedure would so have moved the equilibrium between products and reagents towards the last ones.

5.2 - $[(PPh_3)(CH_2)_{12}(PPh_3)]Br_2$ (tppdodBr$_2$)

5.2.1 Synthesis

Phosphonium salts are assuming a relevant role in different fields, moving from Medicine, to organic chemistry and material science. They find application as phase transfer agents and ionic liquid, as conducting materials and anti-flame agents.

Moreover, the lipophylic properties of aryl substituted phosphonium salts are exploited in cellular biology, for disease treatment and as drug carrier.

In this case we decided to prepare a particular bis-phosphonium salt, where two PPh_2R^+ groups are separated by a long alkyl chain. This characteristic could have a role in the crystal packing of anionic carbonyl cluster, for example in inducing a 1D or 2D infinite packing.

The bis-phosphonium salt was obtained via catalytic reaction from bromobenzene and 1,12-bis(diphenylphosphano)dodecane. The catalyst was $NiBr_2$ with 1:40 molar ratio respect to the diphosphane. The reaction was conducted by suspending 1,12-bis(diphenylphosphano)dodecane in ethylene glycol, adding nickel bromide and bromobenzene and stirring at 180°C for 4 hours. The reaction scheme was the following:

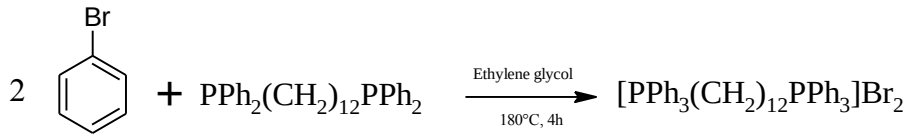

The product was then isolated in good yield and characterized by elemental analysis and ^{31}P-NMR, showing a singlet peak at 25,1 ppm (**Figure 129**).

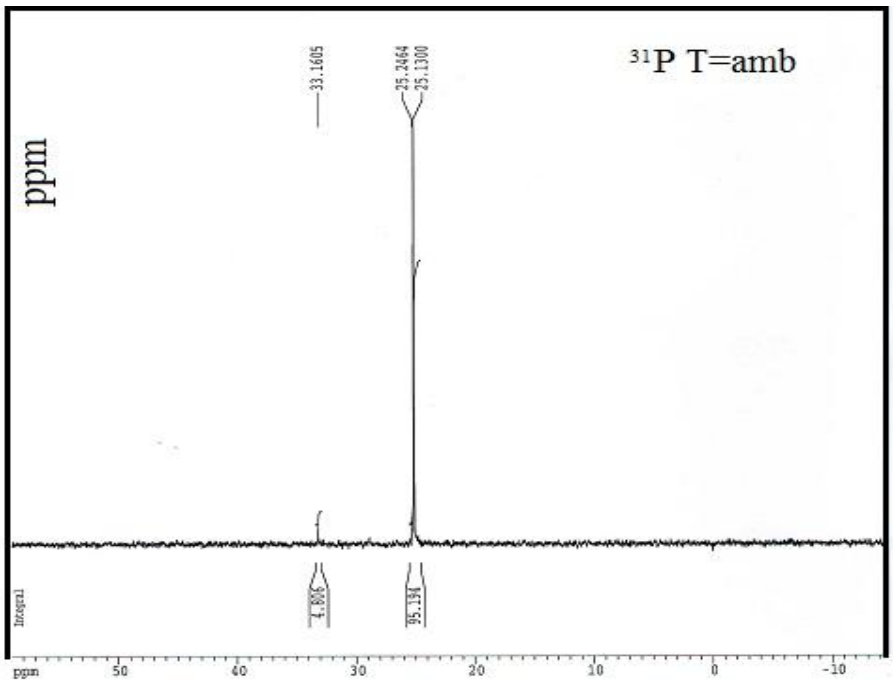

Figure 129 - ^{31}P-NMR in $CDCl_3$ of $[(PPh_3)(CH_2)_{12}(PPh_3)]Br_2$

5.2.2 Synthesis of [tppdod][Pt$_{15}$(CO)$_{30}$]

The sodium salt of platinum cluster $[Pt_{15}(CO)_{30}]^{2-}$ was obtained according to the reported procedure.[238] A subsequent methathesis reaction allowed to isolate the anion as bis(tetraphenylphosphonium)dodecane salt. The product was then checked by IR spectroscopy and investigated in oxidation reactions, with the aim to grow up the column of platinum atoms. Different oxidizing agents were tried the best resulting the trifluoroacetic acid, CF_3COOH.

5.2.3 Reaction of [tppdod][Pt$_{15}$(CO)$_{30}$] with trifluoroacetic acid

The reactivity of platinum columnar cluster $[\{Pt_3(CO)_3(\mu_2\text{-}CO)_3\}_n]^{2-}$ depends on the value of n. An increase of n results into an increased reactivity towards nucleophiles and

reductants, while a decrease turns into a better reactivity with electrophiles and oxidizing agents.

Two remarkable results, previously obtained by oxidation of such clusters can be cited. The first deals with the synthesis and structural characterization, as tetrabutylammonium, of $[Pt_{24}(CO)_{48}]^{2-}$, obtained starting from $[Pt_6(CO)_{12}]^{2-}$ anion, by oxidation with $SbCl_3$.

The second one is the oxidation of $[Pt_{15}(CO)_{30}]^{2-}$ to $[Pt_{18}(CO)_{36}]^{2-}$ by using H^+ as oxidizing agent and PPN^+ as counterion.

In our experiments, a THF solution of $[tppdod][Pt_{15}(CO)_{30}]$ was prepared and IR monitored (Figure 130).

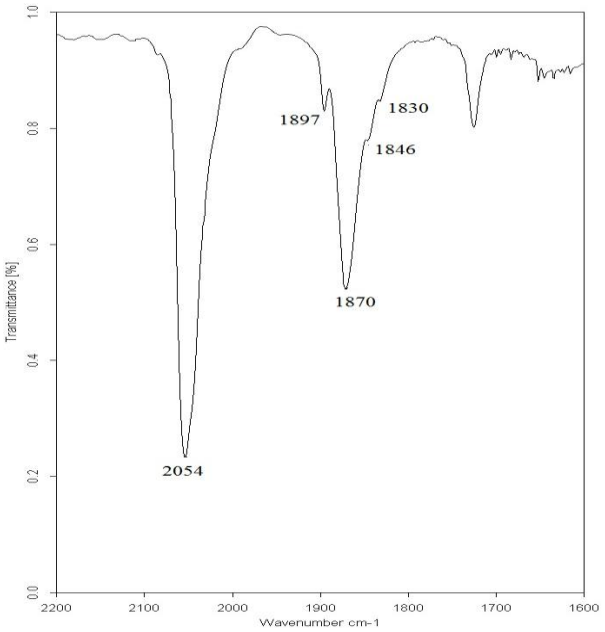

Figure 130 - IR spectrum in THF of $[tppdod][Pt_{15}(CO)_{30}]$

The IR spectrum is identical to that one of $[NBu_4]_2[Pt_{15}(CO)_{30}]$ dissolved in THF.[33]

The solution was put under CO static atmosphere and pure trifluoroacetic acid was added dropwise. Carbon monoxide atmosphere was usefull (even if CO is not a reagent) in order to depress a possible decarbonylation of platinum cluster in the presence of an excess of oxidizing agent.

The reaction quickly leaded to the formation of a dark violet precipitate. IR spectrum, of the surnatant solution exhibits weak bands at higher wavenumbers respect to the starting cluster, 2066(s), 2041(m), 1881(m) cm^{-1}.

The precipitated solid was so separated from the solution, resulting sparingly soluble in THF and acetone and well soluble in DMF.

IR spectrum of the solid redissolved in DMF shows carbonyl stretching bands at 2059(vs), 1902(sh), 1875(s), 1853(sh), 1840(sh) cm^{-1} (**Figure 131**).

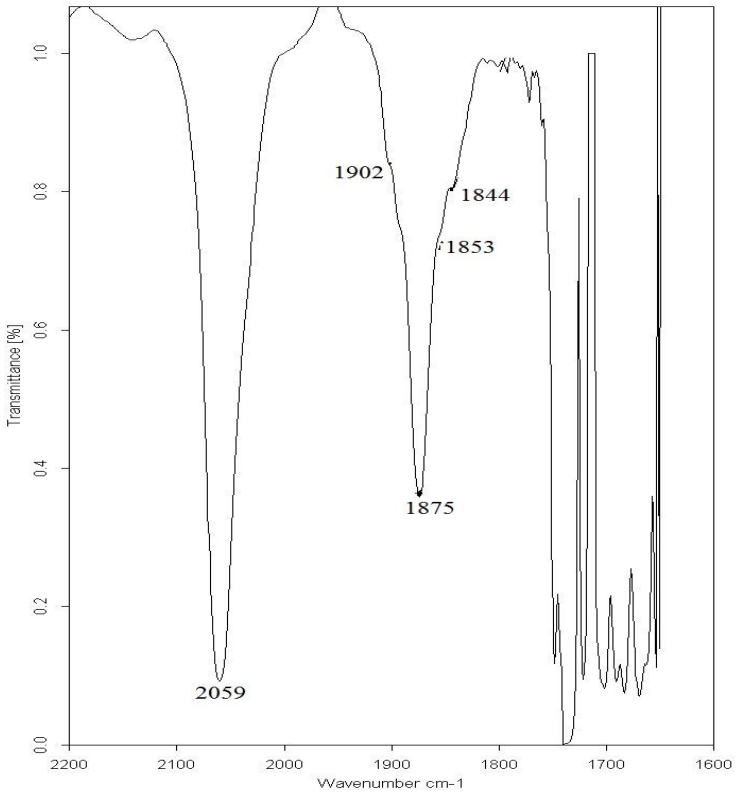

Figure 131- IR spectrum in DMF of [tppdod][$Pt_{18}(CO)_{36}$]

A stoichiometry justifying this result is the following:

$$6\ [Pt_{15}(CO)_{30}]^{2-} + 2\ H^{+} \rightarrow 5\ [Pt_{18}(CO)_{36}]^{2-} + H_2$$

DMF solution of the product was layered with 2-propanol resulting, after about ten days, in the formation of dark violet crystals, suitable for X-ray analysis, which was conducted by Prof. Stefano Zacchini of University of Bologna.

Data obtained from X-ray diffraction analysis allowed to formulate the compound as [Ph_3P-$(CH_2)_{12}$-PPh_3][$Pt_{18}(CO)_{36}$].

Figure 132 reports the elemental cell of the compound, where a whole dication and two $[Pt_9(CO)_{18}]^-$ units at bond distance are present. The cluster units remain at bond distance from other units owning to contiguous cells.

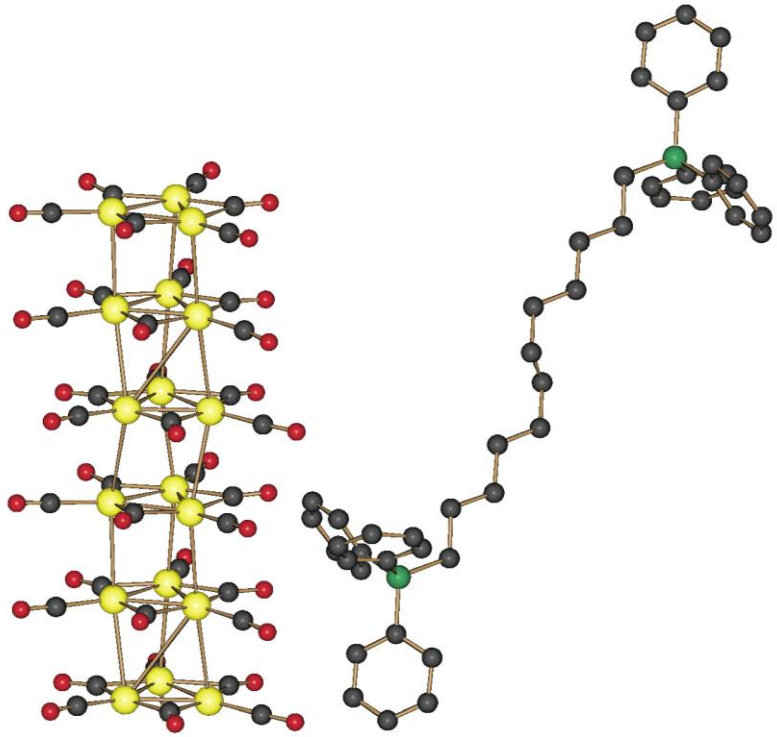

Figure 132 - Elemental cell of $[Ph_3P\text{-}(CH_2)_{12}\text{-}PPh_3][Pt_{18}(CO)_{36}]$

In the solid state, $[PPh_3\text{-}(CH_2)_{12}\text{-}PPh_3][Pt_{18}(CO)_{36}]$ is a 1D polymer and $[Pt_9(CO)_{18}]$ represents the monomeric unit (

Figure 133 and Figure 134).

Each $[Pt_9(CO)_{18}]^-$ unit is constituted by three packed Pt_3 triangles, which arbitrarerly we name as a, b, c.

Table 11 reports the average Pt-Pt bond lengths between triangles owning to a single $[Pt_9(CO)_{18}]^-$ unit (a-b, b-c) and between triangles owning to contiguous monomeric units (c-a').

Average distance	Å
a-b	3.112
b-c	3.151
c-a'	3.283

Table 11 - Average distances between Pt_3 triangles

The longest average distance (3.283 Å) exists between monomeric units. Absolutely the longest Pt-Pt bond measures 3.320 Å. All these values are lower than the double of platinum Van der Waals radius (3.4 Å). This means that an even weak bond interaction exists between monomeric units.

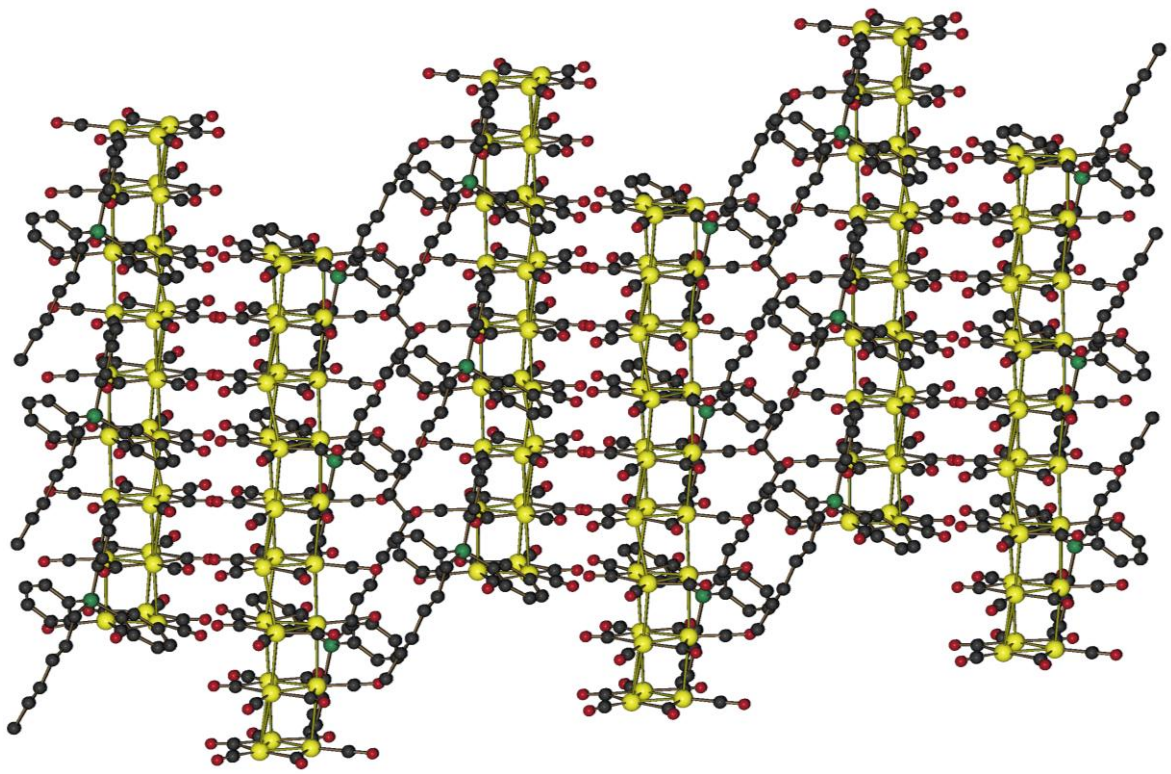

Figure 133 - View along 0, -1, 0 axe of $[Ph_3P\text{-}(CH_2)_{12}\text{-}PPh_3][Pt_{18}(CO)_{36}]$

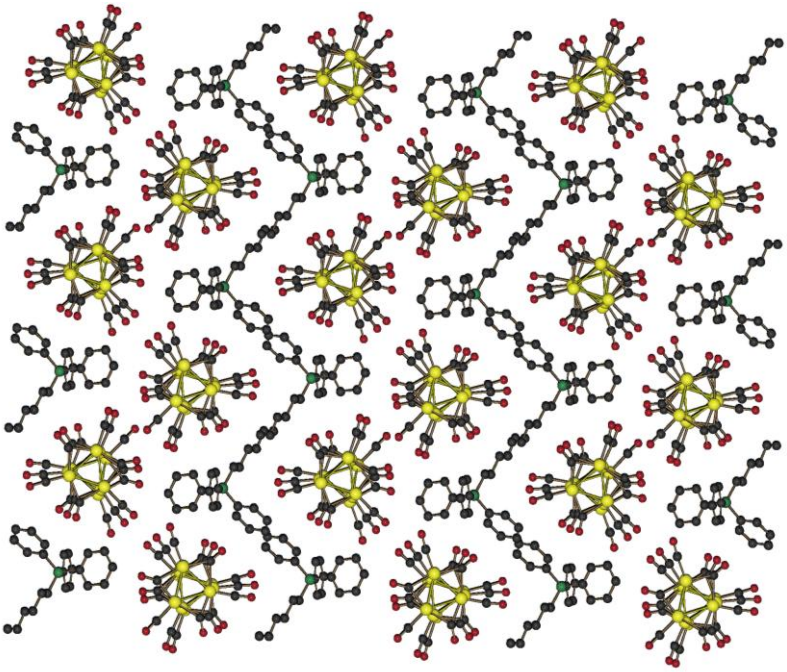

Figure 134 - View along -1, 0, 0 axe of $[Ph_3P\text{-}(CH_2)_{12}\text{-}PPh_3][Pt_{18}(CO)_{36}]$

Peierls distortion theory[239] should disfavour the formation of infinite $[Pt_{3n}(CO)_{6n}]^{2-}$ wires and a gap between adjacent molecule is requested. As otherwise demonstrated,[240] an increasing of L/D shape ratio enables the formation of such a kind of structure.

In this cases, a gap, anyway in the bonding distance limits, is not displayed between $[Pt_{18}(CO)_{36}]^{2-}$ units but between $[Pt_9(CO)_{18}]^{-}$ and this fact seems to be a direct consequence of the particular shape of the bis-monocation.

About the real identity of the species present in DMF solution, it is worth remembering that the metallic atom number / charge ratio for $[Pt_{18}(CO)_{36}]^{2-}$ and $[Pt_9(CO)_{18}]^{-}$ is exactly the same. This results in a same carbonyl stretching bands in IR spectrum. So this analytical technique could not distinguish the two species. Anyhow, considering that $[Pt_9(CO)_{18}]^{-}$ would be a radical species while the stable and known anion is $[Pt_9(CO)_{18}]^{2-}$, is very likely that $[Pt_{18}(CO)_{36}]^{2-}$ is the species present in solution.

5.2.4 Reaction of [tppdod][Pt$_{15}$(CO)$_{30}$] with silver nitrate

In this case the reaction was conducted by using DMF as solvent, under CO atmosphere (in order to prevent possible decarbonylation) and Ag^+ as oxidizing agent.

After the addition of five equivalent of $AgNO_3$ the solution turned from green to brown, while IR spectrum showed ν_{CO} bands typical for $[Pt_{18}(CO)_{36}]^{2-}$ (**Figure 135**).

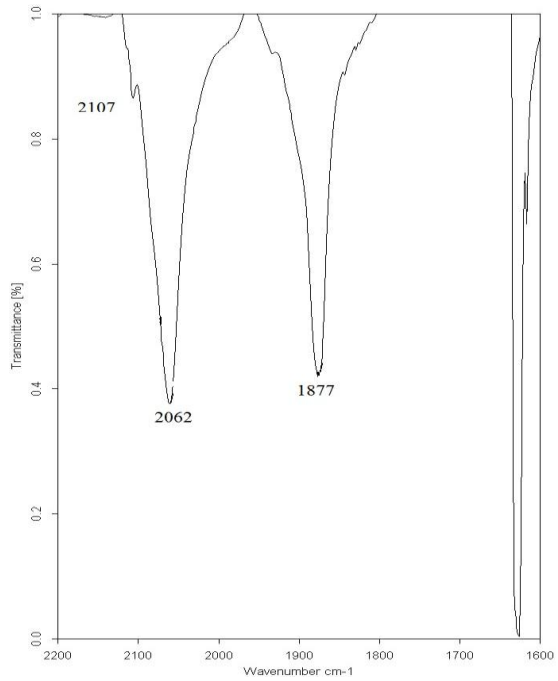

Figure 135 - IR spectrum in DMF after $AgNO_3$ addition

The product was then isolated by precipitation with water. The resulting brown solid was then sparingly soluble in THF or DMF. It was possible to suppose that a cluster higher nuclearity formed during the precipitation step.

In order to verify this hypothesys, the product was chemically reduced under nitrogen atmosphere, with the aim to reobtain a smaller soluble carbonyl cluster.

Therefore the solid was suspended in THF and a little amount of sodium tetrahydroborate was added. Quickly the suspended solid passed in solution which became red-brown in colour. IR spectrum showed ν_{CO} bands at 1970(s), 1947(m) and 1757(m) (**Figure 136**).

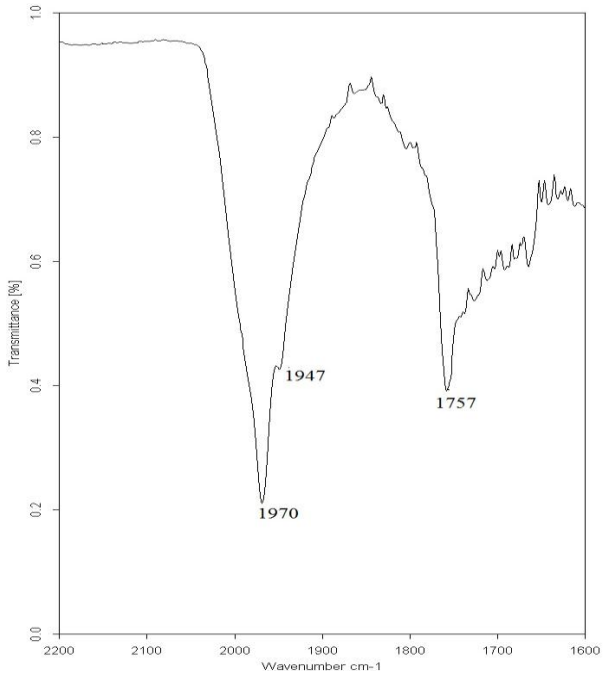

Figure 136 - IR spectrum in THF of the reduced species

This spectrum does not behave to any cluster of the series $[Pt_3(CO)_6]_n^{2-}$, but clearly indicates that, after the precipitation with water, the solid remained a carbonyl cluster and the insolubility was due to its high nuclearity.

5.2.5 Reaction of [tppdod][$Pt_{15}(CO)_{30}$] with other oxidizing agents

Other oxidizing agent were tested, like $(NH_4)_2Ce(NO_3)_6$, $[C_7H_7](PF_6)$ (tropilium) and Ph_3CCl (tritylium). No reactivity was noted with all these reagents: so they are too weak oxidants for Pt_{15} species. On the contrary, they selectively oxidized $[Pt_{12}(CO)_{24}]^{2-}$ to $[Pt_{15}(CO)_{30}]^{2-}$. In fact, by preparing a DMF solution containing a mixture of Pt_{12}/Pt_{15} (**Figure 137**) and adding one equivalent of i.e. Ce^{IV}, only $[Pt_{15}(CO)_{30}]^{2-}$ bands remain in the IR spectrum (**Figure 138**) and further additions of Ce^{IV} or other cited oxidants does not cause any change in the IR spectrum.

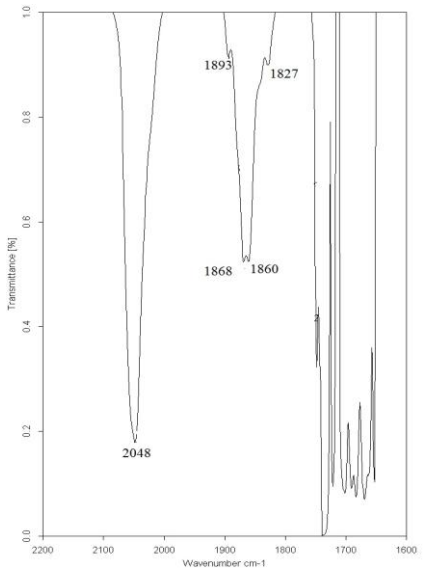

Figure 137 - IR spectrum in DMF of a $[Pt_{12}(CO)_{24}]^{2-}$ / $[Pt_{15}(CO)_{30}]^{2-}$ mixture

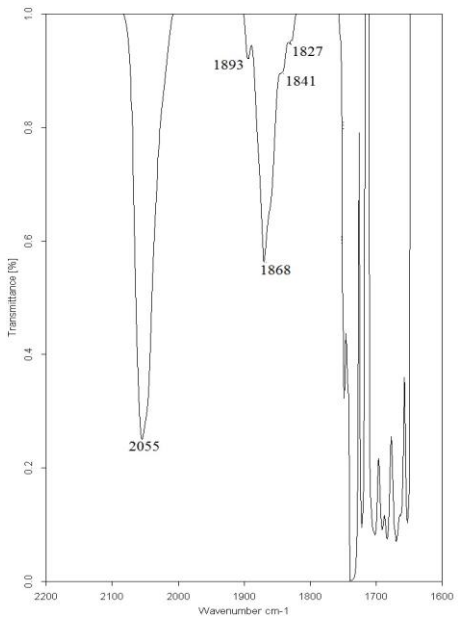

Figure 138- IR spectrum in DMF after Ce(IV addition

5.3 - $[N(C_8H_{17})_4]Br$, tetra-n-octylammonium bromide (toctaBr)

5.3.1 Synthesis of $[tocta]_2[Pt_{15}(CO)_{30}]$

Another tested cation was tetra-n-octylammonium, $[N(C_8H_{17})_4]^+$, commercially available as bromide. The long alkyl chains, exhibiting many freedom degrees, should partially disfavour the solid aggregation and consequently confer an high solubility to their compounds even in the presence of high nuclearity anionic carbonyl clusters.

$[N(C_8H_{17})_4]_2[Pt_{15}(CO)_{30}]$ was obtained from the sodic salt by methathesis reaction.

5.3.2 Reaction of $[N(C_8H_{17})_4]_2[Pt_{15}(CO)_{30}]$ with silver triflate

The starting material was dissolved in DMF and an IR spectrum was collected, even the carbonyl stretching bands were attributable to $[Pt_{12}(CO)_{24}]^{2-}$ instead of $[Pt_{15}(CO)_{30}]^{2-}$ (**Figure 139)**. After a change to CO atmosphere, silver trifluoromethansulphonate caused a shift in the CO bands, now attributable to a $[Pt_{15}(CO)_{30}]^{2-}$ (**Figure 140**). After further addition of Ag^+ and some hours stirring, the reaction mixture turned into a suspension. The solid was separate by centrifugation.

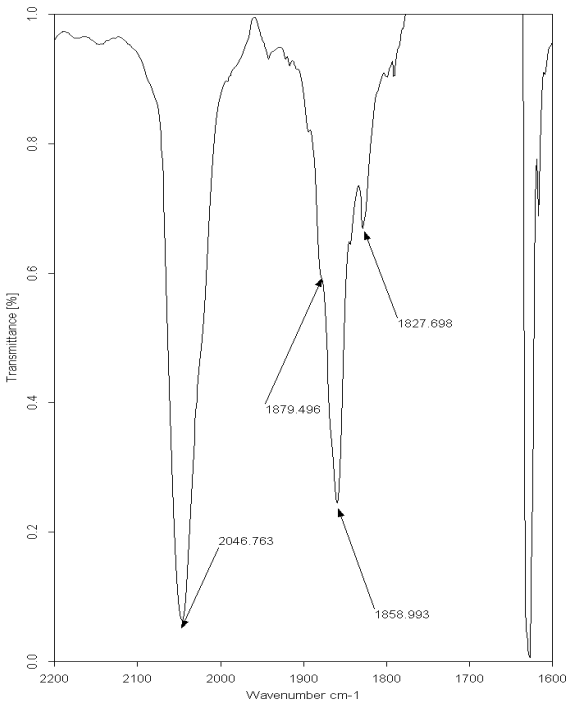

Figure 139 - IR spectrum in DMF of $[tocta]_2$ $[Pt_{12}(CO)_{24}]$

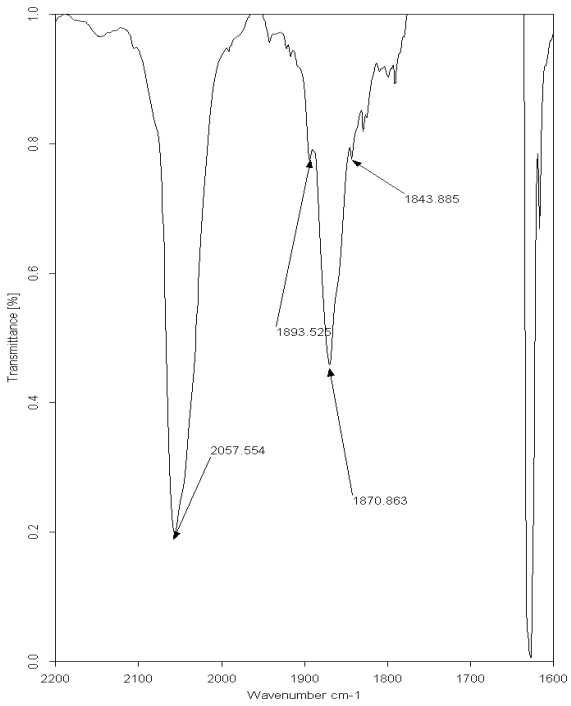

Figure 140 - IR spectrum in DMF after addition of silver triflate

The resulting solid was dark violet and sparingly soluble in all common organic solvents. ATR-IR (Total Attenuated Reflectance- IR) was collected, which showed bands at 2108(m), 2082(m), 1990(b) cm^{-1} (**Figure 141**).

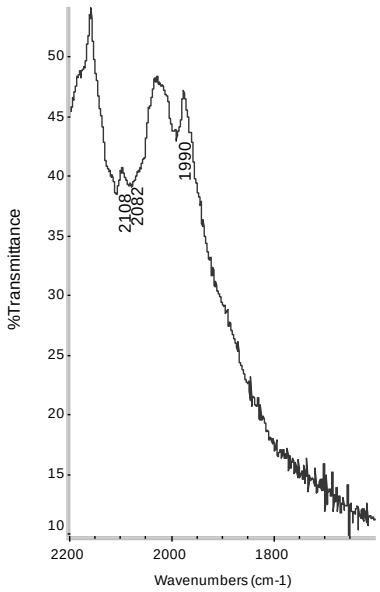

Figure 141 - ATR-IR spectrum of the product coming from the reaction between $[tocta]_2[Pt_{15}(CO)_{30}]$ and AgOTf

Elemental analysis (Table 12) suggests the formulation $[N(C_8H_{17})_4]_2[Pt_{30}(CO)_{60}]$.

% calculated	% found
C = 17,58	C = 16,80
H = 1,60	H = 1,73
N = 0,33	N = 0,42

Table 12

It is so clear that the cation plays a key role in the growing of columnar platinum carbonyl clusters.

6 - Electrochemical investigation on $[Pt_{26}(CO)_{32}]^{2-}$

Although this compound was already reported, its preparation was not optimized.
With some slightly modifications with respect to the past we have been able to obtain a highly pure product. This allowed us to perform electrochemical and spectroelectrochemical studies. The species shows a redox behaviour less rich than its analogous $[Pt_{19}(CO)_{22}]^{4-}$, $[Pt_{24}(CO)_{30}]^{2-}$, $[Pt_{38}(CO)_{44}]^{2-}$. In the ciclyc voltammetry, collected in THF, we can see three cathodic and one anodic processes, all reversible (**Figure 142**). The spectroelectrochemical trend for the oxidation step $[Pt_{26}]^{2-/-}$ displays two isosbestic points, which confirms the stability of the two oxidation states (**Figure 143**). One isosbestic point is shown by the reduction step $[Pt_{26}]^{2-/3-}$ too.

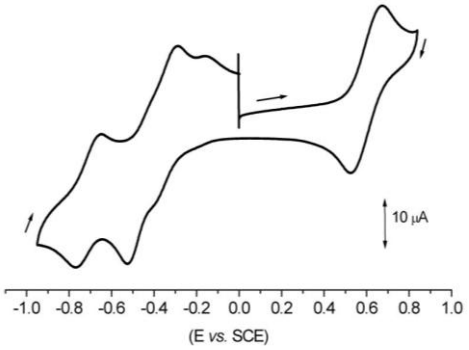

Figure 142 - Cyclic voltammetric profile of $[PPh_4]_2[Pt_{26}(CO)_{32}]$

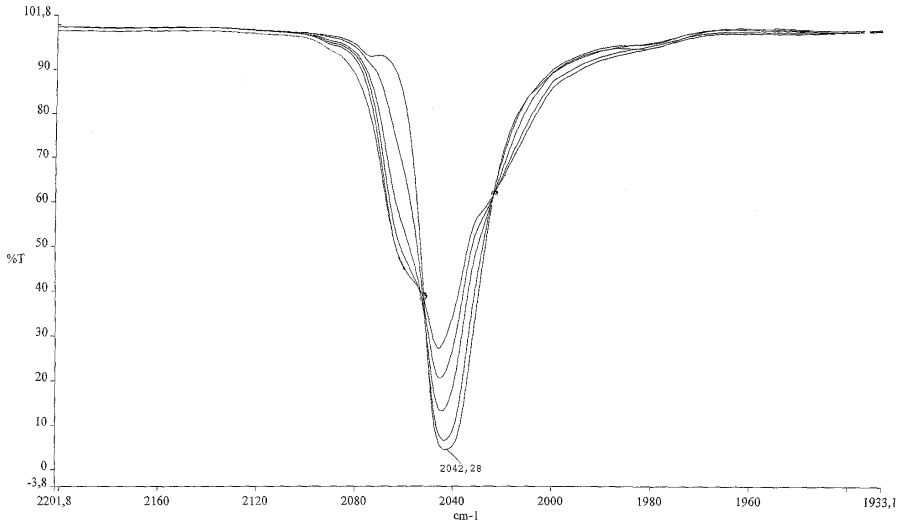

Figure 143 Spectroelectrochemistry of $[PPh_4]_2[Pt_{26}(CO)_{32}]$ in THF

Experimental Section

$[PPh_4][Ir(CO)_4]$

In a 300 mL Schlenk tube DMSO (30 mL) is degassed and put under CO atmosphere. Then $IrCl_3 \cdot 3H_2O$ is dissolved and triturated KOH (3-4 tablets) is added. The resulting suspension is stirred under CO for 3-4 days, adding further amounts of KOH once a day. When the reaction is completed (IR ν_{CO} 1890 cm^{-1}) a solution of PPh_4Cl (1 g) in water (100 mL) is added. This allowed a beige solid to precipitate, which is filtered under nitrogen and washed with water.

THF IR: ν_{CO} 1890 cm^{-1}

$[Ir_4(CO)_{12}]$

In a glass 8,69 g of $IrCl_3 \cdot 3H_2O$ ($2{,}46 \cdot 10^{-2}$ mol) and about 300 mL of formic acid (98%) were introduced. The glass has been put in autoclave. Then it was heated under stirring at 130°C for 12 hours and allowed to cool for 24 hours. The resulting suspension of a pale yellow solid and a uncoloured solution has been poured in about 2 L of water. The resulting solid has been filtered over Buchner and the product washed with methanol (200 mL) and acetone (200 mL).

Obtained 5,52 g, 81%, yield.

ATR-IR ν_{CO} 2053, 2018, 2002, 1995 cm^{-1})

Estimate of the pressure inside the autoclave

For the synthesis of $[Ir_4(CO)_{12}]$, two extreme stoichiometry are possible, while the real is an intermediate one.

A

$4\ IrCl_3 \cdot 3H_2O + 18\ HCOOH \rightarrow Ir_4(CO)_{12} + 6\ COCl_2 + 30\ H_2O$

B

$4\ IrCl_3 \cdot 3H_2O + 18\ HCOOH \rightarrow Ir_4(CO)_{12} + 12\ HCl + 24\ H_2O + 6\ CO_2$

In our autoclave there was a free volume of about 0,133 L. We have overlooked the partial dissolution of HCl, CO_2, and $COCl_2$ in formic acid. We have considered an intermediate

stoichiometry between A and B, by assuming that 9,75 moles of gas are formed per mole of $IrCl_3 \cdot 3H_2O$, so ¼[(36+42)/2], where 36 are the moles of gases forming per 4 moles of iridium trichloride in A and 42 those of B.

So the pressure inside the autoclave, at a given temperature, is:

$$P = \frac{nRT}{V_0\left(1+\frac{p_s}{RT(d_s/M_s - p_s/RT)}\right)} + p_s$$

where

n = moles of gases forming during the reaction

R = gas constant, 0,082 atm·l/mol·K

T = temperature, K

V_0 = starting free volume in the autoclave, L

p_s = solvent vapour tension at T, atm

d_s= solvent density at T, g/L

M_s= solvent molar mass, in g/mol

In the reported synthesis, at 120°C the resulting pressure is 67,8 atm

$[PPh_4][Ir_4Br(CO)_{11}]$

In a 250 mL two necked flask, $[Ir_4(CO)_{12}]$ (1,52 g, $1,38 \cdot 10^{-3}$ mol), LiBr (0,72 g, $8,26 \cdot 10^{-3}$ mol) and THF (40 mL) were introduced. This suspension has been stirred at 75°C in nitrogen atmosphere for 10 hours. During this time the suspension turns into a red solution. A solution of PPh_4Br (1,64 g) in 100 mL of 2-propanol has been added. The resulting solution has been concentrated in order to remove most of THF. This allowed an orange solid to precipitate, filtered under nitrogen and washed with 2-propanol (4x25 mL).

Obtained 1,12 g, 55% yield.

CH_2Cl_2 IR: ν_{CO} 2081-2050-2042-2007-1821 cm^{-1}

$[PPh_4]_2[Ir_6(CO)_{15}]$

In a 250 mL two necked flask, $[Ir_4(CO)_{12}]$ (0,5 g, $4{,}52 \cdot 10^{-4}$ mol), $[PPh_4][Ir(CO)_4]$ (0,5 g, $7{,}7 \cdot 10^{-4}$) and THF (40 mL) were introduced. The resulting suspension was refluxed under nitrogen atmosphere until the $[Ir_4(CO)_{12}]$ was consumed. Sometimes a further addition of $[PPh_4][Ir(CO)_4]$ was necessary. This red solution was added to a solution prepared from PPh_4Br (0,5 g) in 2-propanol (80 mL). After partial remotion of the solvents by vacuum pump, the precipitated solid was filtered under nitrogen and washed with 2.propanol.

THF IR: ν_{CO} 1980(s), 1770(m) cm^{-1}

Recovery of metallic platinum from Pt containing residues

During the research work, all the platinum containing residues (filtration waters, undesired products, filters, papers) are disposed together in a suitable becker.

When they reached a sufficient amount, the mixture is heated by a sand-oven in order to evaporate all the solvents. Then papers are burnt by Bunsen flame and all the solid is treated with oxygen reach flame for some minutes and heated by Bunsen for some hours. The resulting mixture is grossly grinded and treated with aqua regia, stirring at 80°C for 12 hours. To the filtrated resulting solution, ammonium sulphate is added, resulting in the precipitation of pale orange ammonium platinate, which is filtered, washed with water and dried. Solid ammonium platinate is then decomposed to metallic platinum by heating with Bunsen for some hours.

Metallic platinum is then converted to Na_2PtCl_6.

$Na_2PtCl_6\ 6H_2O$

Metallic platinum is treated with a mixture of concentrated HCl and HNO_3 (volume ratio 3:1), stirring at 70°C until its complete dissolution. Then a stoichiometric amount of NaCl is added and the solution concentrated by heating for some hours. The solution is allowed to cool down at RT, resulting in the crystallization of $Na_2PtCl_6\ 6H_2O$. After filtration by Buchner, the filtrate solution is concentrated again and the previous operation repeated until complete recovery of $Na_2PtCl_6\ 6H_2O$.

$[NBu_4]_2[Pt_9(CO)_{18}]$

In a 500 mL 2 necked flask, a solution made from NaOH (8 g) in methanol (120 mL) is put under CO atmosphere for about 30 minutes. Na_2PtCl_6 (10 g) is added and the resulting orange suspension is stirred under CO for about 24 hours. The resulting suspension is filtered in order to eliminate NaCl and Na_2CO_3. and a solution made from $[NBu_4]Cl$ (2 g) in water (100 mL) is added to the violet solution of the cluster. This allowed the product to precipitate, which is filtered under nitrogen and washed with water.

THF: ν_{CO} 2030(s), 1855(m) cm^{-1}

$[NBu_4]_4[Pt_{19}(CO)_{22}]$

$$3\ [Pt_9(CO)_{18}]^{2-} \xrightarrow{CH_3CN,\ riflusso} [Pt_{19}(CO)_{22}]^{4-} + [Pt_8(CO)_x]^{2-} + (32-x)\ CO$$

In a 500 mL 2 necked flask $[NBu_4]_2[Pt_9(CO)_{18}]$ (3,5 g, 1,275 mmol) was dissolved in acetonitrile (150 mL) and heated at 85°C under nitrogen flow for 5 hours, until the solution became brown-orange in colour. Than it was completely dried by vacuum pump and the resulting solid was washed with methanol (5x20 mL) and dried by vacuum pump.

$[PPh_4]_4[Pt_{19}(CO)_{22}]$

$[PPh_4]_4[Pt_{19}(CO)_{22}]$ has been obtained by methathesis reaction dissolving $[NBu_4]_4[Pt_{19}(CO)_{22}]$ in acetonitrile and adding $[PPh_4]Cl$ dissolved in 2-propanol.

IR spectrum (CH_3CN) : ν_{CO} 2005(s), 1800(m) cm^{-1}

$[PPh_4]_2[Pt_{15}(CO)_{30}]$

$CH_3COONa\ 3H_2O$ (3,80 g, 28 mmol) was dissolved in CH_3OH (35 mL) and two tablets of NaOH were added. The solution was saturated with CO, for twenty minutes and then 2,0 g (4,41 mmol) of $Na_2PtCl_6\ 6H_2O$ were added. The resulting solution was allowed to stir at RT for 48 hours, while the colour turned from orange to bright green passing from a beige suspension. The resulting suspension was filtered in order to eliminate NaCl and Na_2CO_3. To the filtrate solution 1,30 g of $[PPh_4]Cl$ dissolved in water (50 mL di H_2O) were added in order to precipitate the cluster as tetrabutylammonium salt. The resulting solid was

filtered under nitrogen atmosphere, washed twice with 50 mL of water and dried by vacuum pump.

IR spectrum (THF) ν_{CO} 2055 (vs), 1898 (sh), 1874 (m), 1845 (sh) cm^{-1}

$[PPh_4]_2[Pt_{24}(CO)_{30}]$

$$2\ [Pt_{15}(CO)_{30}]^{2-} \xrightarrow{THF,\ riflusso} [Pt_{24}(CO)_{30}]^{2-} + [Pt_6(CO)_x]^{2-} + (30\text{-}x)\ CO$$

$[PPh_4]_2[Pt_{15}(CO)_{30}]$ (3 g, 0.675 mmol) was dissolved in THF (150 mL) and the resulting solution was heated at 90°C under nitrogen flow for about 8 hours. The solution became brown and a dark oleum shows up. The solution was separated and treated with a little amount of p-toluensulphonic acid in order to selectively convert the possible presence of $[Pt_{24}(CO)_{30}]^{3-}$ into $[Pt_{24}(CO)_{30}]^{2-}$. Then the solution was added to 250 mL of 2-propanol and concentred by vacuum pump, resulting in an abundant precipitation of the desired product which is filtered, washed with 2-propanol and dried.

$[PPh_4]_2[Pt_{26}(CO)_{32}]$

$$13\ [Pt_6(CO)_x]^{2-} + (96\text{-}13x)\ CO + 20\ H^+ \xrightarrow{THF} 3\ [Pt_{26}(CO)_{32}]^{2-} + 10\ H_2$$

The oil coming from the decomposition of $[PPh_4]_2[Pt_{15}(CO)_{30}]$ was washed with THF (4x30 mL) and 2-propanol (4x40 mL) so making the solid well powdered.

The solid was then suspended in THF (130 mL) and put under CO atmosphere (1 atm); then concentred H_2SO_4 (5 drops) was added and rhe soliution was allowed to stir overnight. Then it was added to 2-propanol (200 mL) and the solution was concentred by vacuum pump, resulting in the precipitation of an abundant solid, which was filtred, washed and dried. $[PPh_4]_2[Pt_{26}(CO)_{32}]$ is finally extracted with methanol (30 mL).

[AuCl(THT)]

$NaAuCl_4$ (0,5 g) is dissolved in ethanol (30 mL) under nitrogen and tetrahydrothiophene (THT) is dropwise added far from light until the white desired product precipitates. It is

filtered under nitrogen, washed with ethanol and ethyl ether (20+20 mL), dried and maintained far from light.

3,3′-5,5′-tetrakis(diphenylphosphano)biphenyl (180tetraphos)

3,3′-5,5′-tetrafluorobiphenyl[241] (0,813 g, 3,59 mmol) was added to a 0,5 M THF solution of $KPPh_2$ (57 ml, 28,5 mmol). The reaction was slightly exotermic and it was stirred at room temperature for an hour and then refluxed at 90°C overnight. The resulting red clear solution was cooled to room temperature and 200 ml of CH_3OH were slowly added. The solution turned pale yellow and a white solid precipitated. The solvent was separated from the solid, 100 ml of CH_3OH added, and the mixture stirred for 30 min. The solid was filtered and washed with CH_3OH, obtaining 2,6 g of a white product. Yield 81%

^{1}H-NMR 300 MHz ($CDCl_3$): 7,41(d) ppm (4H) $^3J_{H-P}$ = 7,8 Hz, 7,31-7,18(m) (40H), 7,14(t) $^3J_{H-P}$ = 6,6 Hz

^{31}P-NMR 127 MHz ($CDCl_3$): -3,85(s) ppm.

Elemental analysis: calculated for $C_{60}H_{46}P_4$ C 80,89%, H 5,20%. Found C 80,62%, H 5,24%

[3,3′-5,5′-tetrakis(diphenylphosphano)biphenyl]tetrakis[chlorogold(I)]

180tetraphos (0,100 g, $1{,}1 \cdot 10^{-1}$ mmol) was dissolved in chloroform (3 mL) and [AuCl(THT)][242] (THT = tetrahydrothiophene) (0,144 g, $4{,}5 \cdot 10^{-1}$ mmol) was added. The resulting solution was stirred for 30 min, then the solvent was removed by vacuum and the resulting white powder was washed with ethanol and diethylether (5+5 mL). Obtained 0,150 g, yield 73,6%

^{31}P-NMR 127 MHz 34,3(s) ppm. Elemental analysis: calculated for $C_{60}H_{46}Au_4Cl_4P_4$ C 39,58%, H 2,55%. Found C 38,57%, H 2,70%

1,3,5-tris(3′-5′-difluorophenyl)benzene

Tetrakis(triphenylphosphino)palladium(0) (0,160 g, 0,14 mmol) was dissolved in 35 ml of degassed dimethylformamide (DMF) and 3,5-difluorobromobenzene (1,74 ml, 15,11 mmol), benzene-1,3,5-tris-(boronic acid)[243] (0,695 g, 2,46 mmol) and Na_2CO_{3aq} 2M (35 ml) were in sequence added. The resulting mixture was stirred at 90°C overnight. Then the

crude was filtered and washed with water, resulting a light brown solid that was suspended in diethyl ether and treated in an ultrasound bath, affording a white solid that was filtered and dried. Obtained 1,0 g, yield 99%.

^{1}H NMR 300 MHz (DMSO, 60°C) 8,13(s) ppm (3H), 7,81(d) ppm (6H) $^{3}J_{H-F}$ = 8,4 Hz, 7,26(t) ppm $^{3}J_{H-F}$ = 8,7 Hz ^{19}F-NMR 282 MHz (DMSO, 60°C, ^{1}H decoupled) -110,1(s) ppm. Elemental analysis: calculated for $C_{24}H_{12}F_6$ C 69,57%, H 2,92%. Found C 66,78%, H 3,05%

1,3,5-tris[3′-5′-bis(diphenylphosphano)phenyl]benzene (120hexaphos)

1,3,5-tris(3′-5′-difluorophenyl) benzene (0,500 g, 1,21 mmol) was added to a 0,5 M THF solution of $KPPh_2$ (30 ml, 15 mmol) and the resulting solution stirred at room temperature for an hour. Then it was stirred at 90°C overnight. After re-cooling the solution to room temperature, 60 ml of CH_3OH were added, the red solution turned pale yellow and a white solid precipitated. Then the solvent was removed, 100 ml of CH_3OH were added and this suspension stirred for half an hour, after which the solid was filtered and washed with additional CH_3OH, affording 1,6 g of a white solid, 93% yield.

^{1}H NMR 300 MHz ($CDCl_3$) 7,48(d) ppm (6H) $^{3}J_{H-P}$ = 7,8 ppm, 7,40(s) ppm (3H), 7,30-7,25(m) ppm (60H), 7,10(t) ppm (3H) $^{3}J_{H-P}$ = 6 Hz. ^{31}P-NMR 127 MHz ($CDCl_3$) -4,0(s) ppm. Elemental analysis: calculated for $C_{96}H_{72}P_6$ C 81,69%, H 5,14%. Found C 79,52%, H 6,31%

[1,3,5-tris[3′-5′-bis(diphenylphosphano)phenyl]benzene]hexakis[chlorogold(I)]

120hexaphos (0,080 g, $5{,}6 \cdot 10^{-2}$ mmol) was dissolved in chloroform (6 mL) and [AuCl(THT)][242] (THT = tetrahydrothiophene) (0,107 g, $3{,}4 \cdot 10^{-1}$ mmol) was added. The resulting solution was stirred for 30 min, then the solvent was removed by vacuum and the resulting white powder was washed with ethanol and diethylether (5+5 mL). Obtained 0,094 g, yield 57,8%

^{31}P-NMR 127 MHz 33,7 (s) ppm. Elemental analysis: calculated for $C_{96}H_{72}Au_6Cl_6P_6$ C 41,09%, H 2,59%. Found C 40,54%, H 3,10%

$[PPh_4]_4[\{Ir_6Au(CO)_{15}\}_4$(180tetraphos)]

$[PPh_4]_2[Ir_6(CO)_{15}]$ (0,110 gr, 4,89x10^{-5} mol) was dissolved in THF (3 mL) under nitrogen atmosphere. In a second Schlenk tube protected from light $[\{AuCl\}_4$(180tetraphos)] (0,022 gr, 1,22x10^{-5} mol) was dissolved in THF (5 mL) and silver trifluoromethansulphonate (0,012 gr, 4,89x10^{-5} mol) was added, resulting in the precipitation of AgCl. The surnatant solution was added to the cluster solution and the system was allowed to react for 30 minutes. Then 2-propanol (20 mL) was added, resulting in the precipitation of a brown solid, which was washed twice with 2-propanol (6 mL).

IR spectrum (THF) ν_{CO}: 2020(vs), 1788(m) cm^{-1}

^{31}P-NMR: 97.70(s), 23,64(s) ppm

Elemental analysis: calculated for $P_8Ir_{24}Au_4C_{216}H_{126}O_{60}$ C 27,82%, H 1,32%,

Found C 27,48%, H 1,81%.

$[PPh_4]_6[\{Ir_6Au(CO)_{15}\}_6$(120hexaphos)]

$[PPh_4]_2[Ir_6(CO)_{15}]$ (0,163 gr, 7.26x10^{-5} mol) was dissolved in THF (3 mL) under nitrogen atmosphere. In a second Schlenk tube protected from light $[\{AuCl\}_6$(120hexaphos)] (0,0340 gr, 1,21x10^{-5} mol) was dissolved in THF (5 mL) and silver trifluoromethansulphonate (0,0190 gr, 7.26x10^{-5}mol) was added, resulting in the precipitation of AgCl. The surnatant solution was added to the cluster solution and the system was allowed to react for 30 minutes. Then 2-propanol (20 mL) was added, resulting in the precipitation of a brown solid, which was washed twice with 2-propanol (6 mL).

Elemental analysis: calculated for $P_{12}Ir_{36}Au_6C_{330}H_{212}O_{90}$ C 28,17%, H 1,37%,

Found C 29,37%, H 1,90%.

IR spectrum (THF): ν_{CO} 2062(w), 2019(vs), 1781(m) cm^{-1}.

Bis(tetraphenylborate)-N,N′-dimethyl-9,9′-bis-acridinium $[Acr][B(C_6H_5)_4]_2$

Dinitrate of N,N′-dimethyl-9,9′-bis-acridinium (1,00 g, 1,95 mmol) was dissolved in water (200 mL) by heating at 50 °C. Then $Na[B(C_6H_5)_4]$ (1,34 g, 3,917 mmol) was added and the

mixture was stirred. After then the precipitation was completed the solution was filtered off *via* Buchner and the solid washed with water (3 x 10 mL) and dried by vacuum pump, obtaining 1,70 g of $[Acr][B(C_6H_5)_4]_2$.

Yield 84.6%

$[Acr][Ir_6(CO)_{15}]$

$[PPh_4]_2[Ir_6(CO)_{15}]$ (0,120 g, 0,045 mmol) was dissolved in THF (7 mL). Then $[Acr][B(C_6H_5)_4]_2$ (0,046 g, 0,045 mmol) was added to the stirred solution. After twenty minutes the precipitated white $[PPh_4][B(C_6H_5)_4]$ was separated and n-heptane (15 mL) was added to the solution. After filtration the solid was washed with n-heptane and dried by vacuum pump.

IR spectrum (THF) ν_{CO} 2033(s), 2020(vs), 2010(vs), 1987(m), 1821(m), 1778(m) cm^{-1}

Elemental analysis: calculated for $[Acr][Ir_6(CO)_{15}]$, C 39,45% H 2,06% N 1,38%.

Found C 40,80 % H 2,89% N 0,9%.

1,12 bis(diphenylphosphano)dodecane [Ph_2P-$(CH_2)_{12}$-PPh_2]

In a Schlenk tube $KP(C_6H_5)_2$ (16.3 mL, 0.5 M in THF) have been introduced and cooled at -78°C. A solution prepared from 1,12-dichlorododecane (1,01 g, $4.24 \cdot 10^{-3}$ mol) and THF (1.5 mL) has been dropwise added under stirring, getting to the precipitation of a white solid. After one hour 15 mL of water have been added and the suspension vigorously stirred. Then the organic phase has been separated, the solvent evacuated and the resulting white solid has been dissolved in toluene (35 mL) and dried with Na_2SO_4. Methanol (80 mL) has been added to the toluene solution, allowing the precipitation of the product as a white powder, that has been filtered over Buchner and washed with methanol.

Obtained 1.55 g, 68% yield

^{31}P-NMR: -15,63(s) ppm (CD_2Cl_2)

Elemental analysis: calculated for $C_{36}H_{44}P_2$ C 80,48% H 8,70%. Found C 80,27% H 8,23%

1,12-bis(triphenylphosphonium)dodecane dibromide [tppod]Br_2

In a neck glass tube 0,80 g (1,49 mmol) of [Ph_2P-$(CH_2)_{12}$-PPh_2], 0,02 g of $NiBr_2$ (0,09 mmol), 0,3 mL of bromobenzene (3,0 mmol, d=1,49 g/mL) and 1 mL of ethylene glycol were

added. The mixture was then heated at 180 °C for 4 hours. The resulting solution was then cooled down to RT and 20 mL of CH_2Cl_2 was added. Then the solution was put in a separating funnel and three washing with 30 mL of water were performed. The organic phase was then anhydrified with $MgSO_4$, filtered and concentrated by vacuum pump until the obtainment of a sticky pale yellow solid. It was redissolved in 5 mL of CH_2Cl_2 and 20 mL of diethylether was added. This resulted in the precipitation of a white solid which was filtered, washed with diethylether and dried by vacuum pump, finally becoming well powdered.

Obtained 0,560 g, yield 44,3 %.

^{31}P-NMR 121 MHz ($CDCl_3$) 25 (s) ppm.

Elemental analysis: calculated for $C_{48}H_{54}Br_2P_2$ C 67,6%, H 6,3%. Found C 70,4%, H 6,8%.

[tppod][Pt$_{15}$(CO)$_{30}$]

The synthetic procedure for obtaining $Na_2[Pt_{15}(CO)_{30}]$ was the same previously reported. To the cluster methanolic solution 2.5 equivalents of [tppod]Br_2 dissolved in water was added, leading to precipitation of the desired product. After filtration under nitrogen atmosphere, it was washed twice with 30 mL of water and dried by vacuum pump.

IR spectrum (THF) ν_{CO} 2056 (vs), 1896 (sh), 1874 (m), 1845 (sh) cm^{-1}

[tppod][Pt$_{18}$(CO)$_{36}$]

[tppod][$Pt_{15}(CO)_{30}$] (0,100 g, 0,022 mmol) was dissolved in THF (10 mL). Then CF_3COOH was added dropwise under CO atmosphere until the abundant precipitation of a violet solid (about 10 drops needed). The solution showed weak carbonyl stretching bands at (2066(s), 2041(m), 1881(m) cm^{-1}). The solid was isolated and washed with THF (2 mL).

IR spectrum (DMF) ν_{CO} 2059 (vs), 1902(sh) 1875(s), 1853(sh), 1840 (sh) cm^{-1}.

Crystals suitable for X-ray diffraction analysis were obtained by carefully layering a concentrated DMF solution of the product with 2-propanol.

[tocta]$_2$[Pt$_{15}$(CO)$_{30}$]

The synthetic procedure for obtaining $Na_2[Pt_{15}(CO)_{30}]$ was the same previously reported. To the cluster methanolic solution four equivalents of $[N(C_8H_{17})_4]Br$ (toctaBr$_2$) dissolved in

water was added, leading to precipitation of the desired product. After filtration under nitrogen atmosphere, it was washed twice with 30 mL of water and dried by vacuum pump. The product looks like a sticky solid.

IR spectrum (THF) ν_{CO} 2055 (vs), 1898 (sh), 1874 (m), 1845 (sh) cm^{-1}

$[tocta]_2[Pt_{30}(CO)_{60}]$

$[tocta]_2[Pt_{15}(CO)_{30}]$ (0,060 g, 0,013 mmol) was dissolved in DMF (6 mL). Under CO atmosphere 0,069 g (0,27 mmol) of silver triflate was added resulting in the formation a very dense suspension green-yellow in colour which was allowed to stir overnight. After centrifugation the resulting solid was washed twice with acetone (3 mL) and dried by vacuum pump.

Solid state ATR-IR ν_{CO} 2108 , 2082 , 1990 cm^{-1}

Elemental analysis: calculated for $[N(C_8H_{17})_4]_2[Pt_{30}(CO)_{60}]$ C17,58% H 1,60% N 0,33%.

Found C 16,80% H 1,73% N 0,42%.

$[PPh_4]_3[Pt_5(CO)_5\{Cl_2Sn(\mu\text{-}OMe)SnCl_2\}_3]$

Anhydrous $SnCl_2$ (0.489 g, 2.58 mmol) was added in solid to a solution of $[NBu_4]_2[Pt_{15}(CO)_{30}]$ (0.604 g, 0.142 mmol) in CH_3OH (75 mL). The solution turned from green to brown-red and it was stirred at room temperature for 1 h. Then Na_2CO_3 (0.100 g, 0.943 mmol) was added. The suspension was stirred at room temperature for additional three hours. This resulted in the precipitation of an unknown species, removed by filtration, which was soluble in acetone with a single carbonyl stretching band at 2066 cm^{-1}. To the filtrate solution an excess of $[PPh_4]Cl$ (0,503 g) was added, allowing the product to precipitate. After filtration and washing with CH_3OH, the crude product $[PPh_4]_3[Pt_5(CO)_5\{Cl_2Sn(\mu\text{-}OMe)SnCl_2\}_3]$ was recovered by extraction with acetone. Polycrystalline powder was obtained from acetone/methanol. (yield 0.76 g, 55% based on Pt). The product is soluble in thf, acetone, CH_3CN and dmf.

$C_{80}H_{66}Cl_{12}O_8P_3Pt_5Sn_6$ (3361.26): calcd. C 28.56, H 1.98, Sn 21.40, Pt 29.00; found C 28.72, H 2.09, Sn 21.58, Pt 29.16. IR (acetone, 293 K) ν(CO): 2034(s), 2008(ms) cm−1.

$[PPh_4]_4[Pt_6(SnCl_2)_2(SnCl_3)_4(CO)_6]$

$[PPh_4]_2[Pt_{15}(CO)_{30}]$ (0,578 g, 0,130 mmol) was dissolved in acetone (20 mL) under nitrogen atmosphere. Then $SnCl_2$ (0,371 g, 1,96 mmol) and $[PPh_4]Cl$ (0,487 g, 1,30 mmol) were added, while the solution quickly turned from green to brown. Then the solution was allowed to stir for 2 hours, resulting in the precipitation of abundant $[PPh_4]_4[Pt_6(SnCl_2)_2(SnCl_3)_4(CO)_6]$. It was separated from the mother liquor (which contained an unknown by-product) by filtration, washed with acetone and dried by vacuum pump.

IR spectrum (CH_3CN): ν_{CO} 2038(s) cm^{-1}

$[PPh_4]_2[Pt_6(SnCl_2)_2(SnCl_3)_2(CO)_6\{P(C_6H_5)_3\}_2]$ hypothetic

$[PPh_4]_4[Pt_6(SnCl_2)_2(SnCl_3)_4(CO)_6]$ (0,115g, 0,029 mmol) was dissolved in CH_3CN (5 mL) under nitrogen atmosphere and $P(C_6H_5)_3$ (0,007 g, 0,029 mmol) was added. Then the system was allowed to react for an hour, while the solution turned colour from green to red-brown.

Then 2-propanol was added (15 mL) and the solution partially evaporated by vacuum pump, until the formation of a precipitate which was separated by decantation. It was then washed with 2-propanol (3x5 mL) and dried.

$[PPh_4]_2[Pt_6(SnCl_2)_2(SnCl_3)_2(CO)_6\{P(C_6H_5)_3\}_2]$ was separated from the unreacted starting material by extraction with acetone (10 mL).

IR spectrum (CH_3CN): ν_{CO} 2031 (s), 2013 (ms), 1813(m) cm^{-1}.

$[PPh_4]_2[Pt_6(SnCl_2)(SnCl_3)_2(CO)_8\{P(C_6H_5)_3\}_2]$

$[PPh_4]_2[Pt_6(SnCl_2)_2(SnCl_3)_2(CO)_6\{P(C_6H_5)_3\}_2]$ (0,385 g, 0,091 mmol) was dissolved in CH_3CN (20 mL) and the solution was stirred under CO atmosphere for 20 minutes, while it became brown-orange in colour. From this point all the subsequent steps are performed under CO atmosphere.

2-propanol (20 mL) was added, leading to the precipitation of a solid which was separated by decantation. $[PPh_4]_2[Pt_6(SnCl_2)(SnCl_3)_2(CO)_8\{P(C_6H_5)_3\}_2]$ was washed with 2-propanol (3x5 mL) and dried.

Crystals suitable for X-ray diffraction were obtained by layering an acetone solution of the product with 2-propanol.

IR spectrum (CH_3CN): ν_{CO} 2042 (s), 1881 (w), 1829 (m) cm^{-1}.

$[PPh_4]_4[Pt_6(SnCl_2)(SnCl_3)_4(CO)_8]$

$[PPh_4]_4[Pt_6(SnCl_2)_2(SnCl_3)_4(CO)_6]$ (1,0415 g, 0,262 mmol) was dissolved in CH_3CN (20 mL) and the solution stirred under CO atmosphere for 20 minutes. Then $[PPh_4]Cl$ (0,102 g) was added and the solution turned colour to brown-orange. 2-propanol (80 mL) was added under CO atmosphere, until the formation of a brown precipitate which was separated, washed twice with 2-propanol (5 mL) and dried. Obtained 0,8575 g

Yield 85,2 %

IR spectrum (CH_3CN): ν_{CO} 2042 (s), 1840 (m) cm^{-1}.

The compound is stable under nitrogen atmosphere in the solid state, while the solution is stable under CO atmosphere. The $[PPh_4]_4[Pt_6(SnCl_2)(SnCl_3)_4(CO)_8]$ salt is sparingly soluble in acetone and well soluble in CH_3CN.

Crystals suitable for X-ray analysis were obtained by layering a CH_3CN with cyclohexane and diisopropylic ether (volume ratio 2:1:3) under CO atmosphere.

$[\{Ir_4(CO)_{11}\}_2(dppa)]$

To a solution of $[PPh_4][Ir_4Br(CO)_{11}]$ (0,176 g, $1,2 \cdot 10^{-4}$ mol) in acetonitrile (15 mL), dppa (0,024 g, $6,1 \cdot 10^{-5}$ mol) has been added under stirring. A yellow microcrystalline solid has quickly precipitated and it has been separated and washed with acetonitrile.

Obtained 0,11 g, 72% yield.

ATR IR ν_{CO}: 2091, 2047, 2030, 2002, 1987,1959, 1845, 1827 cm^{-1}

Nujol ν_{CO}: 2092, 2048, 2036, 2019, 2006 cm^{-1}

Elemental analysis C 22,65%, H 0,81%

Crystals suitable for X-ray analysis have been obtained by layering a solution made from $[PPh_4][Ir_4Br(CO)_{11}]$ (0,061 g, $4,1 \cdot 10^{-5}$ mol) and dichloromethane (4 mL) with a solution made from dppa (0,008 g, $2,1 \cdot 10^{-5}$ mol) and *n*-eptano +dichloromethane (4 mL + 0,5 mL)

Obtained 0,025 g, 48% yield.

[{$Ir_4(CO)_{11}$}$_2$(t-dppethe)]

In a Schlenk tube [PPh_4][$Ir_4Br(CO)_{11}$] (0,074 g, $4{,}9\cdot10^{-5}$ mol) has been dissolved in acetonitrile (4 mL). The addition of *t*-dppethe (0,024 g, $2{,}7\cdot10^{-5}$ mol) has yielded to the precipitation of the product as a yellow microcrystalline solid separated and washed with acetonitrile.

Obtained 0,048 g, 70% yield

ATR-IR ν_{CO}: 2089, 2043, 2035, 2002, 1974, 1958, 1842, 1821 cm^{-1}

Nujol ν_{CO}: 2091, 2048, 2035, 2010, 1994, 1973 cm^{-1}

Crystals suitable for X-ray analysis have been obtained maintaining for 3 days at 3°C a solution obtained dissolving [PPh_4][$Ir_4Br(CO)_{11}$] (0,08 g, $5{,}3\cdot10^{-5}$ mol) in dichloromethane (4 mL), adding *t*-dppethe (0.011 g, $2{,}7\cdot10^{-5}$ mol) and stirring for 1 hour.

[{$Ir_4(CO)_{11}$}$_2$(dppbut)(dppbut)$_2$]

In a Teflon lined steel vessel [$Ir_4(CO)_{12}$] (51 mg, 0,046 mmol), dppbut (60 mg, 0,14 mmol), CH_2Cl_2 (2,5 mL) and n-heptane (5,5 mL) have been loaded. The vessel has been heated at 130°C for 18 hours and allowed to slowly cool down to room temperature. Orange crystals of the product have been so recovered

Obtained 36 mg

ATR-IR 2040(w), 1980(w), 1954(m), 1789(s), 1771(vs) cm^{-1}

Elemental analysis: calculated for $Ir_8C_{102}H_{84}O_{18}P_6$: C 46,35% H 4,63%, found C 43,50% H 4,04%

[{$Ir_4(CO)_{11}$}$_2$(dpphex)$_3$]

[$Ir_4(CO)_{12}$] (0,050 g, $4{,}5\cdot10^{-5}$ mol) and dpphex (0,061 g, $1{,}3\cdot10^{-4}$ mol) were suspended in a CH_2Cl_2 (2,5 ml) *n*-heptane (5,5 ml) mixture and kept in a Teflon lined steel vessel. It was then heated in an oven at 130°C for 18 hours. After *ca* 8 (rate of cooling 0,2°C/min), yellow/orange powder and crystals of [{$Ir_4(CO)_9$}$_2$(dpphex)$_3$] were recovered and washed with dichloromethane (40 mg, 52% yield based on Ir).

ATR-IR ν_{CO}: 2037(m), 1994(m), 1972(s), 1952(s) cm^{-1} (terminal COs), 1776(s), 1761(vs) cm^{-1} (edge-bridged COs).

Elemental analysis: calculated for $Ir_8C_{108}H_{96}O_{18}P_6$ C 38,09% H 2,84% Found C 39,41% H 3,40%

[{$Ir_4(CO)_{11}$}$_4$(180tetraphos)]

In a Schlenk tube 180tetraphos (15 mg, $1.68 \cdot 10^{-2}$ mmol) have been dissolved in chloroform (3 mL) and then [PPh_4][$Ir_4Br(CO)_{11}$] (101 mg, $6.67 \cdot 10^{-2}$ mmol) has been added. The resulting solution was allowed to stir for 24 hours, while it turned from orange to yellow. A TLC (CH_2Cl_2 : hexane 7 : 3) confirmed the presence of a unique product. So the solution has been dried by a vacuum pump and the resulting yellow solid has been washed with acetonitrile (2x5 mL). Obtained 61 mg, yield 69.8%

$CHCl_3$ IR ν_{CO}=2089, 2057, 2019, 1842, 1822 cm^{-1}

^{31}P-NMR: -9.126 ppm.

Elemental analysis: calculated for $Ir_{16}C_{104}H_{46}O_{44}P_4$ C 24.03%, H 0.89%, found C 24.28%, H 1.11%.

[PPh_4][$Pt_{19}(CO)_{24}${$Au(PPh_3)$}$_3$]

In a Schlenk tube 720 mg (0.127 mmol) of [PPh_4]$_4$[$Pt_{19}(CO)_{22}$] were dissolved with 20 ml of CH_3CN; the brown solution was put under a CO atmosphere and stirred. Solid PPh_3AuCl (188 mg, 0.381 mmol) was added in subsequent portions and a brown powder gradually separated. It was recovered in a septum, washed with 2-propanol (2 x 10ml) and dried in vacuum.

ν_{CO}(THF): 2059(w), 2027(s), 1804(w) cm^{-1}

Yield: 515 mg (66 %).

Elem. Anal.: Found: C 20.8 %, H 1.20 %; Calc.: C 20.10%, H 1.07%

[NBu_4][$Pt_{19}(CO)_{24}${$Au(PPh_3)$}$_3$] used for X-ray diffraction was prepared analogously from [NBu_4]$_4$[$Pt_{19}(CO)_{22}$] with comparable yields and satisfactory elemental analises; crystals were grown from THF / 2-propanol.

$[Pt_{19}(CO)_{24}\{Au(PPh_3)\}_4]$

A solution of $[PPh_4][Pt_{19}(CO)_{24}\{Au(PPh_3)\}_3]$ (264 mg, 0.043 mmol) in 25 ml of THF was stirred under a CO atmosphere. In another Schlenk tube PPh_3AuCl (22 mg, 0.044 mmol) and $AgBF_4$ (9 mg, 0.046 mmol) were mixed in 1 ml of THF, giving rise to a fine white powder (AgCl) that was decanted. The colourless solution of PPh_3AuBF_4 was added in small subsequent portions to the cluster solution and the reaction was monitored *via* I.R. spectroscopy. The mixture was filtered and the precipitate was washed with THF until the washings were colourless; 40 ml of 2-propanol were added dropwise and the volume of the solvent was reduced in vacuum. The black precipitate was collected by filtration, washed with several portions of 2-propanol and of cyclohexane and finally dried under reduced pressure. It was extracted to a small Schlenk tube with the minimum amount of THF and cautiously layered with 2-propanol; well shaped black crystals were obtained.

ν_{CO}(THF): 2069(w), 2038(s), 1805(w) cm^{-1}

Yield: 120 mg (45 %)

Elem. Anal.: Found: C 20.0 %, H 1.65 %; Calc.: C 18.55%, H 0.97 %

$[NBu_4]_{12}[\{Pt_{19}Au(CO)_{22}\}_4(180tetraphos)]$

A solution of the dehalogenated gold phosphane complex $[Au_4(180tetraphos]Cl_4$ in THF has been added to a solution of $[NBu_4]_4[Pt_{19}(CO)_{22}]$ in acetone (in 1:4 molar ratio) and the resulting solution has been put in CO atmosphere and stirred for some hours.

Crystals of the reaction product have beew grown by layering the solution with 2-propanol. Unfortunately they were geminate or, in another attempt, their unit cell was too big and so it was not possible to get the structure. Actually the crystallization of such a big species as $[NBu_4]_{12}[\{Pt_{19}Au(CO)_{24}\}_4(180tetraphos)]$ can be really challenging.

The IR spectrum in acetone of the isolated product shows a sharp absorption band in the terminal carbonyl region at 2020 cm^{-1}. The frequency value is in good agreement with the value shown in the corresponding spectrum of the anion $[Pt_{19}(CO)_{24}\{Au(PPh_3)\}]^{3-}$ formally its parent monomeric species.

References

[1] A. Ceriotti, P. Macchi, A. Sironi, S. El Afefey, S. Fedi, F. Fabrizi De Biani, R. Della Pergola, M. Daghetta, **2012,** accepted by *Inorganic Chemistry*

[2] S. Fedi, P. Zanello, F. Laschi, A. Ceriotti, S. El Afefey, *J. of Sol. State Electrochem*., **2009**, 1497-1504.

[3] A.Ceriotti, M. Daghetta, S. El Afefey, A. Ienco, G. Longoni, G. Manca, C. Mealli, S. Zacchini, S. Zarra, *Inorg. Chem*., **2011**, *50(24)*, 12553-12561.

[4] a) H. Willner, F. Aubke et al., *Angew. Chem. Int. Ed.* **1996,** *35*, 1974;

b) H. Willner, F. Aubke et al., *Angew. Chem. Int. Ed.* **2000**, *39*, 168.

[5] F.A. Cotton, *Quart. Rev*, **1966**, *20*, 389; F.A. Cotton, *McGraw-Hill Yearbook of Science e Technology, 1966*.

[6] F.A. Cotton, *Inorg. Chem*., **1964**, *3*, 1217.

[7] J. Dewar, H.O. Jones, *Proc. Roy. Soc*., (London) **1905**, *A76*, 588; **1907**, *A79*, 66.

[8] C.H. Wei, L.F. Dahl, *J. Am. Chem. Soc*., **1966**, *88*, 1821; **1969**, *91*, 1351.

[9] E.R. Corey, L.F. Dahl, *J. Am. Chem. Soc*., **1961**, *83*, 2203.

[10] P. Chini, V.G. Albano, S. Martinengo, *J. Organomet. Chem*., **1969**, *16*, 471.

[11] E.R. Corey, L.F. Dahl, W. Beck, *J. Am. Chem. Soc*., **1963**, *85*, 1202.

[12] http://www.nanotechproject.org.

[13] a) G. Schmid (Ed.), *Nanoparticles: From Theory to Application*, Wiley-VCH, Weinheim, **2010**; b) G. L. Hornyak, J. Dutta, H. F. Tibbals, A. Rao, *Introduction to Nanoscience*, CRC Press, Boca Raton, **2008**; c) G. A. Ozin, A. C. Arsenault, L. Cademartiri, C. A. Mirkin, *Nanochemistry: A Chemical Approach to Nanomaterials*, Royal Society of Chemistry, London, **2008**; d) B. Corain, G. Schmid, N. Toshima (Eds.), *Metal Nanoclusters in Catalysis and Materials Science: The Issue of Size Control, Elsevier B. V., Amsterdam,* ***2008***.

[14]) M. Bruchez Jr., M. Moronne, P. Gin, S. Weiss, A. P. Alivisatos, *Science* **1998**, *281*, 2013–2016; b) J. P. Abid, H. H. Girault, P. F. Brevet, *Chem. Commun.* **2001**, *9*, 829–830.

[15] a) A. C. Templeton, W. P. Wuelfing, R. W. Murray, *Acc. Chem. Res.* **2000**, *33*, 27–36; b) M.-C. Daniel, D. Astruc, *Chem. Rev.* **2004**, *104*, 293–346; c) R. L. Whetten, M. N. Shafigullin, J. T.

Khoury, T. G. Schaaff, I. Vezmar, M. M. Alvarez, A. Wilkinson, *Acc. Chem. Res.* **1999**, *32*, 397–406.

[16] a) J. B. Tracy, G. Kalyuzhny, M. C. Crowe, R. Balasubramanian, J.-P. Choi, R. W. Murray, *J. Am. Chem. Soc.* **2007**, *129*, 6706–6707; b) R. C. Price, R. L. Whetten, *J. Am. Chem. Soc.* **2005**, *127*, 13750–13751; c) Y. Shichibu, Y. Negishi, T. Tsukuda, T. Teranishi, *J. Am. Chem. Soc.* **2005**, *127*, 13464–13465.

[17] a) R. Jin, *Nanoscale* **2010**, *2*, 343–362; b) J. F. Parker, C. A. Fields-Zinna, R. W. Murray, *Acc. Chem. Res.* **2010**, *43*, 1289–1296; c) T. Gutel, C. C. Santini, K. Philippot, A. Padua, K. Pelzer, B. Chaudret, Y. Chauvin, J. M. Basset, *J. Mater. Chem.* **2009**, *19*, 3624–3631.

[18] a) U. Kreibig, M. Vollmer, *Optical Properties of Metal Clusters*, Springer-Verlag, New York, **1995**; b) M. Zhu, W. T. Eckenhoff, T. Pintauer, R. Jin, *J. Phys. Chem. C* **2008**, *112*, 14221–14224; c) M. Zhu, C. M. Aikens, F. J. Hollander, G. C. Schatz, R. Jin, *J. Am. Chem. Soc.* **2008**, *130*, 5883–5885.

[19] a) M. Haruta, T. Kobayashi, H. Sano, N. Yamada, *Chem. Lett.* **1987**, *4*, 405–408; b) G. J. Hutchings, *J. Catal.* **1985**, *96*, 292– 295; c) M. Haruta, *Catal. Today* **1997**, *36*, 153–166; d) A. S. K. Hashmi, G. J. Hutchings, *Angew. Chem.* **2006**, *118*, 8064; *Angew. Chem. Int. Ed.* **2006**, *45*, 7896–7936.

[20] a) G. Schmid (Ed.), *Clusters and Colloids*, Wiley-VCH, New York, **1994**; b) P. Braunstein, L. A. Oro, P. R. Raithby (Eds.), *Metal Clusters in Chemistry*, Wiley-VCH, New York, **1999**; c) G. Schmid, D. Fenske, *Phil. Trans. R. Soc. A* **2010**, *368*, 1207–1210.

[21] P. D. Jadzinsky, G. Calero, C. J. Ackerson, D. A. Bushnell, R. D. Kornberg, *Science* **2007**, *318*, 430–433.

[22] a) N. K. Chaki, Y. Negishi, H. Tsunoyama, Y. Shichibu, T. Tsukuda, *J. Am. Chem. Soc.* **2008**, *130*, 8608–8610; b) Y. Pei, Y. Gao, X. C. Zeng, *J. Am. Chem. Soc.* **2008**, *130*, 7830–7832; c) O. Lopez-Acevedo, J. Akola, R. L. Whetten, H. Grönbeck, H. Häkkinen, *J. Phys. Chem. C* **2009**, *113*, 5035–5038; d) W. Wang, R. W. Murray, *Langmuir* **2005**, *21*, 7015–7022.

[23] a) M. Walter, J. Akola, O. Lopez-Acevedo, P. D. Jadzinsky, G. Calero, C. J. Ackerson, R. L. Whetten, H. Grönbeck, H. Häkkinen, *Proc. Natl. Acad. Sci. USA* **2008**, *105*, 9157–9162; b) H. Häkkinen, *Chem. Soc. Rev.* **2008**, *37*, 1847–1859; c) D. E. Jiang, M. L. Tiago, W. Luo, S. Dai, *J. Am. Chem. Soc.* **2008**, *130*, 2777–2779.

[24] E. G. Mednikov, L. F. Dahl, *Small* **2008**, *4*, 534–537.

[25] C. E. Anson, A. Eichhöfer, I. Issac, D. Fenske, O. Fuhr, P. Sevillano, C. Persau, S. Stalke, J. Zhang, *Angew. Chem.* **2008**, *120*, 1346; *Angew. Chem. Int. Ed.* **2008**, *47*, 1326–1331.

[26] A. Ecker, E. Weckert, H. Schnöckel, *Nature* **1997**, *387*, 379–381.

[27] a) A. Schnepf, H. Schnöckel, *Angew. Chem.* **2001**, *113*, 733; *Angew. Chem. Int. Ed.* **2001**, *40*, 711–715; b) A. Schnepf, B. Jee, H. Schnöckel, E. Weckert, A. Meents, D. Lubbert, E. Herrling, B. Pilawa, *Inorg. Chem.* **2003**, *42*, 7731–7733.

[28] N. T. Tran, D. R. Powell, L. F. Dahl, *Angew. Chem.* **2000**, *112*, 4287; *Angew. Chem. Int. Ed.* **2000**, *39*, 4121–4125.

[29] C. Femoni, M. C. Iapalucci, F. Kaswalder, G. Longoni, S. Zacchini, *Coord. Chem. Rev.* **2006**, *250*, 1580–1604.

[30] G. Hogarth, S. E. Kabir, E. Nordlander, *Dalton Trans.* **2010**, *39*, 6153–6174.

[31] a) D. F. Shriver, H. D. Kaesz, R. D. Adams (Eds.), *The Chemistryof Metal Cluster Complexes*, VCH, New York, **1990**; b) D. M. P. Mingos, D. J. Wales, *Introduction to Cluster Chemistry*, Prentice Hall, Englewood Cliffs, **1990**; c) J. P. Fackler (Ed.), *Metal–Metal Bonds and Clusters in Chemistry and Catalysis*, Plenum, New York, **1992**.

[32] a) B. C. Gates, *Catalytic Chemistry*, Wiley, New York, **1992**; b) G. Gonzales-Moraga, *Cluster Chemistry*, Springer Verlag, Berlin, **1993**; c) C. E. Housecroft, *Metal–Metal Bonded Carbonyl Dimers and Clusters*, Oxford Science Publishers, Oxford, **1994**; d) R. D. Adams, F. A. Cotton (Eds.), *Catalysis by Diand Polynuclear Metal Cluster Complexes*, Wiley-VCH, New York, **1998**.

[33] a) P. Chini, *J. Organomet. Chem.* **1980**, *200*, 37–61; b) K. C. C. Kharas, L. F. Dahl, *Adv. Chem. Phys.* **1988**, *70*, 1–43; c) M. D. Vargas, J. N. Nicholls, *Adv. Inorg. Chem. Radiochem.* **1986**, *30*, 123–222; d) P. R. Raithby, *Platinum Met. Rev.* **1998**, *42*, 146–157; e) B. F. G. Johnson, *Coord. Chem. Rev.* **1999**, *190–192*, 1269–1285.

[34] a) G. Longoni, M. C. Iapalucci in *Clusters and Colloids* (Ed.: G. Schmid), Wiley-VCH, New York, **1994**, pp. 91–177; b) A. Fumagalli, R. Della Pergola in *Metal Clusters in Chemistry* (Eds.: P. Braunstein, L. A. Oro, P. R. Raithby), Wiley-VCH, New York, **1999**, pp. 323–347; c) J. Lewis, P. R. Raithby in *Metal Clusters in Chemistry* (Eds.: P. Braunstein, L. A. Oro, P. R. Raithby), Wiley-VCH, New York, **1999**, pp. 348–380.

[35] a) F. Calderazzo, R. Ercoli, G. Natta in *Organic Syntheses via Metal Carbonyls* (Eds.: I. Wender, P. Pino), Interscience Publishers, New York, **1968**, pp. 1–272; b) Ch. Elschenbroich, A. Salzer, *Organometallics: A Concise Introduction*, VCH, Weinheim, **1992**; c) N. N. Greenwood, A. Earnshaw, *Chemistry of the Elements*, Butterworth-Heinemann, Oxford, **1984**.

[36] a) G. Longoni, P. Chini, *J. Am. Chem. Soc.* **1976**, *98*, 7225–7231; b) J. C. Calabrese, L. F. Dahl, P. Chini, G. Longoni, S. Martinengo, *J. Am. Chem. Soc.* **1974**, *96*, 2614–2616.

[37] a) A. Ceriotti, G. Longoni, M. Marchionna, *Inorg. Synth.* **1989**, *26*, 316–319; b) M. J. D'Aniello, C. J. Car, M. G. Zammit, *Inorg. Synth.* **1989**, *26*, 319–323.

[38] B. Le Gratiet, H. Remita, G. Picq, M. O. Delcourt, *Radiat.Phys. Chem.* **1996**, *47*, 263–268.

[39] C. Femoni, F. Kaswalder, M. C. Iapalucci, G. Longoni, M. Mehlstäubl, S. Zacchini, *Chem. Commun.* **2005**, 5769–5771.

[40] a) S. Kawi, B. C. Gates in *Clusters and Colloids* (Ed.: G. Schmid), Wiley-VCH, New York, **1994**, pp. 299–372; b) M. Ichikawa in *Metal Clusters in Chemistry* (Eds.: P. Braunstein, L. A. Oro, P. R. Raithby), Wiley-VCH, New York, **1999**, pp. 1273–1301; c) A. Kulkarni, R. J. Lobo-Lapidus, B. C. Gates, *Chem. Commun.* **2010**, *46*, 5997–6015.

[41] a) M. Ichikawa, *Platinum Met. Rev.* **2000**, *44*, 3–14; b) A. Fukuoka, N. Higashimoto, Y. Sakamoto, M. Sasaki, N. Sugimoto, S. Inagaki, Y. Fukushima, M. Ichikawa, *Catal. Today* **2001**, *66*, 23–31.

[42] E. G. Mednikov, L. F. Dahl, *Phil. Trans. R. Soc. A* **2010**, *368*, 1301–1322.

[43] a) W. Hieber, H. Lagally, *Z. Anorg. Allg. Chem.* **1943**, *251*, 96–113; b) B. L. Booth, M. J. Else, R. Fields, H. Goldwhite, R. N. Haszeldine, *J. Organomet. Chem.* **1968**, *14*, 417–422; c) P. Chini, S. Martinengo, *Inorg. Chim. Acta* **1969**, *3*, 315–318.

[44] V. G. Albano, D. Braga, S. Martinengo, *J. Chem. Soc., Dalton Trans.* **1981**, 717–720.

[45] C. Femoni, M. C. Iapalucci, G. Longoni, C. Tiozzo, S. Zacchini, B. T. Heaton, J. A. Iggo, P. Zanello, S. Fedi, M. C. Garland, C. Li, *Dalton Trans.* **2009**, 2217–2223.

[46] a) E. Charalambous, L. H. Gade, B. F. G. Johnson, J. Lewis, M. McPartlin, H. R. Powell, *J. Chem. Soc., Chem. Commun.* **1990**, 688–690; b) A. J. Amoroso, L. H. Gade, B. F. G. Johnson, J. Lewis, P. R. Raithby, W. T. Wong, *Angew. Chem.* **1991**, *103*, 102; *Angew. Chem. Int. Ed. Engl.* **1991**, *30*, 107–109.

[47] V. G. Albano, A. Ceriotti, P. Chini, G. Ciani, S. Martinengo, M. Anker, *J. Chem. Soc., Chem. Commun.* **1975**, 859 860.

[48] D. M. Washecheck, E. J. Wucherer, L. F. Dahl, A. Ceriotti, G. Longoni, M. Manassero, M. Sansoni, P. Chini, *J. Am. Chem. Soc.* **1979**, *101*, 6110–6112.

[49] F. Gao, C. Li, B. T. Heaton, S. Zacchini, S. Zarra, G. Longoni, M. Garland, *Dalton Trans.* **2011**, *40*, 5002–5008.

[50] a) V. G. Albano, L. Grossi, G. Longoni, M. Monari, S. Mulley, A. Sironi, *J. Am. Chem. Soc.* **1992**, *114*, 5708–5713; b) V. G. Albano, F. Calderoni, M. C. Iapalucci, G. Longoni, M. Monari, P. Zanello, *J. Cluster Sci.* **1995**, *6*, 107–123; c) D. Collini, C. Femoni, M. C. Iapalucci, G. Longoni, *Compt. Rend. Chim.* **2005**, *8*, 1645–1654.

[51] a) V. G. Albano, F. Demartin, M. C. Iapalucci, G. Longoni, A. Sironi, V. Zanotti, *J. Chem. Soc., Chem. Commun.* **1990**, 547– 548; b) V. G. Albano, F. Demartin, M. C. Iapalucci, F. Laschi, G. Longoni, A. Sironi, P. Zanello, *J. Chem. Soc., Dalton Trans.* **1991**, 739–748.

[52] C. Femoni, M. C. Iapalucci, G. Longoni, J. Wolowska, S. Zacchini, P. Zanello, S. Fedi, M. Riccò, D. Pontiroli, M. Mazzani, *J. Am. Chem. Soc.* **2010**, *132*, 2919–2927.

[53] a) V. G. Albano, D. Braga, D. Strumolo, C. Seregni, S. Martinengo, *J. Chem. Soc., Dalton Trans.* **1985**, 1309–1313; b) V. G. Albano, D. Braga, P. Chini, D. Strumolo, S. Martinengo, *J. Chem. Soc., Dalton Trans.* **1983**, 249–252.

[54] J. J. Brunet, *Chem. Rev.* **1990**, *90*, 1041–1059, and ref. therein.

[55] a) J. C. Calabrese, L. F. Dahl, A. Cavalieri, P. Chini, G. Longoni, S. Martinengo, *J. Am. Chem. Soc.* **1974**, *96*, 2616–2618; b) G. Longoni, P. Chini, A. Cavalieri, *Inorg. Chem.* **1976**, *15*, 3025–3029; c) G. Longoni, P. Chini, L. D. Lower, L. F. Dahl, *J. Am. Chem. Soc.* **1975**, *97*, 5034–5036; d) G. Longoni, P. Chini, *Inorg. Chem.* **1976**, *15*, 3029–3031.

[56] R. Della Pergola, F. Demartin, L. Garlaschelli, M. Manassero, S. Martinengo, M. Sansoni, *Inorg. Chem.* **1987**, *26*, 3487–3491.

[57] a) J. D. Roth, G. J. Lewis, L. K. Safford, X. Jiang, L. F. Dahl, M. J. Weaver, *J. Am. Chem. Soc.* **1992**, *114*, 6159–6169; b) A. Ceriotti, N. Masciocchi, P. Macchi, G. Longoni, *Angew. Chem.* **1999**, *111*, 3941; *Angew. Chem. Int. Ed.* **1999**, *38*, 3724–3727.

[58] D. Collini, F. Fabrizi de Biani, S. Fedi, C. Femoni, F. Kaswalder, M. C. Iapalucci, G. Longoni, C. Tiozzo, S. Zacchini, P. Zanello, *Inorg. Chem.* **2007**, *46*, 7971–7981.

[59] A. Ceriotti, G. Longoni, M. Manassero, M. Perego, M. Sansoni, *Inorg. Chem.* **1985**, *24*, 117–120.

[60] C. Femoni, M. C. Iapalucci, G. Longoni, S. Zacchini, *Chem. Commun.* **2008**, 3157–3159.

[61] C. Femoni, M. C. Iapalucci, G. Longoni, P. H. Svensson, *Chem. Commun.* **2000**, 655–656.

[62] C. Femoni, M. C. Iapalucci, G. Longoni, C. Tiozzo, S. Zacchini, B. T. Heaton, J. A. Iggo, *Dalton Trans.* **2007**, 3914–3923.

[63] C. Femoni, M. C. Iapalucci, G. Longoni, S. Zacchini, *Eur. J. Inorg. Chem.* **2010**, 1056–1062.

[64] A. Ceriotti, F. Demartin, B. T. Heaton, P. Ingallina, G. Longoni, M. Manassero, M. Marchionna, N. Masciocchi, *J. Chem. Soc., Chem. Commun.* **1989**, 786–787.

[65] C. Femoni, M. C. Iapalucci, G. Longoni, S. Zacchini, *Eur. J. Inorg. Chem.* **2009**, 2487–2495.

[66] B. R. Whittlesey, *Coord. Chem. Rev.* **2000**, *206–207*, 395–418.

[67] C. Mealli, D. M. Proserpio, G. Fachinetti, T. Funaioli, G. Fochi, P. F. Zanazzi, *Inorg. Chem.* **1989**, *28*, 1122–1127.

[68] G. Kong, G. N. Harakas, B. R. Whittlesey, *J. Am. Chem. Soc.* **1995**, *117*, 3502–3509.

[69] a) F. Calderoni, F. Demartin, F. Fabrizi de Biani, C. Femoni, M. C. Iapalucci, G. Longoni, P. Zanello, *Eur. J. Inorg. Chem.* **1999**, 663–671; b) F. Calderoni, F. Demartin, M. C. Iapalucci, G. Longoni, *Angew. Chem.* **1996**, *108*, 2393; *Angew. Chem. Int. Ed. Engl.* **1996**, *35*, 2225–2226; c) A. Ceriotti, A. Fait, G. Longoni, G. Piro, F. Demartin, M. Manassero, M. Sansoni, *J. Am. Chem. Soc.* **1986**, *108*, 8091–8092.

[70] A. Ceriotti, G. Longoni, M. Manassero, N. Masciocchi, G. Piro, L. Resconi, M. Sansoni, *J. Chem. Soc., Chem. Commun.* **1985**, 1402–1403.

[71] A. Bernardi, C. Femoni, M. C. Iapalucci, G. Longoni, S. Zacchini, S. Fedi, P. Zanello, *Eur. J. Inorg. Chem.* **2010**, 4831–4842.

[72] J.C. Calabrese, L.F. Dahl, P. Chini, G. Longoni, S. Martinengo, *J. Am. Chem. Soc.* **1974**, *96*, 2614.

[73] C. Femoni, M.C. Iapalucci, G. Longoni, P.H. Svensson, *Chem. Commun.* **2004**, 2274.

[74] K.R. Nary, P.L. Kuhns, M.S. Conradi, *Phys. Rev.*, **1982**, *B 26*, 3370.

[75] G. Longoni, C. Femoni, M. C. Iapalucci, P. Zanello in *Metal Clusters in Chemistry* (Eds.: P. Braunstein, L. A. Oro, P. R. Raithby), Wiley-VCH, New York, **1999**, pp. 1137–1158.

[76] a) G. B. Khomutov, R. V. Gainutdinov, S. P. Gubin, V. V. Kislov, V. V. Khanin, A. A. Rakhnyanskaya, A. N. Sergeev-Cherenkov, E. S. Soldatov, D. B. Suyatin, I. V. Taranov, A. L. Tolstikhina, *Appl. Surf. Sci.* **2004**, *226*, 149–154; b) V. V. Kislov, Y. V. Gulyaev, V. V. Kolesov, I. V. Taranov, S. P. Gubin, G. B. Khomutov, E. S. Soldatov, I. A. Maximov, L. Samuelson, *Int. J. Nanosci.* **2004**, *3*, 137–147.

[77] E. Leary, H. Van Zalinge, S. J. Higgins, R. J. Nichols, F. Fabrizi de Biani, P. Leoni, L. Marchetti, P. Zanello, *Phys. Chem. Chem. Phys.* **2009**, *11*, 5198–5202.

[78] A. Bernardi, C. Femoni, M. C. Iapalucci, G. Longoni, S. Zacchini, *Dalton Trans.* **2009**, 4245–4251.

[79] D. Collini, F. Fabrizi de Biani, D. S. Dolznikov, C. Femoni, M. C. Iapalucci, G. Longoni, C. Tiozzo, S. Zacchini, P. Zanello, *Inorg. Chem.* **2011**, *50*, 2790–2798.

[80] A. Bernardi, C. Femoni, M. C. Iapalucci, G. Longoni, F. Ranuzzi, S. Zacchini, P. Zanello, S. Fedi, *Chem. Eur. J.* **2008**, *14*, 1924–1934.

[81] K.Wade, *J. Chem. Soc., Chem. Commun.* **1971**, 792.

[82] K. Wade, *Adv Inorg. Radiochem*., **1976**, *18*, .1

[83] D.M. Mingos, A. S. May, in D. F. Shriver, H. D. Kaesz, R. D. Adams (Eds.), *The Chemistry of Metal Cluster Complexes*, VCH Publishers, New York, **1990**, p.11.

[84] G. Ciani, A Sironi, *J organomet. Chem*. 241 81983) 385. 4) B.K. Teo, *Inorg. Chem.* **1984**, *23*,1251.

[85] a) P. Lemoine, *Coord. Chem. Rev*. **1982**, *47*,56; b) P. Lemoine, *Coord. Chem. Rev*. **1988**, *83*,169.

[86] a) W. B. Geiger, *Prog. Inorg. Chem*. **1985**, *33*, 275; b) S. R. Drake, *Polyhedron*, **1990**, *9*,455.

[87] a) P. Zanello, in : P.Zanello (Ed.), *Stereochemistry of Organometallic and Inorganic Compounds*, Elsevier, Amsterdam, **1994**, *Vol. 5,* 163; b) P. Zanello, F. Fabrizi de Biani, in: P.Braunstein, L.A. Oro, P.R. Raithby (Eds.), *Metal Clusters in Chemistry*, Wiley-VCH, Weinheim, **1999**, *Vol.2,*.1104; c) P. Zanello, in: P.I. Bernal (Ed.), *Stereochemistry of Organometallic and Inorganic Compounds*, , Elsevier, Amsterdam, **1990**, *Vol. 4*, 181.

[88] G. Longoni, C. Femoni, M.C. Iapalucci, P. Zanello, in: P.Braunstein, L.A. Oro, P.R. Raithby (Eds.), *Metal Clusters in Chemistry*, Wiley-VCH, Weinheim, **1999**, *Vol.2*, 1137.

[89] A. Ceriotti , F. Demartin, B.T. Heaton, P. Ingallina, G.Longoni, M. Massanero, M. Marchionna, N. Masciocchi, *J. Chem. Soc. Chem. Commun*., **1989**, 786.

[90] a) R. Della Pergola, L. Garlaschelli, C. Mealli, D.M. Proserpio, P.Zanello, *J. Cluster Sci.,*. **1990**, *1*, 93; b) A. Fumagalli, M.Costa, R. Della Pergola, P. Zanello, F. Fabrizi de Biani, P. Macchi, A. Sironi, *Inorg Chim. Acta* **2003**, *350*, 187; c) D.F. Rieck, R.A. Montag, T.S. McKechnie, L.F. Dahl*, J. Am. Chem. Soc*., **1986**, *108*, 1330; R. E. Des Enfantes, J.A. Gavney, R.K. Hayashi, A.D. Rae, L.F. Dahl, *J. Organomet. Chem*. **1990**, *383*, 543.

[91] a) D.F. Rieck, J.A. Gavney, R.L. Norman, R.K. Hayashi, L.F. Dahl, *J. Am. Chem. Soc*. **1992**, *114*, 10369; b) P.D. Mlynek, L.F. Dahl, *Organometallics* , **1997**, *16*, 164; c) P.D. Mlynek, L.F. Dahl, *Organometallics*, **1997**, *16*, 1655.

[92] a) L.D. Lower, L.F. Dahl, *J. Am. Chem. Soc*., **1976**, *98*, 5046; b) D.F. Rieck, A.D. Rae, L.F. Dahl, *J. Chem. Soc. Chem. Commun*., **1993**, 585.

[93] a) V.G. Albano, F. Demartin, M.C. Iapalucci, G. Longoni, A. Sironi, V. Zanotti, *J. Chem. Soc. Chem. Commun*., **1990**, 547; b) V.G. Albano, F. Demartin, M.C. Iapalucci, F. Laschi, G. Longoni, A Sironi, P. Zanello, *J. Chem. Soc. Dalton Trans*., **1991**, 739; c) V.G. Albano, F. Demartin, C. Femoni, M.C. Iapalucci, G. Longoni, M. Monari, P. Zanello, *J. Organomet. Chem*., **2000**, *325*, 593.

[94] a) V.G. Albano, F. Demartin, M.C. Iapalucci, G. Longoni, M. Monari, P. Zanello, *J. Chem. Soc. Dalton Trans*. **1992**, 497; b) A.J. Kahaian , J.B. Thoden, L.F. Dahl, *J. Chem. Soc. Chem. Commun*., **1992**, 353; c) J.P. Zebrowski, R.K. Hayashi, L.F. Dahl, *J. Am. Chem. Soc*., **1993**, *115*, 1142.

[95] H. Brunner, H. Cattey, W. Meier, Y. Mugnier, A.C. Stuckl, J. Wachter, R. Wanninger, M. Zabel, *Chem. Eur. J*., **2003**, *9*, 3796.

[96] C. Femoni, M.C. Iapalucci, G. Longoni, P.H. Svensson, P. Zanello, F. Fabrizi De Biani, *Chem. Eur. J*., **2004**, *10*, 2318.

[97] F. Fabrizi de Biani, C. Femoni, M.C. Iapalucci, G. Longoni, P. Zanello, A. Ceriotti, *Inorg. Chem*., **1999**, *38*, 3721.

[98] J. Sinzig, L.J. de Jongh, A. Ceriotti, R. Della Pergola, G. Longoni, M. Stener, K. Albert, N. R¨osch, *Phys. Rev. Lett*. **1998**, *81*, 3211.

[99] R. Della Pergola, L. Garlaschelli, C. Mealli, D.M. Proserpio, P. Zanello, *J. Cluster Science*, **1990**, *1*, 93; R.C. Adams, G. Chen, J.-G. Wang, *Polyhedron*, **1989**, *8*, 2521.

[100] (a) P.Zanello, in "*Stereochemistry of Organometallic and Inorganic Compounds*" P. Zanello Ed., Elsevier; Amsterdam **1994**, *vol 5*, pag 163; (b) P. Zanello in "*Structure and Bonding*" Sringer-Verlag: Berlin, **1992**, *vol 79*, p 101.

[101] V.G. Albano, F. Demartin, C. Femoni, M.C. Iapalucci, G. Longoni, M. Monari, P. Zanello, *J. Organomet. Chem*., **2000**, *593*, 325.

[102] V.G. Albano, F. Demartin, M.C. Iapalucci, G. Longoni, M. Monari, P. Zanello, *J. Chem. Soc., Dalton Trans*., **1992**, 497.

[103] E. Brivio, A. Ceriotti, R. Della Pergola, L. Garlaschelli, F. Demartin, M. Manassero, M. Sansoni, P. Zanello, F. Laschi, B.T. Heaton, *J. Chem. Soc., Dalton Trans*., **1994**, 3237.

[104] V.G. Albano, F. Demartin, M.C. Iapalucci, F. Laschi, G. Longoni, A. Sironi, P. Zanello, *J. Chem. Soc., Dalton Trans*., **1991**, 739.

[105] P.Zanello, in "*Stereochemistry of Organometallic and Inorganic Compounds*" P. Zanello Ed., Elsevier; Amsterdam **1994**, *vol 5*, pag 163

[106] R. Della Pergola, L. Garlaschelli, M. Manassero, N. Masciocchi, P. Zanello, *Angew. Chem., Int. Ed. Engl*., **1993**, *32*, 3670.

[107] P.Zanello, in "*Stereochemistry of Organometallic and Inorganic Compounds*" P. Zanello Ed., Elsevier; Amsterdam **1994**, *vol 5*, pag 163

[108] V.G. Albano, F. Calderoni, M.C. Iapalucci, G. Longoni, M. Monari, P. Zanello, *J. Cluster Science*, **1995**, *6*, 107.

[109] (a) G.J. Lewis, J.D. Roth, R.A. Montag, L.K. Safford, X. Gao, S.-C Chang, L.F. Dahl, M.J. Weaver, *J. Am. Chem. Soc*., **1990**, *112*, 2381; (b) J.D. Roth, G.J. Lewis, L.K. Safford, X. Jiang, L.F. Dahl, M.J. Weaver, *J. Am. Chem., Soc*., **1992**, *114*, 6159.

[110] F. Calderoni, F. Demartin, F. Fabrizi de Biani, C. Femoni, M.C. Iapalucci, G. Longoni, P. Zanello, *Eur. J. Inorg. Chem*., **1999**, 663.

[111] F. Calderoni, F. Demartin, F. Fabrizi de Biani, C. Femoni, M.C. Iapalucci, G. Longoni, P. Zanello, *Eur. J. Inorg. Chem*., **1999**, 663.

[112] F. Calderoni, F. Demartin, F. Fabrizi de Biani, C. Femoni, M.C. Iapalucci, G. Longoni, P. Zanello, *Eur. J. Inorg. Chem*., **1999**, 663.

[113] G. Longoni, dati da pubblicare.

[114] C. Femoni, M. C. Iapalucci, G. Longoni, P. H. Svensson, *Chem. Commun.* **2004**, 2274–2275.

[115] P. Braunstein, *J. Organomet. Chem.*, **2004**, *689*, 3953

[116] M. Ichikawa, *Metal Clusters in Chemistry*; P. Braunstein, L. A. Oro, P. R. Raithby; Wiley-VCH: Wienheim, Germany, **1999**, Vol. 3, p 1273.

[117] B. F. G. Johnson, *Coord. Chem. Rev.*, **1999**, *190-192*, 1269.

[118] F. Schweyer-Tihay, P. Braunstein, C. Estournes, J. L. Guille, B. Lebeau, J.-L Palliaud, M. Richard-Plouet, J. Rose; *Chem. Mater.*, **2003**, *15*, 57

[119] A. J. Deeming, *J. Cluster Sci.*, **1992**, *3*, 347.

[120] E. W. Ainscough, A. M. Brodie, R. K. Coll, T. G. Kotch, A. J. Lees, A. J. A. Mair, J. M. Waters, *J. Organomet. Chem.*, **1996**, *517*, 173.

[121] J. Zhang, X. -N. Chen, Y. -Q. Yin, W. -L. Wang, X. -J. Huang, *J. Organomet. Chem.*, **1999**, *582*, 252.

[122] V. Torna, O. Vidoni, U. Simon, G. Schmid, *Eur. J. Inorg. Chem.*, **2003**, *1121*.

[123] L. -C. Song, W. -F. Zhu, Q. -M Hua, H. Wua, G. -A. Yu, *J. Organomet. Chem.*, **2003**, *667*, 143.

[124] A. J. Amoroso, B. F. G. Johnson, J. Lewis, A. D. Massey, P. R. Raithby, W. T. Wong, *J. Organomet. Chem.*, **1992**, *440*, 219.

[125] A. J. Amoroso, A. J. Edwards, B. F. G. Johnson, J. Lewis, M. R. Al-Mandhary, P. R. Raithby, V. P. Saharan, W. T. Wong, *J. Organomet. Chem.*, **1993**, *443*, C11.

[126] C. J. Adams, M. I. Bruce, E. Horn, B. W. Skeleton, E. R. T. Tiekink, A. H. White, *J. Chem. Soc. Dalton Trans.*, **1993**, *3299*.

[127] C. E. Housecroft, A. L. Rheingold, A. Weller, G. P. A. Yap, *J. Organomet. Chem.*, **1998**, 565, *105*.

[128] M. Ferrer, A. Julia, O. Rossell, M. Seco, M. A. Pelinghelli, A. Tiripicchio, *Organometalics*, **1997**, *16*, 3715.

[129] D. Imhof, U. Burckhardt, K.-H. Dahmen, F, Joho, R. Nesper, *Inorg. Chem.*, **1997**, *36*, 1813.

[130] N. Feeder, J. Geng, P. G. Goh, B. F. G. Johnson, C. M. Martin, D. S. Shephard, W. Zhou, *Angew. Chem., Int. Ed.* **2000**, *39*, 1661.

[131] J. Geng, H. Li, W. T. S. Huck, B. F. G. Johnson, *Chem.Commun.*, **2004**, 2122.

[132] A. Togni, L. M Venanzi, *Angew. Chem., Int. Ed. Engl.* **1994**, *33*, 7.

[133] G. Chelucci, R. P. Thummel, *Chem. Rev.* **2002**, *102*, 3129.

[134] C. Kaes, A. Katz, M. W. Hosseini, *Chem. Rev.* **2000**, *100*, 3553.

[135] A. J. Deeming, R. Peters, M. B. Hursthouse, J. D. J. Backer-Dirks, *J. Chem. Soc., Dalton Trans.* **1982**, 787.

[136] G. A. Foulds, B. F. G. Johnson, J. Lewis, *J. Organomet. Chem*, **1985**, *294*, 123.

[137] W. Y. Wong, S. H. Cheung, S. M. Lee, S. Y. Leung, *J.Organomet. Chem.*, **2000**, *596*, 36.

[138] W. Y. Wong, S. -H. Cheung, X. Huang, Z. Lin, *J. Organomet.Chem.*, **2002**, *655*, 39.

[139] S. Chan, W. T. Wong, *J. Chem. Soc., Dalton Trans.*, **1994**, 1605.

[140] R. Ros, R. Bertani, A. Tassan, D. Braga, F. Grepioni, E. Tedesco, *Inorg. Chim. Acta*, **1996**, *244*, 11.

[141] G. Freeman, S. L. Ingham, B. F. G. Johnsopn, M. McPartlin, I. J. Scowen, *J. Chem. Soc., Dalton Trans.* **1997**, 2705.

[142] S. P. Tunik, I. O. Koshevoy, A. J. Poe, D. H. Farrar, E. Nordlander, M. Haukka, T. A. Pakkanen, *Dalton*, **2003**, 2457.

[143] K. Wajda-Hermanowicz, F. Pruchnik, M. J. Zuber, *J. Organomet. Chem.*, **1996**, *508*, 75.

[144] A. J. Deeming, M. B. Smith, *J. Chem. Soc., Dalton Trans.* **1993**, 3383.

[145] V. I. Ponomarenko, T. S. Pilyugina, V. D. Khripun, E. V. Grachova, S. P. Tunik, M. Haukka, T. A. Pakkanen, *Eur. J. Inorg. Chem.*, in press.

[146] G. Longoni, P. Chini, *J. Am. Chem. Soc.*, **1976**, *98*, 7225.

[147] B.T. Heaton, L. Strona, S. Martinengo, D. Strumolo, V.G. Albano, D. Braga, *J. Chem. Soc. Dalton Trans.*, **1983,** *2175*.

[148] L.H. Gade, B.F.G. Johnson, J. Lewis, M. McPartlin, H.R. Powell, *J. Chem. Soc. Chem. Commun.*, **1990**, *110*.

[149] T. Nakajima, A. Ishiguro, Y. Wakatsuki, *Angew. Chem. Int. Ed.*, **2000**, *39*, 1131.

[150] T. Nakajima, A. Ishiguro, Y. Wakatsuki, *Angew. Chem. Int. Ed.*, **2001**, *40*, 1066.

[151] K.-F. Yung, W.-T. Wong, *Angew. Chem. Int. Ed.*, **2003**, *42*, 553.

[152] F. Demartin, M.C. Iapalucci, G. Longoni, *Inorg. Chem*., **1993**, *32*, 5536.

[153] M.A. Beswick, J. Lewis, P.R. Raithby, M.C. Ramirez de Arellano, *Angew. Chem. Int. Ed*., **1997**, *36*, 291.

[154] M.A. Beswick, J. Lewis, P.R. Raithby, M.C. Ramirez de Arellano, *Angew. Chem. Int. Ed*, **1997**, *36*, 2227.

[155] D.S. Shephard, T. Maschmeyer, B.F.G. Johnson, J.M. Thomas, G. Sankar, D. Ozkaya, W. Zhou, R.D. Oldroyd, R.G. Bell, Angew. *Chem. Int. Ed*., **1997**, *36*, 2242.

[156] S. Zacchini, in preparation.

[157] A. Fumagalli, M.C. Malatesta, A. Tentori, D. Monti, P. Macchi, A. Sironi, *Inorg. Chem*., **2002**, *41*, 76.

[158] I.O. Koshevoy, M. Haukka, T.A. Pakkanen, S.P. Tunik, P. Vainiotalo, *Organometallics*, **2005**, *24*, 3516.

[159] J.L. Segura, N. Martin, *Chem. Soc. Rev*., **2000**, *29*, 13.

[160] N. Dragoe, H. Shimotani, M. Hayashi, K. Saigo, A. de Bettencourt-Dias, A.L. Balch, Y. Miyake, Y. Achiba, K. Kitazawa, *J. Organomet. Chem*., **2000**, *65*, 3269.

[161] N. Dragoe, H. Shimotani, J. Wang, M. Iwaya, A. de Bettencourt-Dias, A.L. Balch, K. Kitazawa, *J. Am. Chem. Soc*., **2001**, *123*, 1294.

[162] K. Lee, H. Song, J. T. Park, *Acc. Chem. Res*., **2006**, *36*, 78.

[163] J.M. Williams, *Adv. Inorg. Chem. Radiochem*., **1983**, *26*, 235.

[164] L. Brossard, M. Ribault, L. Valade, P. Cassoux, *Physica B and C (Amsterdam*), **1986**, *143*, 378.

[165] H. Tajima, M. Inokuchi, A. Cobayashi, T. Ohta, R. Kato, H. Cobayashi, H. Kuroda, *Chem. Lett*., **1993**, 1235.

[166] L.B. Coleman, M.J. Cohen, D.J. Sandman, F.G. Yamagishi, A.F. Garito, A.J. Heeger, *Solid State Commun*., **1973**, *12*, 1125.

[167] K. Bechgaard, K. Carneiro, F.B. Rasmussen, H. Olsen, G. Rindorf, C.S. Jacobsen, H. Pedersen, J.E. Scott, *J. Am. Chem. Soc*., **1981**, *103*, 2440.

[168] A.F. Diaz, K.K. Kanazawa, G.P. Gardini, *J. Chem. Soc. Chem. Commun*., **1979**, 635.

[169] J. Roncali, *Chem. Rev*., **1992**, *92*, 711.

[170] W.A. Little, *Phys. Rev. A*, **1964**, *134*, 1416.

[171] D. Jerome, K. Bechgaard, *Nature*, **2001**, *410*, 162.

[172] J.K. Bera, K.R. Dunbar, *Angew. Chem. Int. Ed*., **2002**, *41*, 4453.

[173] G.M. Finniss, E. Canadell, C. Campana, K.R. Dunbar, *Angew. Chem. Int. Ed. Engl.*, **1996**, *35*, 2772.

[174] F. Huq, A.C. Skapski, *J. Cryst. Mol. Struct.*, **1974**, *4*, 411.

[175] F. Bagnoli, D. Belli Dell'Amico, F. Calderazzo, U. Englert, F.Marchetti, G.E. Herberich, N. Pasqualetti, S. Ramello, *J. Chem. Soc. Dalton Trans.*, **1996**, 4317.

[176] F.A. Cotton, E.V. Dikarev, M.A. Petrukhina, *J. Organomet. Chem.*, **2000**, *596*, 130.

[177] F.A. Cotton, E.V. Dikarev, M.A. Petrukhina, *J. Chem. Soc. Dalton Trans.*, **2000**, 4241.

[178] P. Klüfers, *Angew. Chem. Int. Ed*., **1985**, *24*, 70.

[179] N. Masciocchi, M. Moret, P. Cairati, F. Ragaini, A. Sironi, *J. Chem. Soc. Dalton Trans*., **1993**, 471.

[180] J.C. Calabrese, L.F. Dahl, A. Cavalieri, P. Chini, G. Longoni, S. Martinengo, *J. Am. Chem. Soc.* **1974**, *96*, 2616.

[181] D. Braga, F. Grepioni, P. Milne, E. Parisini, *J. Am. Chem. Soc*, **1993**, *115*, 5115.

[182] C.J. McNeal, J.M. Hughes, G.J. Lewis, L.F. Dahl, *J. Am. Chem. Soc*., **1991**i, *113*, 372.

[183] P.M.S. Monk, *The Viologens*, John Wiley and Sons, Chichester, **1998**, and references therein.

[184] D. Collini, C. Femoni, M.C. Iapalucci, G. Longoni, *Proceedings of the II National Conference on Nanosciences and Nanotechnologies*, Bologna, **2004**, P1.12.

[185] M. P. Cifuentes, M. G. Humphrey, L. E. McGrady, P. J. Smith, R. Stranger, K. S. Murray, B. Moubaraki, *J. Am. Chem. Soc.* **1997**, *119*, 2647–2655.

[186] P. P. Edwards, M. J. Sienko, *Int. Rev. Phys. Chem.* **1983**, *3*, 83–137.

[187] R. E. Benfield, P. P. Edwards, A. M. Stacy, *J. Chem. Soc., Chem. Commun.* **1982**, 525–526.

[188] a) S. R. Drake, P. P. Edwards, B. F. G. Johnson, J. Lewis, E. A. Marseglia, S. D. Obertelli, N. C. Pyper, *Chem. Phys. Lett.* **1987**, *139*, 336–344; b) R. E. Benfield, *J. Phys. Chem.* **1987**, *91*, 2712–2716; c) D. C. Johnson, R. E. Benfield, P. P. Edwards, W. J. H. Nelson, M. D. Vargas, *Nature* **1985**, *314*, 231–235.

[189] a) B. J. Pronk, H. B. Brom, L. J. de Jongh, G. Longoni, A. Ceriotti, *Solid State Commun.* **1986**, *59*, 349–354; b) B. K. Teo, F. J. DiSalvo, J. V. Waszczak, G. Longoni, A. Ceriotti, *Inorg. Chem.* **1986**, *25*, 2262–2265.

[190] D. A. van Leeuwen, J. M. van Ruitenbeek, L. J. de Jongh, A. Ceriotti, G. Pacchioni, O. D. Häberlein, N. Rösch, *Phys. Rev. Lett.* **1994**, *73*, 1432–1435.

[191] J. Sinzig, L. J. de Jongh, A. Ceriotti, R. Della Pergola, G. Longoni, M. Stener, K. Albert, N. Rösch, *Phys. Rev. Lett.* **1998**, *81*, 3211–3214.

[192] a) N. Rösch, G. Pacchioni in *Clusters and Colloids* (Ed.: G. Schmid), Wiley-VCH, New York, **1994**, pp. 5–88; b) L. J. de Jongh (Ed.), *Physics and Chemistry of Metal Cluster Compounds*, Kluwer, Dordrecht, **1994**.

[193] a) T. Iwasa, K. Nobusada, *Chem. Phys. Lett.* **2007**, *441*, 268–272; b) Y. Negishi, H. Tsunoyama, M. Suzuki, N. Kawamura, M. M. Matsushita, K. Maruyama, T. Sugawara, T. Yokoyama, T. Tsukuda, *J. Am. Chem. Soc.* **2006**, *128*, 12034–12035 and ref. therein.

[194] R. Della Pergola, M. Bruschi, F. Fabrizi de Biani, A. Fumagalli, L. Garlaschelli, F. Laschi, M. Manassero, M. Sansoni, P. Zanello, *Comput. Rend. Chim.* **2005**, *8*, 1850–1855.

[195] M. Costa, R. Della Pergola, A. Fumagalli, F. Laschi, S. Losi, P. Macchi, A. Sironi, P. Zanello, *Inorg. Chem.* **2007**, *46*, 552–560.

[196] M. Riccò, T. Shiroka, S. Caretta, F. Bolzoni, C. Femoni, M. C. Iapalucci, G. Longoni, *Chem. Eur. J.* **2005**, *11*, 2856–2861.

[197] a) I. Robinson, S. Zacchini, L. D. Tung, S. Maenosono, N. T. K. Thanh, *Chem. Mater.* **2009**, *21*, 3021–3026; b) R. D.Rutledge, W. H. Morris, M. S. Wellons, Z. Gai, J. Shen, J. Bentley, J. E.Wittig, C. M. Lukehart, *J. Am. Chem. Soc.* **2006**, *128*, 14210–14211.

[198] C. Rown, B.T. Heaton *J. Chem. Soc., Chem. Commun*., **1977**, 309; C. Brown, B.T. Heaton, A.D.C. Towl, P. Chini, A. Fumagalli, G. Longoni, *J. Organomet. Chem*., **1979**, *181*, 233.

[199] We found about 100 references in the CCDC database; selected examples: a) Bennett, M.A.; D.E., Berry; Beveridge, K. A.; *Inorg. Chem.*, **1990**, *29*, 4148; b) Braunstein, P.; Lehner, H.; Matt, D.; Tiripicchio, A.; Tiripicchio Camellini, M.; *Angew. Chem., Int. Ed. Engl.* **1984**, *23*, 304; c) Parish, R.V.; Moore, L.S.; Dens, A.J.J.; Mingos, D.M.P.; Sherman, D.J.; *J. Chem. Soc., Dalton Trans.* **1989**, 539 d) Briant, C.E.; Gilmour, D.I.; Mingos, D.M.P.; *J.Chem.Soc.,Dalton Trans*, **1986** 835 e) Manojlovic-Muir, L.; Muir, K.W.; Treurnicht,I.;

Puddephatt, R.J.; *Inorg. Chem.* **1987**, *26*, 2418 f) Hallam, M.F.; Luke, M.A.; Mingos, D.M.P.; Williams, I.D.; *J.Organomet.Chem.*, **1987** *325*, 271, g) Mingos, D.M.P.; Oster, P.; Sherman, D.J.; *J.Organomet.Chem.* **1987**, *320*, 257, h) Hallam, M.F.; Mingos, D.M.P.; Adatia, T.; McPartlin, M.; *J.Chem.Soc.,Dalton Trans.*, **1988** 335 i) Payne, N.C.; Ramachandran, R.; Schoettel, G.; Vittal, J.J.; Puddephat, R.J.; *Inorg.Chem.*, **1991** *30*, 4048, l) Yip, J.H.K.; Jianguo Wu, Kwok-Yin Wong, Kam Piu Ho, So-Ngan Pun, C.; Vittal, J.J.; *Organometallics* , **2002** *21*, 5292, m) Imhof, D.; Burckhardt, U.; Dahmen, K.-H.; Ruegger, H.; Gerfin, T.; Gramlich, V.; *Inorg.Chem.* **1993**, *32*, 5206, n) Toronto, D.V.; Balch, A.L.; *Inorg.Chem.* , **1994** *33*, 6132,

[200] a) De Silva, N.; Dahl, L. F.; *Inorg. Chem.*, **2005**, *44*, 9604 b) De Silva, N.; Laufenberg, J.W.; Dahl, L.F.; *Chem.Commun.* **2006**, 4437, c) Spivak, G.J.; Vittal, J.J.; Puddephatt, R.J.; *Inorg.Chem.* **1998**, *37*, 5474

[201] a) Krogstad, D.A.; Young Junior, V.G.; Pignolet, L.H.; *Inorg.Chim.Acta* , **1997** *264*, 19, b) Krogstad, D.A.; Konze, W.V.; Pignolet, L.H.; *Inorg.Chem.* **1996**, *35*, 6763, c) Breuer, M.; Strahle, J.; *Z.Anorg.Allg.Chem.* , **1993** *619*, 1564, d) Schoondergang, M.F.J.; Bour, J.J.; van Strijdonck, G.P.F.; Schlebos, P.P.J.; Bosman, W.P.; Smits, J.M.M.; Beurskens, P.T.; Steggerda, J.J.; *Inorg.Chem.* **1991**, *30*, 2048, e) Bour, J.J.; Schlebos, P.P.J.; Kanters, R.P.F.; Bosman, W.P.; Smits, J.M.M.; Beurskens, P.T.; Steggerda, J.J.; *Inorg.Chim.Acta* , **1990** *171*, 177, f) Ito, L.N.; Sweet, J.D.; Mueting, A.M.; Pignolet, L.H.; Schoondergang, M.F.J.; Steggerda J.J.; *Inorg.Chem.* **1989**, *28*, 3696, g) Kanters, R.P.F.; Bour, J.J.; Schlebos, P.P.J.; Bosman, W.P.; Behm, H.; Steggerda, J.J.; Ito, L.N.; Pignolet, L.H.; *Inorg.Chem.* **1989**, *28*, 2591, h) Kanters, R.P.F.; Schlebos, P.P.J.; Bour, J.J.; Bosman, W.P.; Behm, H.J.; Steggerda J.J.; *Inorg.Chem.* **1988**, *27*, 4034, i) Hallam, M.F.; Mingos, D.M.P.; Adatia, T.; McPartlin, M.; *J.Chem.Soc., Dalton Trans.*, **1988**, 335 l) Bour, J.J.; Kanters, R.P.F.; Schlebos, P.P.J.; Bosman, W.P.; Behm, H.; Beurskens, P.T.; Steggerda J.J.; *Rec.Trav.Chim.Pays-Bas* **1987**, *106*, 157

[202] a) Behm, H.J.; Steggerda, J.J.; *Inorg. Chem.* **1988**, *27*, 4034 b) Bour, J.J.; Kanters, R.P.F.; Schlebos, P.P.J.; Steggerda, J.J.; *Reel. Trau. Chim. Pays-Bas* **1988**, *107,* 211; g) Kanters, R.P.F.; Bour, J.J.; Schlebos, P.P.J.; Bosman, W.P.; Behm, H.; Steggerda, J.J.; Ito, L.N.; Pignolet L.H.; *Inorg. Chem.* **1989**, *28*, 2591; h) Ito, L.N.; Sweet, J.D.; Mueting, A.M.; Pignolet, L.H.; Schoondergang, M.F.; Steggerda, J.J.; *Inorg. Chem.* **1989**, *28*, 3696

[203] a) Qian, L.; Yang, X.; *J. Phys. Chem. B* **2006**, *110*, 16672-8 b) Luo, J. ; Njoki, P.N.; Wang, L.; Zhong, C.J.; *Electrochem. Commun.* **2006**, *8*, 81-7 c) Habrioux, A.; Vogel, W.; Guinel, M.; Guetaz, L.; Servat, K.; Kokoh, B.; Alonso-Vante, N.; *Phys. Chem. Chem. Phys.,* **2009**, *11*, 3573-9 d) Mohamed, M.M.; Khairou, K.S.; *J. Colloid Interf. Sci.,* **2011**, *354*, 100-108

[204] Washecheck, D.M.; Wucherer, E.J.; Dahl, L.F.; Ceriotti, A.; Longoni, G.; Manassero, M.; Sansoni, M.; Chini, P.; *J. Am. Chem. Soc.*, **1979**, *101*, 6110

[205] Ceriotti, A.; Masciocchi, N.; Macchi, P.; Longoni, G.; *Angew. Chem. Int. Ed.*, **1999**, *38*, 3724

[206] Fedi, S.; Zanello, P.; Laschi, F.; Ceriotti, A.; El Afefey, S.; *J. Solid State Electrochem.*, **2009**, *13*, 1497

[207] a) Fumagalli, A.; Della Pergola, R.; Bonacina, F.; Garlaschelli, L.; Moret, M.; Sironi A.; *J.Am.Chem.Soc.*, **1989**,*111*,165 b) Della Pergola, R.; Ceriotti, A.; Garlaschelli, L.; Demartin, F.; Manassero, M.; Masciocchi N.; *Inorg.Chem.*, **1993**, *32*, 3349; c) Femoni, C.; Iapalucci, M.C.; Longoni, G.; Tiozzo, c.; Zacchini, S.; Heaton, B.T.; Iggo, J.A.; Zanello, P.; Fedi, S.; Garland, M.V.; Li, C.; *Dalton Trans.*, **2009**, 2217–2223

[208] a) Khimyak, T.; Johnson, B.F.G.; Hermans, S.; Bond A.D.; *Dalton Trans.*, **2003**, 2651 b) Gould, R.A.T.; Craighead, K.L.; Wiley, J.S.; Pignolet L.H.; *Inorg. Chem.*, **1995**, *34*, 2902

[209] a) Fumagalli, A. Martinengo, S. Albano, V. G. Braga, D. Grepioni F.; *J. Chem. Soc., Dalton Trans.*, **1989**, 2343-6; b) Housecroft, C.E.; Matthews, D.M.; Waller, A.; Edwards, A.J.; Rheingold, A.L.; *J.Chem.Soc.Dalton Trans.,* **1993,** 3057 c) Ceriotti, A.; Della Pergola, R.; Garlaschelli, L.; Manassero, M.; Masciocchi, N.; *Organometallics,* **1995,** *14,* 186-193

[210] P. Zanello, Hexanuclear binary complexes, pag. 362, in "*Stereochemistry of organometallic and inorganic compounds. Vol. 5: chains, clusters, inclusion compounds, paramagnetic labels and organic rings*", Elsevier, **1994**, ISBN 0-444-81581-3

[211] F. P. Pruchnik, K. Wajda-Hermanowicz, M. Koralewicz – J. Organomet. Chem., **1990**,384,381

[212] R. B. Jordan in " Reaction Mechanism of Inorganic and Organometallic Systems", Oxford University Press, **1998**.

[213] P: Chini, B. T. Heaton, in "Tetranuclear Carbonyl Cluster", Topics in Current Chemistry, 71, 1, **1977**, Springer-Verlag, Berlino.

[214] J. R. Shapley, G. F. Stuntz, M. R. Churchill and J. P. Huchinson – J.Chem.Soc.Chem.Commun., **1979**, 219.

[215] a) J.C. Calabrese, L.F. Dahl, P. Chini, G. Longoni, S. Martinengo, J. Am. Chem. Soc., **1974**, 96, 2614, b) P. Zanello, Structure and Bonding, , Springer, Berlin, **1992**. Vol. 79, p.101, c) G.J. Lewis, J.D. Roth, R.A. Montag, L.K. Safford, X. Gao, S.-C. Chang, L.F. Dahl, M.J. Weaver, J. Am. Chem. Soc. **1990**, 112, 2831, d) J.D. Roth, G.J. Lewis, L.K. Safford, X. Jiang, L.F. Dahl, M.J. Weaver, J. Am. Chem. Soc. **1992**, 114, 6159

[216] C. Femoni, M. C. Iapalucci, F. Kaswalder, G. Longoni and S. Zacchini, Coord. Chem. Rev., 2006, 1580-1604.

[217] B. F. G. Johnson, Coord. Chem. Rev., 1999, **190-192**, 1269-1285.

[218] C. Femoni, F. Kaswalder, M.C. Iapalucci, G. Longoni, M. Mehlstaubl, S. Zacchini and A. Ceriotti, Angew. Chem. Int. Ed., 2006, **45**, 2060-2062.

[219] C. Femoni, F. Kaswalder, M. C. Iapalucci, G. Longoni and S. Zacchini, Eur. J. Inorg. Chem., 2007, 1483-1486.

[220] B. T. Heaton, L. Strona, S. Martinengo, D. Strumolo, V. G. Albano and D. Braga, J. Chem. Soc. Dalton Trans., 1983, 2175.

[221] T Nakajima, A. Ishiguro and Y. Wakatsuki, Angew. Chem. Int. Ed., 2001, **40**, 1066-1067.

[222] A. Fumagalli, M. C. Malatesta, A. Tentori, D. Monti, P. Macchi and A. Sironi, Inorg. Chem., 2002, **41**, 76-85.

[223] I. O. Koshevoy, M. Haukka, T. A. Pakkanen, S. P. Tunik and P. Vainiotalo, Organometallics, 2005, **24**, 3516-3526.

[224] C. Femoni, R. Della Pergola, M. C. Iapalucci, F. Kaswalder, M. Riccò and S. Zacchini, Dalton Trans., 2009, 1509-1511.

[225] a) M. Cowie, S.K. Dwight, *Inorg. Chem*., **1980**, 19(9), 2500 b) A.R. Sanger, *JCS, Chem. Comm.*, **1975**, 893 c) A.R. Sanger, *JCS, Dalton Trans.*, **1977**, 1971 d) J.T. Mague, J.P. Mitchener, *Inorg. Chem.*, **1969**, 8(1), 119

[226] M. Daghetta, G. Peli, P. Macchi, L. Garlaschelli, A. Sironi, P7 Communication, *VIII Congresso Interdivisionale di Chimica Organometallica, SCI*, Perugia 25-28/6/2008

[227] a) R. Srinivasan, R. J. De Angeles, B. H. Davis, *J. Catal*., **1987**, *106*, 449, b) R. V. Lindsey, G. W. Parshall, U. G. Stolberg, *Inorg. Chem*., **1966**, *5*, 109

[228] R. Srinivasan, R. Sharma, S. Su, B. H. Davis, *Catal.Today*, **1994**, 83.

[229] H. A. Tayim, J. C. Bailar, *J. Am. Chem. Soc.*, **1967**, *89*, 4330.

[230] I. Schwager, J. F. Knifton, *J. Catal.*, **1976**, *45*, 256

[231] J. F. Knifton, *J. Am. Oil Chem. Soc.*, **1978**, *55*, 496.

[232] C. Cheng, R. Eisemberg, *J. Am. Chem. Soc.*, **1978**, *100*, 2968

[233] D.J. Patmore, W.A. Graham, *Inorg. Chem.*, **1966**, *5*, 1405

[234] D.M.T. Chan, T.B. Marder, *Angew. Chem. Int. Ed. Engl.*, **1988**, *27*, 442

[235] P. Ewing, L. Farrugia, *New J. Chem.*, **1988**, *12*, 409

[236] a) Adams, R. D.; Captain, B.; Hollandsworth, C. B.; Johansson, M.; Smith Junior, J. L. *Organometallics* **2006**, *25*, 3848.

b) Schneider, J. J.; Czap, N.; Hagen, J.; Rust, J.; Kruger, C.; Mason, S. A.; Bau, R.; Ensling, J.; Gutlich, P.; Wrackmeyer, B. *Chem. Eur. J.* **2000**, *6*, 625.

[237] (a) Hoffmann, R.; Rogachev, A. Yu. Private communication of their work in progress on the subject.

(b) *Chemistry of Hypervalent Compounds*; Akiba, K.-y., Ed. ; Wiley, **1999**.

[238] G.Longoni, P.Chini, *JACS*, **1976**, 98 (23), 7225

[239] a) M-H Whangbo, *Acc. Chem. Res.*, **1983**, *16*, 95-101

b) J.K. Burdett in *Chemical Bonding in Solids,* Oxf. Univ. Press, New York, **1995**

[240] C. Femoni, F. Kaswalder, M.C. Iapalucci, G. Longoni, S. Zacchini, *Eur. J. of Inorg. Chem.*, **2007**, 1483-1486

[241] F. Leroux, T.U. Hutschenreuter, C. Charrière, R. Scopelliti, R.W. Hartmann, *Helv. Chim. Acta*, **2003**, *86(7)*, 2671

[242] R. Uson, A. Laguna and M. Laguna, Inorg. Synth., **1989**, *26*, 85

[243] R.W. Tilford, W.R. Gemmill, H-C. zur Loye, J.J. Lavigne, *Chem. Mat.*, **2006**, *18*, 5296